Towards Understanding Flavin Reactivity: A Structural Study of Cholesterol Oxidase

by

Paula I. Lario

A thesis submitted to the Faculty of Graduate Studies and Research in partial fulfillment of the requirement of the degree of Doctor of Philosophy

Department of Biochemistry
McGill University
Montreal, Canada

Your file Votre référence
ISBN: 0-612-88505-4
Our file Notre référence
ISBN: 0-612-88505-4

This thesis is dedicated to Greg for his love and encouragement throughout the years

ABSTRACT

Flavoenzymes catalyze a wide variety of biochemical reactions and are commonly observed as electron transport proteins. The redox reactive portion of the enzymes is the isoalloxazine ring system of the flavin cofactor. It is known that the protein environment modulates the redox potential of the flavin, for example, "tuning" its redox potential to favor either a one-electron transfer (electron transfer proteins) or a two-electron transfer (oxidation reactions). This thesis presents an in depth structural study of the flavoenzyme, cholesterol oxidase (EC 1.1.3.6) from *Streptomyces sp.* SA-COO (SCOA) a multifunctional enzyme that oxidizes and isomerizes 3-β-hydroxysteroids. This work was pursued in order to further our understanding of the mechanisms through which the protein interacts with the isoalloxazine system and modulates reactivity. Previous kinetic experiments have identified an active site asparagine (N485) and a histidine residue (H447) both of which are critical to the oxidative activity of the enzyme. On an atomic scale the role of the asparagine residue was unknown. Using mutagensis and crystallographic techniques we have characterized this novel N-H $\cdots$ π protein-flavin interaction. SCOA crystals diffract to sub-atomic resolution providing us with a unique view of the protein bound isoalloxazine system. These atomic resolution maps have revealed unexpected structural features that were not previously apparent in the 1.5 Å resolution of SCOA. For example, a second narrow pathway leading directly to the isoalloxazine system was discovered, which has provided a more complete mechanistic understanding of the reactions catalyzed by SCOA. Five atomic resolution structures of SCOA at varying pH values are reported. Differences among these structures provide

insight into the affect of pH on protein structure and have revealed structural differences resulting from an inadvertent reduction of the cofactor. For example, these structures support our hypothesis that N485 gates the hydrophobic tunnel by responding to differences in the redox state of the isoalloxazine system. In addition to examining the differences among these structures, having five independently refined structures enables one to examine unusual features in the map, since the persistence of density features in all five structures provides convincing evidence that these features are real and not the result of noise in the maps. For example, a protein-flavin interaction involving an aliphatic C-H bond was observed where the hydrogen atom is elongated towards the π system of the isoalloxazine system. The observation of these atypical protein-flavin interactions in SCOA has lead to a paradigm shift in the way we evaluate the roles of residues surrounding isoalloxazine ring systems. Furthermore, the observed asymmetry in electron density around atoms, in these ultra high-resolution maps, has allowed us to visualize electronic differences between main-chain carbonyl groups as a function of secondary structure. This study provides an example of the value of persuing atomic resolution crystallography and what these structures reveal.

RÉSUMÉ

Les Flavoenzymes catalysent une grande variété de réactions biochimiques et sont souvent observé dans le rôle de protéines qui servent comme transporteurs d'électrons. La portion oxidoréductive de ces enzymes se trouve dans le système isoalloxazine du cofacteur flavin. C'est déjà bien connu que l'environnement a l'intérieur de la protéine peut moduler le potentiel oxidoréductif du flavin qui, par exemple, peut favoriser le transfert de un ou de deux électrons. Cette thèse présente une étude structurelle approfondie de la flavoenzyme Cholesterol Oxidase (EC 1.1.3.6) de l'organisme *Streptomyces sp.* SA-COO (SCOA), une enzyme multifonctionelle qui catalyse l'oxidation et l'isomerisation de 3-β-hydroxystéroides. Ces études ont été menées pour approfondir la comprehension du méchanisme par lequel la protéine interagit avec le système isoalloxazine et peut moduler l'activité de celle-ci. Les résultats antérieurs ont identifiés une asparagine (N485) et une histidine (H447) dans le site actif, qui seraient indispensable à l'activité oxidoréductive de l'enzyme. Sur une échelle atomique, le rôle de l'asparagine était inconnu. En utilisant la mutagénèse et diverses techniques crystallographiques, nous avons caracterisé une nouvelle interaction entre le N-H de l'asparagine et le groupe électronique π du flavin. Les crystaux de SCOA ont une diffraction qui permet une résolution sous l'échelle atomique, qui nous donne une image unique de la protéine liée au système isoalloxazine. Les nouvelles cartes à résolution atomique de la protéine ont démontré des caractéristiques structurelles inattendues et qui n'étaient pas évidentes à une résolution de 1.5 Å. Par exemple, un deuxième corridor menant directement au système isoalloxazine a été découvert, ce qui a permi une

compréhension méchanistique approfondie des réactions catalysées par SCOA. Nous avons publié cinq structures à résolution atomique, chaque a un pH différent. Les différences entre ces structures permettent de comprendre l'effet du pH sur la structure de la protéine et ont révélé des differences structurelles qui résultent de la réduction non-intentioné du cofacteur. Par exemple, ces structures appuient notre hypothèse que N485 forme une barrière qui bloque le corridor hydrophobique et qui repond aux different stades oxidoréductifs du système isoalloxazine. En plus de pouvoir examiner les différences entre les structures, le fait d'avoir cinq structures qui ont été raffiné de facon indépendante nous permet d'examiner des reliefs sur la carte qui ne sont pas souvent observés et qui sont habituellement attribués a l'erreur expérimentale. Leur persistence dans les cinq structures nous permet de conclure que ces résultats sont réels. Par exemple, une autre interaction inattendue entre un lien C-H aliphatique de la protéine et le système π du systême isoalloxazine, qui démontre un allongissement du lien et que l'atome d'hydrogène est attiré par le systême isoalloxazine, a été observé. L'observation de ces interactions non-typiques dans SCOA ont causé un changement dans la façon dont on évalue le role des acides aminés qui entourent les systêmes isoalloxazine. De plus, la forme non-symmétrique des électrons contournant les atomes impliqués, dans les cartes haute-résolution, nous permet de visualiser les différences électroniques entre les groupes carbonyles de la chaine principale. Cette étude nous donne un exemple du potentiel de la crystallographie a haute résolution et ce que ces structures peuvent révéler.

ACKNOWLEDGEMENTS

The constant support offered by my thesis supervisor, Dr. Alice Vrielink is gratefully acknowledged. She has provided me a wonderful project and taught me the necessary skills to apply my background knowledge to another discipline. Throughout the years her encouragement and flexibility has helped me to develop confidence as a researcher.

I thank Dr. Zheng Huang and members of his group, Susana Lui and France Laliberté, for welcoming me into their laboratory, teaching me vital biochemistry techniques, critical thinking and providing endless guidance and support.

I have been fortunate to be guided by colleagues like Louis Lim, Nathalie Croteau and Rene Coulombe. Their experience, instruction, serenity and warm dispositions will be missed.

I have enjoyed the camaraderie and help of fellow lab mates, Peter Pawelek, Jaime Cheah, Darcy Kohls, Mark Collins, Nick Skouris and Artem Lyubimov. Special thanks goes to my friend Nick Skouris for translating my abstract into French.

I thank our collaborator Dr. Nicole Sampson and her student YeYin for providing purified protein.

I thank the following institutions for funding: McGill University for the Lloyd Carr-Harris Fellowship, the McGill Faculty of Medicine for the Internal Studentship Awards, the Quebec government for a FCAR-Santé Fellowship, the Post-Graduate Students Society of McGill University for the Alma Mater Award and the American Crystallographic Association for both a travel grant and a Peggy Etter Award. In addition this work was supported through the following grants of Dr. Alice Vrielink: the National Institutes of Health Grant GM63262 and Canadian Institutes of Health Research Grant MT-13341.

CLAIM OF CONTRIBUTION TO ORIGINAL KNOWLEDGE

1. The crystallographic structure of a N485L mutant of cholesterol oxidase from *Streptomyces sp*. has been determined.

2. Discovery of a unique protein-flavin interaction involving the side chain amide group of an asparagine residue with the aromatic system of the isoalloxazine group in FAD. This N-H $\cdots$ π interaction modulates the redox potential of the cofactor.

3. The first sub-atomic resolution structure of a flavoenzyme, cholesterol oxidase from *Streptomyces sp*. To date, this structure is one of the largest protein structures refined to atomic resolution.

4. Detection of a second entry pathway to the isoalloxazine ring system in SCOA. The movements of the side chain of residues gate this narrow hydrophobic tunnel.

5. An additional role for N485 has been proposed where its side chain, senses the oxidative state of the cofactor, and subsequently triggers the gating of the hydrophobic tunnel.

6. The oxidative role of the active site histidine residue, H447, was redefined. It is unlikely that this residue has a basic role, as previously proposed, rather it has a role as hydrogen bond donor, necessary for substrate orientation.

7. The Michaelis complex for this enzyme has been proposed which is contrary to the observed position of the steroid in the *Brevibacterium sterolicum* complex structure.

8. The sensitivity of the FAD cofactor to artificial reduction by the X-ray irradiation experiment was discovered. The rate of reduction was found to be dependant on the solution matrix of the crystal.

9. The adenosine ring of the FAD was found to be protonated on the AN7 atom at acidic pH values. The pKa of AN7 of the adenosine ring in the FAD was estimated based on an observed titration in the varying pH structures.

10. Unique electron density for the pyrophosphate linkage in the FAD cofactor was observed.

11. An unexpected elongation of the CB-H bond towards the N5 atom of the FAD presents experimental evidence that aliphatic hydrogen bonds need to be considered when evaluating protein-flavin interactions.

12. Presentation and evaluation, of the unique electronic features of main chain carbonyl groups; as viewed in the electron density maps of cholesterol oxidase.

CONTRIBUTIONS OF AUTHOURS

In accordance with the guidelines of the Faculty of Graduate Studies and Research, McGill University, concerning thesis preparation, I have opted to present the experimental portion of the thesis (Chapters 2, 3, 4 and 5) in the form of manuscripts. A provision in the guidelines concerning thesis preparation is as follows:

Candidates have the option of including, as part of the thesis, the text of one or more papers submitted or to be submitted for publication, or clearly-duplicated text of one or more published papers. These texts must be bound as an integral part of the thesis.

If this option is chosen, connecting texts that provide logical bridges between the different papers are mandatory. The thesis must be written in such a way that is more than just a mere collection of manuscripts; in other words, results of a series of papers must be integrated.

The thesis must still conform to all other requirements of the "Guidelines Concerning Thesis Preparation". The thesis must include: A Table of Contents, an abstract in English and French, an introduction which clearly states the rationale and objectives of the study, a review of the literature, a final conclusion and summary, and a thorough bibliography or reference list.

Additional material must be provided where appropriate (e.g. appendices) and in sufficient detail to allow a clear and precise judgment to be made of the importance and originality of the research reported in the thesis.

In the case of manuscripts co-authored by the candidate and others, the candidate is required to make an explicit statement in the thesis of who contributed to such work and

what extent. Supervisors must attest to the accurancy of such statements at the doctoral oral defense. Since the task of examiners is made more difficult in these cases, it is in the candidate's interest to make perfectly clear the responsibilities of all the authors of the co-authored papers.

The manuscripts that comprise the experimental chapters of this thesis, are listed below; the contributions of co-authors with respect to each experimental work are specified under each manuscript. I am responsible for the rest of the work presented in each manuscript. Dr. Alice Vrielink edited all of the manuscripts, presented in this thesis.

Chaper 2: "The presence of a hydrogen bond between the asparagine and the π system of FAD modulates the redox potential in the reaction catalyzed by cholesterol oxidase". Yin, Y., Sampson, N.S., Vrielink, A. **Lario, P.I.**, (2001), Biochemisty 40(46), 13779-87.

Chapter 2 is co-authored with Ye Yin who cloned, expressed and purified the N485L mutant. In addition, she preformed the biochemical analysis of the enzyme. The crystallographic structure and the interpretation of the results, were carried out by myself. Based on the hypothesis formulated by my structural interpretation, additional redox potential measurement experiments were carried out by Ye Yin.

Chaper 3: "Sub-atomic resolution crystal structure of cholesterol oxidase: what atomic resolution crystallography reveals about enzyme mechanism and the role of the FAD cofactor in redox activity." **Lario, P.I.**, Sampson, N. & Vrielink, A., submitted to Journal of Molecular Biology.

Dr. N. Sampson supplied the protein. All of the structural work and interpretations were carried out by myself.

Chaper 4: "Effect of pH on the atomic resolution structures of cholesterol oxidase: FAD reduction by synchrotron radiation." **Lario, P.I.**, Sampson, N. & Vrielink, A., to be submitted.

Dr. N. Sampson supplied the protein. All of the structural work and interpretations were carried out by myself.

Chaper 5: "Atomic resolution density maps reveal secondary structure dependant differences in electronic distribution" **Lario, P.I.** & Vrielink, A., submitted to Journal of the American Chemical Society.

TABLE OF CONTENTS

LIST OF FIGURES

LIST OF TABLES

CHAPTER 1. INTRODUCTON

"One of the fundamental and most interesting questions in the action of enzymes is, how do enzymes achieve their catalytic rate enhancement relative to an uncatalyzed reaction?" (Kollman et al., 2001). Flavin enzymes are an ideal system to examine how the protein environment around the active site affects catalysis. The redox chemistry of these macromolecules is very sensitive to the surrounding protein environment and thus it has been used to study a wide variety of intermolecular forces, including hydrogen bonding and π-stacking interactions. The effects of amino acid substitutions on the redox behavior and reaction kinetics of flavin enzymes, has provided a greater understanding of the intermolecular forces that catalyze enzymatic reactions and has helped to characterize less well understood electrostatic interactions. Furthering our knowledge of how electrostatic interactions modulate flavin reactivity provides a greater understanding of how the protein environment modulates catalysis in general.

1.1 FLAVIN MOLECULES

The flavin cofactors (Figure 1.1) FAD (flavin adenine dinucleotide) and FMN (flavin mononucleotide) are involved in the catalysis of a wide variety of biological reactions. The electron deficient flavin is able to accommodate an additional one or two electrons making these cofactors quite versatile redox reagents. They are commonly found in enzymes involved in two-electron oxidation reactions and often associated with proteins implicated in the respiratory chain that involve one-electron transfers. To date, hundreds of enzymes have been identified which contain flavin cofactors and almost all of these enzymes utilize its ability to undergo oxidation and reduction.

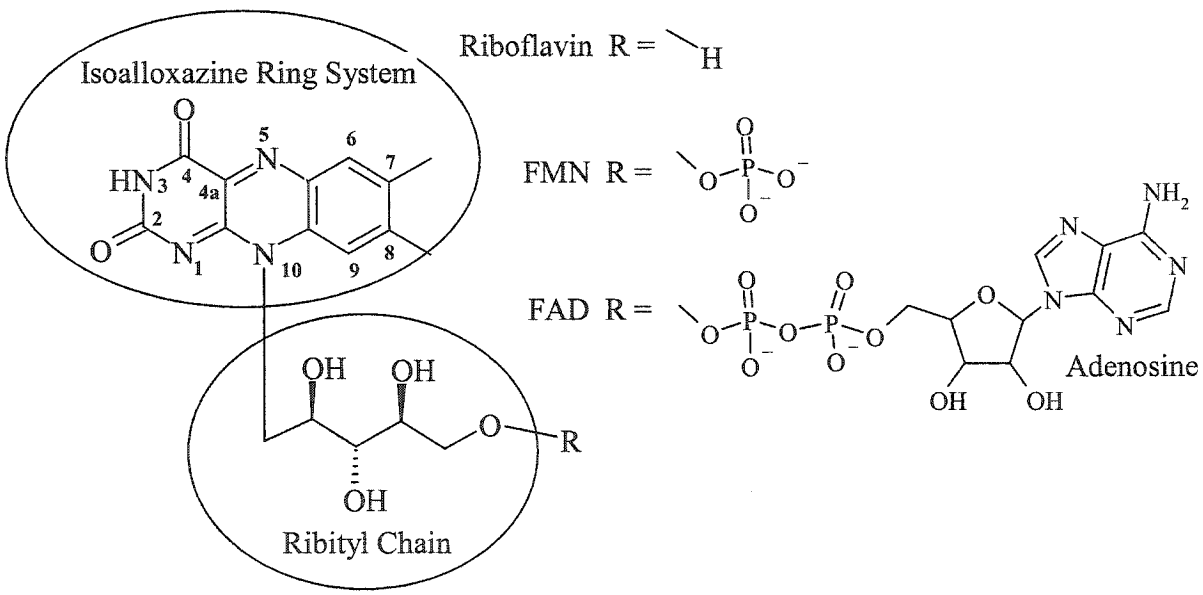

Figure 1.1 Structures of riboflavin, FMN and FAD

1.1.1 Oxidation-reduction reactions

Oxidation-reduction reactions involve the transfer of electrons from an electron donor or reducing agent to an electron acceptor or oxidizing agent. The ability of a reducing agent to lose electrons is represented by its reduction potential. The redox potential of a species is a standardized measure of the electromotive force (emf) in volts observed relative to a reference hydrogen electrode. A strong reducing agent has a large negative reduction potential and a strong oxidizing agent has a large positive reduction potential. Electron transfer can occur between species with different reduction potentials, where the species with the smaller reduction potential will transfer electrons to the species with the larger reduction potential.

1.1.2 Redox states of flavins

The ability of a flavin molecule to accommodate an additional one or two electrons is due to the presence of the isoalloxazine ring system (Figure 1.1). The additional charge gained by the flavin upon reduction can be delocalized onto many different atomic centers within the conjugated ring system. For example, there are two possible tautomers of a two-electron reduced flavin as shown in Figure 1.2. These two tautomers represent the extreme cases of charge distribution where all of the additional charge is located on either of the two oxygen atoms of the isoalloxazine. However, the additional electron charge in the reduced flavin is likely to be distributed throughout the aromatic π system and is better represented by considering partial charges on each atomic center. In fact, an *ab initio* computational study comparing the distribution of charge on

both oxidized and reduced isoalloaxazine systems, have shown that there are larger partial charges observed on both carbonyl oxygen atoms of the reduced state (Breinlinger, 1998).

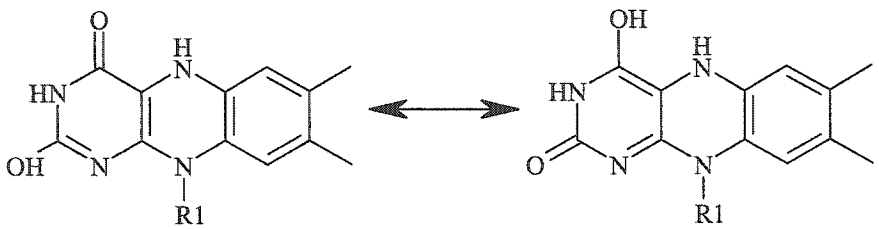

Figure 1.2 Tautomers of a reduced isoalloxazine system

There are three relevant oxidation states observed for flavins: oxidized quinone (F_{ox}), the one-electron reduced semiquinone (F_{rad}), and two-electron reduced hydroquinone (F_{red}). In addition, there are various protonation states possible for each of these redox states. Figure 1.3 represents four commonly considered flavin states.

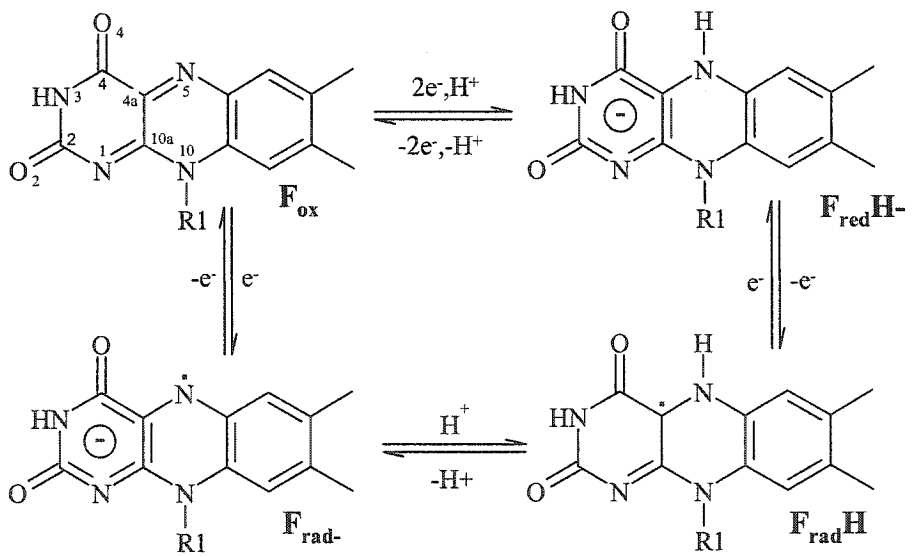

Figure 1.3 Common redox / protonation states of isoalloxazine groups

The redox reactions of flavoproteins can be divided into a reductive and an oxidative half-reaction. The two-electron reduction of a flavin has been proposed to occur

either through two, one-electron transfers or through a two-electron hydride transfer step. Similarly the oxidative half reaction can occur either through either a radical or hydride transfer mechanism. For a number of flavoenzymes the radical mechanism has been clearly established as the presence of the semiquinone intermediate has been detected (Gondry et al., 2001; Mewies et al., 1996; Talfournier et al., 2001). There are also clear examples of single, two-electron transfer mechanism, as in adrenodoxin reductase where a hydride is transferred from an NADPH to the flavin (Ziegler & Schulz, 2000). Radical species have not been detected for many flavoproteins and thus for many of these enzymes a hydride transfer mechanism has been proposed that often involves the cleavage of a stable C-H bond (Gondry et al., 2001; Macheroux et al., 1993; Stenberg et al., 1995; Umhau et al., 2000; Vrielink et al., 1991).

When a hydride mechanism is proposed usually an activating group is also identified. Several flavoenzymes catalyse an α,β dehydrogenation in which an active site base deprotonates the α position and in turn activates the β position for hydride transfer (Rowland et al., 2000; Thorpe & Kim, 1995; Vock et al., 1998; Vrielink et al., 1991). In addition, there is typically a network of hydrogen bonds that lower the pK_a of the α atom to make proton abstraction by a base more feasible (Fraaije et al., 2000).

The actual mechanism for a flavoenzyme is often unclear as the radical intermediates may be very short lived and thus un-detectable with current spectroscopic methods. For example, time resolved (2 ms) rapid fluorescence spectroscopy measurements on pyruvate oxidase revealed only fully oxidized and fully reduced species. This suggests that the enzyme undergoes a hydride transfer mechanism.

However, such a mechanism typically involves a kinetic isotope effect, which was not observed (Tittmann et al., 2000). This mechanistic dilemma is unresolved for many flavoenzymes, however, similarities among enzymes that catalyze dehydrogenation reactions have led to the proposal that these proteins involve hydride transfer mechanisms, rather than the two-step radical mechanism (Kohen & Klinman, 1999; Mattevi et al., 1996; Tittmann et al., 2000; Umhau et al., 2000).

The mechanism of the reoxidation of a flavin by molecular oxygen is believed to go through a flavin-peroxide adduct at the C4a position of the isoalloxazine ring (Ghisla & Massey, 1989; Massey, 1994; Meyer, 1997). *Ab initio* calculations with glucose oxidase have implicated a conserved active site histidine residue that is in a position to stabilize a flavin-peroxide adduct (Meyer et al., 1998).

1.2 Flavin enzymes

Flavoproteins play an important role in a diverse range of biological processes, from embryonic development (Ramana, 1982) to programmed cell death (Susin et al., 1999). They are frequently involved in the oxidation of metabolites through the ability of the flavin to catalyze two-electron dehydrogenations for a wide variety of substrates. In addition, the relative stability of the radical semiquinone state of the flavin allows it to participate in one-electron transfers, which is why these cofactors are regularly found in multi-redox-center enzymes, such as NADPH-cytochrome P450 oxidoreductase (Hubbard et al., 2001).

Hundreds of flavin enzymes have been identified and at present there are around 200 Protein Data Bank (PDB) entries that contain either FAD or FMN dependent

proteins. Most flavoenymes contain a non-covalently bound FAD or FMN, and are specific for binding either of these two flavin forms.

Within the PDB there is a non-redundant subset of 32 FAD-containing protein families, which have been found to adopt one of four FAD-family folds (Dym & Eisenberg, 2001). As would be expected the structural similarities observed within the FAD-family folds is primarily in the FAD binding domains and there are conserved sequence motifs particularly where the protein binds the pyrophosphate moiety. Despite the similarities in the protein folds of these four subfamilies, there is no correlation in enzyme function. Subfamily members catalyze a variety of different reactions.

1.2.1 Glutathione reductase (GR) structural family

Glutathione reductase, GR, family members are identified by similarities in their FAD-binding domains. Despite low sequence identity between GR family members they all adopt a Rossmann fold in their FAD-binding domain, contain a conserved sequence motif (GxGxxG) and are structurally similar in their FAD-binding domain (Dym & Eisenberg, 2001). The FAD cofactor adopts an elongated conformation where the isoalloxazine ring points away from the adenosine ring and towards the active site cavity (Figure 1.4). In addition, the cofactor is found to be either covalently (Trickey et al., 1999), or non-covalently (Vrielink et al., 1991; Wohlfahrt et al., 1999; Ziegler & Schulz, 2000) bound to the protein.

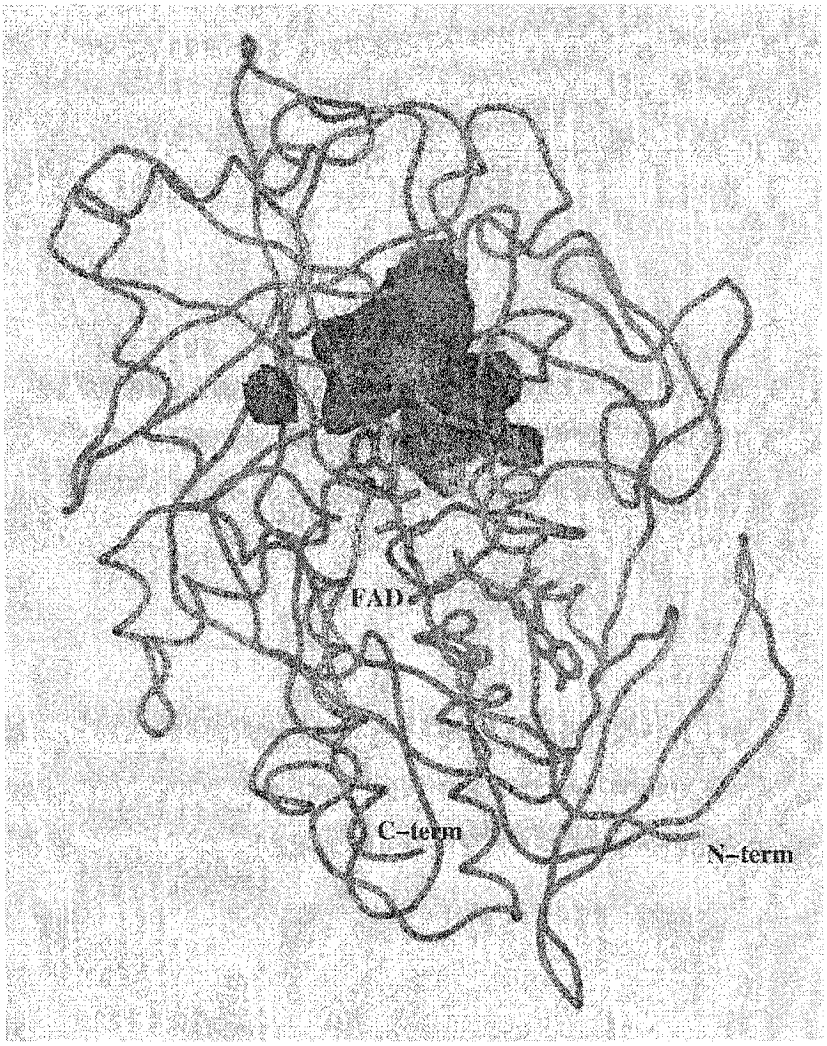

Figure 1.4 Trace diagram of cholesterol oxidase (SCOA). The FAD prosthetic group is shown in purple and the molecular surface of the substrate binding cavity is green. (PDB accession code 1B4V)

Two GR family members, cholesterol oxidase and glucose oxidase, are also known to belong to the glucose-methanol-choline (GMC) oxidoreductase family of enzymes (Cavener, 1992; Kiess et al., 1998; Vrielink et al., 1991). However only the non-covalently bound FAD form of cholesterol oxidase belongs to this enzyme family. The overall fold of the GMC family members is similar, however additional insertions and

deletions occur within family members (Kiess et al., 1998). These enzymes oxidize quite a diverse range of substrates, the requirement of the FAD and conservation of the surrounding active site residues implies that these conserved residues play an important role in the redox reactivity of these enzymes.

The GMC family is characterized by conservation in the general topology and conserved motifs, including two that correspond to FAD-binding. In addition, this family exhibits conservation of key active site residues (Kiess et al., 1998). Within the entire GMC family a histidine residue is absolutely conserved, corresponding to H447 in cholesterol oxidase, BCO1, as well as a H/N corresponding to N485 in BCO1 (Vrielink et al., 1991). Both H447 and N485 are adjacent to the isoalloxazine ring system of the FAD and define part of the substrate-binding pocket (Figure 1.5) The conserved histidine residue (analogous to H447) has been proposed to stabilize the flavin-peroxide adduct in glucose oxidase (Meyer et al., 1998), a possible intermediate in the oxidative half reaction for many of these flavoenzymes.

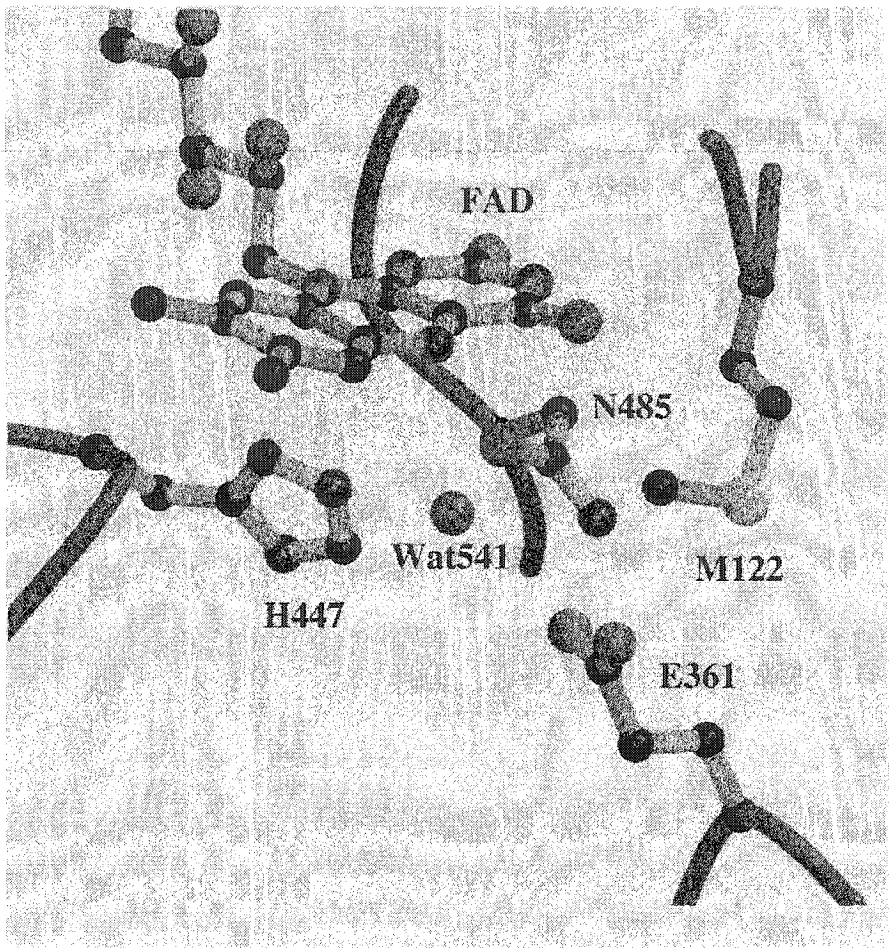

Figure 1.5 Key active site residues of cholesterol oxidase (BCO1).(PDB accession code 3COX)

1.2.2 p-Cresol methylhydroxylase (PCMH) structural family

The most recently identified FAD-binding fold is present in the p-cresol methylhydroxylase, PCMH, structural family [Fraaije, 1998 #201] Similar to the GR family, a conserved protein architecture was observed within the FAD-binding domain. The low sequence homology among the family members, analogous to what was observed for the GR family, may be attributed to the diverse chemistry observed within this family (Dym & Eisenberg, 2001). A recently-discovered, novel cholesterol oxidase

with an FAD covalently bound to the protein (BCO2), was identified as a member of the PCMH family on the basis of structural homology despite the insignificant sequence homology (Coulombe et al., 2001). Although it is frequently found that topologically similar flavoenzymes catalyze different reactions, this second form of cholesterol oxidase (BCO2) is an example where two flavoproteins catalyzing the same reaction have distinct folding architectures.

1.3 ISOALLOXAZINE STRUCTURE AND ENVIRONMENT

The protein environment surrounding the isoalloxazine moiety of the flavin cofactor has been shown to affect its reduction potential. The redox potential for the two-electron reduction of the free flavin, molecule is around –200 mV. However, there are reported potentials of the protein bound oxidized flavins that vary from –500 mV to +60 mV (Fraaije et al., 1999; Ghisla & Massey, 1989; O'Farrell et al., 1998). Previously it was proposed that the protein interactions "tune" the redox potential of flavins through control of their conformation (Hasford, 1997; Massey & Hemmerich, 1980). Additionally it has been shown that specific protein-flavin interactions can modulate the redox potential (Fraaije et al., 2000). In general the presence of a positive charge around the flavin has been shown to increase the redox potential of the enzyme, while the presence of electron rich groups usually lower the potential.

1.3.1 Shape of the isoalloxazine group

There have been a number of crystallographic and computational studies of free flavin molecules. These studies have shown that the oxidized and one-electron reduced semiquinone forms of the isoalloxazine system of the FAD prefer to adopt a planar, conformation while the two-electron reduced isoalloxazine tends to adopt a "butterfly bend" conformation where the bend is along the N5-N10 axis (Lennon et al., 1999; Meyer et al., 1996; Reibenspies et al., 2000) (Figure 1.6)

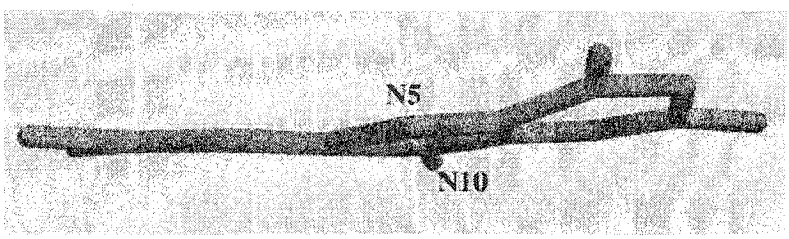

Figure 1.6 Bent isoalloxazine group of the FAD in cholesterol oxidase (*Streptomyces*)

However, the conformation that the isoalloxazine adopts in a protein environment is dependent on the surrounding protein environment. Crystal structures of *Desulfovibrio vulgaris* flavodoxin isolated in its three oxidation states indicated that the flavin is in a planar conformation in all its redox states (Watt et al., 1991). Also, in both crystal structures of cholesterol oxidase, BCO1 and BCO2 the isoalloxazine system adopts a "butterfly bend" despite differences in the oxidation state of their FAD groups (Li et al., 1993; Vrielink et al., 1991). The protein environment in cholesterol oxidase distorts the planar oxidized FAD molecule, to a conformation that is more favorable for the fully reduced FAD, which likely enhances its ability to be reduced.

Ab initio calculations based on both the planar and butterfly conformations have indicated that there is a significantly increased redox potential for the bent conformation relative to the planar oxidized conformation; the respective two-electron reduction potential increases from –200 to –20 mV for lumiflavin and from -174 to 17 mV in C6-methylsulfanyllumiflavin (Trickey et al., 2000). These calculated redox potentials agree well with the experimental two-electron reduction potentials of the planar FMN cofactors in lumiflavin which is –259 mV and –154mV for C6-methylsulfanyllumiflavin (Hasford, 1997) (Ghisla et al., 1980). Also the calculated values for the bent oxidized conformation agree well with the measured potential of +40 mV for the bent FMN in trimethylamine dehydrogenase (Barber et al., 1988). These results strongly support the hypothesis that the conformation of the isoalloxazine ring is a major factor in modulating its redox potential.

1.3.2 Electronic structure

Flavoproteins that catalyze oxidation and reduction reactions typically undergo two-electron transfers and thus the electrostatics of their associated isoalloxazine moieties will change depending on the redox state. In order to understand how the charge is redistributed within the aromatic isoalloxazine system *ab initio* calculations have been used to model the electrostatic distribution (Breinlinger et al., 1998; Cavelier & Amzel, 2001; Trickey et al., 2000). Electrostatic potential maps of the fully oxidized free flavin, in both a planar and a bent butterfly conformation, have shown that there is a positive potential patch adjacent to the C4a-C10a ring juncture in the pyrimidine ring (Figures 1.7 and 1.8). In addition, there is relatively little difference in the electrostatic potential maps between the two conformations (Breinlinger et al., 1998; Trickey et al., 2000). For the

fully reduced isoalloxazine system, the electrostatic surface within the pyrimidine ring is neutral and extra negative charge density is observed in the N1-C2=O2 and C4a-C4=O4 regions (Breinlinger et al., 1998). Therefore, it is apparent, from these theoretical studies, that the additional charge present in the two-electron reduced flavin is delocalized into the aromatic system of the isoalloxazine system and is predominately distributed in the pyrimidine moiety.

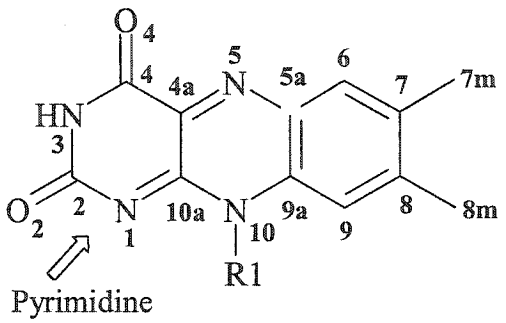

Figure 1.7 Atomic centers of the isoalloxazine system.

Many flavoproteins facilitate oxidation reactions that involve the breaking of a stable C-H bond and it has been proposed that these reactions involve a hydride transfer. Studies have shown that molecular orbital orientations are critical for catalysis involving hydride transfer mechanisms (Mesecar et al., 1997; Umhau et al., 2000). The lowest unoccupied molecular orbital (LUMO) is the most energetically favorable molecular orbital to accommodate an additional two electrons. The orbital of the substrate αC-H needs to overlap (align) with the LUMO of the flavin at N(5) in order to facilitate hydride transfer to that atom. Theoretical studies have provided a model of the LUMO for the oxidized isoalloxazine system and show that there is significant orbital density on the N5 atom of the isoalloxazine ring, which is ideal for optimal orbital overlap (Cavelier &

Amzel, 2001; Trickey et al., 2000) (Figure 1.8a). As expected, the orbital lobes of the calculated LUMO are distributed above and below the plane of the isoalloxazine rings in π shaped orbitals. In addition to the LUMO lobe on N5 there is significant orbital density on the C10a-C4a-C4, N3-C2, O2, O4 atoms of the isoalloxazine ring providing a molecular orbital path for the delocalization of the additional electrons after reduction. These studies show that the orbital distribution of the LUMO in an isoalloxazine system, is consistent with the understanding that the additional electronic charge is redistributed within the π system.

Ab initio quantum mechanical calculations have also been done for the reduced free isoalloxazine system (Cavelier & Amzel, 2001). The highest occupied molecular orbital (HOMO) in the reduced form has a similar configuration to the LUMO of the oxidized isoalloxazine (Figure 1.8b). The HOMO represents the molecular orbital that contains the electrons gained after reduction. There are both increased partial charges as well as increased orbital densities on N1, O2 and O4 atoms in the reduced form with respect to the oxidized form. Depending on the catalytic function of the flavoenzyme, stabilization or destabilization of these charge sinks will play an important role in the redox reactivity of these enzymes.

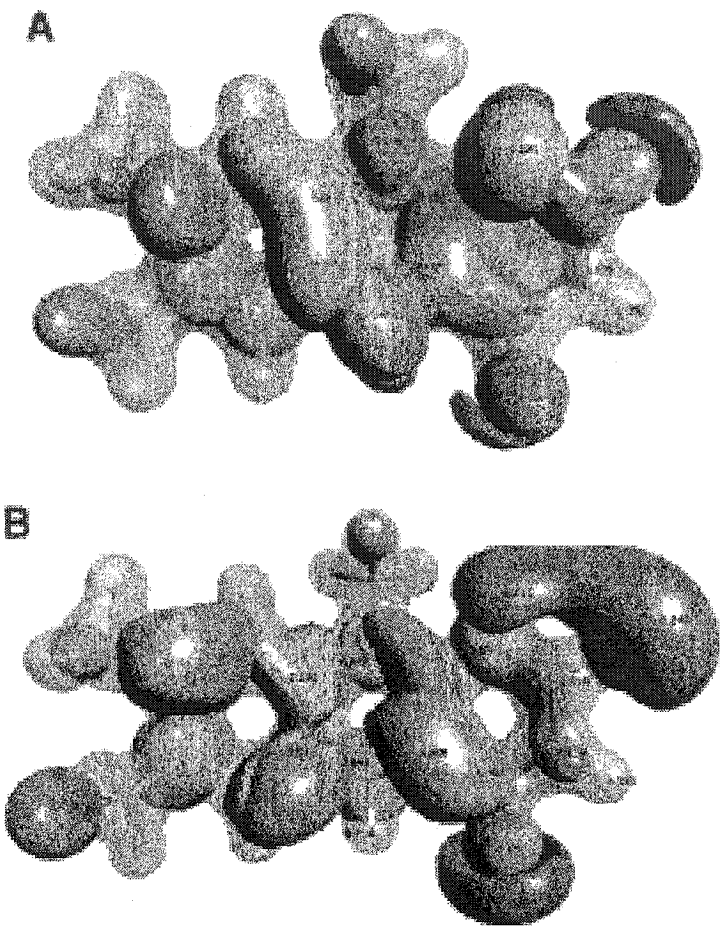

Figure 1.8 Electronic structure results from a DFT B3LYP/6-31G(d) calculation on an isoalloxazine moiety. The electrostatic potential surface is represented in transparent blue (positive) and solid red (negative), the lowest unoccupied molecular orbital (LUMO) is represented by solid green surfaces and the highest occupied molecular orbital (HOMO) is shown in gold. Only one phase of the molecular orbital is shown for clarity; the lobes with the phase of opposite sign are located symmetrically around the cooresponding atoms. The isoalloxazine is shown in two different redox states: (a) oxidized and (b) reduced anionic species. This figure was reproduced from, " Mechanism of NAD(P)H:Quinone Reductase: Ab Initio Studies of Reduced Flavin" Cavelier, G. and Amzel, L,M., PROTEINS: Structure, Function, and Gentics 43:420-432 (2001).

1.3.3 Hydrogen bonding interactions

In general, flavoproteins that are efficient reducing agents tend to form hydrogen bonds that destabilize the reduced flavin, whereas, oxidizing flavins tend to form stabilizing interactions. Aside from the saturated N10 nitrogen atom of the isoalloxazine, all of the electronegative heteroatoms have been identified as forming key hydrogen bonds with the protein.

The presence of a hydrogen bond donor near the N1-C2=O2 locus is a common feature among flavoproteins and has been proposed to facilitate flavin reduction and binding of anionic flavins (Ghisla & Massey, 1989). Frequently there is a strong hydrogen bond donor such as a charged lysine or arginine residue that interacts with this locus, as has been observed in dihydroorotate dehydrogenase (Rowland et al., 2000), cholesterol oxidase (BCO2) (Coulombe et al., 2001), glycolate oxidase (Bradley & Swenson, 1999) and trimethylamine dehydrogenase (Mewies et al., 1996). The presence of an intraflavin hydrogen bond from a hydroxy group on the ribityl chain to the N1 atom of the isoalloxazine in human electron transfer flavoprotein has also been shown to increase the redox potential of the flavin by 116 mV when compared to a 4'-deoxy-FAD mutant (Dwyer et al., 1999) indicating that a hydrogen bond to the N1 atom of the pyrimidine ring facilitates the reduction of this flavin.

It has also been proposed that additional charge on the O2 oxygen atom can be stabilized by a helix dipole. A conserved feature among GMC-oxidoreductases (Vrielink et al., 1991) (Kiess et al., 1998), as well as p-hydroxybenzoate hyroxylase (Schreuder et al., 1989), glutathione reductase (Karplus & Schulz, 1987), polyamine oxidase (Binda et

al., 1999) and D-amino acid oxidase (Mattevi et al., 1996), includes a long helix, where the N-terminus is directed towards the O2 atom of the isoalloxazine moiety.

Despite the recurrent observation of the stabilizing role of interactions with the N1-C2=O2 locus, a recent mutagensis study of morphinone reductase suggests that the presence of a hydrogen donor near this locus does not necessarily imply that its primary role is to stabilize the reduced enzyme (Craig et al., 2001). They have shown that the presence of a positively charged arginine adjacent to the N1-C2=O2 center in morphinone reductase results in only minor decreases to the hydride transfer rate (Craig et al., 2001). Although hydrogen bonds to the N1-C2=O2 atoms of the iosalloxazine moiety likely stabilize the reduced flavin, the degree of stabilization depends on the presence of other protein interactions with the flavin.

Another frequent feature found for flavoproteins is the presence of a hydrogen bond to the O4 oxygen atom of the isoalloxazine ring. The presence of a hydrogen bond donor to the O4 oxygen atom is a conserved feature among related family members of "old yellow enzyme" (OYE) (Xu et al., 1999), such as morphine reductase (Craig et al., 2001) and pentaerythritol tetranitrate reductase (Barna et al., 2001). When the tyrosine that forms a hydrogen bond to O4 in OYE was mutated to an alanine residue, the redox potential of the flavin decreased by 33mV and the rate of the reductive half reaction is decreased 10 fold (Macheroux et al., 1993; Xu et al., 1999). This perturbation of the redox potential by the loss of an O4 hydrogen bonding interaction is also observed for glycolate oxidase (Macheroux et al., 1993). Both of these studies demonstrate the importance of a hydrogen bonding interaction with the C4 carbonyl in stabilizing the reduced flavin.

Other hydrogen bonding interactions have been implicated to play a role in the redox reactivity of the protein-bound flavin. Hydrogen bond acceptors are usually found in close proximity to both N3 and N5 of the isoalloxazine system. A strong hydrogen bond to N(3) has been shown to decrease the redox potential of the flavin making it more difficult to reduce (Cuello, 2000). Many flavodoxin studies have highlighted the importance of hydrogen bonds to both N3 and N5, in stabilizing the semiquinone relative to the fully reduced hydroquinone (Bradley & Swenson, 1999; Chang et al., 2001; Chang & Swenson, 1999; Kasim & Swenson, 2000; Ludwig et al., 1997). In general, it appears that protein-flavin interactions, involving hydrogen bond donation to the isoalloxazine system, typically increase the redox potential while conversely hydrogen bond acceptor-flavin interactions tend to decrease the redox potential.

1.3.4 Aromatic interactions

Early crystallographic studies of isoalloxazine structures have indicated a tendency for these groups to form π-stacking interactions (Ebitani, 1993; Fritchie, 1975; Scarbrough, 1977; Wells, 1974). Usually protein-bound isoalloxazine systems are involved in at least one π-stacking interaction, sometimes on both sides of the isoalloxazine ring as in flavodoxin (Lostao et al., 1997).

Aromatic stacking interactions have been shown to be an important force in ligand binding and protein stability (Hunter et al., 1991; Serrano et al., 1991). Studies have shown that these interactions are also involved in modulating the redox potential of flavins (Breinlinger, 1997; Lostao et al., 1997; Swenson & Krey, 1994; Zhou & Swenson, 1996).

Flavoenzymes that transiently bind the flavin for catalysis often possess an electron-rich donor atom adjacent to the flavin π system. This non-covalent interaction arises from the electrostatic attraction between the electron rich donor and the electron-deficient oxidized flavin (Breinlinger et al., 1998). As mentioned in section 1.3.2, the reduction of the flavin to the radical anion converts the positive potential patch in the pyrimidine ring of the oxidized flavin to a neutrally charged patch. Thus, the favorable binding interaction is attenuated and the apoenzyme–cofactor interaction destabilized.

A sulfur-aromatic interaction in *Clostridium beijerinckii* flavodoxin has been shown by mutagensis studies to regulate its one-electron reduction potentials (Druhan & Swenson, 1998). The midpoint potential for the oxidized-semiquinone (ox/sq) couple of this flavodoxin increased by 20 mV when the methionine residue that interacts with the flavin π system, was mutated to an alanine. In addition, a more dramatic increase of 90 mV was observed for the midpoint potential for the second electron transfer event, the semiquinone-hydroquinone (sq/hq) couple, upon this mutation. Thus the role of the methionine residue appears to be the destabilization of the hydroquinone state relative to the semiquinone, and the separation of the two redox couple reactions which optimizes the physiologically relevant low reduction potential for the sq/hq couple exhibited by the *Clostridium beijerinckii* flavodoxin.

In addition to protein-flavin π interactions that destabilize the reduced isoalloxazine system, we have recently characterized stabilizing π interactions. Rather than involving an electron rich group positioned adjacent to the aromatic π system, a

hydrogen bond donor is present to stabilize the additional charge in the reduced system. These findings are discussed in chapter 2 and chapter 4.

1.3.5 Covalent linkages

There are approximately 25 flavoproteins where the FAD or FMN is covalently attached to the protein (Mewies et al., 1998). This covalent linkage has been observed to occur either at the C6 or C8 carbon atoms on the isoalloxazine group. The covalent linkages involve either a -N-histidyl, -O-Tyrosyl or-S-Cysteinyl.

The direct interaction of these electron rich substituents with the isoalloxazine system is likely to play a role in the electronic properties of the flavin. Removal of the covalent linkage by site directed mutagensis on succinate dehydrogenase / fumarate reductase, SDH, results in an altered activity where the enzyme is still able to reduce fumarate but is unable to oxidize succinate (Blaut et al., 1989). There is still stoichiometric binding of FAD for the SDH mutant which suggests that the covalent linkage alters the flavins redox potentials and/or changes the active site environment (Blaut et al., 1989). Recently a relationship between covalent flavination and redox properties has been identified from studies of a covalent form of cholesterol oxidase, BCO2 (Motteran et al., 2001). In BCO2, the FAD is bound to a histidine residue, H121. When this residue is mutated to an alanine the FAD was found to bind tightly but in a non-covalent manner. This mutant exhibits a 32 fold decrease in its catalytic activity, which has been attributed to a ~100mV decrease in its redox potential. Evidently these studies suggest that covalent modification of the cofactor has a significant affect on the redox potential exhibited by the enzyme.

1.4 CHOLESTEROL OXIDASES

Cholesterol oxidases are bi-functional bacterial enzymes that catalyze the oxidation of the 3β-hydroxysteriods and the isomerization of the intermediate, Δ^{5-6}-ene-3β-ketosteriod to produce Δ^{3-4}-ene-3β-ketosteriod. (Figure 1.9) The oxidation of the substrate is facilitated through the reduction of the FAD prosthetic group, which is subsequently reoxidized by molecular oxygen. Two distinct forms of the enzyme are known, BCO1, where the FAD is non-covalently bound to the protein (EC 1.1.3.6), and the recently-identified form where the FAD is covalently bound to the protein through a FAD_{C8}-histidyl linkage (BCO2) (Coulombe et al., 2001). The non-covalent form of cholesterol oxidase has been isolated from a diverse range bacterium species, including *Bevibacterium sterolicum* (BCO1) (Uwajima et al., 1973), *Streptomyces Sp.* (SCOA) (Corbin et al., 1994; Ishizaki et al., 1989 56), *Streptomyces hydroscopicus* (SCOH) (Motteran et al., 2001), *Rhodococcus, Mycobacterium tuberculosis* and *Mycobacterium leprae* (Navas et al., 2001). Both BCO1 and SCOA are structurally identical which is not surprising considering the high sequence homology observed among the non-covalent enzymes. The covalent form of cholesterol oxidase has been identified in both *Schizophyllum,* (Fukuyama & Miyake, 1979; Kenney et al., 1979) and *Bevibacterium sterolicum* (BCO2) (Coulombe et al., 2001; Gadda et al., 1997; Motteran et al., 2001; Pollegioni et al., 1999).

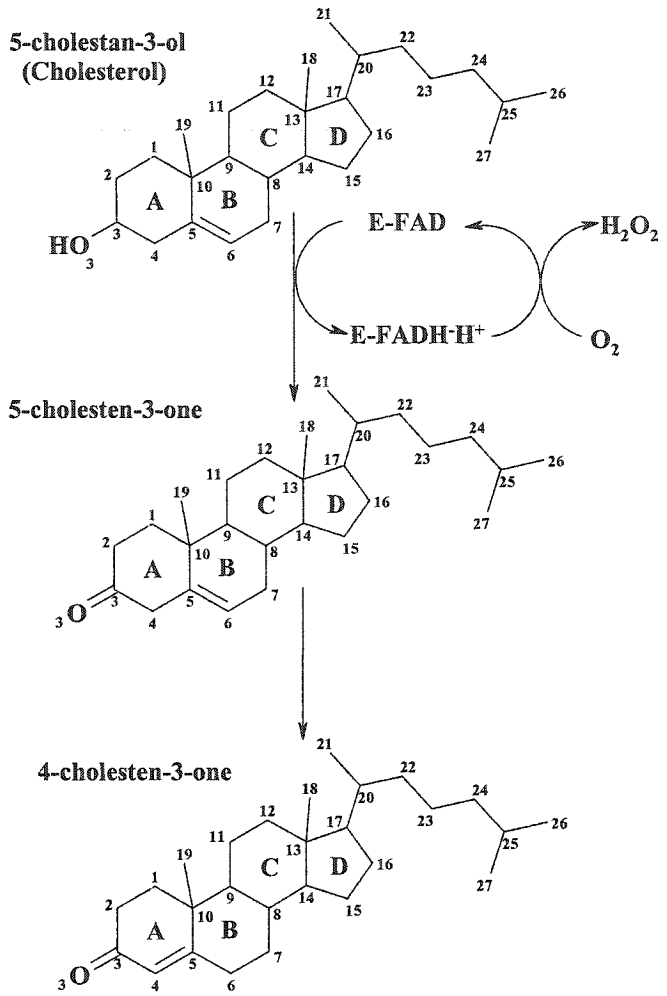

Figure 1.9 Reaction scheme of cholesterol oxidase

Both cholesterol oxidase forms are monomeric (~55 kDa) and while both forms catalyze the oxidation and isomerization of cholesterol, they lack any significant sequence homology with each other. The only structural similarity between the two forms, BCO2 (covalent) and SCOA (non-covalent), is a large active site cavity that can sequester the steroid from the bulk solvent (Figures 1.4 and 1.10). The lack of conserved structural elements around the isoalloxazine ring system of the FAD was not unexpected, as there are large differences in their redox potentials and kinetic properties (Gadda et al., 1997;

Motteran et al., 2001). The redox potential of the FAD is significantly more negative for SCOH compared to BCO1: -101mV and –217 mV respectively (Motteran et al., 2001). In addition, the reaction kinetics for BCO1 indicates an ordered sequential pathway, while BCO2 exhibits a ping-pong mechanism (Pollegioni et al., 1999).

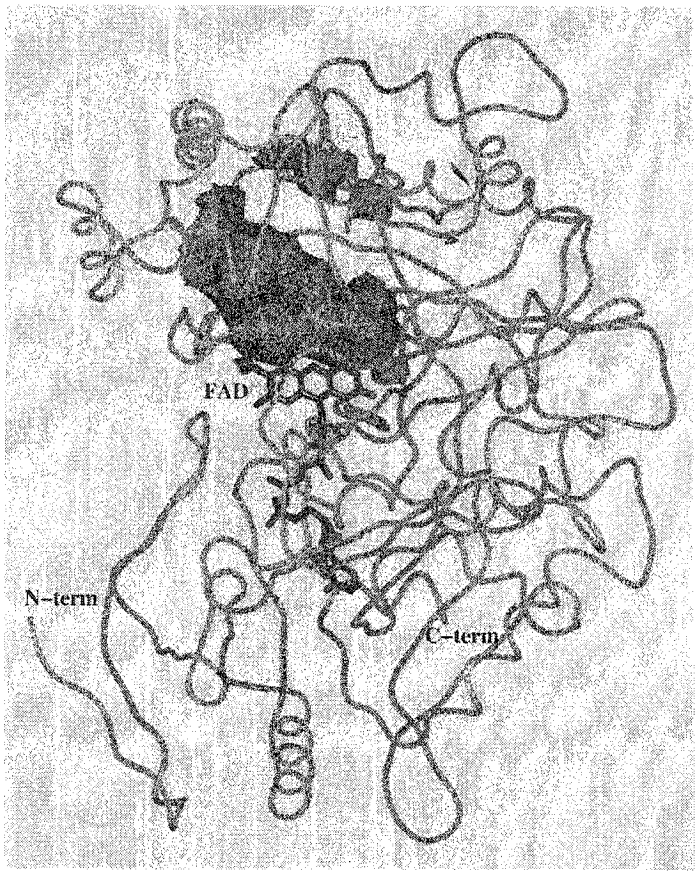

Figure 1.10 Backbone trace of cholesterol oxidase, BCO2 (covalent). The FAD prosthetic group is shown in purple and the molecular surface for the active site cavity is green.

1.4.1 Commercial applications of cholesterol oxidases

Historically, the primary interest in cholesterol oxidases have been as a reagent in clinical assays for the determination of serum cholesterol levels (MacLachlan et al., 2000). Elevated cholesterol concentrations have long been correlated to an increased risk of heart disease (Rose & Shipley, 1980). Development of an efficient assay to determine cholesterol content in plasma was possible due to the specific and highly sensitive properties of cholesterol oxidase (Richmond, 1973). In general, most methods rely on an indirect determination of cholesterol content based on the coupling of the H_2O_2 product of the oxidative half reaction (Figure 1.9). Cholesterol oxidases are stable enzymes, and as such they have even been incorporated on disposable cholesterol test strips (Gottschling et al., 1995).

Cholesterol oxidases have also been used to characterize cellular membranes and to determine their cholesterol content (Lange, 1992), (Slotte, 1992). An interesting study to assess the degree of membrane disruption by cholesterol oxidase, found that conversion of cholesterol to the 4-cholesten-3-one, and not the intermediate 5-cholesten-3-one, was responsible for vesicle lysis (Ghoshroy et al., 1997). These dye leakage experiments also confirmed that it was formation of the product, and not the direct interaction of cholesterol oxidase with the membrane, that results in membrane lysis.

Cholesterol oxidase has also been found to exhibit potent insecticidal activity and is being developed by Monsanto as a potential pesticide (Corbin et al., 1994). Its biological toxicity has been associated with its ability to lyse the midgut epithelium of boll weevils larvae, a common pest for both tobacco and cotton crops (Purcell et al., 1993). It is hypothesized that when boll weevils larvae ingest cholesterol oxidase, its

enzymatic activity converts the cholesterol to 4-cholesten-3-one disrupting the epithelium cell membrane.

1.4.2 Native functions of cholesterol oxidases

The first identified role of cholesterol oxidase was in metabolism, however since then additional functions for this enzyme have been recognized. *Bevibacterium sterolicum,* has been shown to survive on cholesterol as its sole carbon source. The activity of the non-covalent form of cholesterol oxidase, BCO1, is the first step in the breakdown of cholesterol (Uwajima et al., 1973). A putative cholesterol oxidase gene product, *pimE*, was identified in a large gene cluster of the *Streptomyces natalensis* genome (Aparicio et al., 2000). *PimE* has approximately 80% sequence homology to the BCO1 gene (*choB*), (Ohta et al., 1991) as well as both *Streptomyces sp.* strains of this enzyme, A19249 (*choM*) (Corbin et al., 1994) and SA-COO (*choA*) (Ishizaki et al., 1989). The large gene cluster, to which the putative cholesterol oxidase, PIME, is associated, is responsible for the biosynthesis of the anti-fungal agent pimaricin. The role that a cholesterol oxidase has in the synthetic pathway of pimaricin has not yet been elucidated but since this antibiotic is widely used in the food industry as an anti-fungal agent this work is likely underway (Bullerman, 1977; Holley, 1981; Mahjoub & Bullerman, 1986).

Recently, another cholesterol oxidase homologue gene, *choE*, has been identified in the *Rhodococcus equi* parasite (Navas et al., 2001). More importantly, *choE* has been identified as one of the parasite's virulence factors. The 3-hydroxyl group of cholesterol is believed to form an important stabilizing interaction to the phospholipid (Linder, 1984). Oxidation of the hydroxysteroid to form the keto-steroid has been proposed to disrupt this

interaction, facilitating the observed membrane disruption. It is unclear if it is solely the conversion of the hydroxyl group to a ketone that results in membrane disruption or if conformational changes in the steroid A and B rings, as a result of the double bond shift upon isomerization, play a role as had been observed for the dye leakage experiments using egg phosphatidylcholine membranes (Ghoshroy et al., 1997).

Genomic tools have also identified potential cholesterol oxidase homologues in *Mycobacterium tuberculosis* and *Mycobacterium leprae*. It has been proposed that these cholesterol oxidase homologues are one of the bacterial virulence factors (Navas et al., 2001). Navas and coworkers have shown that these putative cholesterol oxidases are secreted by the bacterium and speculate that the enzyme plays a role in membrane disruption of the host's cells and causing the characteristic lesions observed in both animals and humans infected with these bacterium. Clearly, further work is necessary to establish the role of cholesterol oxidase in these pathogenic bacteria.

1.4.3 Structural characterization of the Brevibacterium sterolicum cholesterol oxidase

The first cholesterol oxidase to be structurally characterized by crystallographic methods was that from *Brevibacterium sterolicum* (BCO1) (PDB accession code 3COX) (Vrielink et al., 1991). BCO1 is an example of a non-covalently bound form of cholesterol oxidase and the FAD was found deeply buried in the center of the enzyme. This structure reveals two domains: the FAD-binding domain and the substrate-binding domain. The FAD-binding region shares the highest sequence homology with that of other glutathione reductase structural family members (Dym & Eisenberg, 2001). The

predominant topological similarity in the substrate-binding domain is a large β-sheet structure that forms the roof of the active site (Vrielink et al., 1991).

The active site of BCO1 is located near to the FAD cofactor and comprises a large cavity (Figure 1.11). This cavity is completely sequestered from the bulk solvent indicating that protein loops at the surface of the enzyme must move in order to allow for entry of the substrate into this cavity. Two loops, at the end of the cavity were found to have higher than average crystallographic thermal parameters suggesting that they move to allow binding of the steroid in the active site cavity.

A substrate complex of BCO1 was obtained by soaking the protein crystals in an anaerobic solution containing a steroid substrate, dihydroisoandosterone, DHA, which has a carbonyl group in place of the terpene tail of cholesterol (Figure 1.11b). The presence of a 3-hydroxy substrate reduces the enzyme and the exclusion of O_2 in the soaking experiment effectively traps the enzyme in its reduced state (Li et al., 1993). Cholesterol oxidase is a yellow colored enzyme due to the presence of an oxidized FAD. When the protein is reduced the enzyme becomes colorless due to the electronic change in the flavin. These spectral properties were used to confirm the reduced state of the BCO1/DHA co-crystal. The crystal structure of the DHA complex, confirmed that the large sequestered cavity is the substrate binding pocket and that the 4-ring steroid backbone is accommodated (Figure 1.11b).

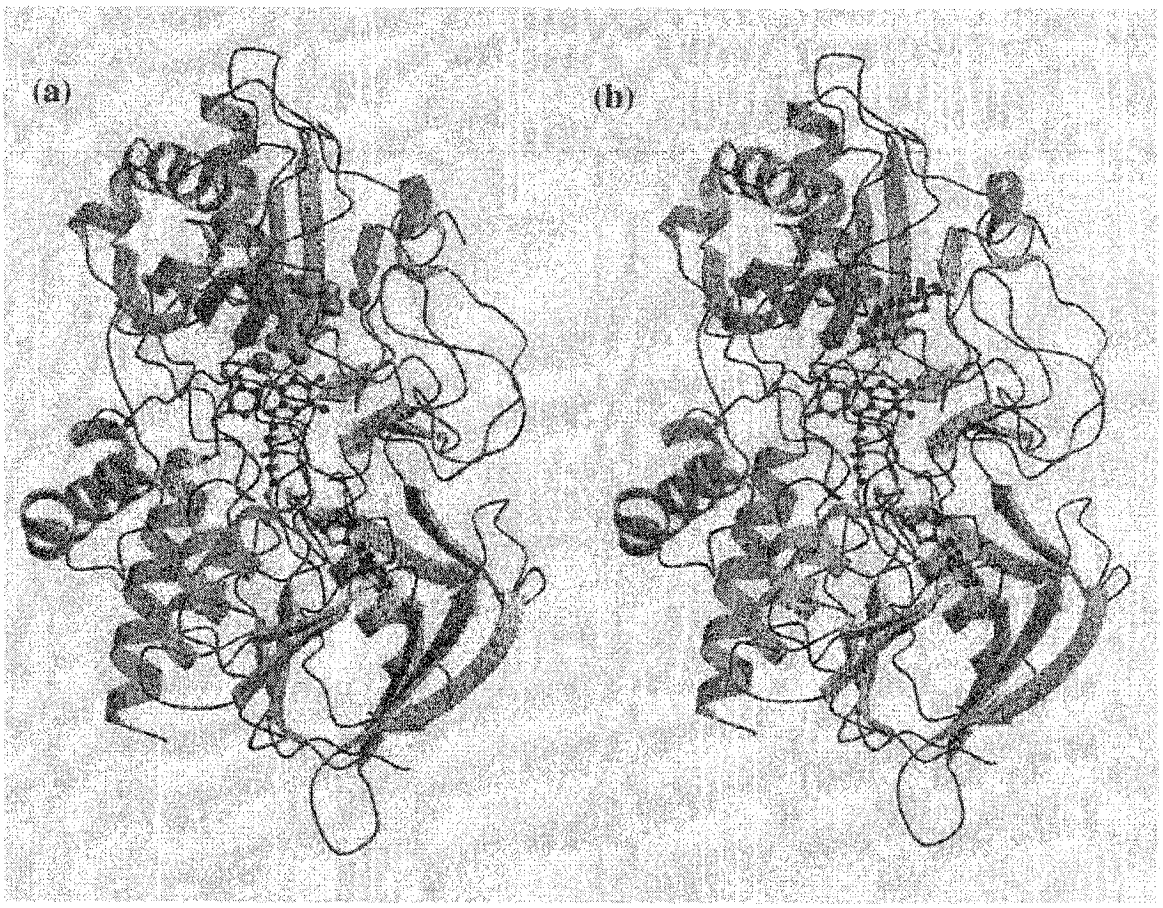

Figure 1.11 Ribbon diagrams of (a) native BCO1 and (b) BCO1 complexed with dehydroisoandosterone. DHA (PDB accession codes 3COX and 1COY). The FAD-binding domain is shown in purple and the substrate-binding domain is blue. Water molecules present in the native BCO1 substrate-binding cavity are shown as red spheres.

1.4.4 Key active-site residues of BCO1

Both crystal structures of BCO1 identified the active site residues and revealed specific conformational changes of these residues upon binding of the steroid (Figure 1.12). In the complex structure, the hydroxyl group of the steroid is within hydrogen bonding distance of both the N5 nitrogen atom and the O4 oxygen atom of the isoalloxazine system of the FAD. The steroid binding pocket is predominately

hydrophobic aside from the residues adjacent to the isoalloxazine system and the hydroxyl end of the steroid. The environment of the active site appears to be dynamic as all of these residues except for H447 are in different conformations when the steroid is bound (Figure 1.12). As mentioned earlier, BCO1 belongs to the glucose-methanol-choline (GMC) oxidoreductase family, that includes glucose oxidase, GOX (Cavener, 1992; Vrielink et al., 1991).

Among the entire GMC family there is a conserved histidine residue corresponding to H447 in BCO1 and a conserved H/N corresponding to N485 (Figure 1.5) Although the GMC family oxidizes quite a diverse range of substrates, the requirement for the FAD and conservation of the surrounding residues implies that these residues play an important role in the redox reactivity for these enzymes. Kinetic and structural analysis of these residues will provide important information about their molecular roles.

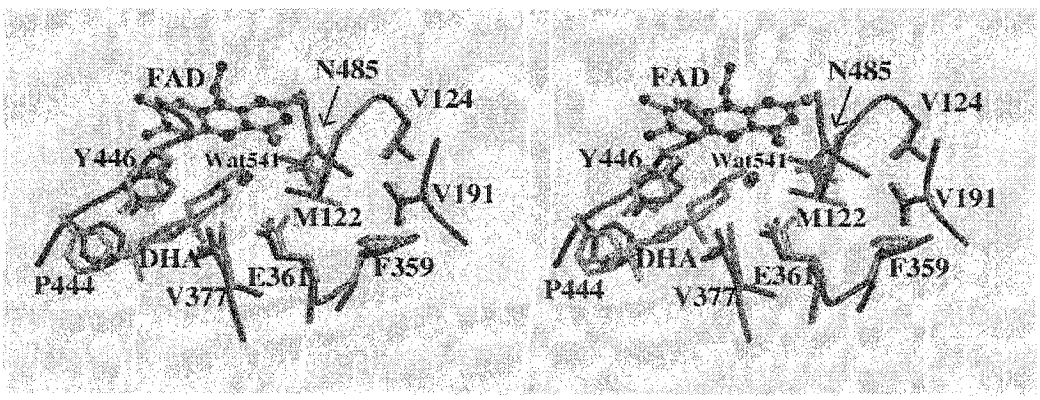

Figure 1.12 Stereoscopic representation of a superposition of the active site region of native BCO1 (purple) and the DHA complex structure (pink) (PDB accession codes 3COX and 1COY).

1.4.5 Proposed reaction mechanism of non-covalent form of cholesterol oxidase

Upon oxidation of 3β-hydroxysteriods by cholesterol oxidase, the FAD cofactor becomes reduced. Regeneration of oxidized FAD is achieved by a reaction of the enzyme with molecular oxygen to produce hydrogen peroxide (Figure 1.9). In the BCO1/DHA complex structure, the conserved histidine, H447, is adjacent to the isoalloxazine ring and involved in a hydrogen bond network including an active site water, Wat541 and the hydroxy oxygen atom, O1' of the steroid (Figure 1.13) (Li et al., 1993). H447 has been proposed to act as both a general base and an acid for this bi-functional enzyme. The histidine was proposed to act as a base through Wat541 abstracting a proton from the C3-hydroxyl group of the steroid, to form an oxyanion intermediate. Such an intermediate is activated for the subsequent oxidation reaction. The oxidation mechanism was proposed to be either a two-electron hydride transfer mechanism or a radical mechanism involving two, one-electron transfers (Figure 1.14) (Vrielink et al., 1991). The protonated histidine residue is then available act as an acid to stabilize a dienolic intermediate for the following isomerization reaction.

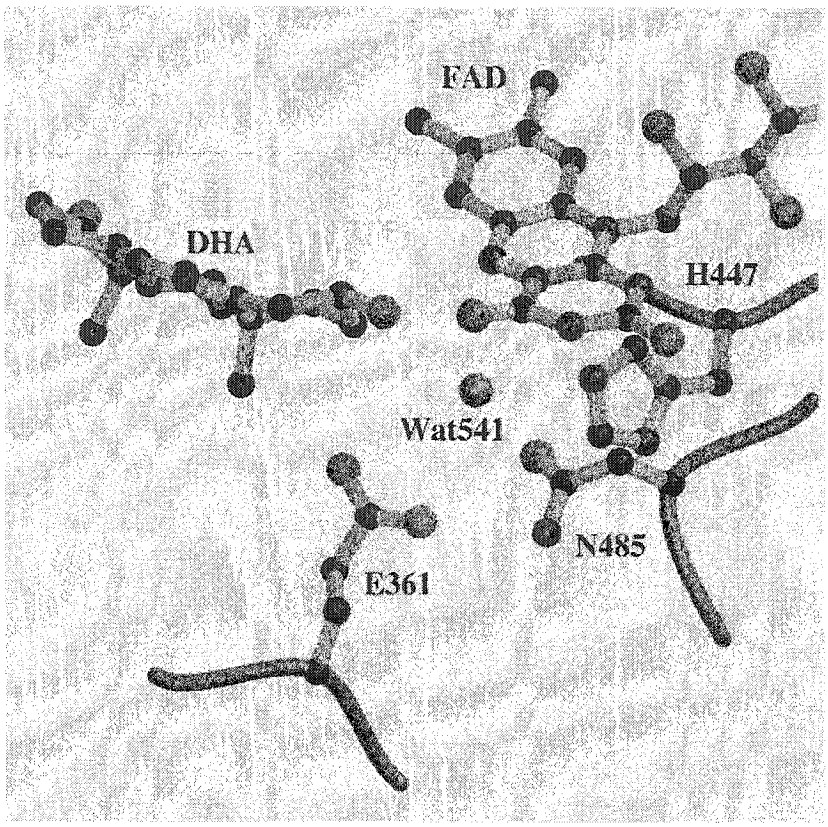

Figure 1.13 Active site of the BCO1/DHA complex structure.

Another key residue is a glutamate residue, E361, which was proposed to act as a base to deprotonate the C4 proton of the 5-cholesten-3-one intermediate and transfer this proton to the C6 position, to form the product, 4-cholesten-3-one. Both H447 and E361 are conserved among all the known non-covalent cholesterol oxidases; BCO1, SCOA, SCOH and PIME, emphasizing their importance in binding and / or catalysis.

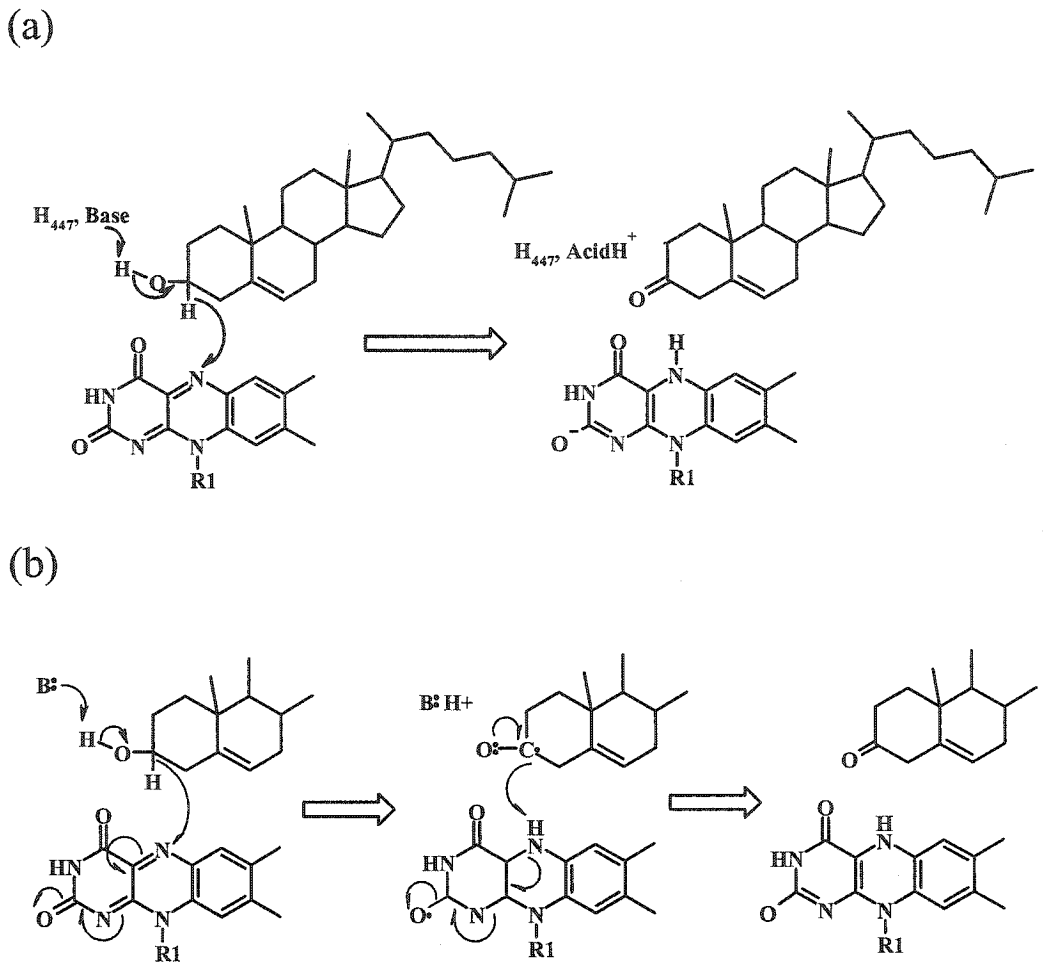

Figure 1.14 Proposed reaction schemes for substrate oxidation BCO1. (a) Two-electron hydride transfer mechanism (b) An example of two step radical mechanism, involving one-electron transfers.

1.4.6 Kinetic characterization of Streptomyces sp. CA_COO, cholesterol oxidase

The activity of the *Streptomyces sp* cholesterol oxidase (SCOA) has been studied using site-directed mutagenesis and kinetic analysis (Kass & Sampson, 1998a; Kass & Sampson, 1995; Kass & Sampson, 1998b; Sampson & Kass, 1997; Yamashita et al., 1998). These studies have provided additional insight into the roles of the active site residues, E361, H447 and N485.

The conserved glutamic acid residue, E361, proposed as the base in the isomerization reaction (Vrielink et al., 1991), was mutated to an isosteric glutamine (E361Q). As expected, the mutation abolished the enzyme's isomerization activity with no significant decrease in the oxidation activity (Kass & Sampson, 1998a). This study confirmed the importance of E361 in the isomerization reaction and indicated that it is not necessary for oxidation. In addition, isotope labeling studies on the substrate, 4β-(H^2)cholest-5-en-3-one, have shown that the deuterium at the C4 position is incorporated at the C6 position of cholest-4-en-3-one (Sampson & Kass, 1997), supporting the proposed mechanism that the active site glutamate residue first acts as a base to abstract a proton from the C4 position of the substrate and then acts as an acid to re-protonate the substrate at the C6 position.

The precise role of the active site histidine residue, H447, is not as well understood and numerous mutants have been created in order to elucidate its catalytic function. Initially, Murooka and coworkers, mutated H447 to an alanine and an asparagine. Both of these mutants exhibited no isomerization or oxidation activity (Yamashita et al., 1998). This agreed well with the proposed roles of H447, as a base to form the oxyanion intermediate necessary for efficient oxidation and as an acid to form an enolic intermediate to facilitate the isomerization reaction (Vrielink et al., 1991). However, a more systematic mutagensis study of this histidine residue, involving 5 different mutants, H447N, H447Q, H447D, H447E and H447K yielded some unexpected results which brings into question its proposed roles (Kass & Sampson, 1998b). There was a significant loss of the oxidation activity for the four mutants, H447N, H447D,

H447E and H447K. In the case of H447E the glutamate side chain can be positioned such that one of the carboxylate oxygen atoms lies in a similar position to the NE2 on the histidine. It was hypothesized that the glutamate side chain could also act as a general base for oxidation. The lack of oxidation activity observed for this mutant was unexpected. It was proposed that the glutamate is protonated and thus unable to act as a base for oxidation. Another unanticipated observation was found with the H447Q mutant, where the oxidation activity (k_{cat}) was only 120-fold lower than that of the wild type. Similar to the glutamate side chain, a gluatamine at the 447 position, can place either its NE2 or OE1 atoms in a similar position to the NE2 of histidine. Again, the retention of oxidation activity for the H447E mutant questions the role of H447 as the base required for oxidation activity. It had been proposed that E361 rescues the oxidative activity for the H447Q mutant by assuming the basic role of H447. However, it is unclear why E361 does not rescue the oxidation activity for other H447 mutants.

The four mutants, H447N, H447Q, H447D and H447E, still possess reasonable isomerization activity showing that the two reactions that cholesterol oxidase catalyzes are separable (Kass & Sampson, 1998b; Yamashita et al., 1998). In addition, these results suggest that the role of H447 forming the proposed enolate intermediate for the isomerization step is unnecessary. This is further supported by the kinetic observation that oxidized SCOH has a faster isomerization rate with the 5-cholesten-3-one, than pre-reduced enzyme where the histidine is expected to be protonated (Gadda et al., 1997).

Substrate and solvent deuterium isotope studies have been carried out for the wild-type and mutant-catalyzed oxidation reactions (Kass & Sampson, 1998b). The primary isotope effect of 2.2 observed on both k_{cat} and k_{cat}/K_m using 3α-(H^2)cholesterol for the

wild-type enzyme indicates that the C-H bond cleavage is at least partially rate-limiting. No primary isotope affect was observed for either the H447N or H447Q mutants indicating a shift in the rate-limiting step. It was proposed that the rate determining step for these mutants is the deprotonation of the 3-hydroxyl group of the substrate as the isomerization kinetics revealed no isotope effect (Kass & Sampson, 1998b; Yue et al., 1999). Alternatively, reoxidation of the flavin may be rate limiting for these mutants, as studies on the oxidative half reaction for glucose oxidase have suggested that the homologous histidine residue is involved in the stabilization of a C4a-hydroperoxy dihydroflavin in the course of the oxidative half reaction (Meyer et al., 1998). No solvent isotope effect was observed for the kinetics of the wild-type enzyme and a small effect of 1.2 was observed for the H447Q mutant.

An intriguing difference in the pH profiles, for the oxidation reaction, between the native and the H447N and H447Q mutants has been observed. There was no appreciable pH effect observed for the kinetics of the wild-type over a very broad pH range from 4.5 to 7 and, over the range from 7.5 –10.6, the k_{cat} decreased 2000-fold (Kass & Sampson, 1998b). The dramatic loss of activity for the native enzyme at higher pH values was reversible and the apparent pK_a was determined to be 8.1. In contrast, the H447Q-catalyzed oxidation reaction was pH independent and the oxidation activity of the H447N could be rescued 10-fold by increasing the pH.

The active-site asparagine residue, N485, is in close proximity to Wat541 and as such is believed to affect the pKa and thus the oxidative activity of the enzyme. This residue is conserved as either an asparagine or a histidine residue among the GMC family members. When this residue was mutated to an alanine no oxidation activity was

observed indicating its importance in oxidation (Yamashita et al., 1998). This drastic mutation results in a considerable change in the active site geometry so an isosteric mutation was the designed where the asparagine was mutated to a leucine residue in order to elucidate its role in changing the electrostatic environment around the flavin. That work is presented in Chapter 2.

1.4.7 Structural characterization of the Streptomyces sp. CA_COO, cholesterol oxidase

In order to correlate the kinetic data with structure, a crystallographic analysis of wild-type SCOA and three mutants (H447N, H447Q, E361Q) was carried out (Yue et al., 1999). As mentioned earlier, SCOA was found to have an identical fold to BCO1, as was predicted from the 58% sequence identity. All of the key active site residues surrounding the isoalloxazine ring of the FAD are conserved (Figure 1.15 *cf.* Figure 1.5). In the native structure there is a hydrogen bond network involving residues, E361, H447, N485 and an active site water molecule, Wat541. This network is preserved in the E361Q mutant structure, however mutation of H447 to an asparagine or glutamine results in a perturbation of the network, particularly a repositioning of Wat541 (Figure 1.16). The oxidative reactivity of the mutant enzymes appears to be correlated with the degree of movement of Wat541 from its position in the native structure. (Yue et al., 1999). In the BCO1 complex structure, Wat541 is hydrogen bonded to O1′ of the dehydroisoandosterone steroid substrate suggesting that the position of the steroid is strongly correlated with that of the water (Figure 1.13). These studies have suggested that H447 plays an important role in orienting the substrate in the active site.

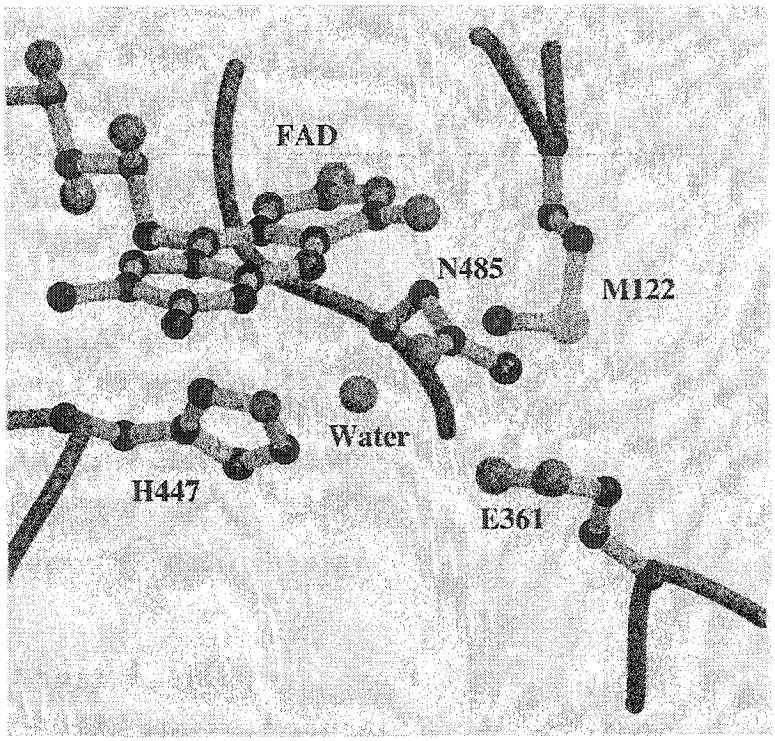

Figure 1.15 Key active site residues of SCOA (PDB accession code 1B4V)

Comparisons of the native structure to the H447Q mutant structure may provide some insight into the role of the histidine in the oxidation reaction. In the H447Q mutant the glutamine side chain is orientated such that its amide nitrogen atom rather than the carbonyl oxygen atom, is in a similar position to NE2 on the imidazole ring (Yue et al., 1999). Examination of the hydrogen bonding network and the temperature factors on residue 447 in the H447Q structure indicate that the correct orientation of the glutamine was modeled. This side chain orientation, directs a hydrogen bond donating group toward Wat541 thus reducing the basicity of the water. As mentioned earlier, the H447Q mutant is only 120 fold less active for oxidation than the wild-type enzyme. If H447 acts as a base through Wat541 it is unclear why this mutation is not detrimental to the oxidation activity as has been observed for the H447E mutant (essentially inactive). Together the

structural and kinetic data support a substrate-positioning role for H447 however these results present some uncertainty into its basic role.

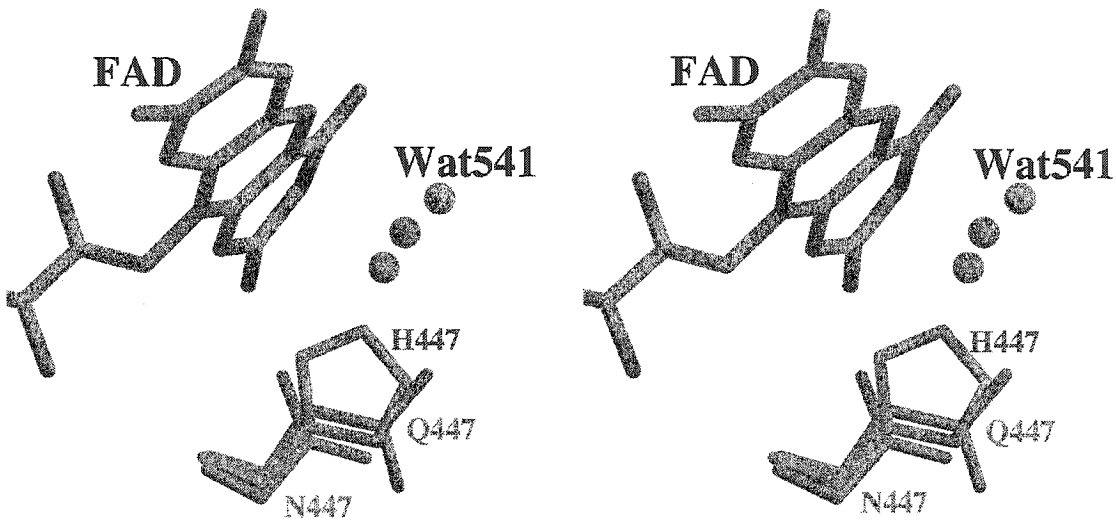

Figure 1.16 Stereoscopic representation of the structural effect of H447 mutations in SCOA. H447, the isoalloxazine system and Wat541 from the wild-type structure are shown in grey. The histidine mutant structures: H447N and H447Q were superimposed on the native structure by a least squares fit of the isoalloxazine group. Shown in pink is the N447 side chain and its associated Wat541. Shown in purple is the Q447 side chain and its associated Wat541.(PDB accession codes 1B4V, 1CBO & 1CC2)

1.4.8 Electronic characterization of the non-covalent form of cholesterol oxidase

The oxidation reaction for BCO1 has been proposed to involve either a hydride transfer mechanism or a radical-mediated mechanism (Vrielink et al., 1991). If the enzyme undergoes a radical mechanism, a transient flavin semiquione intermediate would be generated during the process of oxidation.

Electron spin resonance (ESR) spectroscopy was used to characterize and identify the one-electron reduced, semiquinone intermediate of the FAD in cholesterol oxidase

(Medina et al., 1994). The semiquinone intermediate for cholesterol oxidase can be generated artificially in a basic medium, by reacting the enzyme with sodium dithionite or by light irradiation in the presence of ethylenediaminetetraacetic acid (EDTA). However, no semiquinone intermediate was detected at pH values below 6.5 or at any pH when a steroid substrate, dehydoisoandrosterone, DHA, was used as the reductant. The stability of the semiquinone intermediate may be pH dependent, and thus the occurrence of a transient radical mechanism cannot be ruled out. Similarly the lifetime of the semiquinone species in the presence of the subsequent steroid intermediate may be so short lived that it is undetectable by the methods used. The rate of flavin reduction increased at higher pH (8.6 vs 7.5), suggesting either a change in the flavin protonation state or a change of the protein environment, at higher pH values. In summary, the capability of the flavin to undergo a one-electron reduction appears to be sensitive to changes in the flavin environment.

When BCO1 was reduced to the semiquinone state by photoreduction and then titrated with DHA, further reduction of the flavin was not observed (Medina et al., 1994). This indicates that a one-electron transfer between the flavin semiquinone and the reducing substrate is not possible. Although this finding supports a two-electron hydride transfer mechanism, a radical mechanism still can not be ruled out because the flavin semiquinone is electronically different from the oxidized state. Thus one would expect a different redox potential and also perhaps a different substrate binding interaction unfavorable for one electron transfer.

Re-oxidation experiments for the reduced flavin in BCO1, have shown that it occurs rapidly. When O_2 is gradually re-introduced, only fully oxidized or fully reduced

species were detectable by EPR methods (Medina et al., 1994). Again, these results do not exclude the possibility of a transient radical mechanism, including the proposed C4a flavin-peroxide adduct, as the lifetime of this species is assumed to be very short lived (Ghisla & Massey, 1989).

1.5 Rationale and objectives of the thesis

The aim of this thesis is to further an understanding of how the protein environment can modulate the reactivity for a flavoenzyme. Specifically, we initiated a structural study of the flavoenzyme, cholesterol oxidase, from *Streptomyces sp* (SCOA). Crystals of SCOA are exceptional in that they diffract to sub-atomic resolution. This level of resolution, allows one to differentiate one-electron differences and thus these structures will be instrumental in our understanding of flavin–redox properties. To date, there is no sub-atomic crystal structure of a protein-bound flavin, thus we have a unique opportunity to visualize the electronic properties of a protein-bound FAD cofactor.

Another specific goal of this dissertation is to eluicidate the catalytic roles of the residues surrounding the isoalloxazine system. Prior mutagensis studies have identified active-site residues in SCOA important for catalysis: E361, H447 and N485. These experiments have probed the catalytic roles of E361 and H447, however the nature of the catalytic role(s) of N485 is less well understood.

Mutagenesis and kinetic studies have shown that N485 plays an important role in substrate oxidation. An understanding of how this uncharged residue affects substrate oxidation, will introduce a more comprehensive mechanistic model for the reactions catalyzed by cholesterol oxidase. In addition, these studies provide general insights into

the catalytic roles available for amide side chains. In Chapter 2 we initiated a structural and kinetic study of the N485L mutant in order to probe its catalytic functions. It appears that N485 is involved in a novel flavin-protein interaction that modulates the redox potential of the isoalloxazine system. In addition, the atomic resolution crystallographic study, in Chapter 3, reveals a dynamic role for N485 in flavin re-oxidation.

New mechanistic questions about the basic role of H447 are raised from the unexpected oxidative activity observed for the H447Q mutant. Does E361 rescue the oxidative activity for the H447Q mutant as previously proposed? Why is the H447E mutant essentially inactive? Is a base necessary for substrate oxidation? If so, is H447 the active-site base? What are the oxidative role(s) of H447? As many hydrogen atoms are visible in atomic resolution structures, we not only pursued a single atomic resolution structure, but rather we decided to determine structures of SCOA over a pH range in order to observe and estimate the pKa of H447. In addition, to H447 with these structures we are able to compare the effect of pH on protein structure. The pH study of SCOA is presented in Chapter 4.

The database of information from five independently refined atomic resolution structures of SCOA provides a useful statistical sampling with which to study protein features and how they may be affected by pH. Structural features in the electron density, like hydrogen atoms, are close to the noise levels of the map. Having multiple structure maps to compare enables one to convincingly identify unusual hydrogen atom positions. That is, the persistence of a particular feature throughout all six structures supports the assumption that the observed phenomenon is real and not noise due to the limitations of the experiment. These atomic resolution structures provide an experimental database that

is useful for computer modelers, to compare how well their theoretical models can predict the effect of pH on a protein structure. In addition, the precise coordinates of a protein-bound FAD can be compared with small molecule structures, to compare how the protein affects the isoalloxazine geometry. This analysis is presented in Chapter 4.

Cholesterol oxidase is a relatively large enzyme (499 residues) and one of the largest to be structurally characterized at sub-atomic resolution. We have observed electronic differences between amide carbonyl groups. The size and secondary structure distribution in SCOA has enabled us to correlate these differences to the secondary structure. Chapter 5 incorporates our analysis of this observation and provides an example of how these atomic resolution structures will further our understanding of protein structure.

1.6 References

Aparicio, J. F., Fouces, R., Mendes, M. V., Olivera, N. & Martin, J. F. (2000). A complex multienzyme system encoded by five polyketide synthase genes is involved in the biosynthesis of the 26-membered polyene macrolide pimaricin in *Streptomyces natalensis*. *Chem Biol* **7**(11), 895-905.

Barber, M. J., Pollock, V. & Spence, J. T. (1988). Microcoulometric analysis of trimethylamine dehydrogenase. *Biochem J* **256**(2), 657-9.

Barna, T. M., Khan, H., Bruce, N. C., Barsukov, I., Scrutton, N. S. & Moody, P. C. (2001). Crystal structure of pentaerythritol tetranitrate reductase: "flipped" binding geometries for steroid substrates in different redox states of the enzyme. *J Mol Biol* **310**(2), 433-47.

Binda, C., Coda, A., Angelini, R., Federico, R., Ascenzi, P. & Mattevi, A. (1999). A 30-angstrom-long U-shaped catalytic tunnel in the crystal structure of polyamine oxidase. *Structure Fold Des* **7**(3), 265-76.

Blaut, M., Whittaker, K., Valdovinos, A., Ackrell, B. A., Gunsalus, R. P. & Cecchini, G. (1989). Fumarate reductase mutants of *Escherichia coli* that lack covalently bound flavin. *J Biol Chem* **264**(23), 13599-604.

Bradley, L. H. & Swenson, R. P. (1999). Role of glutamate-59 hydrogen bonded to N(3)H of the flavin mononucleotide cofactor in the modulation of the redox potentials of the *Clostridium beijerinckii* flavodoxin. Glutamate-59 is not responsible for the pH dependency but contributes to the stabilization of the flavin semiquinone. *Biochemistry* **38**, 12377-12386.

Breinlinger, E. C., C.J., K. & V.M., R. (1998). Modulation of Flavin Recognition and Redox Properties through Donor Atom-π Interactions. *Journal of American Chemical Society* **120**(34), 8606-8609.

Breinlinger, E. C. R. V. M. (1997). Model Systems for Flavoenzyme Activity. Modulation of Flavin Redox Protentials through-Stacking Interactions. *Journal of American Chemical Society* **119**(5), 1165-1166.

Bullerman, L. B. (1977). Incidence and control of mycotoxin producing molds in domestic and imported cheeses. *Ann Nutr Aliment* **31**(4-6), 435-46.

Cavelier, G. & Amzel, L. M. (2001). Mechanism of NAD(P)H:quinone reductase: Ab initio studies of reduced flavin. *Proteins* **43**(4), 420-32.

Cavener, D. (1992). GMC oxidoreuctases. A newly defined family of homologous proteins with diverse catalytic activities. *J. Mol. Biol.* **223**, 811-814.

Chang, F., Bradley, L. H. & Swenson, R. P. (2001). Evaluation of the hydrogen bonding interactions and their effects on the oxidation-reduction potentials for the riboflavin complex of the *Desulfovibrio vulgaris* flavodoxin. *Biochim Biophys Acta* **1504**(2-3), 319-28.

Chang, F. C. & Swenson, R. P. (1999). The midpoint potentials for the oxidized-semiquinone couple for Gly57 mutants of the *Clostridium beijerinckii* flavodoxin correlate with changes in the hydrogen-bonding interaction with the proton on N(5) of the reduced flavin mononucleotide cofactor as measured by NMR chemical shift temperature dependencies. *Biochemistry* **38**(22), 7168-76.

Corbin, D. R., Greenplate, J. T., Wong, E. Y. & Purcell, J. P. (1994). Cloning of an Insecticidal Cholesterol Oxidase Gene and Its Expression in Bacteria and in Plant Protoplasts. *Applied and Environmental Microbiology* **60**(12), 4239-4244.

Coulombe, R., Yue, K. Q., Ghisla, S. & Vrielink, A. (2001). Oxygen access to the active site of cholesterol oxidase through a narrow channel is gated by an Arg-Glu pair. *Manuscript submitted.*

Craig, D. H., Barna, T., Moody, P. C., Bruce, N. C., Chapman, S. K., Munro, A. W. & Scrutton, N. S. (2001). Effects of environment on flavin reactivity in morphinone reductase: analysis of enzymes displaying differential charge near the N-1 atom and C-2 carbonyl region of the active-site flavin. *Biochem J* **359**(Pt 2), 315-23.

Cuello, A. O. M., C.M.; Rotello, V.M. (2000). Model Systems for Flavoenzyme Activity. The Role of N(3)-H Hydrogen Bonding in Flavin Redox Processes. *Journal of American Chemical Society* **122**(14), 3517-3521.

Druhan, L. J. & Swenson, R. P. (1998). Role of methionine 56 in the control of the oxidation-reduction potentials of the *Clostridium beijerinckii* flavodoxin: effects of substitutions by aliphatic amino acids and evidence for a role of sulfur-flavin interactions. *Biochemistry* **37**(27), 9668-78.

Dwyer, T. M., Mortl, S., Kemter, K., Bacher, A., Fauq, A. & Frerman, F. E. (1999). The intraflavin hydrogen bond in human electron transfer flavoprotein modulates redox potentials and may participate in electron transfer. *Biochemistry* **38**(30), 9735-45.

Dym, O. & Eisenberg, D. (2001). Sequence-structure analysis of FAD-containing proteins. *Protein Sci* **10**(9), 1712-28.

Ebitani, M. I., Y.In,T.;Sakaguchi, K.-i.; Flippen-Anderson, J.L.; Karle, I.L. (1993). Structures of riboflavin tetraacetate and tetrabutyrate: molecular packing mode of riboflavin tetracarboxylate and its extensive stacking and hydrogen-bonding characteristics. *Acta Cryst.* **B49**, 136-144.

Eric C. Breinlinger, C. J. K., and Vincent M. Rotello. (1998). Modulation of Flavin Recognition and Redox Properties through Donor Atom-Interactions. *J. Am. Chem. Soc.* **120**(34), 8606-8609.

Fraaije, M. W., van den Heuvel, R. H., van Berkel, W. J. & Mattevi, A. (1999). Covalent flavinylation is essential for efficient redox catalysis in vanillyl-alcohol oxidase. *J Biol Chem* **274**(50), 35514-20.

Fraaije, M. W., van Den Heuvel, R. H., van Berkel, W. J. & Mattevi, A. (2000). Structural analysis of flavinylation in vanillyl-alcohol oxidase. *J Biol Chem* **275**(49), 38654-8.

Fritchie, C. J. R. M. J. (1975). Molecular complexes of flavins. The crystal structure of lumiflavin-bis(naphthalene-2,3-diol) trihydrate. *Acta Cryst.* **B31**, 454-461.

Fukuyama, M. & Miyake, Y. (1979). Purification and some properties of cholesterol oxidase from *Schizophyllum commune* with covalently bound flavin. *J Biochem (Tokyo)* **85**(5), 1183-93.

Gadda, G., Wels, G., Pollegioni, L., Zucchelli, S., Ambrosius, D., Pilone, M\. S. & Ghisla, S. (1997). Characterization of cholesterol oxidase from *Streptomyces hydroscopicus* and *Brevibacterium sterolicum*. *Eur. J. Biochem.* **250**, 369-376.

Ghisla, S., Kenny, W. E., Knappe, W. R., McIntire, W. & Singer, T. P. (1980). Chemical synthesis of some properties of 6-substituted flavin. *Biochemistry*

19(2537-2544).

Ghisla, S. & Massey, V. (1989). Mechanism of flavoprotein-catalysed reactions. *Eur. J. Biochem.* **181**, 1-17.

Ghoshroy, K. B., Zhu, W. & Sampson, N. S. (1997). Investigation of membrane disruption in the reaction catalyzed by cholesterol oxidase. *Biochemistry* **36**, 6133-6140.

Gondry, M., Dubois, J., Terrier, M. & Lederer, F. (2001). The catalytic role of tyrosine 254 in flavocytochrome b2 (L-lactate dehydrogenase from baker's yeast). Comparison between the Y254F and Y254L mutant proteins. *Eur J Biochem* **268**(18), 4918-27.

Gottschling, H. D., Reuter, W., Ronquist, G., Steinmetz, A. & Hattemer, A. (1995). Multicentre evaluation of a non-wipe system for the rapid determination of total cholesterol in capillary blood, Accutrend Cholesterol on Accutrend GC. *Eur J Clin Chem Clin Biochem* **33**(6), 373-81.

Hasford, J. K., W.; Rizzo, C. J. (1997). Conformational effects on Flavin Redox Chemistry. *Journal of Organic Chemistry* **62**(16), 5244-5245.

Holley, R. A. (1981). Prevention of surface mold growth on Italian dry sausage by natamycin and potassium sorbate. *Appl Environ Microbiol* **41**(2), 422-9.

Hubbard, P. A., Shen, A. L., Paschke, R., Kasper, C. B. & Kim, J. J. (2001). NADPH-cytochrome P450 oxidoreductase. Structural basis for hydride and electron transfer. *J Biol Chem* **276**(31), 29163-70.

Hunter, C. A., Singh, J. & Thornton, J. M. (1991). Pi-pi interactions: the geometry and energetics of phenylalanine-phenylalanine interactions in proteins. *J Mol Biol* **218**(4), 837-46.

Ishizaki, R., Hirayama, N., Shinkawa, H., Nimi, O. & Murooka, Y. (1989). Nucleotide sequence of the gene for cholesterol oxidase from a *Streptomyces* sp. *J. Bacteriol.* **171**(1), 596-601.

Karplus, P. A. & Schulz, G. E. (1987). Refined structure of glutathione reductase at 1.54 A resolution. *J Mol Biol* **195**(3), 701-29.

Kasim, M. & Swenson, R. P. (2000). Conformational energetics of a reverse turn in the *Clostridium beijerinckii* flavodoxin is directly coupled to the modulation of its oxidation-reduction potentials. *Biochemistry* **39**(50), 15322-32.

Kass, I., J. & Sampson, N. S. (1998). The importance of Glu^{361} position in the reaction catalyzed by cholesterol oxidase. *Bioorganic and Medicinal Chemistry Letters* **8**, 2663-2668.

Kass, I. J. & Sampson, N. S. (1995). The isomerization catalyzed by *Brevibacterium sterolicum* cholesterol oxidase proceeds stereospecifically with one base. *Biochem. Biophys. Res. Commun.* **206**(2), 688-693.

Kass, I. J. & Sampson, N. S. (1998). Evaluation of the role of His447 in the reaction catalyzed by cholesterol oxidase. *Biochemistry* **37**(51) ,17990-18000.

Kenney, W. C., Singer, T. P., Fukuyama, M. & Miyake, Y. (1979). Identification of the covalently bound flavin prosthetic group of cholesterol oxidase. *J Biol Chem* **254**(11), 4689-90.

Kiess, M., Hecht, H.-J. & Kalisz, H. M. (1998). Glucose oxidase from *Penicillium amagasakiense*: Primary structure and comparison with other glucose-methanol-choline (GMC) oxidoreductases. *Eur. J. Biochem.* **252**, 90-99.

Kohen, A. & Klinman, J. P. (1999). Hydrogen tunneling in biology. *Chem Biol* **6**(7), R191-8.

Kollman, P. A., Kuhn, B., Donini, O., Perakyla, M., Stanton, R. & Bakowies, D. (2001). Elucidating the nature of enzyme catalysis utilizing a new twist on an old methodology: quantum mechanical-free energy calculations on chemical reactions in enzymes and in aqueous solution. *Acc Chem Res* **34**(1), 72-9.

Lange, Y. (1992). Tracking cell cholesterol with cholesterol oxidase. *Journal of Lipid Research* **33**(3), 315-321.

Lennon, B. W., Williams, C. H., Jr. & Ludwig, M. L. (1999). Crystal structure of reduced thioredoxin reductase from Escherichia coli: structural flexibility in the isoalloxazine ring of the flavin adenine dinucleotide cofactor. *Protein Sci* **8**(11), 2366-79.

Li, J., Vrielink, A., Brick, P. & Blow, D. M. (1993). Crystal structure of cholesterol oxidase complexed with a steroid substrate: Implications for flavin adenine dinucleotide dependent alcohol oxidases. *Biochemistry* **32**, 11507-11515.

Linder, R. (1984). Alteration of mammalian membranes by the cooperative and antagonistic actions of bacterial proteins. *Biochim Biophys Acta* **779**(4), 423-35.

Lostao, A., Gomez-Moreno, C., Mayhew, S. G. & Sancho, J. (1997). Differential stabilization of the three FMN redox forms by tyrosine 94 and tryptophan 57 in

flavodoxin from Anabaena and its influence on the redox potentials. *Biochemistry* **36**(47), 14334-44.

Ludwig, M. L., Pattridge, K. A., Metzger, A. L., Dixon, M. M., Eren, M., Feng, Y. & Swenson, R. P. (1997). Control of oxidation-reduction potentials in flavodoxin from *Clostridium beijerinckii*: the role of conformation changes. *Biochemistry* **36**(6), 1259-80.

Macheroux, P., Kieweg, V., Massey, V., Soderlind, E., Stenberg, K. & Lindqvist, Y. (1993). Role of tyrosine 129 in the active site of spinach glycolate oxidase. *Eur J Biochem* **213**(3), 1047-54.

MacLachlan, J., Wotherspoon, A. T. L., Ansell, R. O. & Brooks, C. J. W. (2000). Cholesterol oxidase: sources, physical properties and analytical applications. *Journal of Steroid Biochemistry and Molecular Biology* **72**, 169-195.

Mahjoub, A. & Bullerman, L. B. (1986). Effects of natamycin and potassium sorbate on growth and aflatoxin production in olives. *Arch Inst Pasteur Tunis* **63**(4), 513-25.

Massey, V. (1994). Activation of molecular oxygen by flavins and flavoproteins. *J Biol Chem* **269**(36), 22459-62.

Massey, V. & Hemmerich, P. (1980). Active-site probes of flavoproteins. *Biochem Soc Trans* **8**(3), 246-57.

Mattevi, A., Vanoni, M. A., Todone, F., Rizzi, M., Teplyakov, A., Coda, A., Bolognesi, M. & Curti, B. (1996). Crystal structure of D-amino acid oxidase: a case of active site mirror-image convergent evolution with flavocytochrome b2. *Proc Natl Acad Sci U S A* **93**(15), 7496-501.

Medina, M., Vrielink, A. & Cammack, R. (1994). ESR and electron nuclear double resonance characterization of the cholesterol oxidase from *Brevibacterium sterolicum* in its semiquinone state. *Eur J Biochem* **222**(3), 941-7.

Mesecar, A. D., Stoddard, B. L. & Koshland, D. E., Jr. (1997). Orbital steering in the catalytic power of enzymes: small structural changes with large catalytic consequences. *Science* **277**(5323), 202-6.

Mewies, M., McIntire, W. S. & Scrutton, N. S. (1998). Covalent attachment of flavin adenine dinucleotide (FAD) and flavin mononucleotide (FMN) to enzymes: The current state of affairs. *Protein Science* **7**, 7-20.

Mewies, M., Packman, L. C., Mathews, F. S. & Scrutton, N. S. (1996). Flavinylation in wild-type trimethylamine dehydrogenase and differentially charged mutant enzymes: a study of the protein environment around the N1 of the flavin isoalloxazine. *Biochem J* **317**(Pt 1), 267-72.

Meyer, M. (1997). Density functional study of isoalloxazine and C4a-hydroperoxidihydroisoalloxazine. *Journal of Molecular Structure: THEOCHEM* **417**(1-2), 163-168.

Meyer, M., Hartwig, H. & Schomburg, D. (1996). Semiempirical and ab initio study of closed and open shell derivatives of 10-methylisoalloxazine: a model of flavin redox states. *Journal of Molecular Structure: THEOCHEM* **364**(2-3), 139-149.

Meyer, M., Wohlfahrt, G., Knablein, J. & Schomburg, D. (1998). Aspects of the mechanism of catalysis of glucose oxidase: a docking, molecular mechanics and quantum chemical study. *J Comput Aided Mol Des* **12**(5), 425-40.

Motteran, L., Pilone, M. S., Molla, G., Ghisla, S. & Pollegioni, L. (2001). Cholesterol oxidase from *Brevibacterium sterolicum*. The relationship between covalent flavinylation and redox properties. *J Biol Chem* **276**(21), 18024-30.

Navas, J., Gonzalez-Zorn, B., Ladron, N., Garrido, P. & Vazquez-Boland, J. A. (2001). Identification and mutagenesis by allelic exchange of *choE*, encoding a cholesterol oxidase from the intracellular pathogen Rhodococcus equi. *J Bacteriol* **183**(16), 4796-805.

O'Farrell, P. A., Walsh, M. A., McCarthy, A. A., Higgins, T. M., Voordouw, G. & Mayhew, S. G. (1998). Modulation of the redox potentials of FMN in *Desulfovibrio vulgaris* flavodoxin: thermodynamic properties and crystal structures of glycine-61 mutants. *Biochemistry* **37**(23), 8405-16.

Ohta, T., Fujishiro, K., Yamaguchi, K., Tamura, Y., Aisaka, K., Uwajima, T. & Hasegawa, M. (1991). Sequence of gene *choB* encoding cholesterol oxidase of *Brevibacterium sterolicum*: comparison with *choA* of *Streptomyces* sp. SA-COO. *Gene* **103**, 93-96.

Pollegioni, L., Wels, G., Pilone, M. S. & Ghisla, S. (1999). Kinetic mechanisms of cholesterol oxidase from *Streptomyces hygroscopicus* and *Brevibacterium sterolicum*. *Eur. J. Biochem.* **263**, 1-13.

Purcell, J. P., Greenplate, J. T., Jennings, M. G., Ryerse, J. S., Pershing, J. C., Sims, S. R., Prinsen, M. J., Corbin, D. R., Tran, M., Sammons, R. D. & Stonard, R. J. (1993). Cholesterol Oxidase - a Potent Insecticidal Protein Active against Boll Weevil Larvae. *Biochemical and Biophysical Research Communications* **196**(3), 1406-1413.

Ramana, C. V. M., P.; Radhakantha, A. (1982). Pregnancy Suppression by Active Immunization against Gestation-Specific Riboflavin Carrier Protein. *Science* **216**(4542), 191-193.

Reibenspies, J. H., Guo, F. & Rizzo, C. J. (2000). X-ray crystal structures of conformationally biased flavin models. *Org Lett* **2**(7), 903-6.

Richmond, W. (1973). Preparation and properties of a cholesterol oxidase from *Nocardia sp.* and its application to the enzymatic assay of total cholesterol in serum. *Clin Chem* **19**(12), 1350-6.

Rose, G. & Shipley, M. J. (1980). Plasma lipids and mortality: a source of error. *Lancet* **1**(8167), 523-6.

Rowland, P., Norager, S., Jensen, K. F. & Larsen, S. (2000). Structure of dihydroorotate dehydrogenase B: electron transfer between two flavin groups bridged by an iron-sulphur cluster. *Structure Fold Des* **8**(12), 1227-38.

Sampson, N. S. & Kass, I. J. (1997). Isomerization, but not oxidation, is suppressed by a single point mutation, E361Q, in the reaction catalyzed by cholesterol oxidase. *J. Am. Chem. Soc.* **119**(5), 855-862.

Scarbrough, F. E. S., H.-S. & Voet, D. (1977). The X-ray crystal structure of the molecular complexbis(lumiflavin-2,6-diamino-9-ethylpurine)-ethanol-water. *Acta Cryst.* **B33**, 2512-2523.

Schreuder, H. A., Prick, P. A., Wierenga, R. K., Vriend, G., Wilson, K. S., Hol, W. G. & Drenth, J. (1989). Crystal structure of the p-hydroxybenzoate hydroxylase-substrate complex refined at 1.9 A resolution. Analysis of the enzyme-substrate and enzyme-product complexes. *J Mol Biol* **208**(4), 679-96.

Serrano, L., Bycroft, M. & Fersht, A. R. (1991). Aromatic-aromatic interactions and protein stability. Investigation by double-mutant cycles. *J Mol Biol* **218**(2), 465-75.

Slotte, J. P. (1992). Enzyme-catalyzed oxidation of cholesterol in mixed phospholipid monolayers reveals the stoichiometry at which free cholesterol clusters disappear. *biochemistry* **31**, 5472-5477.

Stenberg, K., Clausen, T., Lindqvist, Y. & Macheroux, P. (1995). Involvement of Tyr24 and Trp108 in substrate binding and substrate specificity of glycolate oxidase. *Eur J Biochem* **228**(2), 408-16.

Susin, S. A., Lorenzo, H. K., Zamzami, N., Marzo, I., Snow, B. E., Brothers, G. M., Mangion, J., Jacotot, E., Costantini, P., Loeffler, M., Larochette, N., Goodlett, D. R., Aebersold, R., Siderovski, D. P., Penninger, J. M. & Kroemer, G. (1999). Molecular characterization of mitochondrial apoptosis-inducing factor. *Nature* **397**(6718), 441-6.

Swenson, R. P. & Krey, G. D. (1994). Site-directed mutagenesis of tyrosine-98 in the flavodoxin from *Desulfovibrio vulgaris* (Hildenborough): regulation of oxidation-reduction properties of the bound FMN cofactor by aromatic, solvent, and electrostatic interactions. *Biochemistry* **33**(28), 8505-14.

Talfournier, F., Munro, A. W., Basran, J., Sutcliffe, M. J., Daff, S., Chapman, S. K. & Scrutton, N. S. (2001). alpha Arg-237 in *Methylophilus methylotrophus* (sp. W3A1) electron-transferring flavoprotein affords approximately 200-millivolt stabilization of the FAD anionic semiquinone and a kinetic block on full reduction to the dihydroquinone. *J Biol Chem* **276**(23), 20190-6.

Thorpe, C. & Kim, J. J. (1995). Structure and mechanism of action of the acyl-CoA dehydrogenases. *Faseb J* **9**(9), 718-25.

Tittmann, K., Golbik, R., Ghisla, S. & Hubner, G. (2000). Mechanism of elementary catalytic steps of pyruvate oxidase from *Lactobacillus plantarum*. *Biochemistry* **39**(35), 10747-54.

Trickey, P., Basran, J., Lian, L. Y., Chen, Z., Barton, J. D., Sutcliffe, M. J., Scrutton, N. S. & Mathews, F. S. (2000). Structural and biochemical characterization of recombinant wild type and a C30A mutant of trimethylamine dehydrogenase from *methylophilus methylotrophus* (sp. W(3)A(1)). *Biochemistry* **39**(26), 7678-88.

Trickey, P., Wagner, M. A., Jorns, M. S. & Mathews, F. S. (1999). Monomeric sarcosine oxidase: structure of a covalently flavinylated amine oxidizing enzyme. *Structure Fold Des* **7**(3), 331-45.

Umhau, S., Pollegioni, L., Molla, G., Diederichs, K., Welte, W., Pilone, M. S. & Ghisla, S. (2000). The x-ray structure of D-amino acid oxidase at very high resolution identifies the chemical mechanism of flavin-dependent substrate dehydrogenation. *Proc Natl Acad Sci U S A* **97**(23), 12463-8.

Uwajima, T., Yagi, H., Nakamurs, S. & Terada, O. (1973). Isolation and crystallization of extracellular 3β-hydroxysteroid oxidase of *Brevibacterium sterolicum* nov. sp. *Agr. Biol. Chem.* **37**(10), 2345-2350.

Vock, P., Engst, S., Eder, M. & Ghisla, S. (1998). Substrate activation by acyl-CoA dehydrogenases: transition-state stabilization and pKs of involved functional groups. *Biochemistry* **37**(7), 1848-60.

Vrielink, A., Lloyd, L. F. & Blow, D. M. (1991). Crystal structure of cholesterol oxidase from *Brevibacterium sterolicum* refined at 1.8Å resolution. *J. Mol. Biol.* **219**, 533-554.

Watt, W., Tulinsky, A., Swenson, R. P. & Watenpaugh, K. D. (1991). Comparison of the crystal structures of a flavodoxin in its three oxidation states at cryogenic temperatures. *J Mol Biol* **218**(1), 195-208.

Wells, J. L. B. L. T., R. M. Johnston, R. E. Marsh and C. J. Fritchie Jnr. (1974). Crystal structure of the yellow molecular complex lumiflavin-bis(naphthalene-2,3-diol). *Acta Cryst.* **B30**, 1127-1134.

Wohlfahrt, G., Witt, S., Hendle, J., Schomburg, D., Kalisz, H. M. & Hecht, H. J. (1999). 1.8 and 1.9 A resolution structures of *the Penicillium amagasakiense* and *Aspergillus niger* glucose oxidases as a basis for modelling substrate complexes. *Acta Crystallogr D Biol Crystallogr* **55**(5), 969-77.

Xu, D., Kohli, R. M. & Massey, V. (1999). The role of threonine 37 in flavin reactivity of the old yellow enzyme. *Proc Natl Acad Sci U S A* **96**(7), 3556-61.

Yamashita, M., Toyama, M., Ono, H., Fujii, I., Hirayama, N. & Murooka, Y. (1998). Separation of the two reactions, oxidation and isomerization, catalyzed by *Streptomyces* cholesterol oxidase. *Protein Eng* **11**(11), 1075-81.

Yue, Q. K., Kass, I. J., Sampson, N. S. & Vrielink, A. (1999). Crystals Structure Determination of Cholesterol Oxidase from *Streptomyces* and Structural Characterization of Key Active Site Mutants. *Biochemistry* **38**, 4277-4286.

Zhou, Z. & Swenson, R. P. (1996). The cumulative electrostatic effect of aromatic stacking interactions and the negative electrostatic environment of the flavin

mononucleotide binding site is a major determinant of the reduction potential for the flavodoxin from *Desulfovibrio vulgaris* [Hildenborough]. *Biochemistry* **35**(50), 15980-8.

Ziegler, G. A. & Schulz, G. E. (2000). Crystal structures of adrenodoxin reductase in complex with NADP+ and NADPH suggesting a mechanism for the electron transfer of an enzyme family. *Biochemistry* **39**(36), 10986-95.

PREFACE TO CHAPTER 2

Cholesterol oxidase is a selective oxidizing agent for β-hydroxy steroids. One of the key amino acids necessary for efficient oxidation is an asparagine residue. Among other GMC oxidoreductases this residue is highly conserved as either an asparagine or a histidine residue. In the native structures of BCO1 and SCOA, this N485 is involved in a hydrogen bonding network with the active site water, Wat541. It was speculated that this residue could be important for the orienting H447 in the active site. Thus, the structure of the N485L mutant was pursued to determine if the mutation results in a mis-orientation of H447. Surprisingly, the mutation did not significantly affect the position of the histidine residue but rather noticeably affects the orientation of M122. The close proximity and orientation of N485 relative to the pyrimidine ring of the isoalloxazine system led us to postulate that perhaps this residue interacts directly with the flavin. Redox potential measurements between the wild-type and the N485L mutant did indeed reveal that the asparagine interacts and modulates the reactivity of the FAD. This work introduces a novel amide N-H ...π interaction that likely stabilizes the reduced cofactor.

CHAPTER 2. THE PRESENCE OF A HYDROGEN BOND BETWEEN ASPARAGINE 485 AND THE π SYSTEM OF FAD MODULATES THE REDOX POTENTIAL IN THE REACTION CATALYZED BY CHOLESTEROL OXIDASE

Ye Yin,[‡⊥] *Nicole S. Sampson*[⊥] *Alice Vrielink*[‡,¥] *and Paula I. Lario*[‡,¥]

[‡]Department of Molecular, Cellular and Developmental Biology, Sinsheimer Laboroatory, University of California Santa Cruz, Santa Cruz, CA, 95064, [¥]Biochemistry Department, McGill University, Montréal, QC, H3G-1Y6, and [⊥]Department of Chemistry, State University of New York, Stony Brook, NY 11794-3400.

Reproduced with permission from Biochemistry, (2001) Nov 20;40(46):13779-87.

Footnotes

[1]Abbreviations: chox, cholesterol oxidase; choA, *Streptomyces* cholesterol oxidase; LB, Luria broth; IPTG, isopropyl β–D-thiogalactoside; SDS-PAGE, sodium dodecylsulfate polyacrylamide gel electrophoresis; DEAE, diethylaminoethyl; TLC, thin layer chromatography; HRP, horseradish peroxidase. 2 x YT, 2x yeast-tryptone broth; BSA, bovine serum albumin; GMC, glucose-methanol-choline; FAD, flavin adenine dinucleotide; OPA, opal stop codon.

[2]This numbering refers to the X-ray crystal structure system for numbering amino acid residues (Ohta et al., 1991). Asn485 is encoded by codon 522 in the *Streptomyces* gene (Ishizaki et al., 1989).

[3]The oxidation reaction catalyzed by chox utilizes a FAD cofactor, and thus may proceed as a hydride transfer, or it may proceed as two 1 e^- transfer steps, one of which is a hydrogen atom transfer. Both mechanisms would proceed more efficiently with general base catalysis, and from a structural viewpoint, both are feasible. For the sake of simplicity, we will discuss our experiments in reference to the hydride mechanism, although the arguments presented apply equally well to a two step mechanism, i.e., hydrogen atom transfer followed by fast e^- transfer.

2.1 ABSTRACT

Cholesterol oxidase catalyzes the oxidation and isomerization of cholesterol to cholest-4-en-3-one. An asparagine residue (Asn485) at the active site is believed to play an important role in catalysis. In order to test the precise role of Asn485 we mutated it to a leucine and carried out kinetic and crystallographic studies. Steady-state kinetic analysis revealed a 1300-fold decrease in oxidation k_{cat}/K_m for the mutant enzyme whereas k_{cat}/K_m for isomerization is only 60-fold slower. The primary kinetic isotope effect in the mutant-catalyzed reaction indicates that 3α-H transfer remains the rate-determining step. Measurement of the reduction potentials for the wild-type and N485L enzymes reveals a 76mV decrease in the reduction potential of the FAD for the mutant enzyme relative to wild type. The crystal structure of the mutant, determined to 1.5 Å resolution, reveals a repositioning of the side chain of Met122 near to Leu485 to form a hydrophobic pocket. Furthermore, the movement of Met122 facilitates the binding of an additional water molecule, possibly mimicking the position of the equatorial hydroxyl group of the steroid substrate. The wild type enzyme shows a novel N-H···π interaction between the side chain of Asn485 and the pyrimidine ring of the cofactor. The loss of this interaction in the N485L mutant destabilizes the reduced flavin and accounts for the decreased reduction potential and rate of oxidation. Thus, the observed structural rearrangement of residues at the active site, as well as the kinetic data and thermodynamic data for the mutant, suggest that Asn485 is important for creating an electrostatic potential around the FAD cofactor enhancing the oxidation reaction.

2.2 INTRODUCTION

Cholesterol oxidase (EC 1.1.3.6) is a flavoenzyme isolated from a variety of microorganisms. It is able to catalyze two reactions in one active site: oxidation of the 3β-hydroxyl of cholesterol and subsequent 1,3-allylic isomerization of the oxidation product (Figure 1.9). It is used to clinically determine serum cholesterol levels in the diagnosis of arteriosclerosis and other lipid disorders. The active enzyme is a potent larvicide and is being developed for commercial applications in agriculture as a pest control agent (Corbin et al., 2001; Corbin et al., 1998; Purcell et al., 1993). Moreover, cholesterol oxidase is utilized to study membrane structures, especially the localization of cholesterol. With the precise elucidation of the atomic-level mechanism of cholesterol oxidase catalysis and binding of steroid, both fundamental studies and practical uses will be greatly advanced.

Cholesterol oxidases from Streptomyces sp. SA-COO and B. sterolicum are monomeric (55kD) proteins (60% identical in amino acid sequence) containing one FAD[1] per active site (Yue et al., 1999). There is little (<10%) primary sequence similarity between cholesterol oxidase and other members of the glucose-methanol-choline oxidoreductase (GMC) family (Cavener, 1992; Kiess et al., 1998). However, comparison with the tertiary structures of GMC oxidoreductase enzymes shows that their overall architecture is conserved. His447, Asn485, Glu361 and Wat541 are all highly conserved amongst cholesterol oxidases where the FAD cofactor is non-covalently bound to the enzyme. We have proposed that a hydrogen-bonding network between these residues, helps to position the substrate relative to the FAD cofactor and coordinates general base

and electrophilic catalysis for oxidation (Kass & Sampson, 1998a; Yue et al., 1999). The X-ray crystal structure suggested that His447 could coordinate general base catalysis of oxidation via Wat541 (Li et al., 1993; Yue et al., 1999). We showed that His447 is important for oxidation, but is not essential. Replacement of the imidazole with a glutamine amide resulted in a 100-fold reduction in overall rate of oxidation, and hydride transfer was no longer rate-determining[3]. This suggested that additional residues might contribute to catalysis of oxidation. In this work, we investigated the role of Asn485 in the reaction catalyzed by cholesterol oxidase by a combination of site-directed mutagenesis, kinetics and X-ray crystallography. We found that this residue is crucial for defining the electrostatic environment around the FAD that determines its reduction potential.

2.3 Experimental Procedures

2.3.1 Materials.

Cholest-5-en-3-one, 4-aminoantipyrine and Triton X-100 were from Aldrich Fine Chemical Co., (Milwaukee, WI). Cholesterol and horseradish peroxidase were purchased from Sigma Chemical Co. (St. Louis, MO). The plasmid for heterologous expression of *Streptomyces sp. SA-COO* cholesterol oxidase, pCO202 has been described previously (Sampson et al., 1998), and is a derivative of pCO117, a generous gift from Y. Murooka (Nomura et al., 1995). Restriction endonucleases, T4 DNA ligase, calf intestinal alkaline phosphatase, and T4 kinase were purchased from New England Biolabs (Beverly, MA). Oligonucleotides were purchased from IDT, Inc. (Coralville, IA). All other chemicals

and solvents, of reagent or HPLC grade, were supplied by Fisher Scientific (Pittsburgh, PA). Water for assays and chromatography was distilled, followed by passage through a Barnstead NANOpure filtration system to give a resistivity better than 18 MΩ.

2.3.2 General methods.

CD spectra were acquired on an Aviv Model 62A Circular Dichroism spectrophotometer. A Shimadzu UV2101 PC Spectrophotometer was used for assays and acquisition of UV spectra. Fluorescence measurements were taken on a Spex Fluorolog 3-11 spectrofluorometer. Restriction digests and ligations were performed according to procedures described in Sambrook et al. (Sambrook et al., 1989). The ABI PRISM BigDye Terminator Cycle Sequencing technique was applied to all mutated regions following the manufacturer's protocol (Perkin Elmer, Foster City, CA), and the plasmids were purified with the Wizard Plus DNA Purification System (Promega, Madison, WI) with water elution. The buffers used were A: 50 mM sodium phosphate, pH 7.0; B: buffer A + 0.025% triton X-100 (w/v); C: buffer B + 0.020% BSA (w/v); D: buffer A + 1.0 M $(NH_4)_2SO_4$; E: 100 mM citrate-phosphate, pH 5.10, 0.025% triton X-100 (w/v); F: 100 mM sodium phosphate, pH 5.90, 0.025% triton X-100 (w/v); G: 100 mM sodium phosphate, pH 6.96, 0.025% triton X-100; H: 100 mM sodium phosphate, pH 8.18, 0.025% triton X-100; I: 100 mM glycine-NaOH, pH 9.06, 0.025% triton X-100; J: 100 mM glycine-NaOH, pH 9.98, 0.025% triton X-100.

2.3.3 Construction of N485L ChoA mutant expression plasmid, pCO237.

In addition to introducing the N485L mutation, the extraneous *Streptomyces* DNA between the OPA and the HindIII site in pCO200 (Sampson et al., 1998) was removed by PCR using two primers. Primer 1 was a 67-base oligonucelotide that corresponded to the sequence of the coding strand (5'-ggCTggggCCCCAACggTAACATCATgACCgCCC-gggCCAACCACAtgKBTAACCCCACCggCgCCC-3'). This primer was upstream of a StuI site that was used for subcloning the PCR fragment. Primer 2 was a 99-base oligonucleotide that possessed the actual mutation N485L, introduced a HindIII site after the TAA stop codon and corresponded to the anticoding strand (5'-gCTCACAAgCTTACgACgCCgTgACgTCCTgCTTgATgAtgCgCTCgACgTTCCgCT-CggCCAgCgCCgTgATggTCACgAACgggAggACgCCgACgg-3'). Using XhoI restricted pCO202 (Kass & Sampson, 1998a) as a template, 31 cycles of PCR were performed with Pfu polymerase at an annealing temperature of 75°C. The 500 bp PCR fragment was digested with StuI and HindIII, purified, and subcloned into pCO200 (Kass & Sampson, 1998a) that had been similarly digested to yield the mutant expression plasmid pCO237.

2.3.4 Purification of wild-type cholesterol oxidase.

Cell paste of E. coli BL21(DE3)plysS(pCO117) (Sampson et al., 1998) was obtained from 1 L of 2 x YT-ampicillin (200 μg/mL) medium grown at 28 °C for 8 h after addition of IPTG (100 μg/mL) at A_{600} = 0.8 by centrifugation at 4 000 g for 30 min. The pellet was resuspended in 20 mL of buffer A and lysed by French press at 18 000 psi. All subsequent steps for wild-type cholesterol oxidase were conducted at 4 °C. Cell debris

was removed by centrifugation at 135 000 g for 60 min. The supernatant was precipitated by 1.0 M $(NH_4)_2SO_4$ and the pellet was discarded. $(NH_4)_2SO_4$ was added to the supernatant to a final concentration of 2 M. The pellet was obtained by centrifugation at 4 000g. This pellet was resuspended in buffer A (5 mL) and desalted using dialysis (nMWCO 6 000-8 000) against buffer A. The dialysate was loaded onto a column of DEAE-cellulose (30 mm x 25 cm, DE-52, Whatman) preequilibrated with buffer A. Fractions were collected by elution with buffer A (100 mL). Typically, 15 mL fractions were collected, however, fractions that appeared yellow in color were limited to 7.5 mL. Fractions containing cholesterol oxidase (as determined by SDS-PAGE) were combined and concentrated by $(NH_4)_2SO_4$ precipitation (3.0 M). The pellet was redissolved in buffer A to give a final concentration between 10 to 20 mg/mL of protein and $(NH_4)_2SO_4$ was slowly added until the solution turned slightly turbid (typically, 2.5 M). The precipitate formed was pelleted by centrifugation and the clarified supernatant was transferred to a fresh container where it was allowed to crystallize over 2 days at 4 °C. The microcrystalline protein was collected by centrifugation, dissolved in buffer A and ultrafiltered (YM30 membrane, Amicon, Inc., Danvers, MA) into buffer A. The protein was further purified on a butyl-Sepharose column (30 mL butyl-Sepharose-4 Fast Flow, XK 16/40, Pharmacia Biotech, Upsala, Sweden) preequilibrated with buffer D. The protein was eluted by running a linear gradient from 100% buffer D to 100% buffer A (270 mL). Fractions (4.5 mL) were collected and the elution profile was monitored at A_{280}. Fractions were assayed for content and purity by SDS-PAGE. Fractions containing pure cholesterol oxidase (>98%) were combined and ultrafiltered (YM30 membrane) into buffer A. Typically 30-40 mg of pure cholesterol oxidase was obtained per L of culture.

2.3.5 Purification of N485L cholesterol oxidase.

The mutant N485L cholesterol oxidase was prepared as described above for wild type. The yield of N485L was 75 mg/L. Protein concentrations were determined by UV absorbance using ε_{280} = 81,924 $M^{-1}cm^{-1}$ (calculated from the molar extinction coefficients of tryptophan and tyrosine (Fasman, 1992).)

2.3.6 UV, fluorescence, and CD spectra.

Solutions of cholesterol oxidases were prepared in buffer A. A baseline spectrum of buffer A was subtracted from the sample spectrum. The concentrations of wild type and N485L used were 19 μM and 21 μM, respectively. CD spectra were recorded in the near UV from 300 to 255nm, and in the far UV from 250 to 185 nm. The Uv/vis spectra of the semiquinone and reduced flavin enzyme species were obtained during the anaerobic titration (*vide infra*) and the spectra were deconvoluted by subtracting the spectra of the other species present from the observed spectrum. The concentration of cholesterol oxidases used for fluorescence spectra was 2 μM.

2.3.7 Steady-state enzyme kinetics.

Stock solutions of cholesterol and 3α-[^{2}H]-cholesterol were prepared by dissolving the appropriate sterol in propan-2-ol. The concentration of each solution was determined using cholesterol oxidase and standard assay condition 1 (*vide infra*). Stock solutions of cholest-5-en-3-one were prepared and stored in the dark in foil wrapped containers because the cholest-5-en-3-one decomposes via autooxidation in solution, TLC (15:85, EtOAc:Hexane) was employed to assay the solutions for purity prior to use each day.

HRP (1000 U/mL), phenol (113 mM) and 4-aminoantipyrine (440 mM) stock solutions were prepared in buffer B. Dilute enzyme stock solutions were prepared in buffer C. The concentration of each enzyme used in assays with cholesterol was: wild type, 0.55 nM; N485L, 86 nM. The concentration of each enzyme used in assays with cholest-5-en-3-one was: wild type, 0.44 nM; N485L, 12 nM. Initial velocities were measured in one of three ways. (1) The formation of conjugated enone was followed as a function of time at 240nm (ε_{240} =12,100 M^{-1} cm^{-1}) (Smith & Brooks, 1977). (2) The activity also was determined using a horseradish peroxidase coupled assay to quantitate the rate of formation of H_2O_2. The formation of quinoneimine at 510 nm was followed as a function of time. The standard assay conditions were the same as the UV A_{240} assay with addition of 1.13 mM phenol, 0.87mM 4-aminoantipyrine and 10 U of horseradish peroxidase. (3) The reaction was followed by excitation at 325 nm and monitoring the fluorescence emission at 415 nm (slits = 1.5 nm) using an HRP-coupled assay to quantitate the rate of formation of H_2O_2. The standard assay conditions were the same as the UV A_{240} assay with the addition of 1.0 mM p-hydroxyphenylacetic acid and 10 U of horseradish peroxidase. Independent sets of data were fit simultaneously to the hyperbolic form of the Michaelis-Menten equation using Grafit (Erithacus, London, UK). Primary isotope effects were determined in a similar fashion fitting all the possibilities and selecting the best fit (^{D}V, $^{D}V/K$, or ^{D}V and $^{D}V/K$). pH profiles were determined using buffers E-J that had equal ionic strengths.

2.3.8 Determination of reduction potentials.

The redox potentials of wild-type and mutant cholesterol oxidases were determined at pH 7.0, at 15 °C using the dye-equilibration method and xanthine/xanthine oxidase reduction system described by Massey (Massey, 1991). Enzyme (10-15 μM) was placed in an anaerobic cuvette in buffer A, together with 0.2-0.3 mM xanthine and 1-10 μM concentrations of safranin T that has an E_m of -276 mV. To ensure rapid equilibration of reducing equivalents, 5 μM benzyl viologen was added to the enzyme solution. The closed cuvette was made anaerobic by repeated cycles of evacuation and flushing with argon. After anaerobiosis had been established, the spectrum of the enzyme solution was recorded. The reaction was initiated by adding xanthine oxidase from the side-arm and absorbance spectra were recorded (300-800 nm). The absorbance spectra were collected until the contribution of the benzyl viologen radical became apparent.

The concentrations of the oxidized, semiquinone, and reduced forms of cholesterol oxidases, and of the oxidized and reduced forms of the reference dye were determined from the absorbance values at various wavelengths (using an isosbestic point for the oxidized and semiquinone enzyme forms of 524.5 nm and 525.0 nm for wild type and N485L, respectively). The redox potential, E_h, for the system at equilibrium was calculated using the standard Nernst equation:

$$E_h = E_m + (2.3RT/nF) \log ([\text{oxidized form}]/[\text{reduced form}]) \quad (1)$$

The data were plotted as described previously (Massey, 1991). Briefly, the oxidation/reduction potential for the couple EFl_{ox}/EFl_{seq} (E_1) was determined by plotting the ratio of the concentrations of the oxidized and semiquinone forms of cholesterol

oxidase, and the potential for the couple EFl_{seq}/EFl_{red} (E_2) was determined by plotting the ratio of the concentration of the semiquinone and reduced forms of the enzyme. The separation between the two single-electron transfers was estimated from the maximal percentage of the semiquinone form of the enzyme reached during a reduction experiment in the absence of the reference dye (Gadda et al., 1997):

$$\Delta E_m = 59 \text{ mV} \times \log K \quad (2)$$

$$K = [EFl_{seq}]^2 / [EFl_{red}]\,[EFl_{ox}] \quad (3)$$

Semiquinone formation was graphically determined by plotting the changes in absorbance at the maximum wavelength for this form (372.5 nm and 376.5 nm for wild-type and N485L cholesterol oxidase, respectively) and for the oxidized enzyme (390.5 nm and 394.0 nm for wild-type and N485L cholesterol oxidase, respectively). The ΔE_m between the reference dye and cholesterol oxidase was determined from the value of log (oxidized/reduced) for the enzyme at the point where the log (oxidized/reduced) for the reference dye is zero.

2.3.9 Crystallographic structure determination.

Crystals of the N485L mutant of cholesterol oxidase were obtained as described previously (Yue et al., 1999). X-ray diffraction data were collected at 115K in order to minimize crystal decay. The crystals were transferred briefly to a cryoprotectant solution containing 20% glycerol in the crystal mother liquor. A single crystal was mounted in a cryoloop (Hampton Research, Laguna Hills, CA) and placed in a cold nitrogen stream at 115 K. The data were collected on a MAR image plate detector with a double focussing mirror system (Supper Ltd.) mounted on a Rigaku RU-200 rotating anode X-ray

generator (CuKα radiation). A data set to 1.5Å resolution was collected using a single crystal of dimensions 0.1 x 0.1 x 0.08 mm. The completeness of the data collected was 93% with a redundancy of 4 and a merging R factor of 0.045. The X-ray images were processed, merged and scaled with the HKL suite of software (Minor, 1993; Otwinowski, 1993). The mutant structure was solved by difference Fourier techniques using the native structure (PDB code 1b4v) which had been modified such that all active site water molecules and water molecules located on the surface of the structure were removed. In addition, the proposed catalytic residues, H447, N485 and E361 were mutated to alanines. Refinement was carried out using SHELX-97 (Sheldrick & Schneider, 1997) and SIGMAA-weighted maps calculated with coefficients 2Fo - Fc and Fo – Fc. The free R-factor was monitored during the course of the refinement using a subset of 10% of the data randomly chosen from the total diffraction data. The entire structure was rebuilt and the side chains for H447 and E361 as well as the leucine mutation at position 485 were included in the model. Water molecules were included where difference electron density above 3σ was observed and where hydrogen-bond contacts were made to other polar atoms. Multiple conformations were included for a loop region of the structure (256 – 260) as well as 10 amino acid side chain. In addition, the side chains of 9 surface residues were modeled with partial occupancy. The final refinement statistics are given in Table 2.1. The coordinates have been deposited in the Protein Data Bank (Bernstein et al., 1977).

Table 2.1: Crystallographic refinement statistics

Resolution Range (Å)	25 – 1.5
Total Reflections Used in Refinement	57,331
R factor	0.163
25.5	0.213 (6,632 reflections)
Rmsd bond lengths (Å)	0.009
Rmsd bond angle distances (Å)	0.024
Number of non hydrogen atoms	
Protein	3,901
FAD	53
Water	611
Average B factors (Å^2)	
Overall	16.8
Protein atoms	15.6
FAD atoms	10.3
Water molecules	

2.4 Results

2.4.1 Physical characterization.

The N485L cholesterol oxidase was heterologously expressed in *E. coli.* The purity was confirmed by SDS-PAGE analysis, UV/vis and CD spectroscopy. The UV spectrum of the bound FAD cofactor for the purified N485L cholesterol oxidase has red-shifted λ_{max}'s at 394 nm and 472 nm compared to wild type at 390.5 nm and 468 nm

(Figure 2.1). The fluorescence emision maxima for wild-type and N485L are the same: 338 nm (280 nm, excitation), 526 nm (450 nm, excitation). The CD spectra (far and near UV) confirm that N485L mutant is folded identically to wild type.

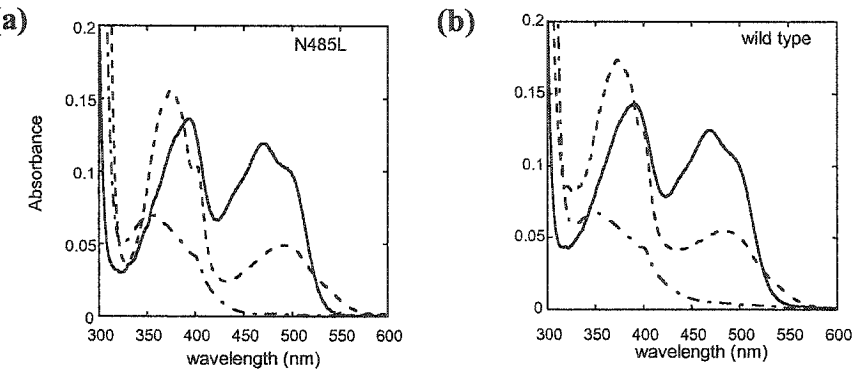

Figure 2.1. Visible spectra of a) N485L, and b) wildtype cholesterol oxidases for each oxidation state as determined by anaerobic reduction.. (—) Oxidized, FAD; (---) semiquinone, FADH·; (- - -) reduced, $FADH_2$. All spectra were acquired in 50 mM sodium phosphate buffer, pH 7.0. The semiquinone and reduced spectra were acquired under anaerobic conditions with benzyl viologen, xanthine, and xanthine oxidase as the reducing system, and the spectra of xanthine were subtracted for clarity. The semiquinone spectrum was determined by subtracting the small amount of oxidized species present near the midpoint of the titration and rescaled to 100%.

2.4.2 Steady-state kinetics.

The catalytic capability of the N485L mutant is summarized in Table 2.2 along with previously obtained data on the H447Q mutant. The Michaelis-Menten parameters of the active mutants using both cholesterol and cholest-5-en-3-one as substrates are reported. In the wild-type catalyzed reaction using cholesterol as a substrate, the A_{240}-based assay that follows the rate of product cholest-4-en-3-one formation, and the H_2O_2-

based assay that follows the rate of intermediate product H_2O_2 formation, measure the same steady-state rates. The rate constants for both assays of the N485L mutant are also the same. This means that N485L catalyzes oxidation and isomerization, i.e., it converts cholesterol to cholest-4-en-3-one. However, the k_{cat}/K_m is 1300-fold reduced compared to wild type.

The mutant isomerization activity using cholest-5-en-3-one as a substrate was compared with wild-type cholesterol oxidase by monitoring the rate of cholest-4-en-3-one appearance at 240 nm. The ability of wild-type enzyme to catalyze the isomerization of the cholest-5-en-3-one is as efficient as its ability to oxidize and isomerize cholesterol. The isomerization k_{cat}/K_m of N485L is 60-fold slower than wild type.

2.4.3 Primary isotope effects.

The same substrate primary kinetic isotope effects were observed for wild-type cholesterol oxidase and the N485L mutant using 3α-[^{2}H]-cholesterol. The isotope effects are 2.2 ± 0.1 on both k_{cat} and k_{cat}/K_m.

Table 2.2. Michaelis-Menten rate constants for wild-type and mutant cholesterol oxidases.

	Turnover (oxidation and isomerization) cholesterol[a]			Isomerization cholest-5-en-3-one[b]		
	k_{cat} (s^{-1})	K_m (μM)	$(k_{cat}/K_m)_{mut}/(k_{cat}/K_m)_{wt}$	k_{cat} (s^{-1})	K_m (μM)	$(k_{cat}/K_m)_{mut}/(k_{cat}/K_m)_{wt}$
wild type	44 ± 2	3.0 ± 0.4		64 ± 3	6.2 ± 0.7	
H447Q[c]	0.32 ± 0.01	3.0 ± 0.3	0.0036	81 ± 4	7.1 ± 0.8	1.1
N485L	0.046 ± 0.004	4.2 ± 0.1	0.00075	3.2 ± 0.3	18 ± 0.6	0.017

[a]Measured by H_2O_2 formation with HRP coupling. [b]Measured by cholest-4-en-3-one formation at 240 nm. [c]As reported in (Kass & Sampson, 1998a).

2.4.4 pH rate profile.

The pH dependence of the cholesterol oxidation reaction was measured by following the appearance of cholest-4-en-3-one, the product of oxidation and isomerization. For wild-type cholesterol oxidase, the value of k_{cat} decreased 2,000-fold with increasing pH with an apparent pK_a of 8.3 ± 0.1, K_m was independent of pH. The loss of activity is reversible. In contrast, an increase in pH for the N485L mutant resulted in a 6-fold increase in the k_{cat}. The pK_a(app) for k_{cat} is 9.5 ± 0.3, again, K_m did not

change with pH. The isomerization activity of N485L or wild type did not change with increasing pH.

2.4.5 Reduction potential of FAD.

The reduction potentials of the wild-type and N485L cofactors were measured spectroscopically using the dye-equilibration method of Massey (Massey, 1991). The 1 e^- reduction potentials of the N485L oxidized FAD and semiquinone FAD are significantly reduced compared to wild type (Table 2.3). The midpoint potential is correspondingly reduced from –278 mV to –354 mV. The reduction potentials for cholesterol oxidase from *Streptomyces hygroscopicus* have been reported previously (Gadda et al., 1997). The E_m of this enzyme is –217 mV, 60 mV higher than the cholesterol oxidase used in our work. Because there is no sequence or structural information available for the *Streptomyces hygroscopicus* enzyme, it is not possible to explain the difference between the two. It is clear, however, that bacteria produce multiple cholesterol oxidases with very different redox properties. For example, *Brevibacteria* produce one cholesterol oxidase that is structurally very similar to that used in this work (Vrielink et al., 1991; Yue et al., 1999), and a second that is structurally distinct with a covalently-bound FAD (Coulombe et al., 2001) that has an increased redox potential (Gadda et al., 1997; Motteran et al., 2001).

Table 2.3: Reduction potentials for wild-type and N485L cholesterol oxidases.[a]

	Maximal amount of semiquinone formed	ΔE (mV)	E_1 (mV)	E_2 (mV)	E_m (mV)
wild type	98%	-112	-222 ± 14	-334 ± 11	-278
N485L	95%	-108	-300 ± 5	-408 ± 8	-354

[a]Determined spectroscopically using the xanthine and xanthine oxidase system (Massey, 1991) in 50 mM sodium phosphate, pH 7.0 at 15 °C. Safranin T was used as the redox standard (E_m = -276 mV).

2.4.6 Crystallographic structure analysis.

As predicted from the CD spectra, the overall fold of N485L is identical to those of the native enzyme from *Streptomyces sp. SA-COO* (Yue et al., 1999) and *B. sterolicum* (Vrielink et al., 1991). Slight differences in the main chain atom positions between the mutant and native structures are localized at two loop regions (256 – 260 and 434 – 438). The electron density for the loop from residues 256 – 260 indicated a second conformation that was included in the final model. The loop from residues 434 – 438 forms part of the entrance to the active site cavity of the enzyme and has previously been observed to be poorly defined and highly mobile (Vrielink et al., 1991; Yue et al., 1999). In the mutant structure, the temperature factors for the main chain atoms in this loop region (28 $Å^2$) are significantly higher than the average observed for the entire protein (14 $Å^2$).

The substrate-binding site of the native enzyme revealed 14 water molecules (Yue et al., 1999). All but one of these water molecules is retained in the active site of the

N485L mutant. In the native structure, Wat1148 lies in a hydrophobic pocket, bounded by the side chains of Phe359, Trp351, Val124 and Ile379 and makes hydrogen bond contacts to both the side chain and main chain atoms of Asn485 (Figure 2.2a). Due to the leucine mutation at this site, this water molecule is no longer present in the structure and the residues surrounding this hydrophobic pocket are slightly repositioned to optimize van der Waals interactions (Figure 2.2b). The side chain of Met122 adopts a different conformation in the mutant structure (χ_3 = 85°) compared to that of the native (χ_3 = -100°) (Figure 2.3). Interestingly, the orientation of the methionine side chain is identical in the mutant and the dehydroisoandosterone complex structures (Li et al., 1993). An additional water molecule (Wat543) is observed in the mutant structure in hydrogen bond contact to O4 of FAD. This water molecule lies near to the position of the Cε methyl group of Met122 in the native structures of both the *Streptomyces sp. SA-COO* and *B. sterolicum* enzymes. Furthermore, this water molecule lies in a similar position to the hydroxyl oxygen atom, O1', of the dehydroisoandosterone steroid substrate in the complex structure.

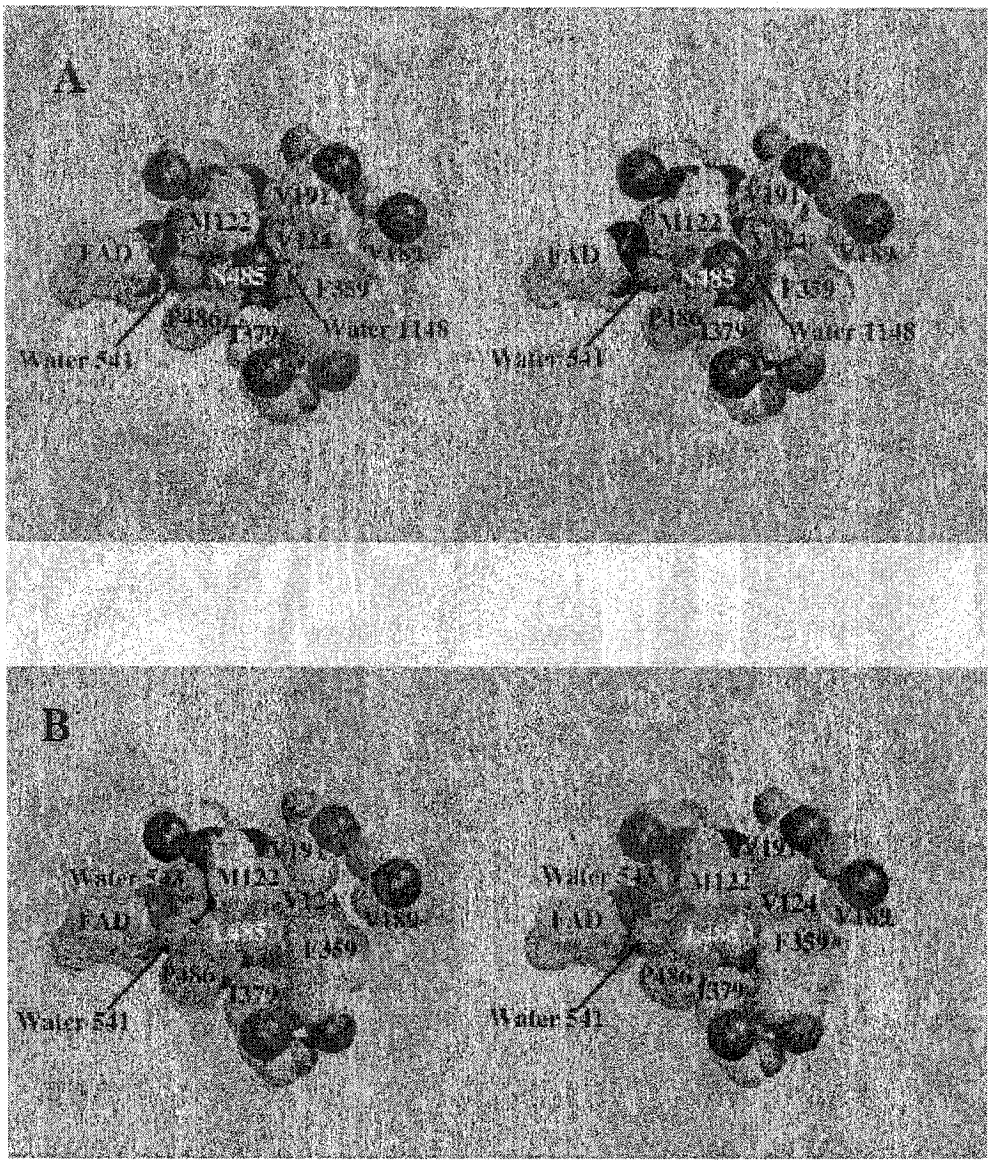

Figure 2.2. Stereo figure showing a CPK representation of the region around residue 485 in a) the native enzyme structure and b) the N485L mutant structure.

Further changes in the active site of the mutant include a repositioning of Wat541 and His447. Both have been strongly implicated in substrate oxidation (Kass & Sampson, 1998a; Yue et al., 1999). In the native structure, Wat541 forms strong hydrogen bonds with the side chains of Asn485 and His447. In the mutant structure, the water molecule moves away from the side chain of Leu485, by 0.6 Å relative to the

native water position (Figure 2.3). However the hydrogen bond with His447 is still preserved due to a slight shift of the histidine side chain (0.3 Å).

Finally, changes in the active site of the mutant are observed for Glu361. In previously determined structures of the enzyme, this side chain exhibits high temperature factors suggesting significant mobility. Furthermore, isotope labeling studies and site directed mutagenesis of this residue have indicated it to be essential for the isomerization reaction of the enzyme (Kass & Sampson, 1995; Kass & Sampson, 1998b; Sampson & Kass, 1997; Yue et al., 1999). In the mutant structure, this glutamate side chain still has relatively high temperature factors (21.3 $Å^2$) and its alpha carbon position has shifted by 0.4 Å relative to the native enzyme. These observed structural changes in Glu361 place the carboxylate moiety within hydrogen bond distance to both the active site water molecule (541) and Wat543 (Figure 2.3).

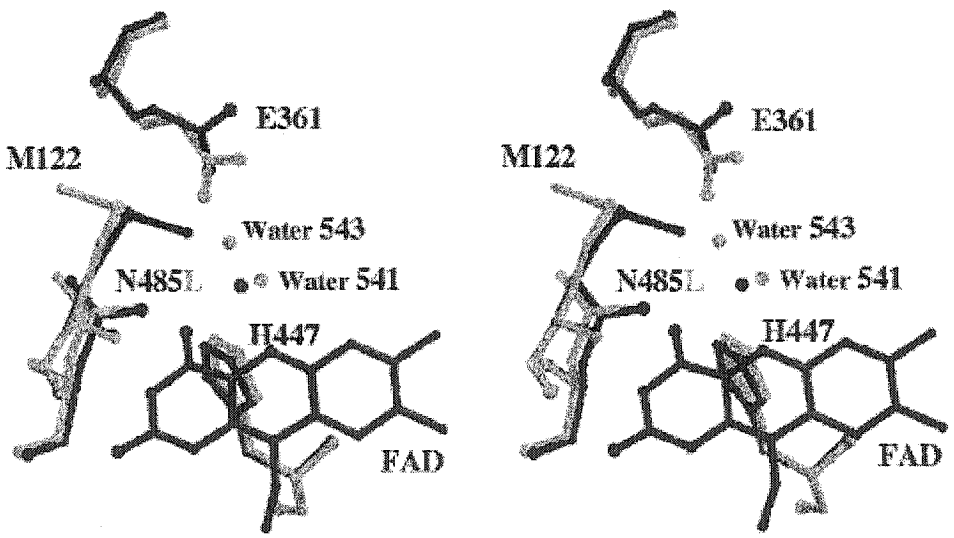

Figure 2.3. Stereo superposition of the active site residues for the native enzyme and the N485L mutant enzyme. The native structure is shown in black and the mutant in gray.

2.5 Discussion

The crystallographic models of *Streptomyces sp. SA-COO* and *B. sterolicum* cholesterol oxidase have revealed a structurally conserved active-site. The positions of residues His447, Glu361, Asn485 and Wat541 suggest they play a role in the catalytic mechanism. (It should be noted that *B. sterolicum* has a second cholesterol oxidase that has a covalently-bound FAD and is structurally distinct from the non-covalent form of the enzyme (Coulombe et al., 2001; Gadda et al., 1997).) Previously, we have shown that His447 via Wat541 is the general base for oxidation of the sterol (Kass & Sampson, 1998a; Yue et al., 1999). Glu361 is the base that catalyzes the isomerization of cholest-5-en-3-one to cholest-4-en-3-one (Kass & Sampson, 1995; Kass & Sampson, 1998b; Sampson & Kass, 1997). Here, we investigated the importance of Asn485 in catalysis.

Asn485 plays a central role in forming the active site hydrogen-bonding network. It is positioned at the N-terminal end of helix 14 however, it is not involved in hydrogen bonding with the helix (Figure 2.4). The structures of the native enzyme from both *Streptomyces sp. SA-COO* and *B. sterolicum* show the Asn485 side chain oriented such that the amide nitrogen atom is within hydrogen bonding distance of Wat541 (Li et al., 1993; Vrielink et al., 1991). However, the lack of a hydrogen bonding network involving the amide nitrogen and oxygen atoms and discrete atoms on the protein make unequivocal conformational assignment of the asparagine side chain impossible.

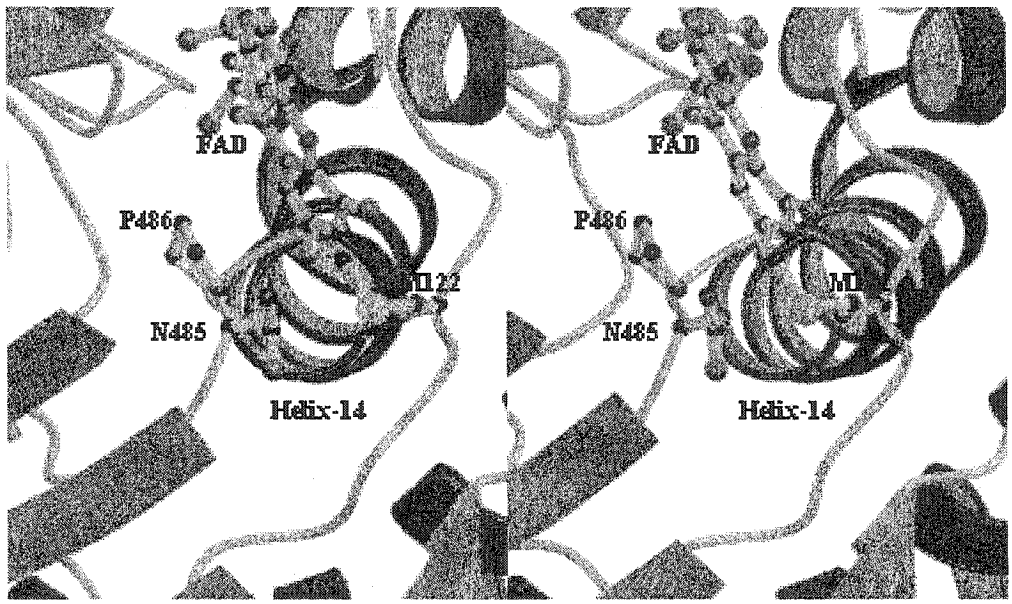

Figure 2.4. Stereo view of helix-14 in the native structure. The pyrimidine ring of the FAD cofactor and the side chains of Asn485, Pro486 and Met122 are shown located at the N terminus of the helix.

If the side chain nitrogen atom of Asn485 is hydrogen-bonded to Wat541, the helix dipole would increase hydrogen-bond donation by Asn485, and increase the general acidity of Wat541. This orientation might lower the activation barrier to form the dienol intermediate of isomerization, but would simultaneously make the general-base catalyzed oxidation more difficult. However, this side chain orientation would position the amide nitrogen atom within close contact with the isoalloxazine ring of FAD. This interaction would stabilize the electron-rich reduced form of the cofactor, thus promoting the oxidation reaction.

On the other hand, if the amide oxygen of Asn485 is hydrogen-bonded to Wat541, it would be poised to increase the general basicity of Wat541. However, the helix dipole would not favor reduction of negative charge on the amide oxygen. In addition, this

orientation would position the electron rich oxygen atom in close contact with the pyrimidine moiety of the isoalloxazine ring. This close interaction is unlikely and would decrease the reactivity of the FAD cofactor for oxidation.

Murooka and coworkers have reported that substitution of Asn485 with alanine and glutamine resulted in a lowering of oxidation activity, but not isomerization (Yamashita et al., 1998). However, they did not probe the reasons for these decreases in oxidation activity. To further test our proposition about the importance of Asn485, we designed and prepared an N485L mutant. Because leucine is isosteric with asparagine but is not polarizable or able to hydrogen bond, we expected to disturb the hydrogen-bonding network and disrupt the assistance from helix14. Furthermore this mutation would affect the electrostatic environment around the isoalloxazine ring and hence the reactivity of FAD. This mutation allowed us to assess Asn485's importance for maintaining the position of Wat541, effecting general acid or base catalysis, and for altering the reduction potential of FAD.

Our kinetic results indicate that Asn485 plays a crucial role in the oxidation activity of the enzyme. When Asn485 was substituted with a leucine, the oxidation activity was greatly impaired. Steady-state kinetic analysis shows that k_{cat} for N485L is 1000-fold slower than wild type in oxidation and for isomerization is only 20-fold slower (Table 2.2). Increasing the reaction pH of the wild-type enzyme decreases the oxidation activity 2000-fold and does not affect the isomerization activity. In contrast, for N485L, a 6-fold increase in oxidation activity was observed upon increasing pH. Although, we cannot assign the pK_a to a single residue or site, the mutation of Asn485 to a more hydrophobic residue will change the electrostatic environment around the isoalloxazine ring system of

the cofactor. These changes would affect the pKa of the isoalloxazine N3 position which will alter the pH dependence of the oxidative activity of the enzyme. The presence of a leucine in place of an asparagine near the cofactor likely results in an increased pKa for the isoalloxazine N3. This altered electrostatic environment around the cofactor in the mutant enzyme may account for the retention of oxidative activity at high pH.

The slightly reduced isomerization rates upon mutation are probably due to a small shift in the position of the water structure in the active site. By analogy, the substrate position would be similarly shifted and the substrate may no longer be ideally aligned with Glu361. Previously, we have observed that the position of Wat541 is important for maximal catalytic activity (Yue et al., 1999). This shift in position will also affect the alignment of the substrate with the FAD. However, the markedly lower oxidation activity of N485L implies that the major effect of the mutation is not primarily due to the misalignment of the substrate in the active site. Rather, it is the electrostatics of this residue that are most important for catalysis of oxidation.

Although the k_{cat}/K_m for the reaction is 1300-fold slower than wild type, 3α-H transfer is still rate-determining in the mutant reaction. This means that mutation of Asn485 reduces the rate of 3β-hydroxy oxidation, rather than decreasing the rate of another kinetic step. These primary isotope effects support the importance of Asn485 for FAD reduction. In contrast, when His447 is mutated, 3α-H transfer is no longer rate determining (Kass & Sampson, 1998a). Mutation of His447 reduces the steady-state rate of oxidation at least 100-fold, however, either 3β-hydroxyl deprotonation (Kass & Sampson, 1998a) or $FADH_2$ oxidation becomes rate-determining (Su & Klinman, 1999).

We examined the X-ray crystal structure of the N485L mutant in order to determine the effect of the mutation on the active site structure. The most significant change observed in the mutant structure is a repositioning of Met122. In the native *B. sterolicum* and *Streptomyces* structures, the Cε of Met122 lies 3.3Å and 3.0Å respectively from O4 of FAD, suggestive of a C-H···O contact. In the mutant structure, the Cε of Met122 is repositioned due to the mutation to a leucine, forming a hydrophobic pocket made up of Val191, Leu485, Phe359 and Met122 (Figure 2). This altered side chain orientation recruits an additional water molecule (543) that forms a hydrogen bond with O4 of the FAD in the unliganded protein. Comparison of the structures of the N485L mutant with the dehydroisoandosterone complex reveals that, in the mutant, Wat543 is in a similar position to the hydroxyl oxygen of the steroid substrate in the complex. Interestingly, the Met122 is in the hydrophobic pocket and does not contact O4 of the FAD. Moreover, the side chain Asn485 has rotated away from the pyrimidine ring of the cofactor ($\chi 1$ of Asn485 is -96° and –65° for the substrate free and substrate bound structures respectively). Thus, the wild-type position of the methionine methyl group orients the amide group of Asn485 over the FAD. In addition, this close contact is observed in the native *B. sterolicum* structure as well as the E361Q and H447Q mutant structures from *Streptomyces* (Yue et al., 1999). In all of these structures, the position of Met122 is correlated with the position of residue 485.

The structural and kinetic data for N485L suggest that Asn485 and Met122 are important for creating an electrostatic potential around the FAD that is favorable for oxidation of alcohol substrates. Indeed, the UV/vis spectrum of the FAD region of

N485L is red-shifted relative to wild-type, indicating that the electronic environment around the FAD has been altered. In addition, the mutation of Asn485 to leucine and its associated structural changes result in a 76 mV decrease in the reduction potential of the FAD (Table 2.3). In other words, the N485L mutant is a much poorer oxidizing agent, and the reduction of the N485L-bound FAD is not as thermodynamically favorable as that of wild-type. This is consistent with the kinetic properties that we observe, i.e., a higher activation barrier to FAD reduction.

Thus, it appears that the most important role of Asn485 is to form an N-H···π electrostatic interaction to facilitate reduction of the FAD. Similar N-H···π interactions have been reported by Levitt and Perutz in studies of hemoglobin-drug interactions (Levitt & Perutz, 1988; Perutz, 1993; Perutz et al., 1986) and have been analyzed by Thornton (Mitchell et al., 1993; Mitchell et al., 1994; Singh & Thornton, 1990). This is the first reported example of such an interaction between a protein residue and a flavin nucleus. Stabilization of the reduced flavin has been shown to involve interactions between protein atoms and discrete atoms on the isoalloxazine ring system of the cofactor, e.g., N1, and N5 (Chang & Swenson, 1999; Fraaije & Mattevi, 2000; Hoover et al., 1999; van den Heuvel et al., 2000; Wagner et al., 2000). Rather than an atom – atom interaction between the protein and the cofactor, cholesterol oxidase reveals an atom - π interaction as providing the stabilization to the reduced form of the cofactor. Furthermore, the strength of this hydrogen bond is amplified by the presence of the dipole through helix 14 (Figure 2.4). This novel mechanism for flavin stabilization is supported by both structural and kinetic analysis. Empirical potential energy calculations

have suggested that an N-H···π interaction has a stabilization energy of approximately 3 kcal/mol (Perutz et al., 1986). This magnitude is consistent with a rate reduction of approximately 100-fold. The remainder of the 1300-fold rate reduction observed may be attributed to mis-positioning of the substrate.

We conclude that the most important roles of Asn485 are two-fold. First, to position Wat541, and consequently the substrate 3α-H, relative to the FAD and Glu361 to promote oxidation and isomerization. Second, to create an electrostatic environment around the isoalloxazine ring that favors reduction of FAD by unactivated alcohols. The combination of kinetic, thermodynamic, and X-ray crystallographic data that we have acquired suggest that the polarity of the environment surrounding the isoalloxazine ring is as important for oxidation as a general base catalyst.

2.7 Acknowledgments

We thank Prof. Giovanni Gadda for his assistance with the redox potential measurements. We also thank Nathalie Croteau for crystallization of the mutant enzyme.

2.8 References

Bernstein, F. C., Koetzle, T. F., Williams, G. J., Meyer, E. E. J., Brice, M. D., Rodgers, J. R., Kennard, O., Shimanouchi, R. & Tasumi, M. (1977). The Protein Data Bank: a computer-based archival file for macromolecular structures. *J. Mol. Biol.* **112**, 535-542.

Cavener, D. R. (1992). GMC oxidoreductases. A newly defined family of homologous proteins with diverse catalytic activities. *J. Mol. Biol.* **223**, 811-814.

Chang, F.-C. & Swenson, R. P. (1999). The midpoint potentials for the oxidized-semiquinone couple for Gly57 mutants of the *Clostridium beijerinckii* flavodoxin correlate with changes in the hydrogen-bonding interaction with the proton on N(5) of the reduced flavin mononucleotide cofactor as measured by NMR chemical shift temperature dependencies. *Biochemistry* **38**, 7168-7176.

Corbin, D. R., Grebenok, R. J., Ohnmeiss, T. E., Greenplate, J. T. & Purcell, J. P. (2001). Expression and chloroplast targeting of cholesterol oxidase in transgenic tobacco plants. *Plant Physiol.* **126**, 1116-1128.

Corbin, D. R., Greenplate, J. T. & Purcell, J. P. (1998). The identification and development of proteins for control of insects in genetically modified crops. *Hortscience* **33**(4), 614-617.

Coulombe, R., Yue, K. Q., Ghisla, S. & Vrielink, A. (2001). Oxygen access to the active site of cholesterol oxidase through a narrow channel is gated by an Arg-Glu pair. *J. Biol. Chem.* **276**, 30435-30441.

Fasman, G. D. (1992). *Practical Handbook of Biochemistry and Molecular Biology.* Practical Handbook of Biochemistry and Molecular Biology (Fasman, G. D., Ed.), C. R. C. Press, Boca Raton, FL.

Fraaije, M. W. & Mattevi, A. (2000). Flavoenzyme: diverse catalysts with recurrent features. *Trends. Biochem. Sci.* **25**, 128-132.

Gadda, G., Wels, G., Pollegioni, L., Zucchelli, S., Ambrosius, D., M.S., P. & Ghisla, S. (1997). Characterization of cholesterol oxidase from *Streptomyces hygroscopicus* and *Brevibacterium sterolicum*. *Eur. J. Biochem.* **250**(2), 369-376.

Hoover, D. M., Drennan, C. L., Metzger, A. L., Osborne, C., Weber, C. H., Pattridge, K. A. & Ludwig, M. L. (1999). Comparisons of wild-type and mutant flavodoxins from *Anacystis nidulans*. Structural determinants of the redox potentials. *J. Mol. Biol.* **294**, 725-743.

Ishizaki, T., Hirayama, N., Shinkawa, H., Nimi, O. & Murooka, Y. (1989). Nucleotide sequence of the gene for cholesterol oxidase from a *Streptomyces* sp. *J. Bacteriol.* **171**, 596-601.

Kass, I. J. & Sampson, N. S. (1995). The isomerization catalyzed by *Brevibacterium sterolicum* cholesterol oxidase proceeds stereospecifically with one base. *Biochem. Biophys. Res. Commun.* **206**, 688-693.

Kass, I. J. & Sampson, N. S. (1998a). Evaluation of the role of His^{447} in the reaction catalyzed by cholesterol oxidase. *Biochemistry* **37**, 17990-18000.

Kass, I. J. & Sampson, N. S. (1998b). The importance of Glu^{361} position in the reaction catalyzed by cholesterol oxidase. *Bioorg. Med. Chem. Lett.* **8**, 2663-2668.

Kiess, M., Hecht, H. J. & Kalisz, H. M. (1998). Glucose oxidase from *Penicillium amagasakiense* - Primary structure and comparison with other glucose-methanol-choline (GMC) oxidoreductases. *Eur. J. Biochem.* **252**(1), 90-99.

Levitt, M. & Perutz, M. F. (1988). *J. Mol. Biol.* **201**, 751-754.

Li, J., Vrielink, A., Brick, P. & Blow, D. M. (1993). Crystal structure of cholesterol oxidase complexed with a steroid substrate: implications for flavin adenine dinucleotide dependent alcohol oxidases. *Biochemistry* **32**, 11507-11515.

Massey, V. (1991). A simple method for the determination of redox potentials. In *Flavins and Flavoproteins 1990* (Curti, B., Ronchi, S. & Zanetti, G., ed.), pp. 59-66. Walter de Gruyter & Co., Berlin, Germany.

Minor, W. (1993). XDISPLAYF Program, Purdue University.

Mitchell, J. B. O., Nandi, C. L., Ali, S., McDonald, I. K., Thornton, J. M., Price, S. L. & Singh, J. (1993). *Nature* **366**, 413.

Mitchell, J. B. O., Nandi, C. L., MacDonald, I. K., Thornton, J. M. & Price, S. L. (1994). *J. Mol. Biol.* **239**, 315-331.

Motteran, L., Pilone, M. S., Molla, G., Ghisla, S. & Pollegioni, L. (2001). Cholesterol oxidase from *Brevibacterium sterolicum*. *J. Biol. Chem.* **276**(21), 18024-18030.

Nomura, N., Choi, K.-P. & Murooka, Y. (1995). Genetic Modification of the *Streptomyces* Cholesterol Oxidase Gene for Expression in *Escherichia coli* and Development of Promoter-Probe Vectors for Use in Enteric Bacteria. *J. Ferm. Bioeng.* **79**(5), 410-416.

Ohta, T., Fujishiro, K., Yamaguchi, K., Tamura, Y., Aisaka, K., Uwajima, T. & Hasegawa, M. (1991). Sequence of Gene ChoB Encoding Cholesterol Oxidase of

Brevibacterium sterolicum: Comparison with ChoA of *Streptomyces* sp. SA-COO. *Gene* **103**, 93-96.

Otwinowski, Z. (1993). Oscillation data reduction program. In *Data collection and Processing: Proceedings of the CCP4 Study Weekend* (Sawyer, L., Isaccs, N. & Bailey, S., eds.), pp. 56-62. SERC Daresbury Laboratory, Warrington, U.K.

Perutz, M. F. (1993). *Phil. Trans. R. Soc. A* **345**, 105-112.

Perutz, M. F., Fermi, G., Abraham, D. J., Poyart, C. & Bursaux, E. (1986). *J. Am. Chem. Soc.* **108**, 1064-1078.

Purcell, J. P., Greenplate, J. T., Jennings, M. G., Ryerse, J. S., Pershing, J. C., Sims, S. R., Prinsen, M. J., Corbin, D. R., Tran, M., Sammons, R. D. & Stonard, R. J. (1993). Cholesterol oxidase: a potent insecticidal protein active against boll weevil larvae. *Biochem. Biophys. Res. Commun.* **196**(3), 1406-13.

Sambrook, J., Fritsch, E. F. & Maniatis, T. (1989). *Molecular Cloning: A Laboratory Manual.* 2nd edit, Cold Spring Harbor Laboratory Press, Cold Spring Harbor, New York.

Sampson, N. S. & Kass, I. J. (1997). Isomerization, but not oxidation, is suppressed by a single point mutation, E361Q, in the reaction catalyzed by cholesterol oxidase. *J. Am. Chem. Soc.* **119**, 855-862.

Sampson, N. S., Kass, I. J. & Ghoshroy, K. B. (1998). Assessment of the role of an Ω loop of cholesterol oxidase: a truncated loop mutant has altered substrate specificity. *Biochemistry* **37**, 5770-5778.

Sheldrick, G. M. & Schneider, T. R. (1997). SHELXL: High-resolution refinement. In *Methods in Enzymology* (Carter, C. W. J. & Sweet, R. M., eds.), Vol. 277, pp. 319-343. Academic Press, Boston.

Singh, J. & Thornton, J. M. (1990). *J. Mol. Biol.* **211**, 595-615.

Smith, A. G. & Brooks, C. J. W. (1977). The substrate specificity and stereochemistry, reversiblility and inhibition of the 3-oxo steroid Δ^4-Δ^5 isomerase component of cholesterol oxidase. *Biochem. J.* **167**, 121-129.

Su, Q. & Klinman, J. P. (1999). Nature of oxygen activation in glucose oxidase from *Aspergillus niger*: the importance of electrostatic stabilization in superoxide formation. *Biochemistry* **38**, 8372-8381.

van den Heuvel, R. H. H., Fraaije, M. W., Mattevi, A. & Van Berkel, W. J. H. (2000). Asp-170 is crucial for the redox properties of vanillyl-alcohol oxidase. *J. Biol. Chem.* **275**, 14799-14808.

Vrielink, A., Lloyd, L. F. & Blow, D. M. (1991). Crystal structure of cholesterol oxidase from *Brevibacterium sterolicum* refined at 1.8 Å resolution. *J. Mol. Biol.* **219**, 533-554.

Wagner, M. A., Trickey, P., Chen, Z.-W., Matthews, F. S. & Jorns, M. S. (2000). Monomeric sarcosine oxidase: 1. Flavin reactivity and active site binding determinants. *Biochemistry* **39**, 8813-8824.

Yamashita, M., Toyama, M., Ono, H., Fujii, I., Hirayama, N. & Murooka, Y. (1998). Separation of the two reactions, oxidation and isomerization, catalyzed by *Streptomyces* cholesterol oxidase. *Protein Eng.* **11**(11), 1075-1081.

Yue, K., Kass, I. J., Sampson, N. & Vrielink, A. (1999). Crystal structure determination of cholesterol oxidase from *Streptomyces* and structural characterization of key active site mutants. *Biochemistry* **38**, 4277-4286.

PREFACE TO CHAPTER 3

In this chapter we present a 0.95 Å crystal structure of native cholesterol oxidase from *Streptomyces sp.* SA-COOA. This structure represents the first sub-Ångstrom structure of a flavin enzyme. Atomic resolution data dramatically improves the quality of the model. It allows one to model the directional nature in the local atomic movements, with anisotropic temperature factors. The correct orientation for asparagine, glutamine and histidine residues is usually unambiguous as one-electron differences are apparent directly from the electron density for most of the residues. In addition, these maps often enable a better description of the disordered regions of the enzyme.

We have observed dramatic enhancements in the 0.95 Å structure of SCOA model, compared to the earlier 1.5 Å resolution structure. Residues with high temperature factors in the lower resolution model are clearly separable into discrete alternate conformations using the atomic resolution maps. Quite unexpectedly many of the active-site residues were found to adopt multiple conformations, despite being unresolved in the lower resolution maps. This additional model information has allowed us to identify a previously unobserved narrow hydrophobic tunnel leading directly to the isoalloxazine system and propose a different substrate position that displaces Wat541 from the active site.

The proposed active site base H447, necessary for oxidative activity is more likely a hydrogen bond donor critical for substrate orientation. Unambiguous side chain assignments and the visibility of hydrogen atoms support this modified role for H447. In addition, these findings account for the unanticipated kinetics observed for the H447Q

mutant. These results question the necessity of an active site base for oxidation and suggest that the electrophilicity of the isoalloxazine is enough to initiate hydride transfer. While this postulate is not new among flavin oxidoreductases, SCOA provides a clear example where it is unlikely that the substrate to be oxidized binds in a pre-activated un-protonated state.

Observed correlations between the alternate residue conformations in the active site, has enabled us to propose dynamic mechanisms for substrate binding, tunnel gating and product release. These new mechanistic models are consistent with the previously reported kinetic data and can be used to design new experiments, perhaps, to further an understanding of the more elusive oxidative half reaction.

CHAPTER 3. SUB-ATOMIC RESOLUTION CRYSTAL STRUCTURE OF CHOLESTEROL OXIDASE: WHAT ATOMIC RESOLUTION CRYSTALLOGRAPHY REVEALS ABOUT ENZYME MECHANISM AND THE ROLE OF THE FAD COFACTOR IN REDOX ACTIVITY

Paula I. Lario[⊥], Nicole Sampson[¥] and Alice Vrielink[⊥]

[⊥]Department of Molecular, Cellular and Developmental Biology, Sinsheimer Laboratory, University of California Santa Cruz, Santa Cruz, CA, 95064, Biochemistry Department, McGill University, Montréal, QC, H3G-1Y6., [¥]Department of Chemistry, State University of New York, Stony Brook, NY 11794-3400.

Submitted Manuscript, October 2002

3.1 ABSTRACT

The crystal structure of cholesterol oxidase, a 56 KDa flavoenzyme was anisotropically refined to 0.95Å resolution. The final crystallographic *R*-factor and R_{free} is 11.0 % and 13.2 % respectively. The quality of the electron density maps has enabled modeling of alternate conformations for 83 residues in the enzyme, many of which are located in the active-site. The additional observed structural features were not apparent in the previous high resolution structure (1.5 Å resolution) and have enabled the identification of a narrow tunnel leading directly to the isoalloxazine portion of the FAD prosthetic group. The hydrophobic nature of this narrow tunnel suggests it is the pathway for molecular oxygen to access the isoalloxazine group for the oxidative half reaction. Resolving the alternate conformations in the active site residues provides a model for the dynamics of substrate binding and a potential oxidation triggered gating mechanism involving access to the hydrophobic tunnel. This structure reveals that the NE2 atom of the active site histidine residue, H447, critical to the redox activity of this flavin oxidase, acts as a hydrogen bond donor rather than as hydrogen acceptor. The atomic resolution structure of cholesterol oxidase has revealed the presence of hydrogen atoms, dynamic aspects of the protein and how side chain conformations are correlated with novel structural features such as the oxygen tunnel. This new structural information has provided us with the opportunity to re-analyze the roles played by specific residues in the mechanism of the enzyme.

3.2 INTRODUCTION

Cholesterol oxidase (CO) (EC 1.1.3.6) is a bi-functional bacterial flavoenzyme that catalyzes the oxidation of 3β-hydroxysteroids and the isomerization of the intermediate, Δ^{5-6}-ene-3β-ketosteroid to produce Δ^{3-4}-ene-3β-ketosteroid (Figure 1.9). This enzyme, produced by a diverse range of bacteria, was originally found to have a metabolic role in the breakdown of cholesterol (Ohta et al., 1991; Uwajima et al., 1973). There is considerable commercial interest in this flavoenzyme, as a method for determining serum cholesterol levels (reviewed in (MacLachlan et al., 2000)). Recently, a putative cholesterol oxidase gene, *pimE*, has been identified by its sequence homology to both the *Brevibacterium sterolicum* (BCO1) and *Streptomyces sp.* SA-COO (SCOA) cholesterol oxidases. *PimE* is present in a large gene cluster involved in the biosynthesis of the commercially valuable antibiotic pimaricin (Aparicio et al., 2000). Sequence similarity studies have also identified CO homologues that are secreted by life-threatening pathogens, including *Rhodococcus equi, Mycobacterium tuberculosis* and *Mycobacterium leprae* (Navas et al., 2001). Gene disruption studies of the cholesterol oxidase gene, *choE* in *Rhodococcus equi* have indicated that this homologue may play a role in the lysis of macrophages and leucocytes, leading to characteristic lesions found in infected humans and animals. As these cholesterol oxidases are unique to bacteria they present a potential target for a new class of antibiotics. Moreover, cholesterol oxidases are larvicidal and are being developed as insecticides against Coeloptera (Corbin et al., 2001; Shen et al., 1997).

The oxidative activity of cholesterol oxidases is facilitated by its flavin adenine dinucleotide, FAD, prosthetic group. FAD cofactors are commonly found within proteins involved in electron transport and are often utilized by enzymes whose reaction mechanisms involve oxidation and/or reduction. Moreover, the oxidized cofactor can accept either 1 or 2 electrons to form a semiquinone or reduced isoalloxazine in the reductive half-reaction. The cofactor is then recycled to the oxidized state by oxygen oxidation in the oxidative half-reaction.

Structural comparisons of flavin oxidases have indicated that these enzymes share common active site features despite very distinct and divergent active site architectures (Fraaije & Mattevi, 2000). For example, there are two structurally distinct cholesterol oxidases from *Brevibacterium sterolicum*, BCO1 in which the FAD is not covalently bound to the enzyme (Vrielink et al., 1991) and BCO2, in which the FAD is covalently bound to the protein through a histidine linkage (Coulombe et al., 2001). Both of these enzymes catalyze the oxidation and isomerization of cholesterol despite having completely different folds and active site residues. Common features among flavin oxidases include an active site sequestered from the bulk solvent, a hydrogen bond donor to the N5 atom of FAD and a similar substrate binding position for the hydride donor atom relative to the isoalloxazine (Fraaije & Mattevi, 2000). Despite these conserved active site features, there are considerable differences among the flavin oxidase active sites. The surrounding protein environment of the FAD isoalloxazine system alters its geometry and modulates its redox potential and hence the reactivity of the enzyme (Chang & Swenson, 1999; Dwyer et al., 1999; Fraaije & Mattevi, 2000; Hasford, 1997; O'Farrell et al., 1998; Yin et al., 2001). In fact, the 100 mV difference in the redox

potential between BCO1 and BCO2 suggested that these two cholesterol oxidases had unique active site environments, as was later observed from crystallographic studies (Coulombe et al., 2001; Gadda et al., 1997; Vrielink et al., 1991).

Here we present the first sub-Ångstrom structure (0.95 Å) of cholesterol oxidase from *Streptomyces sp. SA-COO* (SCOA) (Ishizaki et al., 1989). The high quality electron density maps have enabled us to observe one-electron differences in the isoalloxazine ring system of the FAD cofactor. This high resolution study is instrumental for further theoretical and experimental studies of cholesterol oxidase and will improve our understanding of how the protein environment modulates the reactivity of the enzyme. Finally, the additional information gained from this atomic resolution structure has enabled us to identify hydrogen atoms on specific active site residues and to resolve numerous multiple conformations of protein residues. Based on these novel structural features a potential oxygen channel linking the exterior of the protein to the buried FAD has been identified and has lead to a re-analysis of the enzyme mechanism.

3.3 Results and Discussion

3.3.1 Structure refinement and model quality

Diffraction data to 0.95 Å resolution was collected using synchrotron radiation on a single crystal of cholesterol oxidase. The final model includes 498 residues, the FAD molecule, a sulfate ion, a di-oxygen molecule and 736 water molecules. The final refinement cycle using all the data, gave an *R*-factor of 11.0 % (the data collection and refinement statistics are give in Table 3.1).

Table 3.1: Crystallographic data and refinement statistics

Crystal parameters:	
Cell dimensions	a = 51.23
	b = 72.90
	c = 62.95
	β = 105.10
Data collection:	
Number of measured reflections	1089496
Number of unique reflections	266037 (4.1 redundancy)
Resolution range (Å)	28.2 – 0.95
Resolution range for the last shell (Å)	0.97 – 0.95
Completeness (%)	94.1
Completeness in the last shell (%)	88.0
R-merge	0.051
Mean I/σ	11.1
Refinement:	
Number of reflections used	250371
Number of reflections set aside for R_{free}	13180 (5 %)
R-factor	11.0
Free R-factor	13.2
R-factor (all data)	11.0

r.m.s. (bond lengths) (Å)	0.015
r.m.s. (angle distances) (Å)	0.031
Protein residues	498
Water molecules	736 (440 full)
Isotropic average temperature factors ($Å^2$)	
All atoms	12.2
Main chain atoms	8.6
Side chains and waters	14.8
FAD molecule	5.6

During the final stage of refinement the restraints applied to bond distances and angles were relaxed, however, no further improvement in the R-factor was observed indicating that the relaxation of the restraints was unwarranted. A final cycle of full-matrix refinement was carried out in order to obtain the errors in the atomic positions for the final model.

The stereochemical quality of the model is comparable to that of other crystal structures refined at atomic resolution. The Ramachandran plot shows that all of the residues are located in allowed regions. Anisotropic temperature refinement for all non-hydrogen atoms resulted in a significant improvement in the quality of the electron density map. The higher resolution of the electron density allows us to model alternate conformations for 82 residues, 71 of which were previously unresolved in the 1.5 Å structure. Despite the excellent quality of the electron density for most of the residues, 15 surface residues were modeled with a portion of their side chain as either partially

occupied or absent. In addition, as observed for the 1.5 Å structure, 3 residues at the N terminus and 2 residues at the C terminus were disordered and excluded from the model.

3.3.2 Flexibility of the active site

The improved resolution of the SCOA structure provides a better description of the flexible nature of the active site than was previously observed in the 1.5 Å structure (Yue et al., 1999). At 0.95Å resolution, most of the active site residues are observed in multiple conformations. In contrast, at 1.5Å resolution the multiple conformations of many of these residues were unresolved. The refinement program SHELXL-97 allows the occupancy for each alternate residue conformation to be refined. These alternate conformations provide important insights into the roles of active site residues in catalysis. For example, in the structures of BCO1 and SCOA (1.5Å) as well as the steroid bound complex of BCO1 (PDB entries: 3cox, 1b4v and 1coy respectively) (Li et al., 1993; Vrielink et al., 1991; Yue et al., 1999) the side chain of N485 has been modeled in different single conformations; however at 0.95Å, two discrete conformations are evident in the electron density (Figure 3.1a). Interestingly, these multiple conformations, seen at 0.95Å, represent the different positions for the steroid bound and unbound structures observed at 1.8Å (Figure 3.1b). Thus, in the absence of a steroid bound complex, higher resolution data from a single crystal structure is able to provide a view of the possible conformations available to the protein and reveals how active site residues adjust to accommodate the substrate. Furthermore, these multiple conformations can show the role certain residues play in catalysis. Previous studies of N485 have shown that this residue affects the oxidative activity of the enzyme and modulates the redox potential of

the flavin (Yamashita et al., 1998; Yin et al., 2001) through an interaction between ND2-H and the ring of FAD which stabilizes the increased charge density in the reduced cofactor. One of the multiple conformations of N485 places the ND2 atom 3.00(3) Å away from C4 of the FAD confirming its role in forming a strong hydrogen bonding interaction with the flavin (Figure 3.1a).

Within the active site cavity several new water sites were observed in the electron density, all of which are partially occupied and are correlated with specific conformations of protein side chains. The presence of these partially occupied water molecules enables us to establish the relationships between conformations of adjacent residues. Using steric considerations and hydrogen bonding networks, the conformations of active site residues were assigned as either A or B. These conformational populations and their significance in the mechanism will be discussed below.

Determining the relationships between active site residues and water molecules provides insight into the flexible nature of the enzyme. Furthermore, it gives us an understanding of the mechanisms by which residues move relative to each other. These features were examined for insight into the catalytic roles of the enzyme and the reaction mechanism.

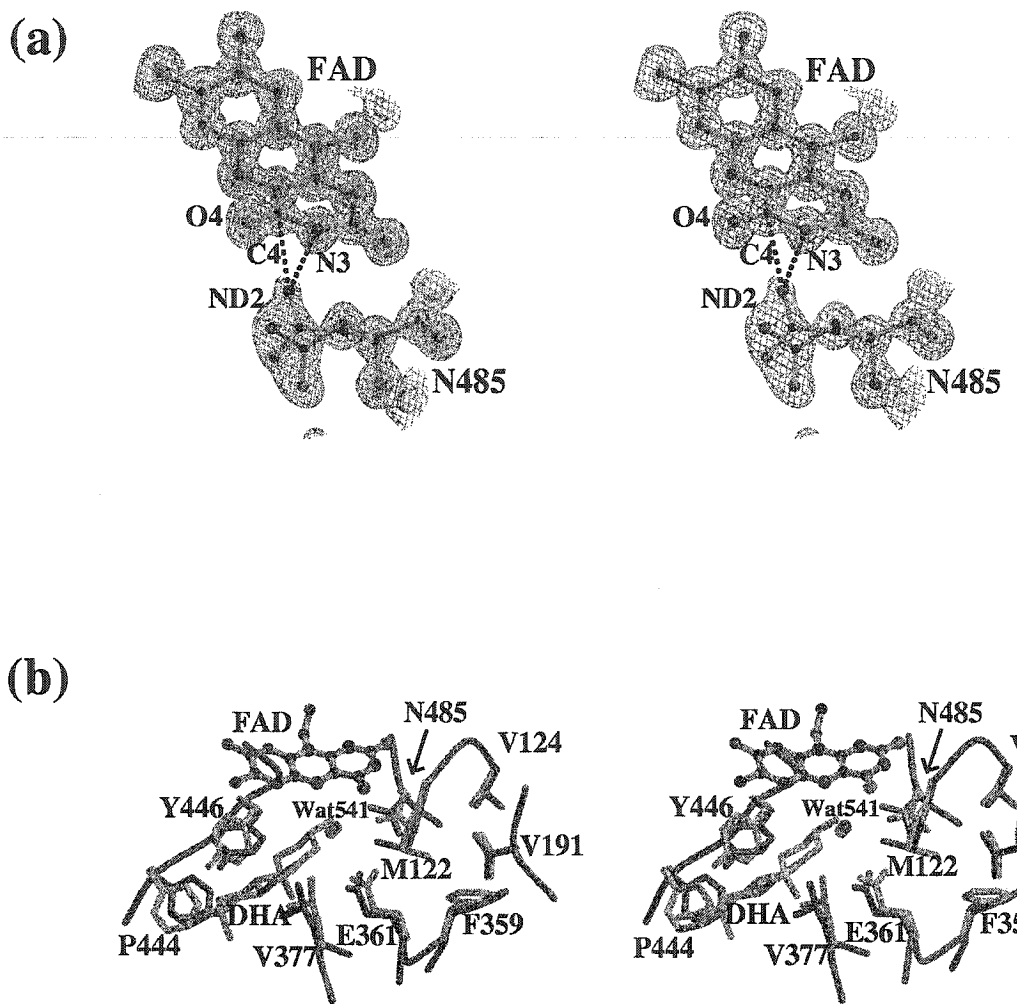

Figure 3.1 (a) The electron density map for the FAD cofactor and N485 modeled in two alternate conformations. The density is computed using the coefficients 2mFo-DFc and is contoured at 1.0 σ (blue) and 4.0 σ (pink). Conformer B, shown in green, is 2.97Å and 3.00 Å from both N3 and C4 of the FAD, respectively. (b) A superposition of the active site region of native cholesterol oxidase and the dehydroisoandosterone steroid complex from *B. sterolicum* (PDB accession codes 3COX and 1COY). The native structure is colored purple and the steroid complex structure is colored peach.

3.3.3 Oxygen tunnel

After the enzyme oxidizes cholesterol to 5-cholesten-3-one, the flavin must be re-oxidized by molecular oxygen (Figure 1.9). Previously it was supposed that molecular oxygen entered the active site of the enzyme via the movement of two surface loops in the structure, in an identical fashion as proposed for the substrate (Vrielink et al., 1991). The higher resolution and the ability to resolve additional alternate conformations in this structure has revealed a second pathway, a narrow tunnel, located at the interface between the FAD and substrate binding domains, that leads directly to the active site and the isoalloxazine system (Figure 3.2a).

This tunnel is only open when the active site residues are modeled in conformation B. Both the entrance and lining of the tunnel are hydrophobic (lined by the M122, V124, V189, V191, P192, F359, A360, I379 and V484) (Figure 3.2). The importance of these residues is evident by the fact that they are highly conserved among cholesterol oxidase homologues. Even in putative cholesterol oxidases from *M.tuberculosis* and *M. leprae* that have low (25%) identity to SCOA, the tunnel residues within this FAD–binding domain are conserved.

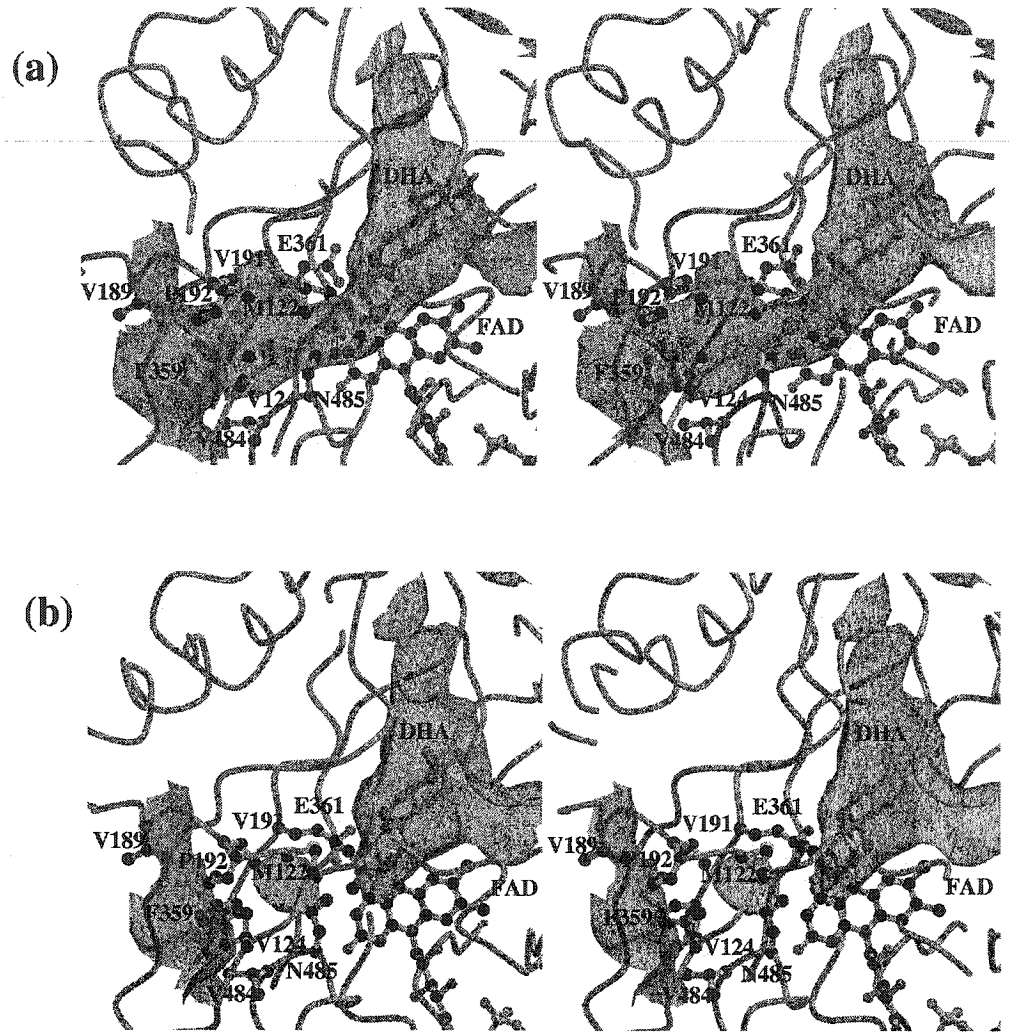

Figure 3.2. Stereoscopic representations showing the active site of the enzyme with (a) the hydrophobic tunnel of the enzyme in the open conformation (corresponding to conformation B) and (b) the tunnel closed conformation (corresponding to conformation A). The molecular surfaces were constructed using the program SPOCK and colored according to residue type: aromatic and hydrophobic residues are colored green, acidic residues are colored red and basic residues are colored blue. The bound water molecules in the tunnel are represented as red spheres. The dehydroisoandosterone molecule, shown in green, has been modeled into the substrate-binding cavity.

The size, location and hydrophobic nature of the tunnel in SCOA is characteristic of molecular oxygen tunnels and thus is the likely route taken by O_2 to FAD for the

oxidative half reaction of the enzyme. A hydrophobic tunnel has also been observed for the structurally distinct cholesterol oxidase, BCO2 (Coulombe et al., 2001). Interestingly, this tunnel is also located between the FAD binding and the substrate binding domains. Narrow hydrophobic tunnels have also been observed in cytochrome C oxidase (Iwata et al., 1995; Riistama et al., 1996; Soulimane et al., 2000), ba3 cytochrome, ribonucleotide reductases (Eriksson et al., 1998), aa3-quinol oxidase (Soulimane et al., 2000), and ferritin (Stillman et al., 2001).

No significant backbone movements are necessary to open the tunnel, which is closed when the active site residues are modeled in conformation A (Figure 3.2B). Active site residues M122, E361 and N485 are positioned where the tunnel meets the isoalloxazine ring. Thus by switching between their side chain conformations, these residues control access of O_2 to the flavin. Two of these residues: N485 and E361, have been identified as critical catalytic residues for the oxidation and isomerization reaction, respectively (Kass & Sampson, 1995; Kass & Sampson, 1998b; Sampson & Kass, 1997; Yamashita et al., 1998; Yin et al., 2001). Their prospective roles in gating the tunnel will be discussed in more detail below.

Kinetic data has indicated that the overall kinetic mechanism for cholesterol oxidase from *Streptomyces hydroscopicus* (SCOH) is sequential and involves a ternary complex consisting of the reduced enzyme, product and O_2 (Pollegioni et al., 1999). Kinetic studies of SCOH indicate that the oxidized form is more efficient at isomerization than a pre-reduced enzyme (Pollegioni et al., 1999). Additionally, the rate of re-oxidation of the pre-reduced enzyme in the absence of the steroid was shown to be significantly slower (~2000 fold) than the turnover rates observed in steady state conditions. The

identification of the hydrophobic tunnel to the active site in SCOA is consistent with the observed sequential reaction mechanism observed for SCOH. A ping-pong mechanism would be expected if oxygen was to enter through the substrate binding loops, since the steroid would have to be displaced for oxygen to enter via this route.

The tunnel in SCOA opens to a hydrophobic cleft on the exterior surface of the protein (Figure 2), providing a potential loading site for O_2. In order for O_2 to react with FAD the steroid needs to move away from its original reactive position. While this might suggest that SCOA may undergo ping-pong kinetics, a pre-binding of O_2 could involve an ordered sequential reaction mechanism. Oxygen may either pre-bind in the hydrophobic cleft or within the oxygen channel, without full release of the steroid from the active site. The presence of the steroid within the substrate cavity, maintains a sequestered hydrophobic environment that would facilitate the oxidative half reaction. In addition, a pre-docking of O_2 in the hydrophobic cleft would prevent competition between O_2 and water within the tunnel, optimizing the rate of re-oxidation of the flavin. This may explain why the turnover rates observed in the steady state are not achievable in the absence of the steroid. In summary, the presence of the putative oxygen tunnel in SCOA is consistent with an ordered sequential reaction mechanism as observed for the potential homologue SCOH.

3.3.4 Substrate oxidation

The mechanism of the oxidation reaction for cholesterol oxidase has been proposed to be either a single 2 electron hydride transfer mechanism or a radical mechanism involving two, 1 electron transfers (Vrielink et al., 1991). EPR studies support a single two electron hydride transfer mechanism for steroid oxidation (Medina et al., 1994; Medina et al., 1997). For simplicity, the discussion presented here will focus on a hydride transfer mechanism, however as a radical mechanism requires similar proximity constraints on the substrate relative to the FAD molecule there are some parallel requirements for the active site geometry.

3.3.4.1 Substrate position.

Flavin assisted oxidation reactions often involve the transfer of a hydride from the substrate to the N5 nitrogen atom of the isoalloxazine ring (Figure 1.9). The electrophilic molecular orbital of the FAD that accepts the 2 electrons from the transferred hydride ion is the lowest unoccupied molecular orbital (LUMO). A number of theoretical studies of isoalloxazine systems, have shown that the LUMO is a π–type molecular orbital with a large π like lobe on N5 (Breinlinger et al., 1998; Cavelier & Amzel, 2001; Trickey et al., 2000). For efficient hydride transfer, optimal orbital overlap would occur when the C-H bond of the substrate is directed towards the π–like "atomic" orbital on N5 of the FAD. This corresponds to positioning C3 of the steroid directly above or below the plane of the isoalloxazine and in a close proximity to N5. Similar substrate positioning has been shown to be a recurring feature of flavin enzymes involved in hydride transfer

mechanisms (Fraaije & Mattevi, 2000) as well as NAD(P)H-dependent dehydrogenase (Mesecar et al., 1997).

Contrary to the conserved substrate geometry observed for flavin enzymes, the steroid substrate in the BCO1 complex structure was bound such that the C3-H points toward the lone pair of electrons on N5 rather than the LUMO of the FAD (Figure 3.3A) (Li et al., 1993). This orbital is electron rich, hence not electrophilic, therefore efficient hydride transfer with substrate geometry as observed in the complex structure is unlikely. Interestingly, the structure of the BCO1/steroid complex was an outlier in Fraaije and Mattevi's study of hydride transfer geometry and led to the suggestion that the steroid in this structure may be positioned for isomerization (Fraaije & Mattevi, 2000). We propose however that the position of the substrate in the BCO1 complex structure is a result of the reduced state of the cofactor. In order to trap the substrate in the active site, Li and coworkers soaked the crystals in an oxygen free environment with an excess of substrate. This essentially resulted in a complex of steroid substrate and reduced enzyme, rather than the Michaelis complex (Li et al., 1993). There are considerable electronic differences between the oxidized and reduced isoalloxazine ring systems. Theoretical calculations carried out on an unbound isoalloxazine have shown that the additional charge in the reduced flavin is redistributed throughout the aromatic system with greater charge density on both O4 and O2 of the FAD (Breinlinger et al., 1998; Cavelier & Amzel, 2001; Trickey et al., 2000). Thus, it is not surprising that the additional charge in the reduced cofactor is stabilized by a hydrogen bond between O4 of the FAD and the hydroxyl group of the substrate as observed in the BCO1 complex structure (Figure

3.3A). The keto-steroid product of the enzymatic reaction would not form such an interaction.

Based on the assumption that the BCO1/steroid structure does not represent the true Michaelis complex for oxidation, we examined the structure in order to determine the optimal substrate binding position. Due to steric constraints, there are few alternate positions available to the steroid in the active site. The hydroxyl group of the steroid substrate might occupy a position similar to that of the bound water molecule (Wat541). Such a position would optimize hydrogen bonding geometries and may represent the true Michaelis complex (Figure 3.3B). The complete absence of water in the active site is supported by pulsed electron paramagnetic resonance studies of BCO1 where no significant changes in the hyperfine coupling were observed upon solvent exchange to $^{2}H_{2}O$ (Medina et al., 1997). The tight fit of the substrate in the active site almost exclusively determines the positioning of the steroid. All of the active site residues must be modeled in conformation A and some additional movement is necessary for residues Y446 and F444. Although these two residues were not observed in multiple conformations in the high resolution structure, both exhibit large anisotropic thermal parameters. Additionally, Y446 and F444 adopt different conformations in the BCO1/steroid complex structure, indicating movement upon substrate binding (Figure 3.1B). The fact that this substrate complex model is only possible when many binding site residues adopt only one alternate conformation reveals the extra information available from atomic resolution structures as the alternate conformations were not resolved in the 1.5 Å resolution structure. This observation is an elegant example of a substrate induced fit into a flexible active site.

(a)

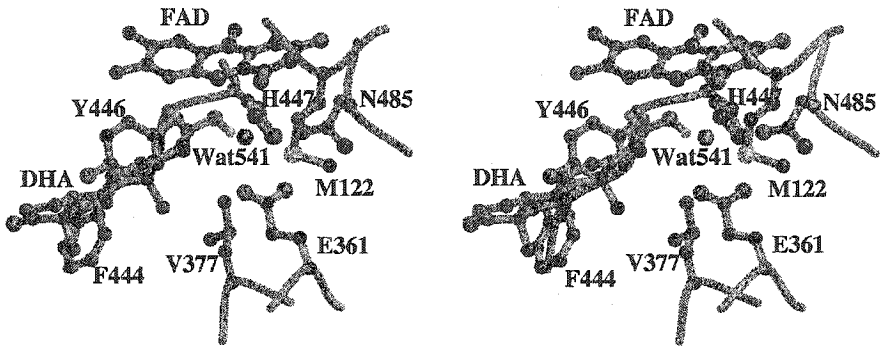

(b)

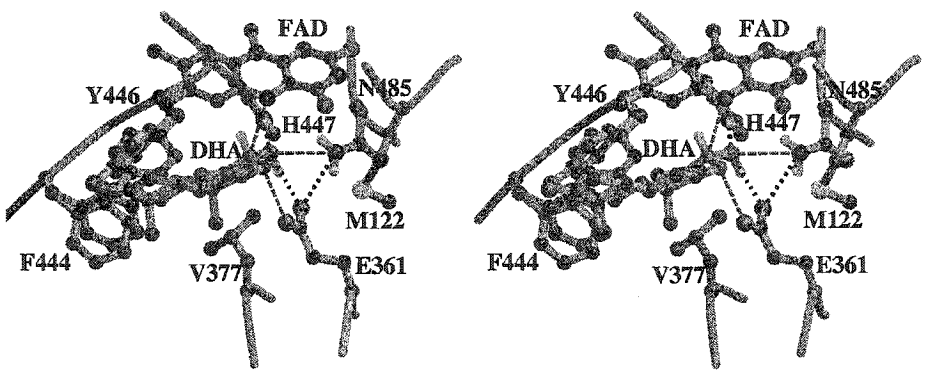

Figure 3.3. (a) Stereoscopic representation of the active site of the dehydroisoandosterone (DHA) complexed crystal structure of cholesterol oxidase (PDB accession code 1COY). The hydrogen atoms on the hydroxyl group of the steroid and the adjacent carbon atom (C3) have been modeled in expected geometrical positions and are represented in white. The hydrogen atom on C3, to be transferred to the flavin during oxidation of the steroid, is directed towards the lone pair of electrons on the FAD. (b) Stereoscopic representation of the active site with the newly interpreted substrate position. The residues shown in grey are in conformation A. Modeled positions are shown in green including the DHA molecule and the side chains of F444 and Y446. Close interactions are represented by dashed lines: those colored in black represent classical hydrogen bonding interactions and those in purple correspond to non-classical hydrogen bonding interactions.

Analysis of the new substrate bound model with the steroid hydroxyl group at the position of Wat541 reveals that the hydride donor atom (C3) is optimally placed for hydride transfer (Figure 3.3B). The C3 atom is positioned 3.1 Å from N5 of the FAD and at an angle of 122° with the plane of the isoalloxazine ring. The hydrogen atom is directed towards the LUMO lobe on the N5 atom of the FAD. This model agrees with the observed geometry among other flavin oxidase complex structures (Fraaije & Mattevi, 2000). Furthermore, the concerted positioning of the active site residues into conformation A upon substrate binding effectively closes the oxygen tunnel creating a sequestered active site (Figure 3.2A). This is a common feature for flavin dependant oxidases (Fraaije & Mattevi, 2000) and is likely to play an important role in facilitating hydride transfer by amplifying electrostatic interactions (Shan & Herschlag, 1993; Warshel & Aqvist, 1981)

3.3.4.2 General base catalysis?

Hydride transfer from a stable aliphatic carbon atom requires an activating environment. Some flavin oxidases have an active-site base that is proposed to deprotonate the substrate to activate it for hydride transfer, e.g., dihydroorotate dehydrogenase (Rowland et al., 1998) and acylCoA dehydrogenase (Rudik et al., 1998). Abstraction of a proton adjacent to the hydride donor atom results in increased electron density near the donor, thus facilitating hydride transfer from the β position. The atoms deprotonated in these enzymes are generally carbons adjacent to carbonyls. That is, atoms of low acidity (pK_a approx. 20), but sufficiently acidic that enzyme bases can deprotonate them. Other flavin oxidases preferentially bind the deprotonated form of

their substrate at their pH optima, for example, D-amino acid oxidase (Harris et al., 2001), L-amino acid oxidase (Pawelek et al., 2000), trimethylamine dehydrogenase (Basran et al., 2001), and vanillyl alcohol oxidase (Mattevi et al., 1997) and do not have an active-site base to form the deprotonated substrate. Sufficient concentrations of the deprotonated substrates of these enzymes are available in solution because the deprotonated atoms are heteroatoms with pK_a's in a physiological range or the electronic environment of the enzyme is able to perturb the pK_a to a physiological pH. However, there are a number of oxidases that fall in between these two extremes of mechanism, the substrates of which are carbons substituted with heteroatoms, for example, glycolate oxidase, flavocytochrome b_2 (lactate dehydrogenase), sarcosine oxidase and cholesterol oxidase. In the cases of glycolate oxidase and flavocytochrome b_2, the pK_a's of the heteroatoms are sufficiently high that adequate quantities of deprotonated substrate are unavailable in solution, however, it is still unclear whether the oxidation reactions proceed via hydride transfer or a covalent-FAD intermediate. This mechanistic ambiguity makes it difficult to assign the role of individual active site residues (Fitzpatrick, 2001). In the case of sarcosine oxidase, it is known that the substrate binds in the protonated, i.e., zwitterionic, form. However, the most promising candidate residue for active-site base, H269, is not a base, but rather serves to position the substrate relative to the flavin cofactor (Zhao et al., 2002).

In the case of SCOA and BCO1, Vrielink and coworkers proposed that H447 facilitates the oxidation reaction for cholesterol oxidase by abstracting the hydroxyl proton from the steroid during hydride transfer Figure 3.4a (Li et al., 1993). This proposal was supported by the high conservation of this histidine among the glucose-methanol-

choline (GMC) oxidoreductase family that includes cholesterol oxidase and glucose oxidase (Cavener, 1992). Furthermore a number of single point mutants of H447 in SCOA have indicated that this residue is important for the oxidative activity (Kass & Sampson, 1998b; Yamashita et al., 1998; Yue et al., 1999). Analogous histidine mutants in glucose oxidase also demonstrate a critical role for this residue (Wohlfahrt et al., 1999) Moreover, kinetic isotope and pH effects support the importance of this residue for $FADH^-$ oxidation by O_2 in the reaction catalyzed by glucose oxidase (Su & Klinman, 1999).

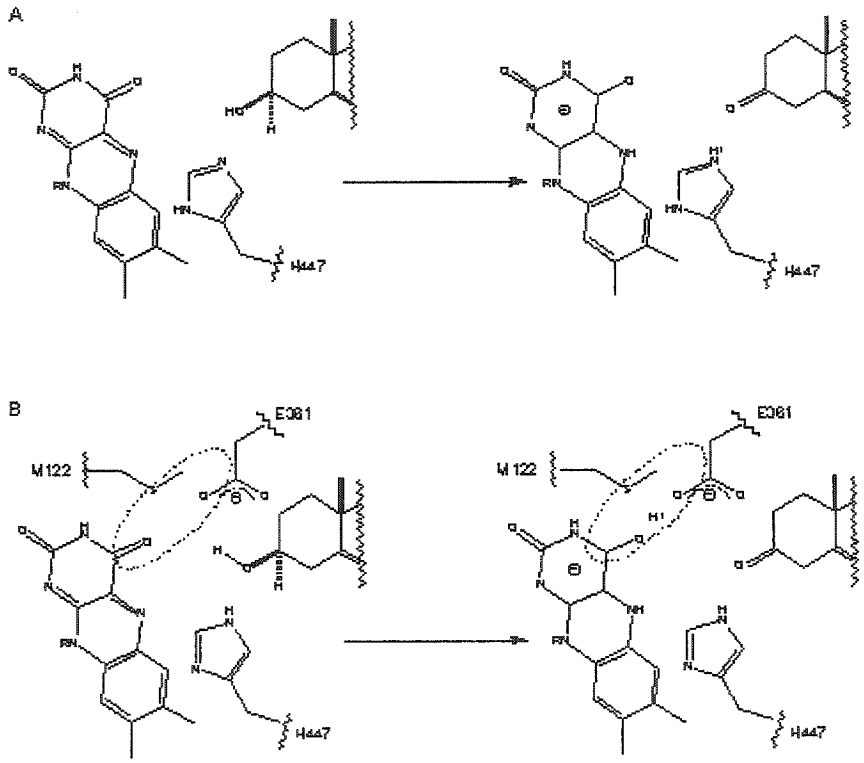

Figure 3.4 Schematic of the oxidation reaction mechanisms

If this residue were to act as the base, the hydrogen atom on the imidazole NE2 must be absent. Initially, the atomic resolution structure of cholesterol oxidase was pursued in order to observe the protonation state of H447 as a function of pH. The

structure clearly reveals hydrogen density for many main chain and side chain atoms. For the imidazole ring of H447, hydrogen atoms are strongly visible for CD1, whereas no density is present near ND1 indicating the absence of a hydrogen atom at this position. Weaker density is seen near CE1 and NE2 (Figure 3.5a) suggestive of the presence of hydrogen atoms on these two atoms, however they exhibit larger anisotropic temperature parameters than other atoms in the imidazole ring (Figure 3.5b). This apparent flexibility results in the weaker electron density peaks for hydrogen atoms bound to CE1 and NE2. Further evidence supporting the presence of a hydrogen atom on NE2 is apparent by examining the hydrogen bonding interactions around ND1 (Figure 3.5c). The structure reveals the ND1 atom of H447 involved in two strong hydrogen bonds with the side chain amide hydrogen atoms from N321 and N323. Indeed the hydrogen atoms on N321 and N323 are clearly observed in the electron density map. This bifurcated hydrogen bonding pattern fixes the imidazole ring within the structure and indicates the presence of a lone pair of electrons on ND1 of H447. If there were no hydrogen atoms on both ND1 and NE2 then H447 would be present as an anionic imidazolate. This is unlikely since an imidazolate is only expected in proteins when the side chain is ligated to an oxidized metal atom, although imidazolates have been proposed as reaction intermediates (Lodi & Knowles, 1991). Although our structure is of the unliganded enzyme, the hydrogen bonding network of H447 is identical in the BCO1 complex, indicating that NE2 is also protonated in the liganded structure, i.e., when water is removed from the active site. Moreover, it is difficult to envision how binding a hydrophobic steroid in the active site could sufficiently alter the pK_a of H447 to stabilize an imidazolate. These observations suggest that H447 may act as a hydrogen bond donor to O1' rather than an acceptor in the

reaction catalyzed by cholesterol oxidase. That is, H447 may serve to position the substrate with respect to the flavin and E361, the active site base for isomerization. This positioning is analogous to what has been deduced from structural and mutagenesis studies of the role of H269 in catalysis by sarcosine oxidase.

If NE2 of H447 remains protonated upon binding substrate, previous mechanistic experiments must be reinterpreted. Mutation of H447 to glutamine resulted in a 140-fold decrease in k_{cat} for oxidation (Kass & Sampson, 1998b) with no change in K_m for cholesterol. This reduction in activity indicates that H447 plays an important, but not essential, role in oxidation. In addition to H447, the active site of the enzyme contains a second basic residue, E361. Kass *et al.* proposed that E361 rescues the oxidative activity of H447Q (Kass & Sampson, 1998b). Studies of the H447Q/E361Q double mutant suggest that it does, but the amount of rescue is only 3–fold (Yin et al., 2002). X-ray crystallographic studies of the H447Q mutant place the NE2 atom of Q447 in a similar position in the active site to the NE2 atom of H447 (Yue et al., 1999). More importantly the expected position of the hydrogen atom on Q447-NE2 is similar to that on H447-NE2 (Figure 3.5d). This shows that glutamine can mimic the histidine protonated on NE2 as a hydrogen bond donor to O1' of the substrate and help position the substrate relative to the FAD. Unlike the wild-type enzyme, the H447Q mutant shows no kinetic isotope effect on hydride transfer. Thus mutation of H447 slows the rate of another step in the reaction besides hydride transfer. As mentioned earlier, the H447 homologue in glucose oxidase has been proposed to be important for the oxidative half–reaction in which O_2 oxidizes $FADH^-$ to FAD. The conservation of histidine at this position in the GMC

oxidoreductase family may be due to its ability to stabilize the 4a-hydroperoxy-flavin as proposed by Meyer and coworkers (Meyer et al., 1998) whose computational studies have indicated that a proptonated histidine in that position is the primary residue involved in the stabilization of such an adduct.

Umhau and coworkers proposed that oxidation of D-amino acid oxidase involves a concerted trans-elimination reaction with an anti-coplanar arrangement of the two sigma bond orbitals of the substrate involved in the reaction (Umhau et al., 2000). Such a trans-elimination mechanism has also been proposed for MCADH dehydrogenases (Ghisla et al., 1984; Pohl et al., 1986). An analogous mechanism can be envisaged for SCOA. The most energetically favorable position of the substrate hydroxyl hydrogen atom is trans to the leaving hydride atom. This conformation directs the hydrogen atom of O1' towards E361 and a lone pair of electrons towards H447 (Figure 3.3 and Figure 3.4b). The orbital interactions resulting from this conformation enable the O1'-H bonding electrons to delocalize into the antibonding orbital of the adjacent C3-H group, thereby destabilizing the bond and facilitating hydride transfer. The role of the hydrogen bond donor group at H447 would therefore assist in optimizing substrate geometry and thus orbital alignment. The importance of orbital overlap in SCOA is further supported by the structural and kinetic data showing that oxidative activity is critically affected by active site geometry (Yue et al., 1999).

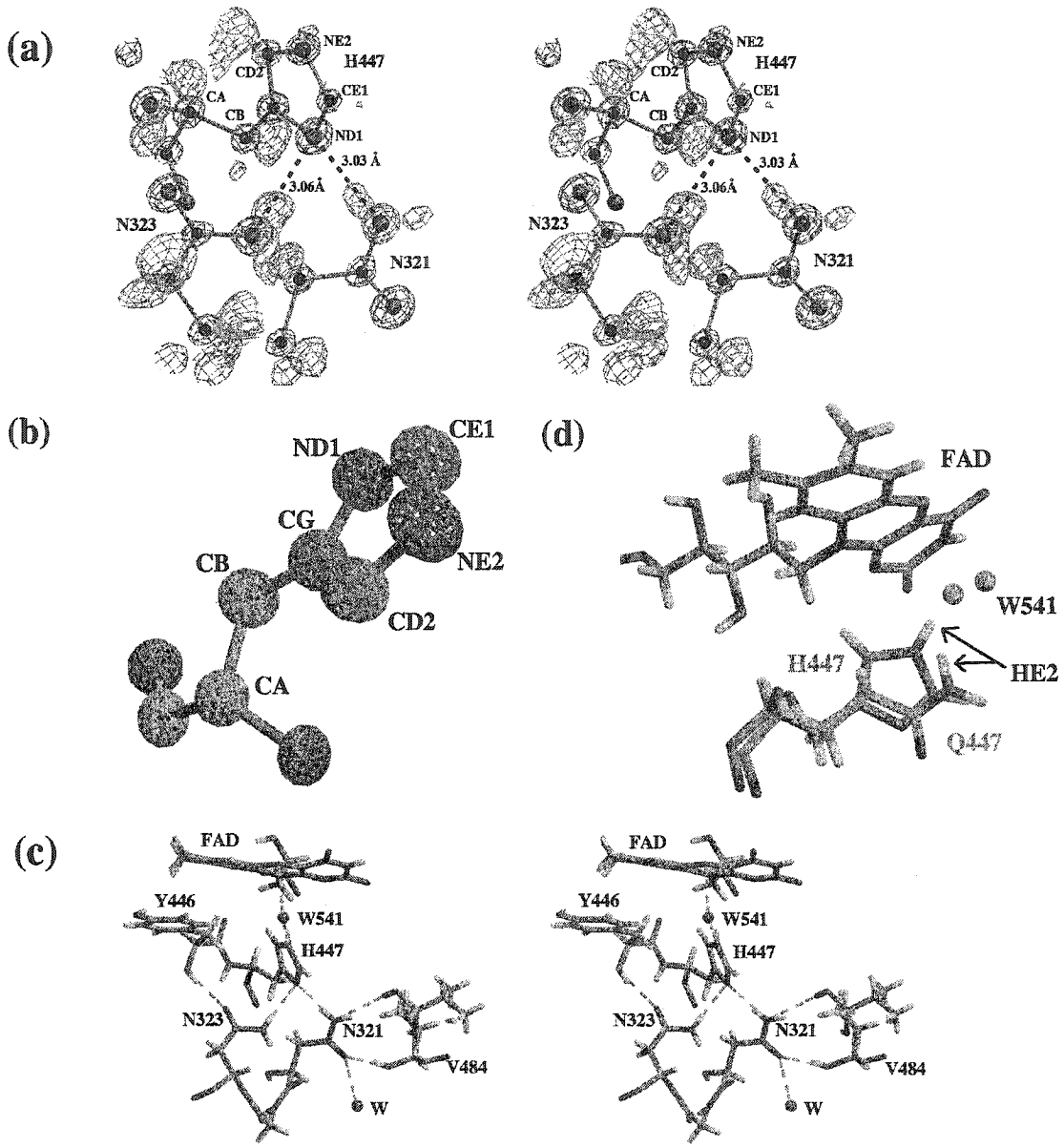

Figure 3.5. (a) Stereoscopic view of the electron density around H447. Green contours represent the Fo-Fc map contoured at 1.5 and magenta represents the SigmaA map contoured at 4 . (b) A representation of H447 showing the thermal ellipsoids plotted at a 50% probability level. (c) Stereoscopic representation of the hydrogen-bonding network around H447. (d) Superposition of residue H447 with the H447Q mutant structure (PDB accession codes 1CC2). The hydrogen atoms are shown in white. The hydrogen atoms for the H447Q structure were modeled in expected geometrical positions. The dashed lines represent hydrogen bonding interactions.

3.3.4.3 An electrostatic patch for general base catalysis.

The proton from O1' of cholesterol ultimately protonates the peroxy product of the oxidative half–reaction to form peroxide. There must, therefore, be a mechanism to transfer this proton from substrate to product. Aside from H447, the only other potentially basic residue in the active site that may act to facilitate hydride transfer is E361. This glutamate residue is optimally positioned to act as a general base catalyst for oxidation (Figure 3.3 and Figure 3.4b), however it is also the base for isomerization of cholest-5-en-3-one to cholest-4-en-3-one. Mutation of E361 to glutamine abolishes isomerization activity. Moreover, the E361Q mutant exhibits only a small decrease in k_{cat} for oxidation (30-fold lower than the wild-type enzyme) with a minimal effect on K_m (Sampson & Kass, 1997) suggesting that a carboxylic acid at this position is not crucial for oxidative activity. The crystal structure of the E361Q mutant revealed a slight mis-positioning of Wat541 (analogous to the position of the substrate hydroxyl), which may account for the reduced oxidation activity (PDB entry:1B8S) (Yue et al., 1999). Alternatively, the reduced rate may be due to rate–determining release of cholest-5-en-3-one, the wild–type reaction intermediate, from the enzyme. Furthermore, the double mutant, H447Q/E361Q, exhibits a 500-fold decrease in k_{cat} relative to the wild-type enzyme (Yin et al., 2002). Despite the significant damping of the oxidation activity, this double mutant it is only 3-fold less active than the H447Q mutant. These mutagenesis results indicate that the factors affecting the oxidation rate of the two separate mutants, H447Q and E361Q, are not entirely additive and may be the result of structural perturbations rather than the absence of an active site base. Interestingly, this double mutation to form a mutant with no "classical" active site bases, still does not completely

prevent hydride transfer suggesting that either the FAD is sufficiently electrophilic to oxidize the substrate without complete proton abstraction or that other active site features are involved in hydrogen atom abstraction, or both.

The micro-environment surrounding the active site may play an important role in decreasing the pKa for the substrate hydroxyl group, much like the trimethylamine pK_a is reduced by the protein environment in trimethylamine dehydrogenase (Basran et al., 2001). When the active site residues adopt conformation A necessary to accommodate the steroid, an electron rich patch is generated, composed of the side chain of E361, the lone pair electrons on the sulfur atom of M122 and O4 of the FAD (Figure 3.3b). The environment formed by this electrostatic patch would increase the basicity of E361 as well as decrease the pKa of the steroid hydroxyl group. Furthermore, the sequestered hydrophobic environment in SCOA amplifies the stabilization gained from this electrostatic patch. It is attractive to speculate that the electrostatic patch acts as a hydrogen accepting network facilitating the movement of the hydroxyl proton from E361 to O4.This movement regenerates a basic E361 necessary for the isomerization reaction and retains the hydroxyl proton in the active site for the oxidative half reaction.

The importance of the methionine in the redox reaction it is supported by the crystal structure and reactivity profile for the structural homologue hydroxynitrile lyase, PaHNL1 (Dreveny et al., 2001) (PDB entry: 1JU2). A superposition of the active site region of the lyase with cholesterol oxidase reveals a remarkably similar architecture (Figure 3.6) with structural conservation of all key active site residues except M122. Interestingly, unlike cholesterol oxidase and glucose oxidase, PaHNL1 is unable to oxidize alcohols. This suggests that features in the active site of cholesterol oxidase and

glucose oxidase, not present in PAHNL1, are necessary for oxidative activity. Within the PaHNL1 sub-family the M122 the position of SCOA is replaced by a valine residue (Dreveny et al., 2001). Among the glucose oxidase structures, this position is either a serine or threonine (Hecht et al., 1993; Wohlfahrt et al., 1999). Serine, threonine and methionine all have polarizable atoms with lone pairs of electrons. Perhaps the absence of such functionality at this position results in the inability of the PaHNL1 lyases to oxidize alcohols despite similar active site architecture. Further mutagenesis work is needed to elucidate the role of M122 in oxidation.

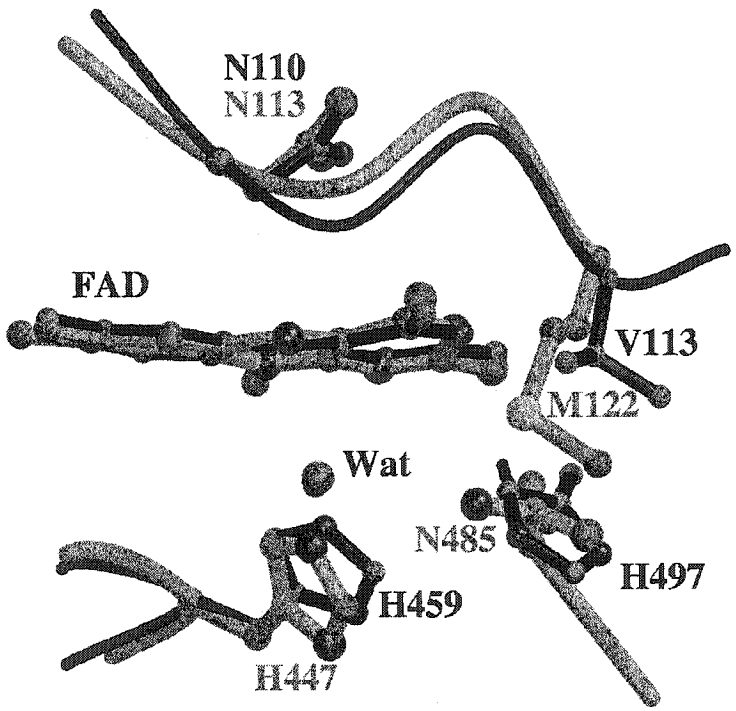

Figure 3.6. Superposition of the crystal structures of cholesterol oxidase from *Streptomyces* and hydroxylnitrile lyase (PDB accession codes 1JU2). The atoms of the isoalloxazine ring of FAD were used to superimpose the two structures. Cholesterol oxidase is shown in grey and the lyase is shown in black. Both structures have a water molecule (shown as a red sphere) bound in an identical position relative to the FAD.

3.3.5 Isomerization

After oxidation of the substrate and reduction of the flavin, the intermediate, cholest-5-en-3-one undergoes isomerization to cholest-4-en-3-one (Figure 1.9). This reaction is not rate limiting for the wild type enzyme and involves proton abstraction by E361 (Kass & Sampson, 1998a; Sampson & Kass, 1997; Yamashita et al., 1998). The positioning of the keto-steroid relative to E361 is thus critical for the isomerization reaction. Our proposed model for the Michaelis complex for oxidation positions the substrate C4 atom in an ideal geometry for proton abstraction by E361 (Figure 3.3b). However, this complex does not represent the Michaelis complex necessary for isomerization since, after oxidation, the steroid C3 position changes its hybridization state from sp^3 to sp^2. In order to maintain ideal hydrogen bond geometry around O1` we believe that the position of the steroid ring system is adjusted after oxidation. Evidence for conserving the position of O1` is implied by the changes observed in the isomerization activity for H447E and H447Q mutants, in which the glutamate mutation results in a 9–fold decrease in k_{cat} while the glutamine mutation exhibits a 1.3–fold increase (Kass & Sampson, 1998b). Thus the presence and position of a hydrogen bond donor at the 447 position appears to be important for the isomerization reaction. In addition to H447, there are two other potential hydrogen bond donors in relatively close proximity: N485 and H-N5 of the reduced FAD. The presence of multiple hydrogen bond donors in the vicinity of the steroid carbonyl oxygen would aid in positioning the steroid and would lower the pK_a of the steroid C4 atom facilitating proton abstraction. Similar hydrogen bonding interactions have been shown to affect the pK_a of the α carbon atom in

acylCoA dehydrogenases, (Thorpe & Kim, 1995; Vock et al., 1998) and in dihydroorotate dehydrogenase (Rowland et al., 1998), as well as the reaction analogue ketosteroid isomerase (Cho et al., 1998).

3.3.6 Gating of the tunnel

In addition to the structural shift proposed for the steroid upon oxidation, the surrounding residues are also likely to move in order to accommodate the keto-intermediate and stabilize the reduced cofactor. Earlier, we proposed that N485 stabilizes the reduced FAD through a hydrogen bond interaction with the π system of the pyrimidine ring (Yin et al., 2001). The multiple side chain positions of N485 and the observed 76mV decrease in redox potential for the N485L mutant supports our proposal that this residue stabilizes the reduced flavin. We propose that N485 initially adopts conformation A (substrate binding conformation) and, after flavin reduction, the side chain moves to conformation B where a hydrogen bond is formed with the pyrimidine ring of the cofactor thereby stabilizing the increased electron density of the flavin.

The stabilization afforded to the reduced flavin by the asparagine side chain also triggers gating of the oxygen tunnel to the active site since many of the active site residue conformations are correlated. Access to the tunnel from the bulk solvent is dependent on the side chain conformations adopted by M122, F359, N485 and E361 (Figure 3.2). The side chain of F359 adopts two distinct alternate conformations separated by a 65° rotation of the benzene group. When F359 is modeled in conformation A, the gate is closed maximizing hydrophobic packing interactions. When F359 is modeled in conformer B, the tunnel becomes solvent accessible. When N485 also adopts conformation B, four

water molecules are observed in this segment of the tunnel, however when in conformation A, there is no space to accommodate these water molecules. The refined conformer populations of both F359 and N485 are correlated with each other ($F359_{confA}$ is 58.4 % and $N485_{confA}$ is 65.1 %). Although F359 has room to adopt conformation B when N485 is positioned in conformation A, the strong correlation of populations suggest it is more energetically favorable for the gate to remain closed. Thus F359 acts as a valve that is gated by the movement of N485.

In addition to F359 the conformation of M122 is correlated to that of N485 (Figure 3.7a). The methyl group of M122 is observed in two positions: one directed towards O4 of the flavin (conformation B) and the other directed into the hydrophobic tunnel (conformation A). Interestingly, the position of M122 in conformation A sterically restricts the side chain of N485 to conformation A. However when N485 is in conformation A no steric constraints are evident on M122. The opposite constraints are observed when N485 is in conformation B; specifically, M122 is constrained to conformation B. However when M122 is in conformation B no steric constraints are observed on the side chain of N485. This arrangement of conformations is analogous to two adjacent swinging doors that overlap with each other. Pushing on either side of the doors open the gate however the gate will not open if both doors are pushed from opposite directions at the same time (Figure 3.7b). Such a correlated movement of side chains could be considered as a functional mechanism for sequestering the active site. Binding of the steroid results in a rotation of the methyl group of M122 from conformation B to A in order to prevent repulsive steric interactions (Figure 3.1b). This in turn pushes N485 to conformation A sealing the tunnel and creating an ideal

environment for oxidation. Conversely, after substrate oxidation, a driving force to reopen the tunnel would be generated by the energy gained from the strong hydrogen bond formed when N485 moves to conformation B near the flavin thereby forcing M122 to conformation B which in turn destabilizes the binding of the oxidized product. In summary, the proposed gating mechanism for the hydrophobic tunnel depends on the state of the enzyme; the Michaelis complex closes the hydrophobic tunnel and the reduced enzyme triggers the re-opening of the tunnel and the enzyme's readiness for re-oxidation.

(a)

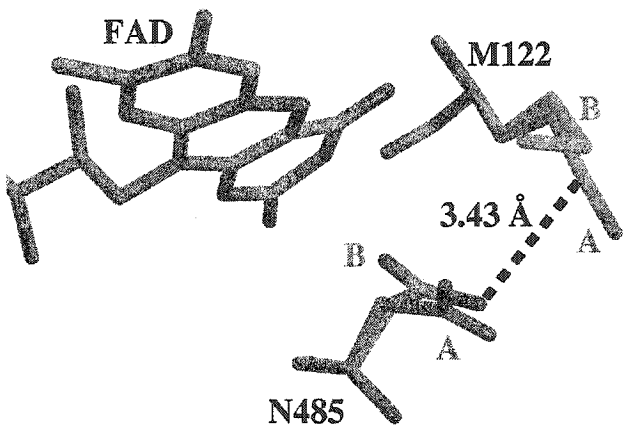

(b)

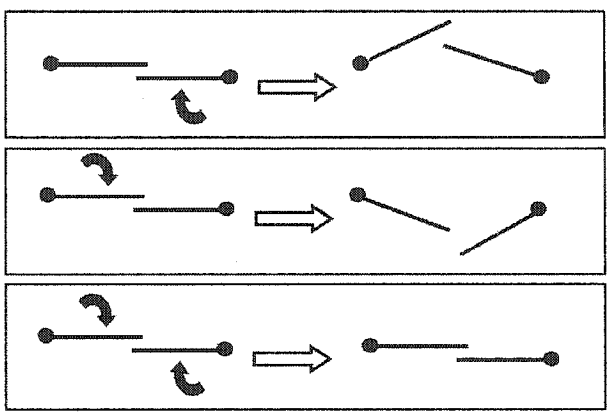

Figure 3.7. The relationship between alternate conformations of the side chains of M122 and N485. (a) The side chain A conformation is shown in grey and the B conformation is shown in pink. The steric clash resulting from the combination of conformer A for M122 and conformer B for N485 is shown by a dashed line. (b) Cartoon representation of the overlapped swinging door mechanism that gates the hydrophobic tunnel. The doors will move when a force is applied from either side but no movement is possible when a force is exerted simultaneously from both sides.

One significant disparity of this gating mechanism is that the 5-cholesten-3-one intermediate would be expelled from the active site if the isomerization reaction does not occur before the oxidative half reaction. The architecture of the active site requires that the O1' atom of the steriod be displaced from its proposed binding position to allow molecular oxygen to be in a similar reactive position relative to the FAD. However, any movement of the intermediate away from this binding position results in an unfavorable geometry for isomerization (Figure 3.3b). Thus, it is more likely that isomerization occurs before the oxidative half reaction, requiring that the combined rate of the tunnel opening and molecular oxygen movement is sufficiently slower than the rate of isomerization. This proposed mechanism of isomerization before flavin re-oxidation is in agreement with the mutagenesis study of E361D, which exhibits much slower isomerization activity to the wild type (Kass & Sampson, 1998a). One would expect this mutant to release the cholest-5-en-3-one intermediate before isomerization occurs. Indeed, HPLC analysis of the reaction products for the E361D mutant have shown that the cholest-5-en-3-one intermediate is released into the reaction medium and then slowly rebound by the enzyme and converted to the product. Based on the proposed gating mechanism, a pre-reduced enzyme would favor the tunnel open state (conformation B) and thus hinder the correct intermediate orientation necessary for isomerization. This may explain the reduced efficiency of isomerization observed for the pre-reduced enzyme of the SCOH homologue to SCOA (Pollegioni et al., 1999). These results support the dynamic nature of the gating mechanism triggered by the reduction of the flavin.

3.3.7 Oxidative half-reaction

The oxidative half reaction of cholesterol oxidase involves re-oxidation of the flavin by molecular oxygen, forming H_2O_2 (Figure 1.9). Flavin monooxygenases have been shown to form a flavin 4a-hydroperoxide intermediate upon reaction with O_2 (Ghisla & Massey, 1989; Massey, 1994). The adduct can be artificially generated in GOX using pulse radiolysis (Massey et al., 1988) indicating that the enzyme is capable of forming such a species. Computational studies of GOX have indicated that the conserved histidine residue among the GMC oxidoreductase family is the primary active site residue involved in stabilization of a 4a-hydroperoxy-flavin (Meyer et al., 1998). Modeling studies have shown that the most stable tautomer for the active site of the 4a-hydroperoxy-flavin involves a hydrogen bond interaction with a proton donor NE2-H516. The hydrophobic tunnel observed in the SCOA structure leads directly towards the re-face of the isoalloxazine and the C4a atom of the FAD supporting a similar mechanism for SCOA. In SCOA, H447 is able to donate a hydrogen bond to stabilize a flavin 4a-hydroperoxide intermediate. The oxidative half reaction occurs very rapidly, thus no flavin-peroxide adduct has been detected by ESR and ENDOR techniques (Medina et al., 1994). In addition, no measurable semiquinone formation was detected. Furthermore, there is no evidence for the formation of a flavin semiquinone or a reduced enzyme-oxygen complex for GOX using similar spectroscopic techniques (Su & Klinman, 1999). Despite the lack of experimental evidence, flavin 4a-hydroperoxide intermediates have been proposed for oxidases and the recent observation of a putative flavin 4a-hydroperoxide species in the

x-ray crystal structure of D-amino acid oxidase supports this analogy to the re-oxidation mechanism observed for monooxygenases (Umhau et al., 2000).

The mechanistic conclusions presented in this structural study of SCOA, combined with the extensive kinetic data and mutagenesis studies of the enzyme, may be useful in identifying a 4a-hydroperoxy-flavin intermediate. The oxidative half reaction is not rate limiting for wild type SCOA. Deuterium labeling experiments using 3α-[^{2}H]cholesterol revealed a isotope effect of 2.2 for both k_{cat} and k_{cat}/K_m with the wild type enzyme, indicating 3α-hydrogen-carbon bond breakage, and not flavin re-oxidation, is rate determining. Unlike wild type, no primary isotope effect was observed for the H447Q mutant indicating that another step in the mechanism has become rate limiting. The unchanged K_m and the increased isomerization activity suggest that the re-oxidation of the flavin could be the rate determining step for this mutant. The small solvent isotope effect (V_{H2O}/V_{D2O} = 1.3(1)) observed for the H447Q mutant (Kass & Sampson, 1998b) could be linked to either the formation of an enzyme-O_2 complex or subsequent steps in the re-oxidation of the flavin. Structural comparisons of the wild type enzyme and the mutant show that the hydrogen bond donor group of the mutant is shifted away from the flavin (Figure 3.5d), resulting in a less ideal hydrogen bond geometry with the 4a-hydroperoxy-flavin. These considerations suggest that further ESR and ENDOR experiments with the H447Q mutant of SCOA could perhaps identify a longer-lived peroxide adduct.

3.4 Conclusions

This atomic resolution structure of SCOA has revealed novel features relating to the dynamic aspects of the protein. These studies have shown that protein dynamics plays a fundamental role in catalysis by cholesterol oxidase. Furthermore, based on these observations we have had a unique opportunity to reinterpret the mechanistic details for this enzyme. Specifically, we have shown that the conformational populations of side chains in the region of the active site result in the appearance of a narrow hydrophobic tunnel, not seen in lower resolution structures. This tunnel is proposed to act as the entry point for molecular oxygen to the active site during the oxidative half reaction. The tunnel is gated by residues proposed to play important mechanistic roles in substrate positioning, oxidation, and isomerization, as well as tuning the redox state of the cofactor. Furthermore, the atomic resolution structure has revealed the location of hydrogen atoms on H447, a residue that was previously proposed to act as the active site base for oxidation and that is now proposed to orient the substrate with respect to the cofactor. This has resulted in a reanalysis of the role of this histidine in the mechanism and a new model for both substrate position and substrate oxidation. These studies demonstrate how an atomic resolution structure provides novel insight into the conformational space available to protein side chains and how the anisotropic thermal parameters can be evaluated to provide an understanding of residue and domain movements.

3.5 MATERIALS AND METHODS

3.5.1 Crystallization, data collection and processing

Crystals of cholesterol oxidase were obtained as described previously (Yue et al., 1999). A single crystal of dimensions 0.16 x 0.16 x 0.05 $Å^3$ was briefly transferred from the mother liquor (11% (w/v) poly(ethyleneglycol) (PEG) MW 8000, 75mM $MnSO_4$, and 100 mM sodium cacodylate, pH 5.2) to a cryo protectant solution (20 % (v/v) in the mother liquor). The crystal was rapidly frozen in a stream of nitrogen gas at 100K. The diffraction data were collected on an ADSC Q4 CCD detector using a synchrotron source at wavelength 0.978 Å (beamline X8C at NSLS, Brookhaven National Laboratory). A complete dataset to 0.95 Å resolution was obtained using two sweeps. The first sweep was measured using longer exposure times in order to optimize the high resolution intensities. The second sweep was measured using a shorter exposure time in order to obtain the low resolution data. The data were processed using the HKL suite of software (Minor, 1993; Otwinowski, 1993; Otwinowski & Minor, 1997) (Table 3.1).

3.5.2 Structure refinement

The atomic resolution structure was refined using the previously solved 1.5 Å resolution structure (PDB code: 1b4v) which had been modified such that all active site water molecules, the FAD molecule and surface water molecules were removed. In addition, the proposed catalytic residues, E361, H447 and N485 were mutated to alanine residues. The refinement was carried out using a restrained conjugate gradient least-

squares algorithm as implemented in the program SHELXL97 (Sheldrick & Schneider, 1997). The default stereochemical restraints were applied to bond lengths, bond angles, chiral volumes and planer groups during the refinement. Additional restraints were applied to the temperature factors of bonded atoms and to solvent molecules, which exhibited high anisotropy.

Manual modeling was carried out using the program XFIT (McRee, 1999) and sigmaA-weighted maps calculated by SHELXPRO with coefficients 2Fo-Fc and Fo-Fc (Sheldrick & Schneider, 1997). The free R-factor was monitored during the refinement using a randomly chosen subset of 5 % of the data (13180 reflections). The initial model was refined with isotropic temperature factors. During the final stages of refinement anisotropic temperature were applied to the non-hydrogen atoms.

The higher resolution data enabled us to resolve multiple conformations for 83 residues (an additional 71 residues from the previously published 1.5 Å structure of the native enzyme (PDB ID: 1b4v). Multiple conformations were observed for 3 surface loops: residues 47-50; 186-188; 256-260. Despite the improved resolution, poor density was still observed for 14 surface residues (73, 87, 127, 156, 163, 183, 241, 273, 365, 396, 398, 435, 436, 468, 507) whose side chains were modeled with either 50 % or 0 % occupancy. Only the backbone amide nitrogen atom of residue 499 was visible in the electron density and modeled. As observed for the 1.5 Å structure, 3 residues (6 - 8) at the N terminus and 2 residues (508 - 509) at the C terminus were disordered and excluded from the model.

Water molecules were added into positive difference density and where hydrogen bond contacts were made to polar atoms. A few exceptions, where persistent difference

density near aromatic rings were observed, were also modeled as water molecules. Seventy two additional water positions were identified when compared to the 1.5 Å structure. Since the occupancy of a water molecule is strongly correlated with its thermal parameter, they were typically modeled with full occupancy. However, if a water molecule was found to be associated through a hydrogen bond network with a multiple conformation residue then is was assigned occupancy of either 75% or 50% or 25% depending on the occupancy of the conformation of the residue to which it is associated. The occupancies of the water molecules in the region of the active site were coupled to those of the surrounding residues, M122, F359, E361 and N485. Hydrogen bonding geometry and steric considerations were used to correlate the association of partially occupied waters and alternate residue side chain conformations. The electron density surrounding the key active site water molecule, Wat541, is triangular, and the anisotropy of its temperature factor suggests that this density shape is the result of alternate positions. Given the number of residues with alternate conformers in the active site, multiple conformations for Wat541 are also expected, however an accurate model of these alternate water positions was not justified due to the lack of definition in the electron density. The correlation between alternate side chain positions for different residues was determined by applying the same principles as used to associate the active site water molecules to their respective residue conformer. Alternate side chain positions that were likely to co-exist were assigned the same part number (i.e. conformation A or B). Many alternate conformations were identified before anisotropic refinement was carried out, however subsequent improvement of the electron density maps enabled lower occupancy conformers to be modeled. In order to remove bias in the temperature factor

each additional residue conformation was first refined isotropically and then allowed to refine anisotropically.

Hydrogen atoms were included after aniostropic refinement and modeling of the alternate conformations. Although over 70 % of the backbone hydrogen atoms were observed, the amount of experimental data does not warrant their positional refinement. Thus, all hydrogen atoms were added such that their positions ride on the associated hetero atom. Hydrogen atoms that reside on hydroxyl groups (serine, threonine and tyrosine side chains) were automatically placed using a SHELX-97 algorithm that first fixes the hydrogen atom distance and angle and then searches around that defined cone for the maximum electron density peak, placing the hydrogen atom at that position. Although this method was quite successful in locating the correct or reasonable positions for most hydroxyl groups a number of examples were observed where the hydrogen atom position required rotation to prevent un-favorable interactions with other residues.

A di-oxygen molecule was modeled in the active site tunnel with a fixed occupancy of 25%. The identification of this species is not certain as the observed density may also represent two alternate water conformations. However, both positions require the adjacent active site residues to be present in conformer B. Furthermore these positions are approximately 1.2 Å from each other suggestive of a di-oxygen molecule.

A two fold relaxation of the default restraints failed to improve the crystallographic R_{free}-factor thus the refinement was pursued with the original values. No restraints were applied to the FAD cofactor. Upon completion of the refinement, an additional10 cycles were performed using all data. Standard deviations for the coordinates were estimated using the full-matrix inversion method (Sheldrick & Schneider, 1997). The final R_{free}-

factor and *R*-factors calculated before inclusion of all the reflections is 13.2% and 11.0% respectively. The final *R*-factor including all of the data is 11.0%. The coordinates have been deposited in the Protein Data Bank, PDB code: 1MXT (Berman et al., 2000).

3.6 Acknowledgement

We thank Nathalie Croteau for crystallization of the enzyme and Rene Coloumbe, Joseph Lauher, and Frank Fowler for useful discussions. This work is supported by the National Institutes of Health Grant GM63262 (A.V.) and HL53306 (N.S.S.) and Canadian Institutes of Health Research Grant MT-13341 (A.V.).

3.7 REFERENCES

Aparicio, J. F., Fouces, R., Mendes, M. V., Olivera, N. & Martin, J. F. (2000). A complex multienzyme system encoded by five polyketide synthase genes is involved in the biosynthesis of the 26-membered polyene macrolide pimaricin in *Streptomyces* natalensis. *Chem Biol* **7**(11), 895-905.

Basran, J., Sutcliffe, M. J. & Scrutton, N. S. (2001). Optimizing the Michaelis complex of trimethylamine dehydrogenase: identification of interactions that perturb the ionization of substrate and facilitate catalysis with trimethylamine base. *Journal of Biological Chemistry* **276**(46), 42887-42892.

Berman, H. M., Westbrook, J., Feng, Z., Gilliland, G., Bhat, T. N., Weissig, H., Shindyalov, I. N. & Bourne, P. E. (2000). The Protein Data Bank. *Nucleic Acids Research* **28**, 235-242.

Breinlinger, E. C., Keenan, C. J. & Rotello, V. M. (1998). Modulation of Flavin Recognition and Redox Properties through Donor Atom-Interactions. *Journal of American Chemical Society* **120**(34), 8606-8609.

Cavelier, G. & Amzel, L. M. (2001). Mechanism of NAD(P)H:quinone reductase: Ab initio studies of reduced flavin. *Proteins* **43**(4), 420-32.

Cavener, D. (1992). GMC oxidoreuctases. A newly defined family of homologous proteins with diverse catalytic activities. *J. Mol. Biol.* **223**, 811-814.

Chang, F. C. & Swenson, R. P. (1999). The midpoint potentials for the oxidized-semiquinone couple for Gly57 mutants of the Clostridium beijerinckii flavodoxin correlate with changes in the hydrogen-bonding interaction with the proton on N(5) of the reduced flavin mononucleotide cofactor as measured by NMR chemical shift temperature dependencies. *Biochemistry* **38**(22), 7168-76.

Cho, H.-S., Choi, G., Choi, K. Y. & Oh, B.-H. (1998). Crystal structure and enzyme mechanism of Δ^5-3-ketosteroid isomerase from *Pseudomonas testosteroni*. *Biochemistry* **37**, 8325-8330.

Corbin, D. R., Grebenok, R. J., Ohnmeiss, T. E., Greenplate, J. T. & Purcell, J. P. (2001). Expression and chloroplast targeting of cholesterol oxidase in transgenic tobacco plants. *Plant Physiol.* **126**, 1116-1128.

Coulombe, R., Yue, K. Q., Ghisla, S. & Vrielink, A. (2001). Oxygen access to the active site of cholesterol oxidase through a narrow channel is gated by an Arg-Glu pair. *Journal of Biological Chemistry* **276**(30435-30441).

Dreveny, I., Gruber, K., Glieder, A., Thompson, A. & Kratky, C. (2001). The hydroxynitrile lyase from almond: a lyase that looks like an oxidoreductase. *Structure* **9**(9), 803-815.

Dwyer, T. M., Mortl, S., Kemter, K., Bacher, A., Fauq, A. & Frerman, F. E. (1999). The intraflavin hydrogen bond in human electron transfer flavoprotein modulates redox potentials and may participate in electron transfer. *Biochemistry* **38**(30), 9735-45.

Eriksson, M., Jordan, A. & Eklund, H. (1998). Structure of *Salmonella typhimurium nrdF* ribonucleotide reductase in its oxidized and reduced forms. *Biochemistry* **37**(13359-13369).

Fitzpatrick, P. F. (2001). Substrate dehydrogenation by flavoproteins. *Acc. Chem. Res.* **34**(4), 299-307.

Fraaije, M. W. & Mattevi, A. (2000). Flavoenzymes: diverse catalysts with recurrent features. *Trends Biochem. Sci.* **25**, 126-132.

Gadda, G., Wels, G., Pollegioni, L., Zucchelli, S., Ambrosius, D., Pilone, M. S. & Ghisla, S. (1997). Characterization of cholesterol oxidase from *Streptomyces hydroscopicus* and *Brevibacterium sterolicum*. *Eur. J. Biochem.* **250**, 369-376.

Ghisla, S. & Massey, V. (1989). Mechanism of flavoprotein-catalysed reactions. *Eur. J. Biochem.* **181**, 1-17.

Ghisla, S., Thorpe, C. & Massey, V. (1984). Mechanistic studies with general acyl-CoA dehydrogenase and butyryl-CoA dehydrogenase: evidence for the transfer of the beta-hydrogen to the flavin N(5)-position as a hydride. *Biochemistry* **23**(14), 3154-61.

Harris, C. M., Pollegioni, L. & Ghisla, S. (2001). pH and kinetic isotope effects in D-amino acid oxidase catalysis. *Eur J Biochem* **268**(21), 5504-5520.

Hasford, J. K., W.; Rizzo, C. J. (1997). Conformational effects on Flavin Redox Chemistry. *Journal of Organic Chemistry* **62**(16), 5244-5245.

Hecht, H. J., Kalisz, H. M., Hendle, J., Schmid, R. D. & Schomburg, D. (1993). Crystal structure of glucose oxidase from *Aspergillus niger* refined at 2.3 A resolution. *J Mol Biol* **229**(1), 153-72.

Ishizaki, R., Hirayama, N., Shinkawa, H., Nimi, O. & Murooka, Y. (1989). Nucleotide sequence of the gene for cholesterol oxidase from a *Streptomyces* sp. *J. Bacteriol.* **171**(1), 596-601.

Iwata, S., Ostermeier, C., Ludwig, B. & Michel, H. (1995). Structure at 2.8-Ångstrom Resolution of Cytochrome C Oxidase from *Paracoccus Denitrificans*. *Nature* **376**(N6542), 660-669.

Kass, I., J. & Sampson, N. S. (1998a). The importance of Glu^{361} position in the reaction catalyzed by cholesterol oxidase. *Bioorganic and Medicinal Chemistry Letters* **8**, 2663-2668.

Kass, I. J. & Sampson, N. S. (1995). The isomerization catalyzed by *Brevibacterium sterolicum* cholesterol oxidase proceeds stereospecifically with one base. *Biochem. Biophys. Res. Commun.* **206**(2), 688-693.

Kass, I. J. & Sampson, N. S. (1998b). Evaluation of the role of His447 in the reaction catalyzed by cholesterol oxidase. *Biochemistry* **37**(51), 17990-18000.

Li, J., Vrielink, A., Brick, P. & Blow, D. M. (1993). Crystal structure of cholesterol oxidase complexed with a steroid substrate: Implications for flavin adenine dinucleotide dependent alcohol oxidases. *Biochemistry* **32**, 11507-11515.

Lodi, P. J. & Knowles, J. R. (1991). Neutral imidazole is the electrophile in the reaction catalyzed by triosephosphate isomerase: structural origins and catalytic implications. *Biochemistry* **30**(28), 6948-6956.

MacLachlan, J., Wotherspoon, A. T. L., Ansell, R. O. & Brooks, C. J. W. (2000). Cholesterol oxidase: sources, physical properties and analytical applications. *Journal of Steroid Biochemistry and Molecular Biology* **72**, 169-195.

Massey, V. (1994). Activation of molecular oxygen by flavins and flavoproteins. *J Biol Chem* **269**(36), 22459-62.

Massey, V., Schopfer, L. M. & Anderson, R. F. (1988). Structural determinants of the oxygen reactivity of different classes of flavoproteins. In *Progress in Clinical and Biological Research. Oxidases and Related Enzyme Systems; 4th International Symposium, Portland, Oregon, USA, October 4-8, 1987* (King, T. E., Mason, H. S. & Morrison, M. M., eds.), pp. 147-166. Alan Liss Inc., New York.

Mattevi, A., Vanoni, A. & Curti, B. (1997). Structure of D-amino acid oxidase: new insights from an old enzyme. *Curr. Opin. Struct. Biol.* **7**(6), 804-810.

McRee, D. E. (1999). XtalView/Xfit - A Versatile Program for Manipulating Atomic Coordinates and Electron Density. *J Structural Biology* **125**, 156-165.

Medina, M., Vrielink, A. & Cammack, R. (1994). ESR and electron nuclear double resonance characterization of the cholesterol oxidase from *Brevibacterium sterolicum* in its semiquinone state. *Eur J Biochem* **222**(3), 941-7.

Medina, M., Vrielink, A. & Cammack, R. (1997). Electron spin echo envelope modulation studies of the semiquinone anion radical of cholesterol oxidase from *Brevibacterium sterolicum*. *FEBS Lett* **400**(2), 247-51.

Mesecar, A. D., Stoddard, B. L. & Koshland, D. E., Jr. (1997). Orbital steering in the catalytic power of enzymes: small structural changes with large catalytic consequences. *Science* **277**(5323), 202-6.

Meyer, M., Wohlfahrt, G., Knablein, J. & Schomburg, D. (1998). Aspects of the mechanism of catalysis of glucose oxidase: a docking, molecular mechanics and quantum chemical study. *J Comput Aided Mol Des* **12**(5), 425-40.

Minor, W. (1993). XDISPLAYF Program, Purdue University.

Navas, J., Gonzalez-Zorn, B., Ladron, N., Garrido, P. & Vazquez-Boland, J. A. (2001). Identification and mutagenesis by allelic exchange of *choE*, encoding a cholesterol oxidase from the intracellular pathogen Rhodococcus equi. *J Bacteriol* **183**(16), 4796-805.

O'Farrell, P. A., Walsh, M. A., McCarthy, A. A., Higgins, T. M., Voordouw, G. & Mayhew, S. G. (1998). Modulation of the redox potentials of FMN in *Desulfovibrio vulgaris* flavodoxin: thermodynamic properties and crystal structures of glycine-61 mutants. *Biochemistry* **37**(23), 8405-16.

Ohta, T., Fujishiro, K., Yamaguchi, K., Tamura, Y., Aisaka, K., Uwajima, T. & Hasegawa, M. (1991). Sequence of gene *choB* encoding cholesterol oxidase of *Brevibacterium sterolicum*: comparison with *choA* of *Streptomyces* sp. SA-COO. *Gene* **103**, 93-96.

Otwinowski, Z. (1993). Oscillation data reduction program. In *Data collection and Processing: Proceedings of the CCP4 Study Weekend* (Sawyer, L., Isaccs, N. & Bailey, S., eds.), pp. 56-62. SERC Daresbury Laboratory, Warrington, U.K.

Otwinowski, Z. & Minor, W. (1997). Processing of X-Ray Diffraction Data Collected in Oscillation Mode. In *Methods in Enzymology* (Carter, C. W. J. & Sweet, R. M., eds.), Vol. 276, pp. 307-325. Academic Press, Boston.

Pawelek, P., Cheah, J., Coulombe, R., Macheroux, P., Ghisla, S. & Vrielink, A. (2000). The structure of L-amino acid oxidase reveals the substrate trajectory into an enantiomerically conserved active site. *EMBO Journal* **19**, 4204 – 4215.

Pohl, B., Raichle, T. & Ghisla, S. (1986). Studies on the reaction mechanism of general acyl-CoA dehydrogenase. Determination of selective isotope effects in the dehydrogenation of butyryl-CoA. *Eur J Biochem* **160**(1), 109-15.

Pollegioni, L., Wels, G., Pilone, M. S. & Ghisla, S. (1999). Kinetic mechanisms of cholesterol oxidase from *Streptomyces hygroscopicus* and *Brevibacterium sterolicum*. *Eur. J. Biochem.* **263**, 1-13.

Riistama, S., Puustinen, A., Garciahorsman, A., Iwata, S., Michel, H. & Wikstrom, M. (1996). Channelling of Dioxygen into the Respiratory Enzyme. *Biochimica Et Biophysica Acta-Bioenergetics* **1275**(N1-2), 1-4.

Rowland, P., Bjornberg, O., Nielsen, F. S., Jensen, K. F. & Larsen, S. (1998). The crystal structure of *Lactococcus lactis* dihydroorotate dehydrogenase A complexed with the enzyme reaction product throws light on its enzymatic function. *Protein Science* **7**(6), 1269-1279.

Rudik, I., Ghisla, S. & Thorpe, C. (1998). Protonic equilibria in the reductive half-reaction of the medium-chain acyl-CoA dehydrogenase. *Biochemistry* **37**(23), 8437-8445.

Sampson, N. S. & Kass, I. J. (1997). Isomerization, but not oxidation, is suppressed by a single point mutation, E361Q, in the reaction catalyzed by cholesterol oxidase. *J. Am. Chem. Soc.* **119**(5), 855-862.

Shan, S. O. & Herschlag, D. (1993). The change in hydrogen bond strength accompanying charge rearrangement: implications for enzymatic catalysis. *Proc. Natl. Acad. Sci. USA* **93**(25), 14474-14479.

Sheldrick, G. M. & Schneider, T. R. (1997). SHELXL: High-resolution refinement. In *Methods in Enzymology* (Carter, C. W. J. & Sweet, R. M., eds.), Vol. 277, pp. 319-343. Academic Press, Boston.

Shen, Z., Corbin, D. R., Greenplate, J. T., Grebenok, R. J., Galbraith, D. W. & Purcell, J. P. (1997). Studies on the mode of action of cholesterol oxidase on insect midgut membranes. *Archives of Insect Biochemistry and Physiology* **34**(4), 429-442.

Soulimane, T., Buse, G., Bourenkov, G. P., Bartunik, H. D., Huber, R. & Than, M. E. (2000). Structure and mechanism of the aberrant ba(3)-cytochrome c oxidase from *Thermus thermophilus*. *Embo Journal* **19**(N8), 1766-1776.

Stillman, T. J., Hempstead, P. D., Artymiuk, P. J., Andrews, S. C., Hudson, A. J., Treffry, A., Guest, J. R. & Harrison, P. M. (2001). The high-resolution X-ray crystallographic structure of the ferritin (EcFtnA) of *Escherichia coli;* comparison with human H ferritin (HuHF) and the structures of the Fe(3+) and Zn(2+) derivatives. *J. Mol. Biol.* **307**(2), 587-603.

Su, Q. & Klinman, J. P. (1999). Nature of oxygen activation in glucose oxidase from *Aspergillus niger*: the importance of electrostatic stabilization in superoxide formation. *Biochemistry* **38**(26), 8572-8581.

Thorpe, C. & Kim, J. J. (1995). Structure and mechanism of action of the acyl-CoA dehydrogenases. *Faseb J* **9**(9), 718-25.

Trickey, P., Basran, J., Lian, L. Y., Chen, Z., Barton, J. D., Sutcliffe, M. J., Scrutton, N. S. & Mathews, F. S. (2000). Structural and biochemical characterization of recombinant wild type and a C30A mutant of trimethylamine dehydrogenase from *methylophilus methylotrophus* (sp. W(3)A(1)). *Biochemistry* **39**(26), 7678-88.

Umhau, S., Pollegioni, L., Molla, G., Diederichs, K., Welte, W., Pilone, M. S. & Ghisla, S. (2000). The x-ray structure of D-amino acid oxidase at very high resolution identifies the chemical mechanism of flavin-dependent substrate dehydrogenation. *Proc Natl Acad Sci U S A* **97**(23), 12463-8.

Uwajima, T., Yagi, H., Nakamurs, S. & Terada, O. (1973). Isolation and crystallization of extracellular 3β-hydroxysteroid oxidase of *Brevibacterium sterolicum* nov. sp. *Agr. Biol. Chem.* **37**(10), 2345-2350.

Vock, P., Engst, S., Eder, M. & Ghisla, S. (1998). Substrate activation by acyl-CoA dehydrogenases: transition-state stabilization and pKs of involved functional groups. *Biochemistry* **37**(7), 1848-60.

Vrielink, A., Lloyd, L. F. & Blow, D. M. (1991). Crystal structure of cholesterol oxidase from *Brevibacterium sterolicum* refined at 1.8Å resolution. *J. Mol. Biol.* **219**, 533-554.

Warshel, A. & Aqvist, J. (1981). Electrostatic energy and macromolecular function. *Annu. Rev. Biophys. Biophys. Chem.* **20**, 267-298.

Wohlfahrt, G., Witt, S., Hendle, J., Schomburg, D., Kalisz, H. M. & Hecht, H. J. (1999). 1.8 and 1.9 A resolution structures of the *Penicillium amagasakiense* and *Aspergillus niger* glucose oxidases as a basis for modelling substrate complexes. *Acta Crystallogr D Biol Crystallogr* **55**(5), 969-77.

Yamashita, M., Toyama, M., Ono, H., Fujii, I., Hirayama, N. & Murooka, Y. (1998). Separation of the two reactions, oxidation and isomerization, catalyzed by *Streptomyces* cholesterol oxidase. *Protein Eng* **11**(11), 1075-81.

Yin, Y., Liu, P., Anderson, R. G. & Sampson, N. S. (2002). Construction of a catalytically inactive cholesterol oxidase mutant: investigation of the interplay between active site-residues glutamate 361 and histidine 447. *Archives of Biochemistry and Biophysics* **402**(2), 235-242.

Yin, Y., Sampson, N. S., Vrielink, A. & Lario, P. I. (2001). The presence of a hydrogen bond between asparagine 485 and the pi system of FAD modulates the redox potential in the reaction catalyzed by cholesterol oxidase. *Biochemistry* **40**(46), 13779-87.

Yue, Q. K., Kass, I. J., Sampson, N. S. & Vrielink, A. (1999). Crystals Structure Determination of Cholesterol Oxidase from *Streptomyces* and Structural Characterization of Key Active Site Mutants. *Biochemistry* **38**, 4277-4286.

Zhao, G., Song, H., Chen, Z. W., Mathews, F. S. & Jorns, M. S. (2002). Monomeric sarcosine oxidase: role of histidine 269 in catalysis. *Biochemistry* **41**(31), 9751-9764.

PREFACE TO CHAPTER 4

Only a subset of proteins diffract to sub-Ångstrom resolution. As has been shown in Chapter 3 a wealth of information is available from these crystal structures. The ability to visualize hydrogen atoms in the electron density can be used as a tool to estimate the pKa of residues in the protein. The size of SCOA (56 KDa) and the presence of numerous titratable residues make the determination of pKa for specific residues impossible by other methods. Originally, base abstraction of the hydroxyl hydrogen atom of cholesterol was proposed to activate the substrate for oxidation. It order to estimate the pKa for this histidine, crystals were grown using a pH range of buffers. In addition we hoped to study the effect of pH on protein structure with an atomic view of the electron density and to observed possible changes in the structure and electron density of the redox active FAD cofactor. We were fortunate to obtain atomic resolution crystallographic data for five crystals in a pH range from 4.5 to 7.4. These studies have revealed structural differences as a result of pH. Furthermore these structures have enabled us to compare the similarities between the five independently refined crystal structures, providing convincing evidence that the unexpected and unusual electron density features are indeed real and not an artifact from the noise of the experiment.

CHAPTER 4. EFFECT OF PH ON THE ATOMIC RESOLUTION STRUCTURES OF CHOLESTEROL OXIDASE: FAD REDUCTION BY SYNCHROTRON RADIATION.

Paula I. Lario[⊥], Nicole Sampson[¥], and Alice Vrielink[⊥*]

[⊥]Department of Molecular, Cellular and Developmental Biology, Sinsheimer Laboratory, University of California Santa Cruz, Santa Cruz, CA, 95064, Biochemistry Department, McGill University, Montréal, QC, H3G-1Y6.

[¥]Department of Chemistry, State University of New York, Stony Brook, NY 11794-3400.

4.1 ABSTRACT

Multiple atomic resolution data sets were collected using cholesterol oxidase crystals at varying pH values from pH 4.5 to 7.4. This 56 KDa flavoenzyme diffracts to sub-atomic resolution, providing high quality electron density maps. Overall, there are small differences observed in the flavin geometry among the five structures, despite the observation that the FAD cofactor in these structures were being reduced at differing rates during data collection. These structures provide further evidence that the narrow hydrophobic tunnel to the active-site is gated by the redox state of the isoalloxazine group. In addition, this study presents some interesting features for the FAD cofactor. The adenosine ring, buried within the structure, clearly has a hydrogen atom visible in the electron density on the AN7 atom in the pH 4.5 structure. Comparisons with the other pH structures have indicated that the apparent pKa for this hydrogen atom is around pH 5. Very unusual electron density was observed for the bridging oxygen atom in the pyrophosphate group. It appears that the density is polarized away from the phosphorus atoms, suggestive of either increased ionic nature or bonding orbitals that are predominatly π in character. Another unexpected finding is an elongated CB-H interaction involving the isoalloxazine system, indicating that similar protein-flavin interactions could be important for the redox reactivity of other flavoenzymes.

4.2 INTRODUCTION

A diverse range of biological reactions are catalyzed by enzymes that contain FAD (flavin adenine dinucleotide) and FMN (flavin mononucleotide) cofactors. The reactive portion of these cofactors is the isoalloxazine group (Figure 1.1). Delocalization of electronic charge enables this aromatic group to adopt 3 different oxidation states: oxidized quinone (F_{ox}), one-electron reduced semiquinone (F_{rad}^{-}), and two-electron reduced hydroquinone (F_{red}). The redox reactivity of flavoproteins is the reason why these enzymes are commonly involved in one-electron transfers and two-electron oxidation reactions.

The protein environment surrounding the isoalloxazine group has been shown to modulate its reduction potential (Fraaije et al., 2000; Ghisla & Massey, 1989; O'Farrell et al., 1998). It has been proposed that protein-flavin interactions modulate the redox potential of the isoalloxazine through control of its conformation (Hasford, 1997; Massey & Hemmerich, 1980). Theoretical studies have shown that the oxidized and the one-electron reduced semiquinone forms of the isoalloxazine prefer a planar conformation, while the two-electron reduced group tends to adopt a "butterfly bend" conformation (Lennon et al., 1999; Meyer et al., 1996; Reibenspies et al., 2000). The isoalloxazine group is bent in the native and the two-electron reduced complex structures of cholesterol oxidase from *Brevibacterium sterolicum*, BCO1 (3cox and 1coy), suggesting that protein-flavin interactions are distorting the geometry of the oxidized co-factor into a conformation favorable for reduction. Specific protein-flavin interactions have been identified that stabilize the reduced isoalloxazine system (Ghisla & Massey, 1989;

Mewies et al., 1996; Rowland et al., 2000; Yin et al., 2001; Bradley & Swenson, 1999, however it is not entirely clear how these interactions affect isoalloxazine geometry.

This structural study of cholesterol oxidase from *Streptomyces* sp. SA-COO (SCOA) (Ishizaki et al., 1989; Yamashita et al., 1998), includes 5 atomic resolution structures from pH 4.5 to pH 7.4. This work provides a better understanding of the environmental factors that affect isoalloxazine geometry. The high quality electron density maps provide precise atomic positions for the protein-bound cofactor. In addition to SCOA, the only other atomic resolution structure of a flavoenzyme is that of D-amino acid oxidase, DAAO (refined to 1.2 Å) (Umhau et al., 2000). Comparison of the isoalloxazine geometry of flavin-oxidase to the theoretical and experimental models provides new insights on how bonding geometries can be distorted in a protein.

SCOA is a relatively large enzyme (~55 KDa) to diffract at sub-atomic resolution and as such has a representative distribution of secondary structural elements. These structures are invaluable for studying protein structure in general and the affect of pH on structural stability and a redox center. In addition, unusual and unexpected protein-flavin interaction are observed in these structures changing our understanding of important catalytic interactions.

4.3 Results and Discussion

Cholesterol oxidase (EC 1.1.3.6) is a multi-functional bacterial enzyme that catalyzes the oxidation of the 3β-hydroxysteriods and the isomerization of the intermediate, Δ^{5-6}-ene-3β-ketosteriod to produce Δ^{3-4}-ene-3β-ketosteriod (Figure 1.9). An active-site histidine residue, H447, conserved among the glucose-methanol-choline

(GMC) family, has been proposed to act as a general base for oxidation and as a general acid for isomerization. Analogous to the pH titration of the protein RNase A by Berisio and co-workers (Berisio et al., 2002,) we originally pursued this study in order to determine the pKa of H447. Previous structural studies have indicated that H447 has low mobility, as judged from the refined atomic displacement parameters (Vrielink et al., 1991; Yue et al., 1999). Rather than soaking the crystals to obtain the desired pH as had been done for the RNase A structures, we grew crystals of SCOA at varying pH values and buffers: 4.5 ($NaKHPO_4$), 5.0 (NaCacodylate), 5.8 (MES), 7.3 (TRIS) and 7.4 (Glycine). Originally we believed that the collected data sets were at the pH of the buffer used. However, subsequent pH measurements have indicated that the actual pH of the crystal grown in pH 9.0 buffer was pH 7.4, primarily a result of the added $MnSO_4$. Although the two crystals grown in pH 7.3 and 7.4 mother liquors are essentially at the same pH, interesting structural differences are observed between these two structures that will be discussed below. Atomic resolution data sets were collected using a single crystal from each condition (Table 4.1).

Table 4.1. Crystallization conditions

Crystal pH	**4.5**	**5.0**	**5.8**	**7.3**	**7.4**
Buffer (100mM)	$NaKHPO_4$	NaCacodylate	NaCacodylate	MOPS	GLYCINE
pH of Buffer	4.0	5.2	6.0	7.5	9.0
Measured pH of mother liquor	4.5	5.0	5.8	7.3	7.4
Salt (75 mM)	$(NH_4)_2SO_4$	$MnSO_4$	$MnSO_4$	$MnSO_4$	$MnSO_4$
Glycerol (%)	20	20	20	20	30

4.3.1 The quality of the models

The five structures of SCOA were independently refined with a truncated starting model derived either from the previous 1.5 Å structure (Yue et al., 1999) or from the first atomic resolution structure (Lario et al., submitted). Before anisotropic refinement, many additional alternate residue conformations were observed and modeled in the structure. On average about 15 % of the residues in a single structure were modeled in alternate conformations. Although many of the hydrogen atoms were clearly visible in the electron density, the hydrogen atoms (except for the titratable hydrogen atoms on histidine residues) were included at riding positions in the refinement. The positions of the hydroxyl group hydrogen atoms of tyrosines, serines and threonines were adjusted as necessary either to prevent steric clashes or to improve the fit to the electron density. The refinement statistics are listed in Table 4.2.

Table 4.2. Refinement statistics

Crystal pH	**4.5**	**5.0**	**5.8**	**7.3**	**7.4**
R (All) (%)	11.4	11.0	12.0	10.4	9.7
R_{free} (All) (%)	13.6	13.2	14.7	12.2	11.9
R (>4σ) (%)	9.9	9.8	10.4	9.5	9.2
R_{free} (>4σ) (%)	12.0	12.0	13.0	11.4	11.2
Peak (e/Å^3)	0.62	0.67	0.47	0.56	0.58
Hole (e/Å^3)	-0.34	-0.34	-0.38	-0.28	-0.42
Data/Parameter	5.8	5.8	4.0	5.3	5.2
Residues modeled in multiple conformers	98	82	89	107	118
Isotropic average temperature factors* **(Å^2)**					
All atoms	10.7	11.4	13.7	12.6	10.4
Main chain atoms	7.8	8.6	10.8	9.8	7.5
Side chains and waters	12.8	13.4	15.9	14.6	12.4
FAD molecule	4.8	5.6	7.8	6.8	4.3

* Hydrogen atoms were not included in the calculations.

4.3.2 Effect of pH on protein structure

Half of the residues that were observed in multiple conformations were found to vary their respective conformer populations with pH. However, most of these apparently pH sensitive residues were not titratable residues. Rather, the predominance of hydrogen bonding networks in the protein, results in large correlated movements of neighboring residues. For example, a histidine residue H331 is likely responsible for affecting the conformer populations of over 15 surrounding residues (including residues in adjacent monomers in the crystal) through a relay system of hydrogen bonding.

4.3.2.1 C-terminus disorder

The positioning of the C-terminal helix of SCOA also appears to be pH sensitive. In three of the structures (crystals at pH 5.8, pH 7.3 and pH 7.4), the end of the helix is very anisotropic and required the modeling of an alternate conformation (Figure 4.1). A single conformation for this helix is observed in the other two structures at acidic pH values. When a residue is found to adopt multiple conformations, its conformers are labeled as A, B or C as necessary. Table 4.3 summarizes the population of conformer A of the C-terminal helix. As the pH of the crystal is increased there is a decrease in population of conformer A. A neighboring bond phosphate group could be responsible for fixing the position of the C-terminal helix in the pH 4.5 crystal structure, however, a similar anion at that position is not observed for the pH 5 structure. This suggests that additional interactions are involved in the flexibility of the C-terminus. Most of the hydrogen bonding interactions involving the C-terminus are maintained with the movement of the

helix, however, one salt bridge between R463 and D505 is disrupted. Examination of the structure does not indicate that any titratable residue in reasonable proximity to the helix causes its movement and the loss of the salt bridge.

Table 4.3. Conformer A population percentages

Crystal pH	4.5	5	5.8	7.3	7.4
C-Term	100	100	70	60	57
M122	63	39	44	40	41
D349	44	64	51	48	50
F359	66	58	55	53	42
E361	47	52	44	49	46
N485	66	65	62	64	49

The pH profile for the oxidative activity of SCOA is consistent with the structural variations observed in the pH 4.5 to 7.4 structures. The value of k_{cat} was essentially independent of pH over the range from pH 4.5 -7.0 (Kass & Sampson, 1998). Over the range from 7.5 - 10.6, the k_{cat} decreased 2000 fold and this loss of activity was reversible. The C-terminal helix has been proposed to have a role in the stabilization of the reduced flavin (Vrielink et al., 1991). The N-terminus of this helix is situated directly adjacent to O2 of the isoalloxazine system (Figure 4.1) and thus it is in a position to stabilize the additional charge on this atom when the FAD is reduced. Such a long helix, with the N-terminus directed towards O2 is a commonly observed structural feature of flavoenzymes (Binda et al., 1999; Karplus & Schulz, 1987; Kiess et al., 1998; Mattevi et al., 1996; Schreuder et al., 1989; Vrielink et al., 1991). It is tempting to speculate, that the reversible loss of activity at basic pH values is a result of the repositioning of this

C-terminal helix. Although, the disorder does not extend to the N-terminus of the helix, the magnitude and the direction of the helix dipole could be affected by the partial disorder at the C-terminus, changing the stabilization effect at the N-terminus of the helix. However, it is unclear if the helix dipole effect is cumulative or rather just a local stabilizing interaction with an amide group at the N-terminus of the helix. The potential correlation between the disorder at the C-terminal helix and enzyme activity is intriguing. Further mutagenesis studies of SCOA may help elucidate the mechanism of helix stabilization in flavoenzymes.

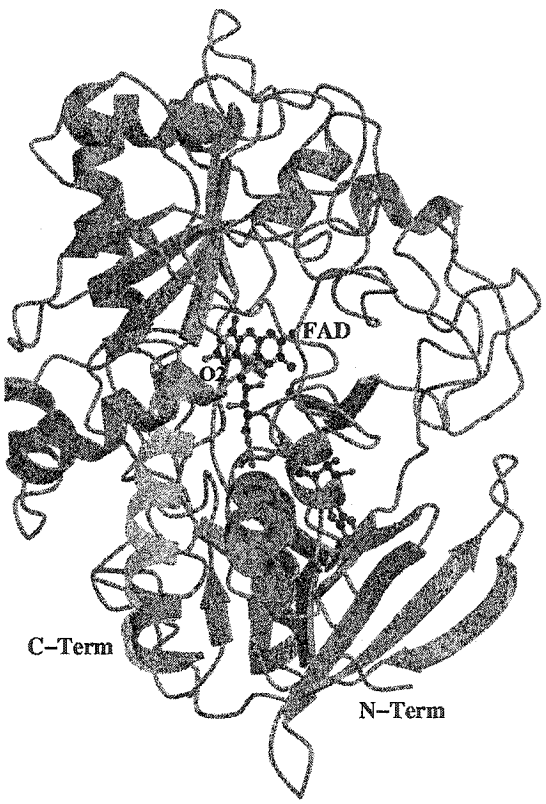

Figure 4.1 Ribbon representation of SCOA. The C-terminal helix is highlighted in yellow and the alternate conformation observed for part of this helix is shown in purple.

4.3.2.2 Potential pH effects on enzyme activity

Apart from the F359-D349 interactions no other structural changes in the close proximity of the isoalloxazine system appear to be correlated to changes in the protonation state of a titratable residue. Both F359 and D349 are observed in multiple conformations where their conformer populations appear to be correlated in the pH 5.0 to 7.4 structures (Table 4.3). One conformer arrangement (conformer A) directs the aromatic hydrogen atoms of F359 towards the π system of the carboxylate group of D349. The conformer B arrangement results in a steric π - π interaction. The observed correlation of the conformer populations for the four structures is not observed in the pH 4.5 crystal structure (Table 4.3). In the latter structure, conformer B of D349 is 66 % populated despite the higher population of conformer A of F359. Thus it appears that the stability of the conformer A arrangement observed in the pH 5.0 to 7.4 structures has shifted to a repulsive interaction at pH 4.5. This observed change in the F359-D349 interactions with pH is consistent with typical pKa value for an aspartate group and suggests that the protonation of residue D349 at pH 4.5 results in the observed changes in conformer populations

An understanding of the interactions with F359 are important as it is a critical surface residue involved in the gating of a narrow tunnel leading to the isoalloxazine group [Refer to Chapter 3]. The alternative conformer populations of F359 are strongly correlated with the alternate conformations of the other residues lining the tunnel (M122, V124, V191 and N485). Thus at a low pH value near the pKa of D349, the change in its interaction with F359 could directly affect the conformer population of N485, an

important residue that modulates the redox activity of the enzyme (Yin et al., 2001). It is unlikely, however, that the F359-D349 interactions are responsible for the slower kinetics observed at basic pH values (Kass & Sampson, 1998). At acidic pH the change in the D349-F359 interaction will likely also affect the gating of the tunnel. This prospective role of D349 in gating the tunnel will be discussed in more detail below.

4.3.2.3 Role of phosphate binding

Interestingly, the cryo-protectant glycerol was observed in the buried active site pocket of the pH 4.5 structure, but was not present in any of the other structures. As glycerol was used to cryo-protect all of the crystals, it appears that either the pH or the phosphate buffer affects the accessibility of the active-site cavity in the crystalline state. Phosphate anions are observed on the surface of the enzyme, however they are not directly adjacent to the loops proposed to move and open the active site for substrate entry (Li et al., 1993). The hydrophobic tunnel to the isoalloxazine group is too narrow to accommodate a glycerol molecule thus it is probable that it enters the active-site cavity via the same route as cholesterol. One of the phosphates is situated at the top of the substrate-binding domain and affects the crystal contacts in that region, perhaps enabling the substrate domain to rotate slightly and consequently affecting access to the active-site cavity.

Kinetic studies on cholesterol oxidase from *Streptomyces hydroscopicus* (SCOH) have indicated that the concentration of HPO_4^{2-} has a significant affect on the activity of this enzyme (Gadda et al., 1997). Clearly additional studies would be useful to determine the effect of HPO_4^{2-} concentration on substrate binding and /or C-terminal helix

orientation. These preliminary observations indicate that phosphate anions play a role in rigidifying the protein structure.

Currently it is not understood how cholesterol oxidase interacts with membranes in order to extract cholesterol. The observation of bound phosphate groups on the surface of the enzyme, provides clues to potential binding sites of the enzyme with the phosphatidyl head groups in cellular membranes. There are five phosphate groups observed in the structure of the crystal grown at pH 4.5 and all of the phosphate-binding positions are partially occupied. The most populated phosphate-binding site is the one on the substrate-binding domain, perhaps suggestive that this is the primary binding site to the phospholipid membrane. In addition, this site is the only one of the five phosphate binding sites that was found to bind a similarly charged sulfate anion in the structure of the crystal grown at pH 5.0, further supporting the role of this position in membrane association. A membrane binding interaction at that site would facilitate membrane interactions with two adjacent hydrophobic surface loops, which have been proposed to move and allow cholesterol to access the active site cavity (Li et al., 1993). Furthermore, as discussed earlier, this phosphate-binding site may be correlated to the observed presence of glycerol in the active site cavity in the pH 4.5 structure. A slight rotation of the substrate domain separates the two loops from each other, thereby facilitating opening of the substrate cavity. Further mutagenesis studies targeting the residues that form this binding site (E179, W333 and N334) along with membrane interaction studies would be useful to identify if this atomic-level interaction plays a key role in membrane association.

4.3.2.4 H447 is a hydrogen bond donor

As mentioned earlier, these structural studies were initially pursued in order to determine the pKa of the active site histidine residue, H447. Unexpectedly, the atomic resolution study of SCOA in the pH 5.0 structure has indicated that this proposed basic residue, does have visible but weak electron density for a hydrogen atom on NE2 of the imidazole (Figure 4.2a) [Refer to Chaper 3]. In addition, this structure revealed that two asparagine residues act as hydrogen bond donors to the ND1 atom of H447, indicating that the lone pair of electrons is on ND1 rather than the NE2 atom proposed as the general base for oxidation. This bifurcated hydrogen-bonding geometry at ND1, the low temperature factors observed for the ND1 atom, and the lack of an hydrogen bond acceptor in close proximity of ND1, indicate that it is unlikely that H447 rotates such that the NE2 atom could accommodate the lone pair of electrons. However, the observed electron density for the hydrogen atom on NE2 in the pH 5.0 structure was close to the noise level of the map making it difficult to rule out the possibility that H447 is not present as a negatively charged imidazolate (Figure 4.2a). Although such a species is unlikely, it could be stabilized by the adjacent N-terminal end of C-terminus α-helix.

The pH 7.4 structure, reported here convincingly shows evidence for a hydrogen atom on NE2 (Figure 4.2b). In addition, the pH 7.3 structure also has electron density indicative of a hydrogen atom on NE2. These independent observations suggest that the other structures at lower pH values, with higher H447 thermal parameters, also have hydrogen atoms at that position. Furthermore, these results confirm our hypothesis that the histidine is not present as an imidazolate in the absence of a substrate and we expect

that such a charged species would not be stabilized in the presence of the hydrophobic substrate.

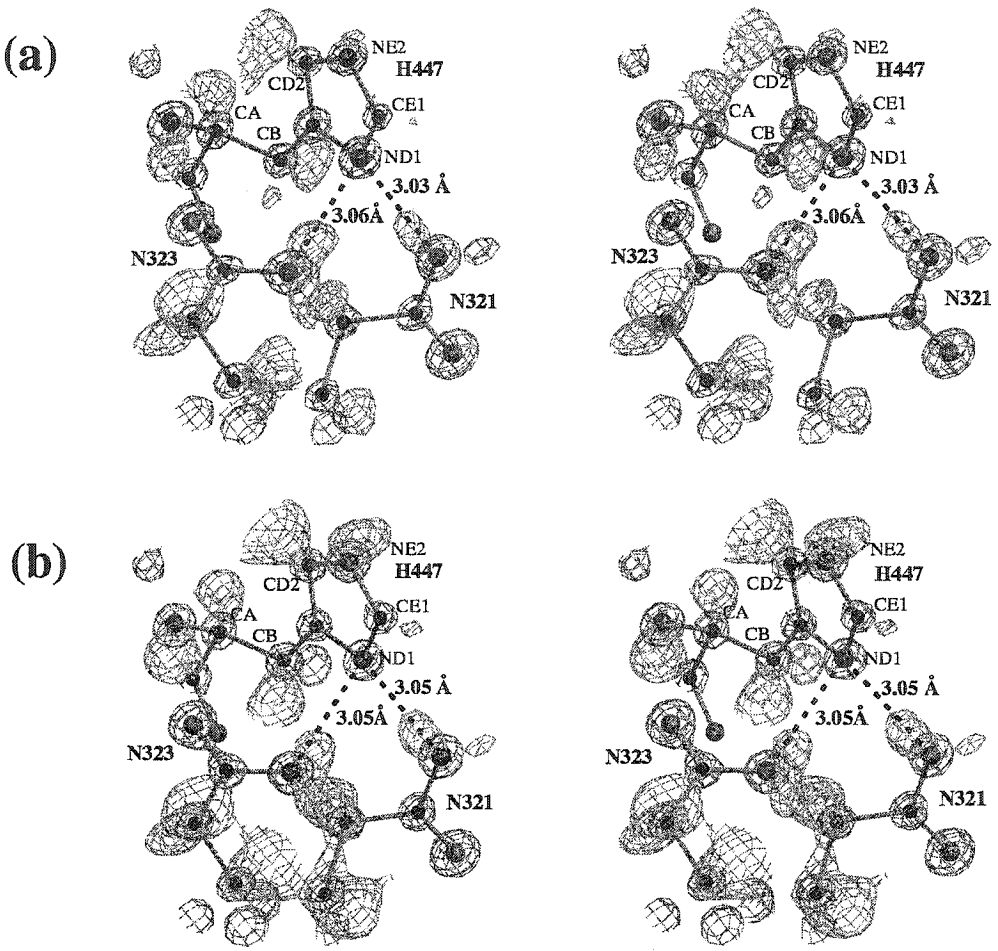

Figure 4.2 Stereoscopic representation of the electron density around H447 for the crystals grown at (a) pH 5.0 and (b) pH 7.4. Green contours represent the Fo - Fc map contoured at 1.5σ and magenta represents the SigmaA map contoured at 4σ. The difference map was calculated with the hydrogen atoms excluded from the model.

The recently proposed role of H447 for the oxidative activity of the SCOA, is as a hydrogen bond donor that orients the substrate [Refer to Chaper 3]. The unambiguous observation of a hydrogen atom on NE2 in the pH 7.4 structure (Figure 4.2b) is consistent with that proposed mechanism.

4.3.3 Reduction of SCOA by X-ray Irradiation

In addition to differences in pH amongst the five atomic resolution structures there are also differences in their respective oxidative state(s). All of the crystals were grown and mounted in cryo-loops in an oxidizing environment. However, a rapid bleaching of the yellow pH 7.4 crystal was observed with synchrotron irradiation, indicating that the FAD cofactor becomes reduced during the course of data collection. Crystal bleaching was not monitored during data collection for the crystals grown at the other pH values. Preliminary tests on a pH 5.0 crystal revealed no color change after one hour of synchrotron irradiation, suggesting that either this crystal is not reduced, or more likely, it is reduced at a slower rate than the pH 7.4 crystal. These observed differences could be the result of variations in the buffering solutions, pH and / or the concentration of glycerol used as a cyro-protectant (Table 4.1). Reduction of iron centers by synchrotron radiation has been reported for ribonucleotide reductases where the rate of reduction was highly dependent on the concentration of glycerol, an effective electron hole-trapping agent (Davydov et al., 1994; Eriksson et al., 1998).

These qualitative color change observations indicate that there are differences in the redox state(s) of the enzyme between the different crystal structures of SCOA. The rapid bleaching observed for the pH 7.4 structure suggests that it represents a predominantly

reduced species for the FAD. The one hour test on a crystal grown at pH 5.0 indicates that a minimum of 10 % of the data of the pH 5.0 crystal was collected with an oxidized FAD. Despite the ambiguity of the redox state(s) of the cofactor for this structure there is no evidence in the electron density for a low population of a planar isoalloxazine group (Figures 4.3a & 4.3b). In addition, the anisotropic temperature factors do not indicate the presence of a planar species (Figure 4.3c). In fact, there is no evidence for a planar isoalloxazine group in any of the five structures.

Another crystal bleaching test was preformed on a crystal grown at pH 5.0 using a rotating anode X-ray generator source. This test was carried out to clarify the redox species present in the previously published structures of BCO1 and SCOA (Vrielink et al., 1991; Yin et al., 2001; Yue et al., 1999) collected on a similar radiation source. No color change was observed when an oxidized pH 5.0 crystal of SCOA was exposed for 48 hours on the rotating anode (unpublished results). This supports our earlier assumption that the FAD is oxidized in these structures. Furthermore these results indicates that the bent geometry observed for the isoalloxazine in these structures represents an oxidized FAD, consistent with the absence of a planar species in any of the atomic resolution structures.

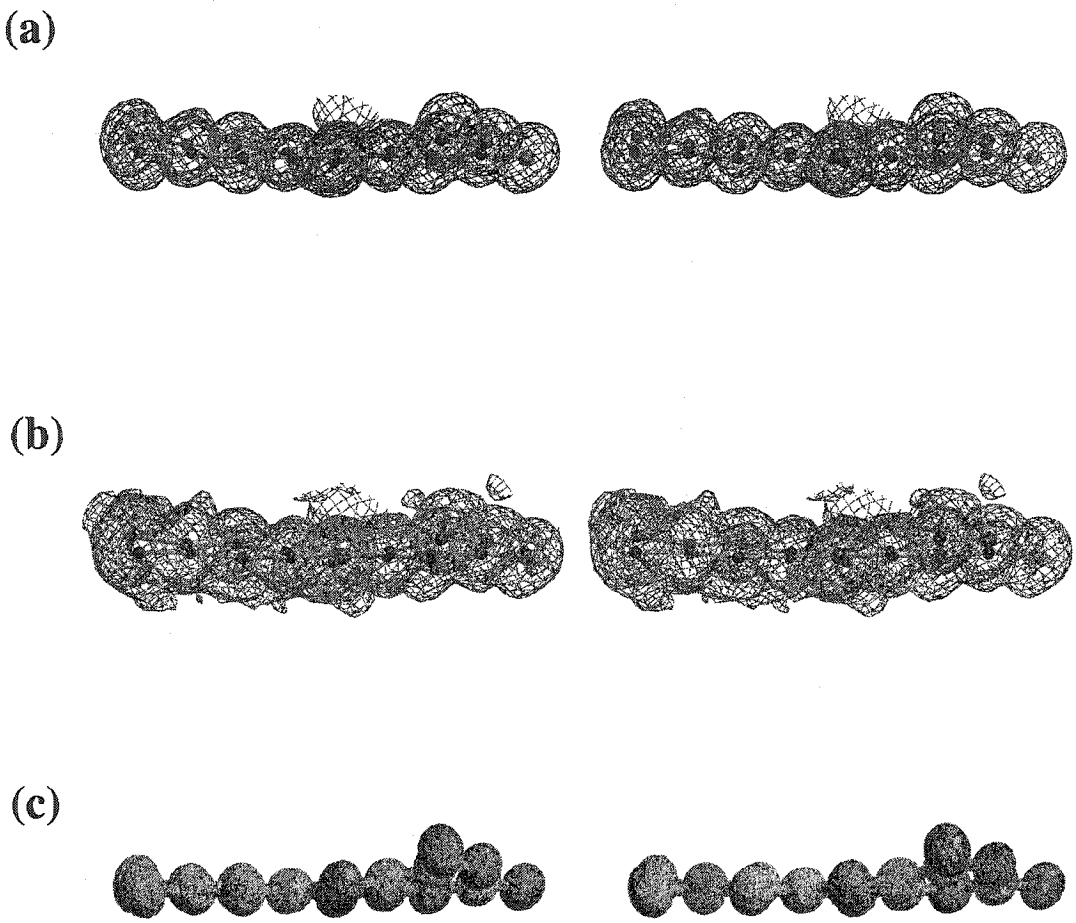

Figure 4.3 Stereoscopic representation of the isoalloxazine system in the pH 5.0 structure. The isoalloxazine is oriented to view its twisted conformation. The SigmaA map is contoured at two levels where (a) blue represents 1σ and (b) purple represents ½ σ. (c) A representation of showing the thermal ellipsoids of the isoalloxazine group plotted at a 50% probability level.

4.3.4 Gating of the oxygen tunnel

The presence of narrow gated tunnel to the active site was observed in the first atomic resolution structure of SCOA [Refer to Chaper 3]. The residues that line this tunnel (M122, V124, V191, F359, E361 and N485) are all modeled in two alternate conformations. The conformer adopted by a residue is correlated to the conformation of its adjacent residues, either through hydrogen bonding networks or to prevent steric clashes. When all of the tunnel residues are modeled in conformation A the tunnel is closed (Figure 4.4a) and conversely when the residues are in conformer B the tunnel is open and water molecules occupy its interior (Figure 4.4b). The observation of two alternate conformations for the tunnel residues indicate that both open and closed forms of the enzyme are present within the single pH 5.0 crystal structure. Similar, mixed open and closed states of the enzyme are observed in each of the other atomic resolution structures. Interestingly, the ratio between the two forms varies among the different pH structures. The pH 4.5 structure has a higher population of proteins present in the closed state (~ 65% conformation A) while the pH 7.4 structure has the highest population of monomers in the open state (~40 % conformation A). These apparent structural differences provide additional insights into the gating of the tunnel.

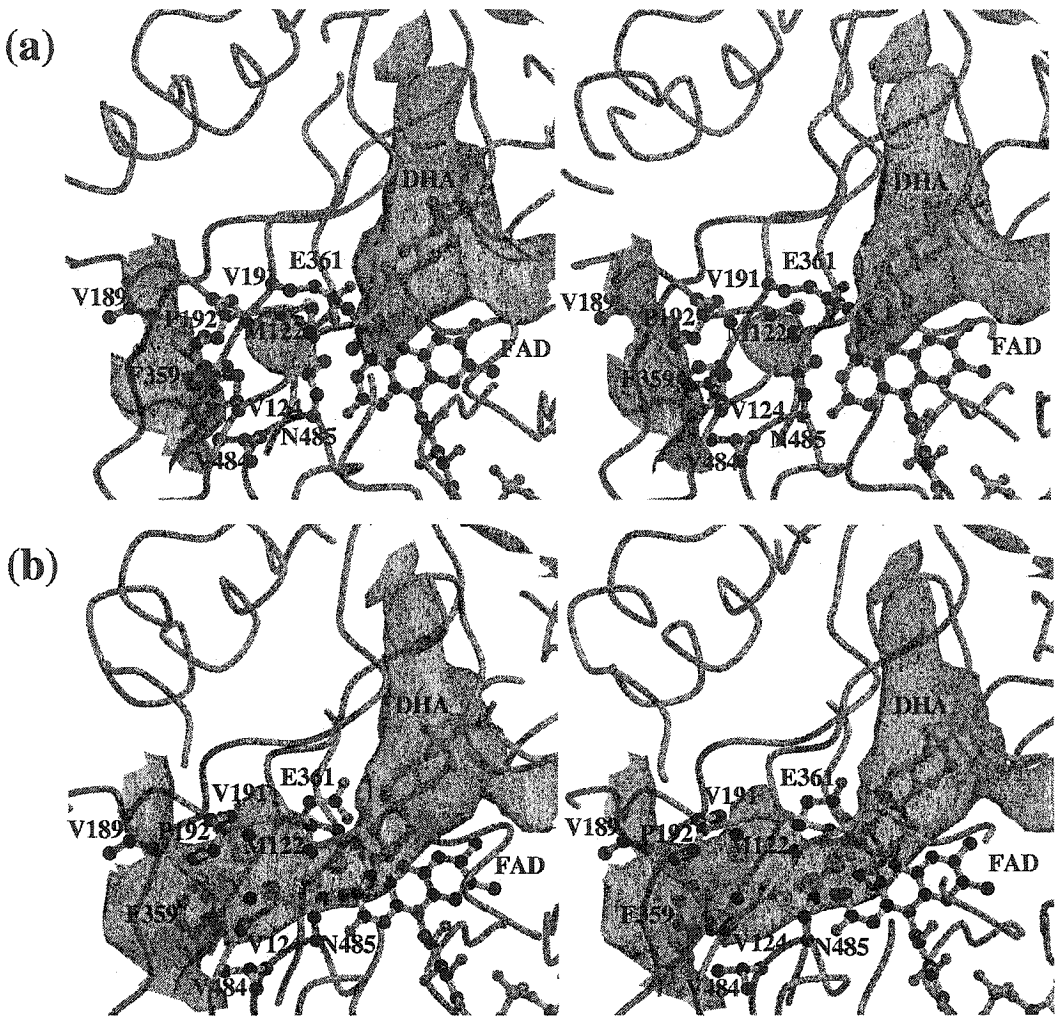

Figure 4.4 Stereoscopic representations showing the active site of the enzyme with (a) the hydrophobic tunnel of the enzyme in a closed conformation (corresponding to conformation A) and (b) the tunnel open conformation (corresponding to conformation B). The molecular surfaces were constructed using the program SPOCK (Christopher, 1998) and colored according to residue type: aromatic and hydrophobic residues are colored green, acidic residues are colored red and basic residues are colored blue. The bound water molecules in the tunnel are represented as red spheres. The dehydroisoandosterone molecule, shown in green, has been modeled into the substrate-binding cavity.

The active site residue N485 was proposed to gate the tunnel via a mechanism dependent on the oxidation state of the FAD [Refer to Chaper 3]. In the pH 5.0 structure, conformer B of this residue positions the side chain nitrogen atom ~3.0 Å from the π system of FAD. This strong hydrogen bonding interaction likely stabilizes the increased electron density in the reduced FAD. Thus it was postulated that with substrate oxidation and subsequent FAD reduction, the side chain of N485 rotates from conformation A (tunnel closed) to B (tunnel open). The pH 7.4 crystal was observed to be rapidly reduced by the synchrotron radiation, unlike the pH 5.0 crystal. These differing rates of FAD reduction are reflected in the different populations of conformation B of N485 where conformer B is 51 % populated in the pH 7.4 structure and 35 % populated in the pH 5.0 structure (Figures 5.5a & 5.5b). These observations suggest that either the reduction rate of the FAD is dependent on the population of conformer B or that the oxidation state of the enzyme affects the observed population of conformation B. While the latter scenario may appear less likely since it requires side chain movements in a frozen crystal, there is precedence for such atomic movements at 100K (Genick et al., 1998; Petsko & Ringe, 2000; Ravelli & McSweeney, 2000; Schlichting et al., 2000; Weik et al., 2001).

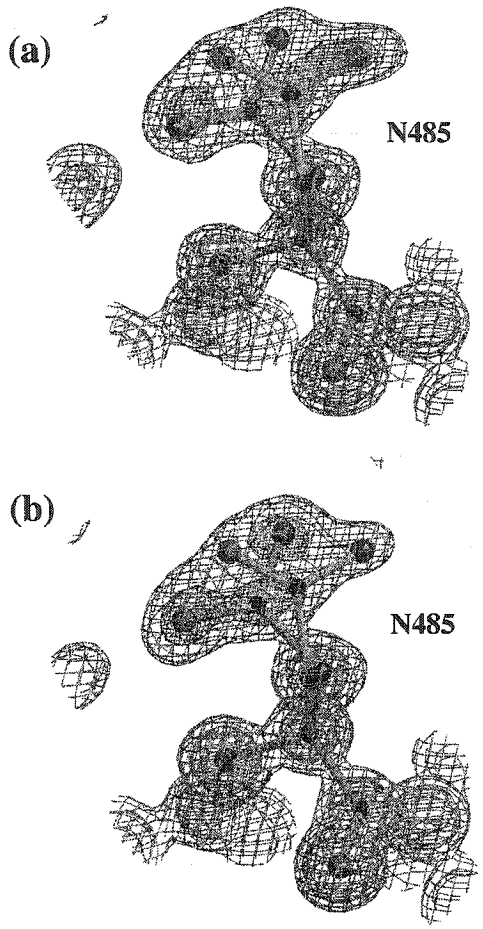

Figure 4.5 Electron density around N485 in the crystals grown at (a) pH 5.0 and (b) pH 7.4. The SigmaA map is contoured at two levels where blue represents 1σ and magenta represents 2.5σ.

In order to gain some insight into the order of events of SCOA reduction, comparisons among the different pH structures were performed to determine if the N485 population of conformer B could be correlated to pH. Evidence suggesting that factors other than pH are responsible for the observed conformation of N485 is provided by the structural differences observed between the pH 7.3 and 7.4 structures, where the conformer B population of N485 is 36 % and 51 % respectively. These results suggest that differences in the populations of N485 are the result of differences in their respective

solution matrices, either buffer and /or glycerol concentration (Table 4.1). Both data sets were collected on the same beamline (X8C at the National Synchrotron Light Source, Brookhaven National Laboratory) with a similar wavelength of radiation used and comparable data collections times (Table 4.4). However the crystals used in each of the experiments differed significantly in the percentage of glycerol used as a cryo-protectant (20 % for pH 7.3 and 30 % for pH 7.4). None of the structural differences observed for the tunnel residues could be directly associated to the presence of additional glycerol. There are no bound glycerol molecules near the tunnel and no noticeable allosteric affect due to glycerol concentration. Therefore, we postulate that the differences in the conformer populations of N485 are the result of differences in the crystal reduction rate. Perhaps as had been observed for ribonucleotide reductase crystals (Eriksson et al., 1998), the rate of SCOA crystal reduction by the synchrotron radiation is also strongly dependent on glycerol concentration and the observed differences in N485 conformer populations are related to the oxidation state(s) of the enzymes in the crystal. This hypothesis is strengthened by the structural similarities of N485 conformer B populations (from 34 - 38 %) for the pH 4.5, 5.0 5.8 and 7.3 structures (Table 4.3), where an identical glycerol concentration of 20 % was used. The higher population of N485 conformer B in the apparently reduced pH 7.4 structure (51 %) supports the hypothesis than the side chain of N485 moves towards the flavin either during or after substrate oxidation in order to form a stabilizing interaction with the reduced flavin.

Table 4.4. Crystallographic data

Crystal pH	4.5	5.0	5.8	7.3	7.4
Space group	$P2_1$	$P2_1$	$P2_1$	$P2_1$	$P2_1$
Cell dimensions (Å)	a = 51.248	a = 51.227	a = 51.354	a = 51.343	a = 51.273
	b = 73.276	b = 72.902	b = 73.291	b = 72.959	b = 72.964
	c = 63.098	c = 62.947	c = 63.171	c = 63.045	c = 63.036
	β = 104.07	β = 105.10	β = 105.10	β = 105.25	β = 105.18
Wavelength (Å)	0.979	0.979	0.9795	0.9795	0.979
Total reflections	1028338	1083885	957755	931572	1029762
Data collection time (hours)	~20	~9	~16	~9	~10
Unique reflections	266037	263559	230865	291204	277783
Resolution range (Å)	47 - 0.95	28 – 0.95	47 – 1.0	31 –0.92	49 – 0.95
(last shell)	(0.97-0.95)	(0.97-0.95)	(1.02-1.00)	(0.94 – 0.92)	(0.97-0.95)
Completeness (%)	94.3	94.1	95.0	94.1	98.8
(last shell)	(89.3)	(88.0)	(90.8)	(66.8)	(98.8)
I/σ	11.1	11.1	7.2	13.8	19.4
(last shell)	(1.5)	(1.5)	(1.7)	(1.4)	(2.2)
Redundancy	3.9	4.1	4.1	3.2	3.7
(last shell)	(3.1)	(3.1)	(3.3)	(2.1)	(3.0)
$\mathbf{R_{merge}}$	0.058	0.051	0.069	0.041	0.046
(last shell)	(0.569)	(0.611)	(0.643)	(0.476)	(0.349)

Based on this proposed role for N485, one may expect that N485 would be observed predominantly in conformation B for the pH 7.4 structure, where the data was collected on a colorless crystal. However, it is clear from the electron density that a significant portion of the monomers in the crystal maintain conformation A (away from the FAD) (Figure 4.5b). Thus, the conformer occupancies of N485 are not representative of the ratio of the different redox species present in the crystal, but rather only reflect differences in the rate of crystal reduction. The lack of a direct relationship is not surprising, as one would expect side chain movements in a frozen crystal to be significantly hindered.

While the conformation of N485 appears to be dependent on the oxidation state of the cofactor, additional factors do affect the side chain conformations of other residues within the tunnel. As discussed earlier, in the pH 4.5 structure, F359 favors conformer A (66 %), likely due in part to steric interactions with a protonated D349. However, in addition to this interaction, a small pH affect is also observed on the conformer populations of F359; a gradual decrease in the occupancy of conformer A, for F359 is observed for pH 5.0, 5.8 and 7.3 (58 %, 55% and 53 % respectively) (Table 4.3). Previously we have proposed that F359 plays a passive role analogous to a valve, in the gating of the tunnel [Refer to Chaper 3]. This residue is situated at the exterior side of the tunnel and, depending upon its adopted conformation, controls access to the tunnel. Aside from D349 no other residue directly affects its adopted conformation. Despite the lack of a direct interaction with N485 there is a strong correlation of their respective side chain conformations (Table 4.3)(Figure 4.6). Conformer A of F359 is preferred when N485 adopts conformer A, likely due to additional hydrophobic packing interactions. When

N485 moves to conformer B away from F359, space in the tunnel is created resulting in a negative pressure. Rotation of the phenylalanine to conformer B, allows this space to be filled with water molecules or molecular oxygen. Based on this mechanism, it appears that a decrease in the barrier to rotation of F359 and/or a change in the energetic stability of its two conformers will have an affect on the opening of the tunnel. Aside from the pH 4.5 structure, there is 7 - 11 % difference between the conformer A populations of F359 and N485, indicating that F359 can adopt conformer B when N485 is in conformation A. The ability of F359 to adopt conformation B without the movement of N485 suggests that the barrier to rotation for this residue is low. The lack of this unusual conformer arrangement in the pH 4.5 structure indicates that there is a change in the energetics of the F359 - D349 interaction that is responsible for the shift in the conformer populations. Thus, the observed pH trend on the conformer populations of F359 is likely a result of a hydrogen atom being titrated from D349. At pH 4.5 it is less favorable for F359 to adopt its B conformer, consequently requiring more energy to open the tunnel. The pH effect on the conformation of F359 could be responsible for a decreased oxidative activity of the enzyme at acidic pH (Kass & Sampson, 1998) by decreasing the accessibility of the oxygen tunnel.

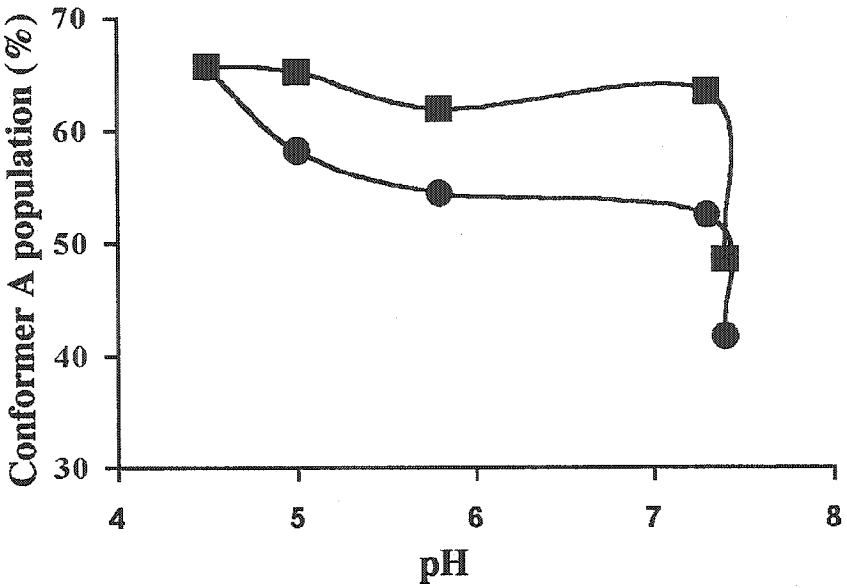

Figure 4.6 Plot of the populations of conformer A for F359 (spheres) and N485 (squares) against the pH of the crystal.

An additional smaller pH effect on conformer populations could be the result of another active-site residue, M122, as the alternate conformations of the tunnel residues are correlated. The tunnel residue M122 also appears to show variations in its conformation among the different structures. Examination of the pH 5.0 structure indicated that, due to steric constraints, the conformation adopted by this residue is dependent on the conformation of N485. This methionine residue can only adopt conformation A when N485 is in conformation A, however it may also adopt conformation B when N485 is in conformation A. Thus the population of M122 conformer A has to be less than or equal to the population of N485 conformer A. Indeed this relationship is consistent with the structures at all pH values (Table 4.3). Unexpectedly, a difference in the occupancy of conformer B for M122 when N485 is in

conformer A was observed between the structures. Approximately 20 % of the monomers in the pH 5.0, 5.8 and 7.3 structures with N485 in conformer A have M122 in conformer B. However, for the pH 7.4 structure with an additional 10 % glycerol concentration, only 8 % adopt the conformer B arrangement for M122 in that condition. This observation may be a result of structural movements in the crystal to stabilize the reduced isoalloxazine. In the absence of the substrate, as in these structures, the terminal methyl group is able to rotate into the observed conformation B which places the methyl group between 3.07 –3.21 Å from the O4 atom of the isoalloxaine group FAD. When M122 is in conformation A, a water molecule occupies a similar position close to O4. This partially-occupied water position is positioned between 2.88 – 2.94 Å (depending on the structure) to the O4 atom forming a hydrogen bond. Theoretical studies on isoalloxazine systems have shown that the increased charge in the reduced flavin is predominately redistributed on both the O2 and O4 atoms of the isoalloxazine (Cavelier & Amzel, 2001). After reduction of the crystal one could expect a shift of the conformer populations of M122 due to the increased stabilization resulting from the hydrogen bonding interaction between the water molecule and O4 rather than the methyl (M122) / O4 interaction. This stabilizing interaction, however, is not likely to play a role in the activity of the enzyme. When the steroid is bound in the active site a water molecule in that position would be displaced by the substrate (Li et al., 1993) [Refer to Chaper 3]. The presence of a glycerol molecule in the active site of the pH 4.5 structure affects the water structure in the substrate binding cavity and thus may be responsible for the inconsistency between the conformer populations observed for M122 at pH 4.5 and at the other pH structures which are similarly cryo-protected (Table 4.3). In summary, the

correlations in the active site residue populations for all of the five atomic resolution structures are consistent with the proposed residue correlations assigned in the pH 5.0 structure [Refer to Chaper 3]. In addition, the corresponding conformer populations are consistent with the proposal that the FAD is more rapidly reduced in the pH 7.4 structure. Furthermore the differences in the adopted conformations of N485 are consistent with the proposal that N485 gates the tunnel residues via a mechanism, dependent on enzymatic reduction.

4.3.5 Geometry of the FAD cofactor

These structures of SCOA represent the first sub-atomic view of a FAD cofactor. The high quality of the electron density improves the precision of the modeled structure and allows for positional refinement in the absence of any constraints. Contouring the electron density of the isoalloxazine system with a 3.3 e/Å^{3}cutoff (~ 4σ), demonstrates the accuracy of the model (Figures 5.7a & 5.7b); clear spherical atomic density is observed and the charge differences between atom types are evident. Despite the low refractive power of hydrogen atoms all of the hydrogen atoms, with the exception of the methyl hydrogen atoms, of the FAD were observed in the difference density before their inclusion in the model at geometrical positions. Slight polarization of the electron density contoured at 0.8 e/Å^3 (~ 1σ), is suggestive of the hydrogen atoms on the isoalloxazine system. Omit maps, where the hydrogen atoms were excluded from the model clearly indicates the positions of the hydrogen atoms on the aromatic heteroatoms of the isoalloxazine group (Figure 4.7c & 4.7d). Contouring the omit map electron density at a lower level will reveal the positions of the methyl hydrogen atom and additional density

in the flavin system that is either noise or a feature of the aromatic density which is unaccounted for in the spherical atom based model used. Further charge density studies, incorporating electron polarization functions on these structural models will help clarify if the additional features observed in the maps are due to the asymmetry in the electron density of the isoalloxazine atoms.

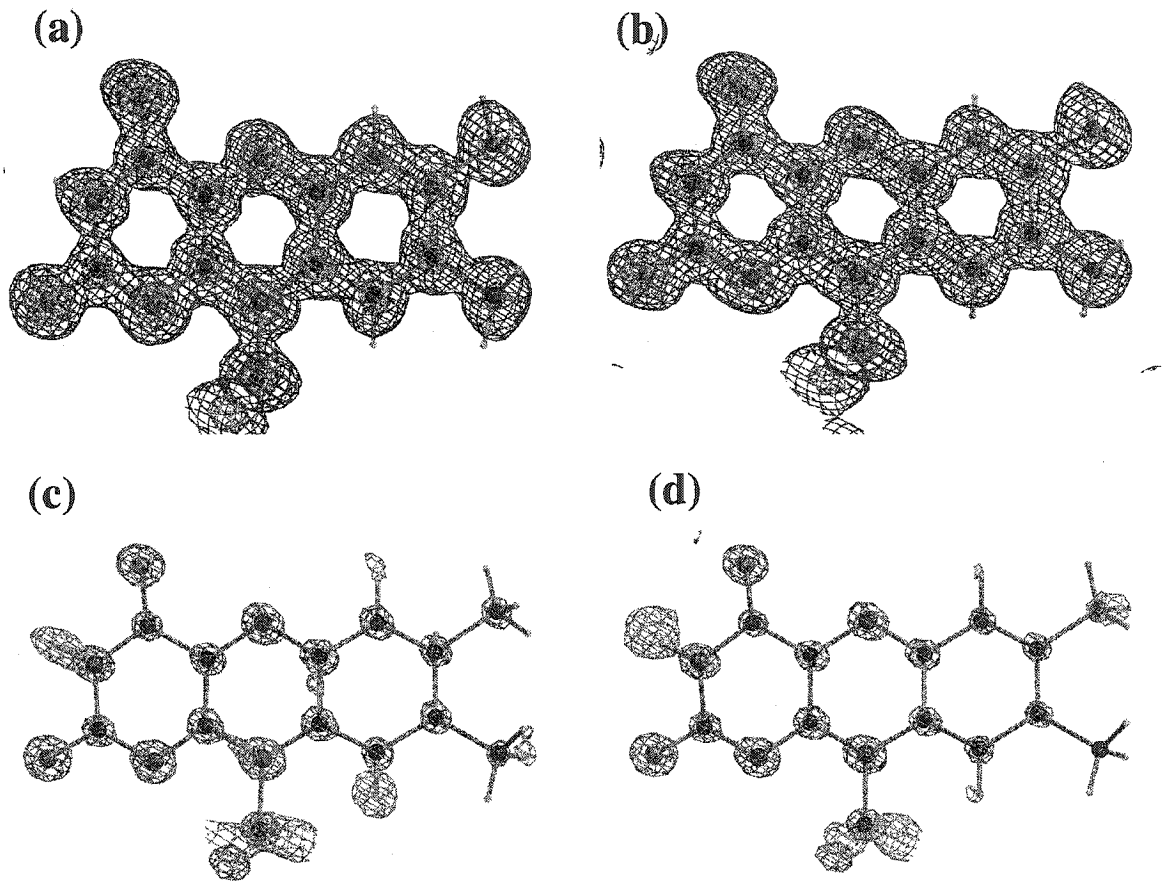

Figure 4.7 Electron density surrounding the isoalloxazine system, where Figures (a) and (c) represent the pH 7.4 structure and Figures (b) and (d) represent the pH 5.0 structure. The blue and magenta contours represent the SigmaA map with cutoffs at 0.8 and 3.3 e/Å^3 respectively. The green contours represent the Fo-Fc map, calculated from a model where the hydrogen atoms were excluded and contoured at 0.2 e/Å^3.

Protein-flavin interactions have been proposed to tune the reactivity of the isoalloxazine group by affecting its geometry. Therefore, one of the original goals of this study was to gain insight into how the surrounding protein environment and pH affects the geometry of the oxidized isoalloxazine group.

4.3.5.1 Isoalloxazine Geometry

The geometry of the isoalloxazine system in SCOA has significant differences in bond lengths and angles when compared to the small molecule crystallographic studies (Ebitani, 1993; Fritchie, 1975; Scarbrough, 1977) and theoretical structures (Cavelier & Amzel, 2001; Trickey et al., 2000; Zheng & Ornstein, 1996) of isoalloxazine systems. It is clear that the protein environment affects the geometry of the isoalloxazine. For example, both carbonyl groups of the isoalloxazine group in the SCOA structures have bond distances that on average are significantly longer (1.26 Å) than those calculated for either a fully oxidized or a fully reduced species (1.19 and 1.22 Å respectively). Small molecule isoalloxazine structures typically have carbonyl bond distances in the 1.19 to 1.24 Å range. The latter extreme was found in a structure where the carbonyl was involved in a hydrogen bonding interaction where the hydrogen atom from the donor was observed closer to the carbonyl group than the hydrogen bond donor atom (Fritchie, 1975). The only other atomic resolution structure with a reportedly long isoalloxazine carbonyl group (1.27 Å) was the 1.2 Å resolution DAAO structure (Umhau et al., 2000) another protein-bound flavin. Apparently, the enzyme environments in SCOA and DAAO stabilize elongated carbonyl groups on the isoalloxazine system. Perhaps, this is an example where the protein environment tunes the redox reactivity of the isoalloxazine

through its geometry. Theoretical calculations for the free isoalloxazine systems have shown a larger charge density on both O2 and O4 for a reduced state relative to an oxidized form (Cavelier & Amzel, 2001; Zheng & Ornstein, 1996). In addition, there are longer carbonyl bond lengths for the fully reduced state compared to the oxidized species (Zheng & Ornstein, 1996). In SCOA the protein environment may play a role in the stabilizing increased charge density on the O2 and O4 atoms by stabilizing the elongated carbonyl geometry. This observation indicates that, in addition to considering the bent geometry of the flavin, other structural features of the surrounding protein environment have a direct role in the geometry of the isoalloxazine system. Thus, accurate QM-MM studies need to include some isoalloxazine geometry optimization for the protein-bound group, rather than just geometries based on isolated systems.

An overall comparison of the isoalloxazine geometry in the SCOA structures to the calculated geometries of isoalloxazines with different redox and protonation states (Zheng & Ornstein, 1996) indicates that these protein-bound isoalloxazine groups more closely represent an anionic fully reduced isoalloxazine than any other species. This analysis involved a summation of the differences in the isoalloxazine bond distances between the structures compared (absolute magnitudes were used). The lowest sum of the differences for all five structures of SCOA was when comparing their respective isoalloxazine geometries to the fully reduced anioinic species calculated by Zheng and coworkers (Zheng & Ornstein, 1996). Perhaps, this is a direct result of the flavin being reduced in our structures, however, it is also likely a reflection of the geometry induced by the surrounding protein.

The twist angle for the isoalloxazine system varies slightly among the five atomic resolution structures of SCOA. The twist angle was calculated by separating the system into two planes, one including the pyrimidine ring and the N5 and N10 atoms and second plane defined by the benzene ring and the N5 and N10 atoms. A small variation of one degree in the twist angle (θ) was observed when comparing the different structures. What is intriguing is that the twist angle (θ) was found to consistently increase among the structures with increasing pH (pH 4.5 θ = 13.9(2); pH 5.0 θ = 14.4(2); pH 5.8 θ = 14.6(3); pH 7.3 θ = 14.8(2); pH 7.4 θ = 14.9(3)) As previously discussed, the redox state(s) of the isoalloxazine groups are uncertain, and likely represent a mixed population of redox states, for the pH 4.5, 5.0, 5.8 and 7.3 structures. The slight increase in the twist angle may reflect a small pH effect on the reduction rate of the isoalloxazine group or perhaps is a reflection of mixed population of redox species in each structure. As would be expected, the largest twist angle was observed in the pH 7.4 structure, which is predominately reduced, consistent with the theoretical calculations that a fully reduced state prefers a bent isoalloxazine geometry.

An unexpected observation is the lack of significant visible differences in the electron density of the isoalloxazine group between the structures. Figures 5.7a & 5.7b shows the electron density of the isoalloxazine for both the pH 5.0 and the pH 7.4 structures. The sigma levels are different between the two structures (0.77 and 0.83 e/Å^3 respectively), thus contour levels based on e/Å^3 were used for comparison. Aside from the N485 interaction with the isoalloxazine group there are no significant differences in the observed hydrogen–bond lengths involving protein-isoalloazine interactions among

the five structures. While some bond length and bond angle differences appear to be significant based on the estimated standard deviations (esds), we are unable to deduce any correlation of these differences to either population of reduced species, pH or structural differences. While it is likely that the apparent geometrical differences are the result of the combination of all three parameters considered (redox species, pH and structural differences), it could also be that the esds are underestimated and / or at these resolutions we are unable to detect the subtle differences among the structures.

4.3.5.2 Protein-isoalloxazine interactions

Unusual protein-flavin interactions are observed in the electron density of SCOA. Mutagenesis studies have indicated the N485 plays an important role in the reactivity of the enzyme (Yamashita et al., 1998; Yin et al., 2001). When N485 was mutated to an isosteric leucine residue the redox potential of the enzyme was reduced by 76 mV (Yin et al., 2001) indicating that it is more difficult to reduce the isoalloxazine system. As discussed earlier the ND2 atom of N485 acts as a hydrogen bond donor to the π system of the pyrimidine ring in the isoalloxazine system and has been proposed that this interaction is important for stabilizing the reduced cofactor. Indeed, the significance of this interaction was apparent in the first atomic resolution structure which indicated that conformer B of N485 places the hydrogen bond donor atom, ND2 around 3 Å from the from the "π" like orbital on the C4 and N3 atoms of the isoalloxazine system [Refer to Chaper 3]. The five structures presented here were refined independently of each other, and this close interaction between the FAD and conformer B of N485 was consistently

observed within hydrogen-bonding distance (where the ND2···π distances range from 2.99(3) to 3.04(4) Å).

Another atypical flavin-protein interaction observed in the SCOA structures involves a second asparagine residue, N119. Unlike the N485-flavin interaction, this residue positions the amide portion of the side chain away from the π system of the isoalloxazine and one of its CB hydrogen atoms is directed towards the N5 atom of the FAD (Figure 4.8). In Figure 4.8 the electron density that is unaccounted for in the model is shown in green (Fo-Fc electron density); the persistence of this density between the CB hydrogen atom and the N5 atom of the FAD suggests that the hydrogen atom is positioned farther from its modeled riding position and is closer to the flavin (Figure 4.8a). In addition to the difference density, shown in green in Figure 4.8a, there is also electron density observed in the sigmaa weighted map, shown in blue, in a similar position close to the N5 atom of the FAD. The appearance of electron density at that position in both maps suggests that this observation represents actual electron density at that position rather than noise in the map. An omit map where the hydrogen atoms are removed from the model was calculated and shown in Figure 4.8b. The electron density clearly reveals the presence of the hydrogen atom on CB of N119 and suggests that the hydrogen atom could be modeled with a longer bond distance to CB. Contouring the electron density with a lower cutoff of ¾ σ, as shown in cyan in Figure 4.8c, provides a clearer view of the actual hydrogen atom positions for both the elongated CB hydrogen atom and the backbone amide hydrogen atom of G120.

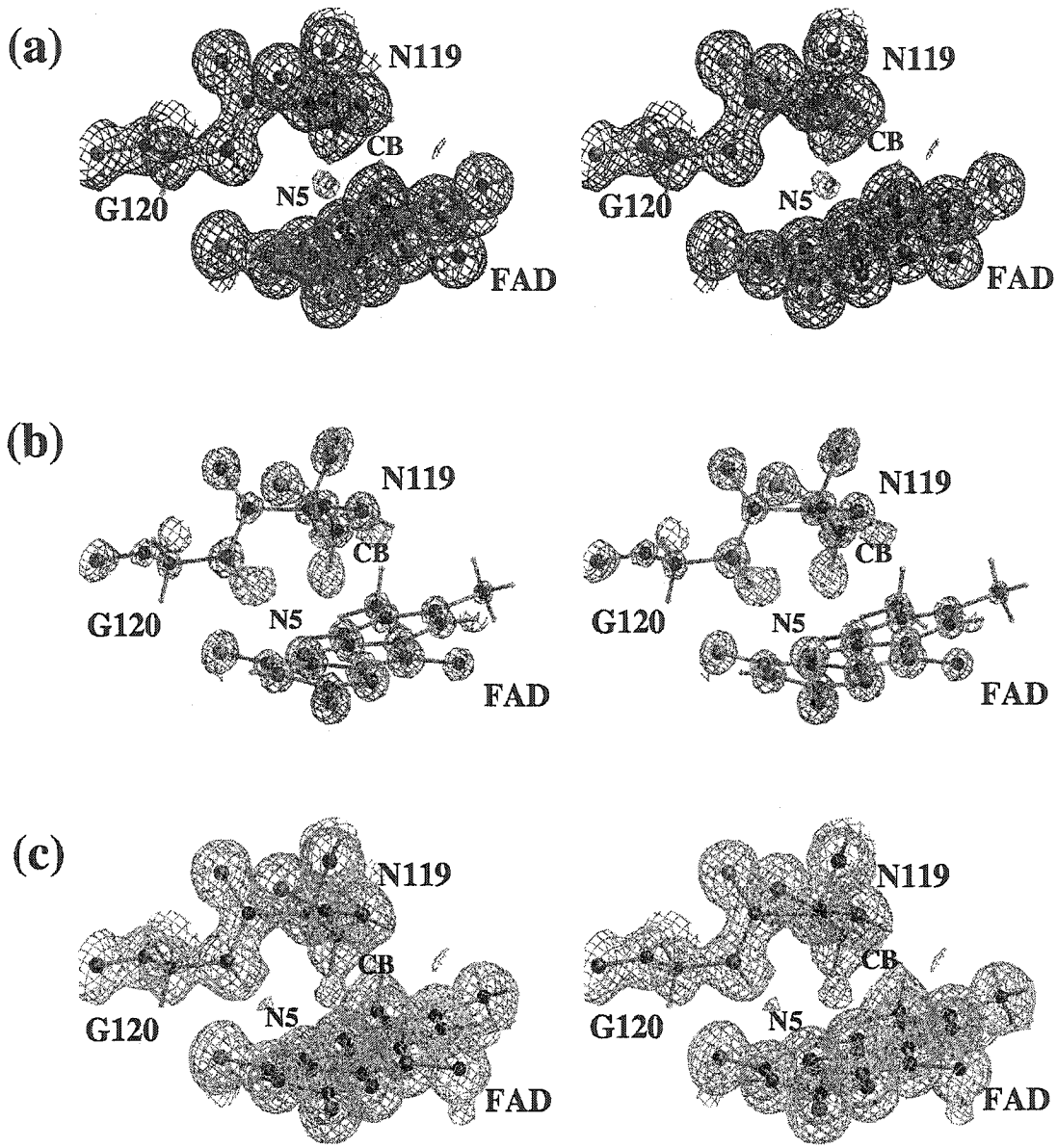

Figure 4.8 Stereoscopic representation of the electron density around N119 and the isoalloxazine system in the pH 7.4 structure. (a) Green contours represent the Fo - Fc map contoured at 2.5σ and magenta represents the SigmaA map contoured at 1σ. (b) Green contours represent the Fo-Fc map, calculated from a model where the hydrogen atoms were excluded and contoured at 2.5σ and magenta contours represent the SigmaA map contoured at 4σ. (c) Cyan contours represent the SigmaA map contoured at ¾ σ.

This unusual structural feature of an elongated CB hydrogen atom is consistently observed in all five structures. The importance of this unusual protein-flavin interaction is supported by the conservation of this residue in the structurally homologous enzyme, glucose oxidase (GOX). A structural comparison of the two enzymes indicates that the corresponding N107 homologue in GOX is identically positioned relative to the FAD. Furthermore, theoretical calculations of GOX have indicated that that asparagine residue contributes as little as 7 kcal/mol to the stabilization of the reduced flavin (Meyer et al., 1998).

Hydrogen bond donor groups in the vicinity of the N5 atom of the isoalloxazine system are a common feature among flavin oxidases (Fraaije & Mattevi, 2000). In addition to the N119 CB-H interaction, there is also a backbone amide hydrogen bond from the *si*-face in SCOA. The role of these hydrogen-bonding interactions can be inferred by considering the orbital geometries of the isoalloxazine system. If the isoalloxazine group is planar, then both of these hydrogen bonding interactions would be directed towards a π like lobe of the LUMO (lowest unoccupied molecular orbital) lobe rather than the lone pair in an sp^2 orbital on N5. However, for a bent isoalloxazine, where the bend is along the N5 - N10 axis, the hybridization of both the N5 and N10 atoms would be between sp^2 and sp^3. Pyrimidalization of the geometry of N5 would position the lone pair orbital closer to the two hydrogen bond donors observed on the *si*-face in SCOA, effectively maximizing the stabilization energy of these interactions. In addition, this orbital permutation would result in a larger LUMO lobe for the N5 atom on the re-face of the isoalloxazine, thereby increasing its reactivity as a hydride acceptor. The

presence of two hydrogen bond donors to N5 in SCOA likely contributes to the observed twist in the isoalloxazine and the reactivity of the cofactor.

4.3.5.3 Adenosine geometry

Some small structural differences in the adenosine ring geometries between the different structures were observed. Many of these differences can be attributed to a protonation at the AN7 atom of the adenosine at acidic pH. The hydrogen atom linked to the AN7 atom is clearly present in the pH 4.5 structure (Figure 4.9a), however the electron density of this hydrogen atom is weak in the pH 5.0 structure (Figure 4.9b) and does not exist in the pH 5.8 structure (Figure 4.9c). Together, Figures 4.9a, 4.9b and 4.9c effectively show a titration of the hydrogen atom on position AN7 of the adensoine ring. Based on these observations the pKa for AN7 is close to pH 5, which is comparable to the pKa of 5.1(1) measured for an adenosine analogue (Kampf et al., 2001). Despite the FAD cofactor being relatively buried in the protein, its adenosine ring portion is solvent accessible and apparently sensitive to the solution pH.

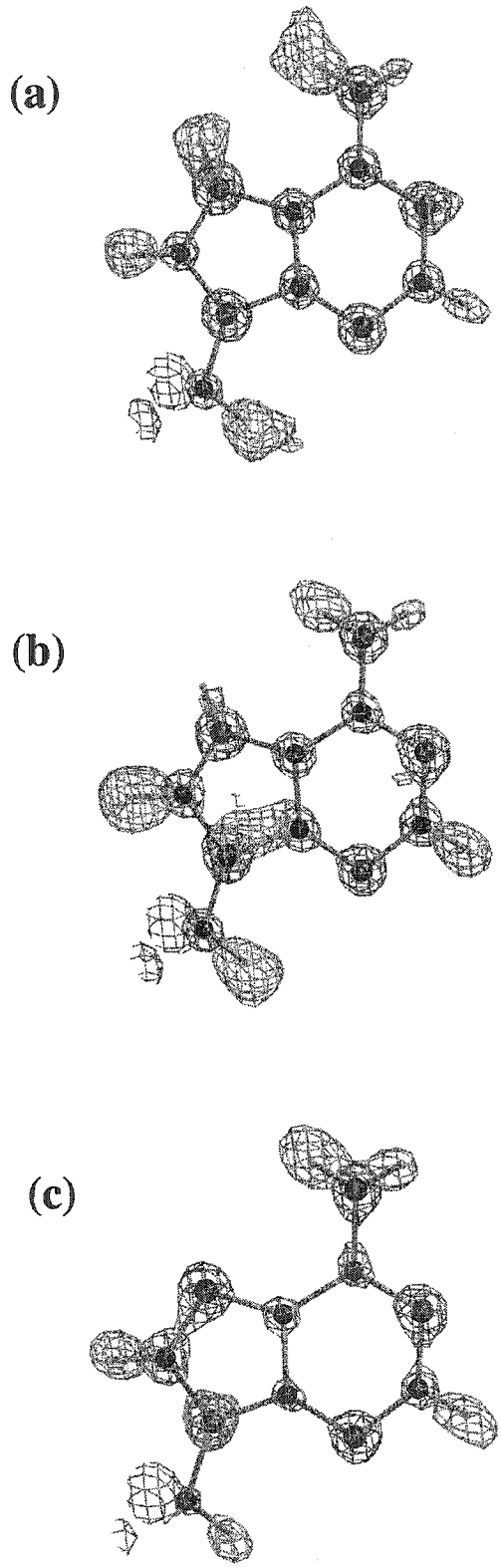

Figure 4.9 The electron density surrounding the adenosine ring of the FAD cofactor showing the protonation of nitrogen atom, AN7, at acidic pH. Figures represent the crystals grown at different pH values; (a) pH 4.5, (b) pH 5.0 and (c) pH 5.8. Green contours represent the Fo - Fc map contoured at 1.5σ and magenta represents the SigmaA map contoured at 4σ. The difference map was calculated with the hydrogen atoms excluded from the model.

4.3.5.4 Pyrophosphate geometry

One of the most important molecular motifs in biological systems are polyphosphate linkages. The FAD cofactor contains a pyrophosphate group connecting the ribityl chain to the ribose ring (Figure 1.1). The average P-O-P bond angle is 136°, the terminal P-O bond average is 1.49 Å and the average bridging P-O bond is 1.60 Å, which are all comparable with those values in related compounds (Guillot et al., 2001). Close examination of this functional group has revealed fascinating electronic features. Clearly polarized and odd-shaped electron density is observed for the oxygen atom that bridges the two phosphate atoms (Figure 4.10). The polarization could be the result of the P-O bonding orbital being more "π" like in nature. Similar flattening of the electron density for the other oxygen atoms within the pyrophosphate group is observed on the side that faces the phosphorous atom. Furthermore, with the electron density contoured at a low level, 1σ, breaks in the density are evident for some of the P-O bonds. This phenomenon is perhaps reflective of the low force constants calculated for these (Ma et al., 1994; McCarthy et al., 1998) and could reflect a more ionic nature for these bonding interactions.

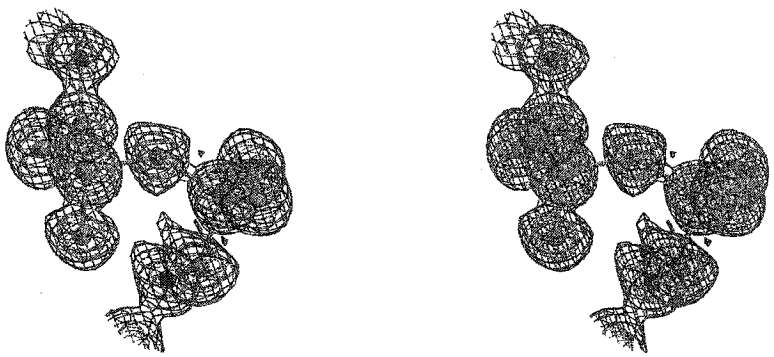

Figure 4.10 Stereoscopic representation of the electron density around the pyrophosphate group of the FAD cofactor. The SigmaA map is contoured at two levels where (a) blue represents 1σ and (b) magenta represents 4σ.

4.4 CONCLUSIONS

Atomic resolution studies present a detailed picture of protein structure. These structural observations can be used to provide insights into the enzyme mechanism. The unambiguous presence of a hydrogen atom on the NE2 atom of H447 in this structure, supports a newly proposed role for this residue as a hydrogen bond donor rather that as a general base. Resolving alternate conformations of residues in the structure and how these conformations can change at different pH values, provides insights into the dynamical nature of proteins. For example, how the conformation of one residue can allosterically effect the conformation of surrounding residues in a cascade-like fashion. In addition, these independently refined structures present unusual but consistently-observed electronic features. Polarization of the electron density surrounding the isoalloxazine system identified an unexpected protein-flavin interaction that likely effects the geometry

and reactivity of the cofactor, presenting a new paradigm for evaluating how the surrounding protein interacts and modulates the reactivity of an isoalloxazine group.

4.5 MATERIALS AND METHODS

4.5.1 Crystallization of SCOA at varying pH values

Crystals of SCOA were grown in a variety of pH values with a similar protocol as previously reported (Yue et al., 1999). Initial crystals were typically grown in 11% (w/v) poly(ethylene glycol) (PEG) MW 8000, 75mM $MnSO_4$, and 100 mM buffer where different buffers were substituted : pH 4.0 ($NaKPO_4$) , 5.2 (NaCacodylate), 6.0 (NaCacodylate), 7.5 (MOPS), and 9.0 (Glycine) (Table 4.1). The use of phosphate buffer for the pH 4.5 crystals necessitated the substitution of 75 mM $MnSO_4$ with 100 mM $(NH_4)_2SO_4$, to prevent $MnPO_4$ crystals. Crystals were cryo-protected with 20 – 30 % glycerol in identical mother liquor concentrations of the other reagents. The final measured pH values of the five differently buffered cryo-solutions were not equivalent to the original pH of the buffer used (Table 4.1). The most dramatic difference was found for the pH 9.0 buffered solution, which was found to be 1.6 pH units lower than the pH of the buffer. With higher pH buffers the manganese in the solution appears to undergo oxidation and produces a brown precipitate in the drop. Effectively, the presence of this precipitate results in a lowering of the pH, perhaps due to the formation of insoluble manganese hydroxide. At low pH values, it was difficult to obtain good quality crystals since the drops contain significant quantities of precipitated protein. Despite the differing

crystallization conditions all of the crystals were isomorphous with each other, adopting the space group P2. The cell dimensions for the five structures are listed in Table 4.4.

4.5.2 Data collection

Single crystals were transferred from their respective crystallization solutions to a glycerol cryo-protected mother liquor. For effective cryo protection an increase in the glycerol concentration from 20% to 30% was required for the crystals grown in glycine buffer. A single crystal at each pH value was used to collect atomic resolution data (Tables 4.1). The pH 4.5, 5.0, 5.8, 7.3 and 7.4 data sets were collected on the beamline X8C at the National Synchrotron Light Source, NSLS (Brookhaven National Labs). Data collection statistics are shown in Table 4.4.

4.5.3 Structure refinement and model quality

The 0.95 Å structure of SCOA at pH 5.0 has been previously reported [Refer to Chaper 3] and the additional structures of SCOA were refined in a similar manner. However, rather than use the 1.5 Å structure of SCOA as a starting model the pH 5.0 structure was modified and used for the initial refinement jobs for the other pH data sets. The modification of the starting model involved the removal of all alternate conformations, re-defining the temperature parameters as isotropic, truncation of the active site and tunnel residues to alanines (residues M122, V124, V191, P344, F359, A360, E361, L377, N485), removal of all of the active site water molecules, water molecules with isotropic temperature factors greater than 0.4, and the FAD cofactor.

The refinement was carried out using a restrained conjugate gradient least-squares algorithm as implemented in the program SHELXL97 (Sheldrick & Schneider, 1997). The default stereochemical restraints were applied to bond lengths, bond angles, chiral volumes and planar groups during the refinement. Additional restraints were applied to the temperature factors of bonded atoms and to solvent molecules, which exhibited high anisotropy. No constraints or restraints were put on the FAD atoms throughout the refinement.

Manual modeling was carried out using the program XFIT (McRee, 1999) and sigma-weighted maps with coefficients 2Fo-Fc and Fo-Fc (Sheldrick & Schneider, 1997). Manual modeling was carried out using the program XFIT (McRee, 1999) and sigmaA-weighted maps calculated by SHELXPRO with coefficients 2Fo-Fc and Fo-Fc (Sheldrick & Schneider, 1997). The free R-factor was monitored during the refinement using a randomly chosen subset of 5 % of the data.

Depending on the structure, 16 - 24 % of the residues were modeled in multiple conformations. While, many of these alternate conformations were observed to be dependent on pH, a large number maintained relatively similar alternative conformer populations for all of the structures. Multiple conformations were observed for 3 surface loops: residues 47-50; 186-188; 256-260. Disorder was observed at both the N-terminus and C-terminus, preventing the modeling of some residues and usually requirng the modeling of alternate conformations for residues close to the termini. Poor density was observed for around 3 % of the residues, all of which are located on the surface of the protein. These residues were modeled with either 50 % or 0 % occupancy.

Water molecules were added into positive difference density and where hydrogen bond contacts were made to polar atoms. A few exceptions, where persistent difference density near aromatic rings was observed, and these positions were modeled with water molecules. Since the occupancy of a water molecule is strongly correlated with its thermal parameter, they were typically modeled with full occupancy. However, if a water molecule was found to be associated through a hydrogen bond network with a multiple conformation residue then is was assigned occupancy of either 75% or 50% or 25% depending on the occupancy of the conformation of the residue to which it is associated. The occupancies of the water molecules in the region of the active site were coupled to those of the surrounding residues, M122, F359, E361 and N485. The shape of the electron density surrounding the key active site water molecule, Wat541, indicates that it is disordered. However an accurate model of these alternate water positions was not justified due to the lack of definition in the electron density.

As expected, when comparing the water positions between the five structures, most water molecules occupied identical positions. Some of the differences in the water positions between the structures were a direct result of differences in side chain conformations. The five structures show a wide variety in the number of modeled water molecules, from around 698 water molecules in the pH 4.0 structure to 818 modeled in the pH 7.4 structure (Table 4.4). The number of modeled water positions in a particular structure depends on the quality and the resolution range of the collected data.

The correlation between alternate side chain positions for different residues was determined by considering hydrogen bonding and steric interactions. Alternate side chain positions in close proximity to each other that were likely to co-exist were assigned the

same part number (i.e. conformation A or B). Many alternate conformations were identified before anisotropic refinement was carried out, however subsequent improvement of the electron density maps enabled lower occupancy conformers to be modeled. In order to remove bias in the temperature factor each additional residue conformation was first refined isotropically and then allowed to refine anisotropically.

In the pH 4.5 and 5.0 structures a di-oxygen molecule was modeled in the active site tunnel with a fixed occupancy of 25%. The identification of this species is not certain as the observed density may also represent two alternate water conformations. However, both positions require the adjacent active site residues to be present in conformer B. Furthermore these positions are approximately 1.2 Å from each other suggestive of a di-oxygen molecule.

Other compounds present in the mother liquor and cryo-protectant solution were observed in the crystal structures. Glycerol was found in the substrate-binding cavity of the pH 4.5 structure and on the surface of the protein in both the pH 7.3 and 7.4 structures. These glycerol molecules are all partially occupied and were found in overlapping positions with partially occupied water molecules. Three surface histidine residues in the pH 7.4 structure and one in the pH 7.3 structure were found to be complexed with an octahedrally coordinated metal ion. This ion was modeled as a manganese atom due to its presence in the mother liquor and the coordination geometry. All of the bound metal ion positions were partially occupied. Five phosphate anions were observed in the pH 4.5 structure and their occupancies were refined and ranged from 76 to 37 %. A similar tetrahedrally coordinated anion was observed in the pH 5.0 structure at the same position as 76% occupied phosphate position in the pH 4.5 structure. Since

the occupancy of the anion in the pH 5.0 structure is low, and its position in the structure is shared with a partially occupied by a water molecule, the occupancies of the anion and water were fixed at 25% and 75 % respectively. No phosphate anions were used in the mother liquor, so the identity of the anion at that position is uncertain. It was modeled as a sulfate anion, as this group is present in the mother liquor at high concentrations.

Hydrogen atoms were included after aniostropic refinement and modeling of the alternate conformations. Although over 70 % of the backbone hydrogen atoms were observed, the amount of experimental data does not warrant their positional refinement. Thus, all hydrogen atoms were added in riding positions. Hydrogen atoms that reside on hydroxyl groups (serine, threonine and tyrosine side chains) were automatically placed using a SHELX-97 algorithm that first fixes the hydrogen atom distance and angle and then searches around that defined cone for the maximum electron density peak, placing the hydrogen atom at that position. Although this method was quite successful in locating the correct or reasonable positions for most hydroxyl groups a number of examples were observed where the hydrogen atom position required rotation to prevent un-favorable interactions with other residues.

Upon completion of the refinement, an additional refinement cycles were performed using all of the data. Standard deviations for the coordinates were estimated using the full-matrix inversion method (Sheldrick & Schneider, 1997). The refinement statistics are presented in Table 4.2. The coordinates for the pH 5.0 structure have been deposited in the Protein Data Bank, PDB code: 1MXT (Berman et al., 2000) and we are in the process of depositing the coordinates for the other four structures.

4.6 ACKNOWLEDGEMENT

We thank Nathalie Croteau for crystallization of the enzyme and Rene Coloumbe and Louis Lim for useful discussions. This work is supported by the National Institutes of Health Grant GM63262 (A.V.) and HL53306 (N.S.S.) and Canadian Institutes of Health Research Grant MT-13341 (A.V.).

4.7 References

Berisio, R., Sica, F., Lamzin, V. S., Wilson, K. S., Zagari, A. & Mazzarella, L. (2002). Atomic resolution structures of ribonuclease A at six pH values. *Acta Crystallogr D Biol Crystallogr* **58**(Pt 3), 441-50.

Berman, H. M., Westbrook, J., Feng, Z., Gilliland, G., Bhat, T. N., Weissig, H., Shindyalov, I. N. & Bourne, P. E. (2000). The Protein Data Bank. *Nucleic Acids Research* **28**, 235-242.

Binda, C., Coda, A., Angelini, R., Federico, R., Ascenzi, P. & Mattevi, A. (1999). A 30-angstrom-long U-shaped catalytic tunnel in the crystal structure of polyamine oxidase. *Structure Fold Des* **7**(3), 265-76.

Bradley, L.H. & Swenson, R.P. (1999). Role of glutamate-59 hydrogen bonded to N(3)H of the flavin mononucleotide cofactor in the modulation of the redox potentials of the *Clostridium beijerinckii* flavodoxin. Glutamate-59 is not responsible for the pH dependency but contributes to the stabilization of the flavin semiquinone. *Biochemistry* **38**(38), 12377-86.

Cavelier, G. & Amzel, L. M. (2001). Mechanism of NAD(P)H:quinone reductase: Ab initio studies of reduced flavin. *Proteins* **43**(4), 420-32.

Christopher, J. A. (1998). SPOCK: The Structural Properties Observation and Calculation Kit (Program Manual)., Texas A&M University.

Davydov, R., Kuprin, S., Graslund, A. & Ehrenberg, A. (1994). Electron Paramagnetic Resonance Study of the Mixed-Valent Diiron Center in *Escherichia Coli* Ribonucleotide Reductase Produced by Reduction of Radical-Free Protein R2 at 77 K. *Journal of the American Chemical Society* **116**(24), 11120-11128.

Ebitani, M. I., Y.In,T.;Sakaguchi, K.-i.; Flippen-Anderson, J.L.; Karle, I.L. (1993). Structures of riboflavin tetraacetate and tetrabutyrate: molecular packing mode of riboflavin

tetracarboxylate and its extensive stacking and hydrogen-bonding characteristics. *Acta Cryst.* **B49**, 136-144.

Eriksson, M., Jordan, A. & Eklund, H. (1998). Structure of *Salmonella typhimurium nrdF* ribonucleotide reductase in its oxidized and reduced forms. *Biochemistry* **37**(13359-13369).

Fraaije, M. W. & Mattevi, A. (2000). Flavoenzymes: diverse catalysts with recurrent features. *Trends Biochem. Sci.* **25**, 126-132.

Fraaije, M. W., van Den Heuvel, R. H., van Berkel, W. J. & Mattevi, A. (2000). Structural analysis of flavinylation in vanillyl-alcohol oxidase. *J Biol Chem* **275**(49), 38654-8.

Fritchie, C. J. R. M. J. (1975). Molecular complexes of flavins. The crystal structure of lumiflavin-bis(naphthalene-2,3-diol) trihydrate. *Acta Cryst.* **B31**, 454-461.

Gadda, G., Wels, G., Pollegioni, L., Zucchelli, S., Ambrosius, D., Pilone, M. S. & Ghisla, S. (1997). Characterization of cholesterol oxidase from *Streptomyces hydroscopicus* and *Brevibacterium sterolicum*. *Eur. J. Biochem.* **250**, 369-376.

Genick, U. K., Soltis, S. M., Kuhn, P., Canestrelli, I. L. & Getzoff, E. D. (1998). Structure at 0.85 A resolution of an early protein photocycle intermediate. *Nature* **392**(6672), 206-9.

Ghisla, S. & Massey, V. (1989). Mechanism of flavoprotein-catalysed reactions. *Eur. J. Biochem.* **181**, 1-17.

Guillot, B., Lecomte, C., Cousson, A., Scherf, C. & Jelsch, C. (2001). High-resolution neutron structure of nicotinamide adenine dinucleotide. *Acta Crystallogr D Biol Crystallogr* **57**(Pt 7), 981-9.

Hasford, J. K., W.; Rizzo, C. J. (1997). Conformational effects on Flavin Redox Chemistry. *Journal of Organic Chemistry* **62**(16), 5244-5245.

Ishizaki, R., Hirayama, N., Shinkawa, H., Nimi, O. & Murooka, Y. (1989). Nucleotide sequence of the gene for cholesterol oxidase from a *Streptomyces* sp. *J. Bacteriol.* **171**(1), 596-601.

Kampf, G., Luth, M. S., Kapinos, L. E., Muller, J., Holy, A., Lippert, B. & Sigel, H. (2001). Formation of ternary complexes by coordination of (diethylenetriamine)-platinum(II) to N1 or N7 of the adenine moiety of the antiviral nucleotide analogue 9. *Chemistry* **7**(9), 1899-908.

Karplus, P. A. & Schulz, G. E. (1987). Refined structure of glutathione reductase at 1.54 Å resolution. *J Mol Biol* **195**(3), 701-29.

Kass, I. J. & Sampson, N. S. (1998). Evaluation of the role of His447 in the reaction catalyzed by cholesterol oxidase. *Biochemistry* **37**(51), 17990-18000.

Kiess, M., Hecht, H.-J. & Kalisz, H. M. (1998). Glucose oxidase from *Penicillium amagasakiense*: Primary structure and comparison with other glucose-methanol-choline (GMC) oxidoreductases. *Eur. J. Biochem.* **252**, 90-99.

Lario, P.I., Sampson, N. & Vrielink, A (2002) Sub-atomic resolution studies of cholesterol oxidase: What atomic resolution crystallography reveals about enzyme mechanism and the role of the FAD cofactor in redox activity. Submitted.

Lennon, B. W., Williams, C. H., Jr. & Ludwig, M. L. (1999). Crystal structure of reduced thioredoxin reductase from *Escherichia coli*: structural flexibility in the isoalloxazine ring of the flavin adenine dinucleotide cofactor. *Protein Sci* **8**(11), 2366-79.

Li, J., Vrielink, A., Brick, P. & Blow, D. M. (1993). Crystal structure of cholesterol oxidase complexed with a steroid substrate: Implications for flavin adenine dinucleotide dependent alcohol oxidases. *Biochemistry* **32**, 11507-11515.

Ma, B. Y., Meredith, C. & Schaefer, H. F. (1994). Pyrophosphate Structures and Reactions - Evaluation of Electrostatic Effects on the Pyrophosphates with and without Alkali Cations. *Journal of Physical Chemistry* **98**(33), 8216-8223.

Massey, V. & Hemmerich, P. (1980). Active-site probes of flavoproteins. *Biochem Soc Trans* **8**(3), 246-57.

Mattevi, A., Vanoni, M. A., Todone, F., Rizzi, M., Teplyakov, A., Coda, A., Bolognesi, M. & Curti, B. (1996). Crystal structure of D-amino acid oxidase: a case of active site mirror-image convergent evolution with flavocytochrome b2. *Proc Natl Acad Sci U S A* **93**(15), 7496-501.

McCarthy, W. J., Smith, D. M. A., Adamowicz, L., SaintMartin, H. & OrtegaBlake, I. (1998). An ab initio study of the isomerization of Mg- and Ca-pyrophosphates. *Journal of the American Chemical Society* **120**(24), 6113-6120.

McRee, D. E. (1999). XtalView/Xfit - A Versatile Program for Manipulating Atomic Coordinates and Electron Density. *J Structural Biology* **125**, 156-165.

Mewies, M., Packman, L. C., Mathews, F. S. & Scrutton, N. S. (1996). Flavinylation in wild-type trimethylamine dehydrogenase and differentially charged mutant enzymes: a study of the protein environment around the N1 of the flavin isoalloxazine. *Biochem J* **317**(Pt 1), 267-72.

Meyer, M., Hartwig, H. & Schomburg, D. (1996). Semiempirical and ab initio study of closed and open shell derivatives of 10-methylisoalloxazine: a model of flavin redox states. *Journal of Molecular Structure: THEOCHEM* **364**(2-3), 139-149.

Meyer, M., Wohlfahrt, G., Knablein, J. & Schomburg, D. (1998). Aspects of the mechanism of catalysis of glucose oxidase: a docking, molecular mechanics and quantum chemical study. *J Comput Aided Mol Des* **12**(5), 425-40.

O'Farrell, P. A., Walsh, M. A., McCarthy, A. A., Higgins, T. M., Voordouw, G. & Mayhew, S. G. (1998). Modulation of the redox potentials of FMN in Desulfovibrio vulgaris flavodoxin: thermodynamic properties and crystal structures of glycine-61 mutants. *Biochemistry* **37**(23), 8405-16.

Petsko, G. A. & Ringe, D. (2000). Observation of unstable species in enzyme-catalyzed transformations using protein crystallography. *Curr Opin Chem Biol* **4**(1), 89-94.

Ravelli, R. B. & McSweeney, S. M. (2000). The 'fingerprint' that X-rays can leave on structures. *Structure Fold Des* **8**(3), 315-28.

Reibenspies, J. H., Guo, F. & Rizzo, C. J. (2000). X-ray crystal structures of conformationally biased flavin models. *Org Lett* **2**(7), 903-6.

Rowland, P., Norager, S., Jensen, K. F. & Larsen, S. (2000). Structure of dihydroorotate dehydrogenase B: electron transfer between two flavin groups bridged by an iron-sulphur cluster. *Structure Fold Des* **8**(12), 1227-38.

Scarbrough, F. E. S., H.-S. ;Voet, D. (1977). The X-ray crystal structure of the molecular complexbis(lumiflavin-2,6-diamino-9-ethylpurine)-ethanol-water. *Acta Cryst.* **B33**, 2512-2523.

Schlichting, I., Berendzen, J., Chu, K., Stock, A. M., Maves, S. A., Benson, D. E., Sweet, R. M., Ringe, D., Petsko, G. A. & Sligar, S. G. (2000). The catalytic pathway of cytochrome P450cam at atomic resoluton. *Science* **287**, 1615-1622.

Schreuder, H. A., Prick, P. A., Wierenga, R. K., Vriend, G., Wilson, K. S., Hol, W. G. & Drenth, J. (1989). Crystal structure of the p-hydroxybenzoate hydroxylase-substrate complex refined at 1.9 A resolution. Analysis of the enzyme-substrate and enzyme-product complexes. *J Mol Biol* **208**(4), 679-96.

Sheldrick, G. M. & Schneider, T. R. (1997). SHELXL: High-resolution refinement. In *Methods in Enzymology* (Carter, C. W. J. & Sweet, R. M., eds.), Vol. 277, pp. 319-343. Academic Press, Boston.

Trickey, P., Basran, J., Lian, L. Y., Chen, Z., Barton, J. D., Sutcliffe, M. J., Scrutton, N. S. & Mathews, F. S. (2000). Structural and biochemical characterization of recombinant wild type and a C30A mutant of trimethylamine dehydrogenase from *methylophilus methylotrophus* (sp. W(3)A(1)). *Biochemistry* **39**(26), 7678-88.

Umhau, S., Pollegioni, L., Molla, G., Diederichs, K., Welte, W., Pilone, M. S. & Ghisla, S. (2000). The x-ray structure of D-amino acid oxidase at very high resolution identifies the chemical mechanism of flavin-dependent substrate dehydrogenation. *Proc Natl Acad Sci U S A* **97**(23), 12463-8.

Vrielink, A., Lloyd, L. F. & Blow, D. M. (1991). Crystal structure of cholesterol oxidase from *Brevibacterium sterolicum* refined at 1.8Å resolution. *J. Mol. Biol.* **219**, 533-554.

Weik, M., Ravelli, R. B., Silman, I., Sussman, J. L., Gros, P. & Kroon, J. (2001). Specific protein dynamics near the solvent glass transition assayed by radiation-induced structural changes. *Protein Sci* **10**(10), 1953-61.

Yamashita, M., Toyama, M., Ono, H., Fujii, I., Hirayama, N. & Murooka, Y. (1998). Separation of the two reactions, oxidation and isomerization, catalyzed by *Streptomyces* cholesterol oxidase. *Protein Eng* **11**(11), 1075-81.

Yin, Y., Sampson, N. S., Vrielink, A. & Lario, P. I. (2001). The presence of a hydrogen bond between asparagine 485 and the pi system of FAD modulates the redox potential in the reaction catalyzed by cholesterol oxidase. *Biochemistry* **40**(46), 13779-87.

Yue, Q. K., Kass, I. J., Sampson, N. S. & Vrielink, A. (1999). Crystal Structure Determination of Cholesterol Oxidase from *Streptomyces* and Structural Characterization of Key Active Site Mutants. *Biochemistry* **38**, 4277-4286.

Zheng, Y.-J. & Ornstein, R. L. (1996). A Theoretical Study of the Stuctures of Flavin in Different Oxidation and Protonation States. *J. Am. Chem. Soc.* **118**(39), 9402-08.

PREFACE TO CHAPTER 5

Protein structures have unique characteristics that make them efficient catalysts and electron transporters. Crystallographic techniques have provided insights into what particular features of the macromolecule are central for function. The emergence of atomic resolution protein structures are redefining our understanding of peptide structure and resulting in a re-parameterization of the models used to characterize lower resolution crystal structures, NMR structures and theoretically-derived structures. Unexpected observations in these structures are expanding our understanding of the multitude of ways the protein environment can tune its reactivity. For example, the helix dipole has been identified to play a role in catalysis for a number of enzymes including cholesterol oxidase. These atomic resolution structures of cholesterol oxidase have revealed numerous examples where the electron density is asymmetrically polarized. One re-occurring electronic feature we observed was electronic differences in the backbone carbonyl groups. While these observed differences were not always absolute, there is a strong correlation of the carbonyl density and the secondary structure of the main chain. These electronic differences have been well characterized through spectroscopic methods, however this is the first example where we visually observe the structural effects on the electron density of the polypeptide.

CHAPTER 5. ATOMIC RESOLUTION DENSITY MAPS REVEAL SECONDARY STRUCTURE DEPENDENT DIFFERENCES IN ELECTRONIC DISTRIBUTION

*Paula I. Lario and Alice Vrielink**

Department of Molecular, Cellular and Developmental Biology & Department of Chemistry and Biochemistry, Sinsheimer Laboratory, University of California Santa Cruz, Santa Cruz, CA, 95064, Biochemistry Department, McGill University, Montréal, QC, H3G-1Y6.

5.1 ABSTRACT

The X-ray crystal structure of the flavoenzyme cholesterol oxidase (*Streptomyces sp.*SA-COO) has been determined to 0.95Å resolution. The large size (55kDa) and the high resolution diffraction of this protein provides a unique opportunity to observe detailed electronic effects within a protein environment and to obtain a statistical sampling for which to analyze these electronic and structural differences. Our analysis indicates an increased tendency for the electron density of the main chain carbonyl groups within α-helices to be polarized towards the oxygen atoms. In contrast, the carbonyl groups tend to exhibit a greater charge density between the carbon and oxygen atoms within β-sheet regions of the structure. Interestingly, the electronic differences observed at the carbonyl groups do not appear to be correlated to the amide geometry. This study gives important insight into the activating effects of α-helix dipoles in enzymes and provides experimentally based observations that will be useful in parameterization of theoretical models.

5.2 INTRODUCTION

Carbonyl groups are perhaps one of the most important functional groups in organic chemistry. The reactivity of a carbonyl group depends on both its substituents and its surrounding environment. For instance, the electronic field generated by an α-helix in acyl-cysteine proteases polarizes the reactive carbonyl group of the substrate thus increasing its reactivity towards nucleophilic attack (Doran and Carey 1996). An α-helix dipole has been proposed to facilitate the oxidation reaction in cholesterol oxidase and other flavin oxidases such as D-amino acid oxidase, by stabilizing the additional negative charge generated on the reduced flavin cofactor (Ghisla and Massey 1989; Vrielink, Li et al. 1994; Fraaije and Mattevi 2000). Direct visualization of the electronic environments of backbone carbonyl groups within different structural elements will help in understanding the effects of electronic properties within a protein. In addition, such an analysis will provide an important link between other observations, including experimental data derived from spectroscopic methods and theoretically derived parameters and will lead to an improved understanding of the electronic features of secondary structure elements within proteins.

The electronic environment of the peptide carbonyl group within a protein is dependent on secondary structure. Environmental differences between carbonyl groups in a protein are responsible for many spectroscopic differences observed between α-helix and β-sheet structures (Haris and Chapman 1995:Shinji, 1996; Zuiderweg 2000). For example, distinct differences are observed in the backbone carbonyl FT-IR stretching

frequencies between α-helices and β-sheets. These differences are routinely used to assign the percentages of secondary structure elements during the characterization of a protein. NMR chemical shift differences between α-helix and β-sheet structures have been associated with varying degrees of polarization of the electron density surrounding the carbonyl group (Shinji 1996).

The resonance model has been used to explain the barrier to rotation around the amide bond and the general reactivity and stability of this functional group. That is, energetic stabilization is a result of π electron interactions where charge is transferred from the lone pair on the nitrogen atom into the carbonyl π system (Figure 5.1a & 5.1b). A systematic study of a series of twisted amide compounds was found to be consistent with the resonance model of an amide (Shinji 1996). However, *ab initio* molecular orbital theoretical studies have lead to a new interpretation about the electronic structure of amides (Wiberg 1992; Wiberg and Castejon 1995). While resonance arguments are concerned with π electrons, there are also usually changes in the σ system. These changes result in amide bonds with more ionic character (Figure 5.1c). Rather than a net charge transfer from the amide nitrogen atom, this electronegative atom withdraws more charge density from the carbonyl carbon atom. Thus Coulombic interactions between the atoms within the amide group, play a large role in both stability and geometry. This ionic nature within an amide group has been extrapolated to account for the stability of particular secondary structure motifs in proteins (Maccallum, Poet et al. 1995; Maccallum, Poet et al. 1995; Milner-White 1997).

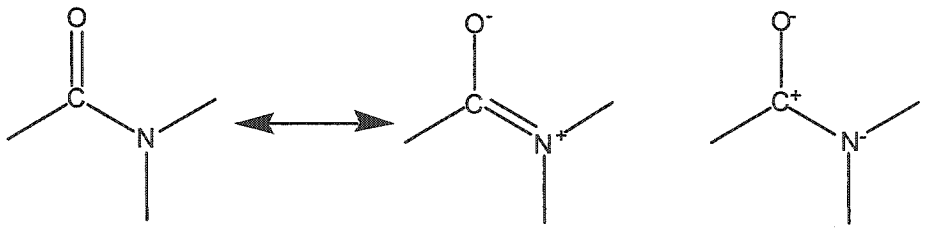

(a) (b) (c)

Figure 5.1 Different resonance and ionic forms of an amide group

Macromolecular systems are unique from small molecules in that they are often comprised of a significant hydrophobic core environment. Coulombic interactions are amplified in such an environment. Further studies of how carbonyl groups are affected by this microenvironment may enhance our understanding of electron polarization effects resulting from electrostatic interactions.

The sub-atomic resolution refinement of cholesterol oxidase, a relatively large enzyme (MWt = 55kDa), has provided us with an opportunity to observe significant differences in the electron density of the amide carbonyl groups. A unique advantage of this large structure is the ability to generate a statistically significant distribution of observations within a single crystal structure. Furthermore, such a large sampling of observations eliminates systematic errors associated with comparing structural differences between multiple crystals. For example, an analysis carried out on multiple crystals may result in bond length differences due to slight variations between the actual and the reported radiation wavelength used in each of the x-ray experiments. Our findings reveal significant electronic differences in the amide carbonyl groups for cholesterol oxidase and show that these differences are correlated with secondary structure.

5.3 METHODS

Cholesterol oxidase is a monomeric 55kDa flavoenzyme that crystallizes in the monoclinic space group P21 with unit-cell parameters a = 51.273Å, b = 72.964Å, c = 63.036Å and $\beta = 105.18°$. The crystals used for this study were grown by vapor diffusion from 12% polyethylene glycol MWt 8000, 75mM $MnSO_4$, 100mM glycine buffer pH 9.0 (The cryo-protected solution was measured and was at pH 7.4). Diffraction data from a single crystal cooled to 100K was collected to a resolution of 0.95 Å. using synchrotron radiation at a wavelength of 0.979Å. The data were collected on a Q4 Quantum detector on beamline X8C at the National Synchrotron Light Source, Brookhaven National Laboratory. The data were processed, merged and scaled with the HKL suite of software (reference from Methods in Enzymology). The data statistics are given in Table 5.1.

Table 5.1. Crystallographic data and refinement statistics

Crystal Parameters:	
Space Group	$P2_1$
Cell Dimensions	a = 51.273
	b = 72.964
	c = 63.036
	β = 105.18
Data Collection :	
Number of measured reflections	2567129
Number of unique reflections	277783
Resolution range (Å)	49 – 0.95
Resolution range for the last shell (Å)	0.97 – 0.95
Completeness (%)	98.8
Completeness in the last shell (%)	98.8
R-merge	0.049
R-merge for the last shell	0.349
Mean I/σ	19.4
Mean I/σ for the last shell	2.22
Refinement:	
Number of reflections used for refinement	239945

Number of reflections used for R_{free}	12008
R-factor (%)	9.7
Free R-factor (%)	11.9
r.m.s (bond lengths) (Å)	0.015
r.m.s (angle distances) (Å)	0.030
Number of protein residues	499
Number of water molecules	818 (436 full)
Isotropic average temperature factors ($Å^2$)	
All atoms	11.1
Main chain atoms	7.5
Side chains and waters	13.6
FAD molecule	5.6

The structure of cholesterol oxidase from *Streptomyces sp.* was previously solved and refined to 1.5 Å resolution (Yue, Kass et al. 1999) (PDB entry 1B4V). The water molecules and the FAD molecule were removed from this model and the active site residues: M122, F359, E361, H447 and N485 were all mutated to alanine. This truncated model was used as the initial model for crystallographic refinement. The program SHELX-97 was used to refine both the atomic positions and the anisotropic thermal parameters (Sheldrick and Schneider 1997). Standard SHELX restraints were used for the refinement however during the final cycle the restraints were removed in order to obtain

estimates of the standard deviations for atomic positions. Most aliphatic hydrogen atoms as well as all backbone hydrogen atoms were included in the model. The hydrogen atom positions were restrained to "ride" on the heteroatom to which they are bound. The free R-factor was monitored during the course of the refinement using a subset of 5% of the reflections randomly chosen from the total diffraction data. The structure refined to a final *R*-factor of 9.7 and a free *R*-factor of 11.9 with no data cutoff. The final refinement statistics are given in Table 5.1. Secondary structure assignments for the refined model were made with the program PROMOTIF (Hutchinson and Thornton 1996).

SIGMAA-weighted electron density maps with a grid set to 0.2Å were calculated with coefficients $2F_o - F_c$ using SHELXPRO (Sheldrick and Schneider 1997) and viewed using XTALVIEW (McRee 1999). MAPMAN (Kleywegt and Jones 1996) was used to extract and sum the electron density values at the atomic centers from the sigma-weighted map. The electron density values were summed for all grid points within a sphere of radius 0.8Å around the atomic position. In addition, the density surrounding each backbone carbonyl group was examined visually at two different electron density cutoff values: 4 sigma (2.2 e/Å^3) and 5 sigma (2.8 e/Å^3). If no separation in the electron density surrounding the carbon and the oxygen atoms within the carbonyl group was observed at 5 sigma then that particular carbonyl was labeled as "share". In contrast, if the electron density surrounding the carbonyl atoms was clearly separated at 4 sigma the carbonyl was labeled as "gap". Carbonyl groups where a gap was observed at 5 sigma but not at 4 sigma were labeled as "middle".

The maximum electron density peak for an individual atom is strongly correlated to the root mean square (rms) deviation of the atomic position. Large atomic movements

cause a smearing of the electron density thereby resulting in a lower peak density value than that for a less mobile atom. Therefore the map cutoff values used to classify the types of carbonyl groups are only useful in comparing atoms exhibiting similar thermal displacement parameters (B-factors). Most of the backbone atoms in the structure of cholesterol oxidase exhibit low B-factors, however, as observed in many protein structures, more mobile regions of the structure are observed. In the structure of cholesterol oxidase, the average B factor for main chain atoms is 7.45Å^2, corresponding to an average rms positional deviation of 0.385Å. Of the 498 amino acid residues modeled in the structure of cholesterol oxidase, 158 were excluded from further study either because they exhibited thermal parameters greater than 8.0Å^2 for the carbonyl carbon atom or because the carbonyl group was modeled in multiple conformations.

5.4 RESULTS

Initial comparison of the 0.95Å resolution electron density maps of cholesterol oxidase clearly revealed that many of the carbonyl groups within α-helices exhibit highly polarized electron density while those found within β-sheet structures show a greater propensity towards a shared density between the atomic centers (Figure 5.2). Based on these observations, a more thorough analysis was carried out in order to confirm whether a statistically significant relationship between the electronic features for carbonyl groups could be observed for different structural elements.

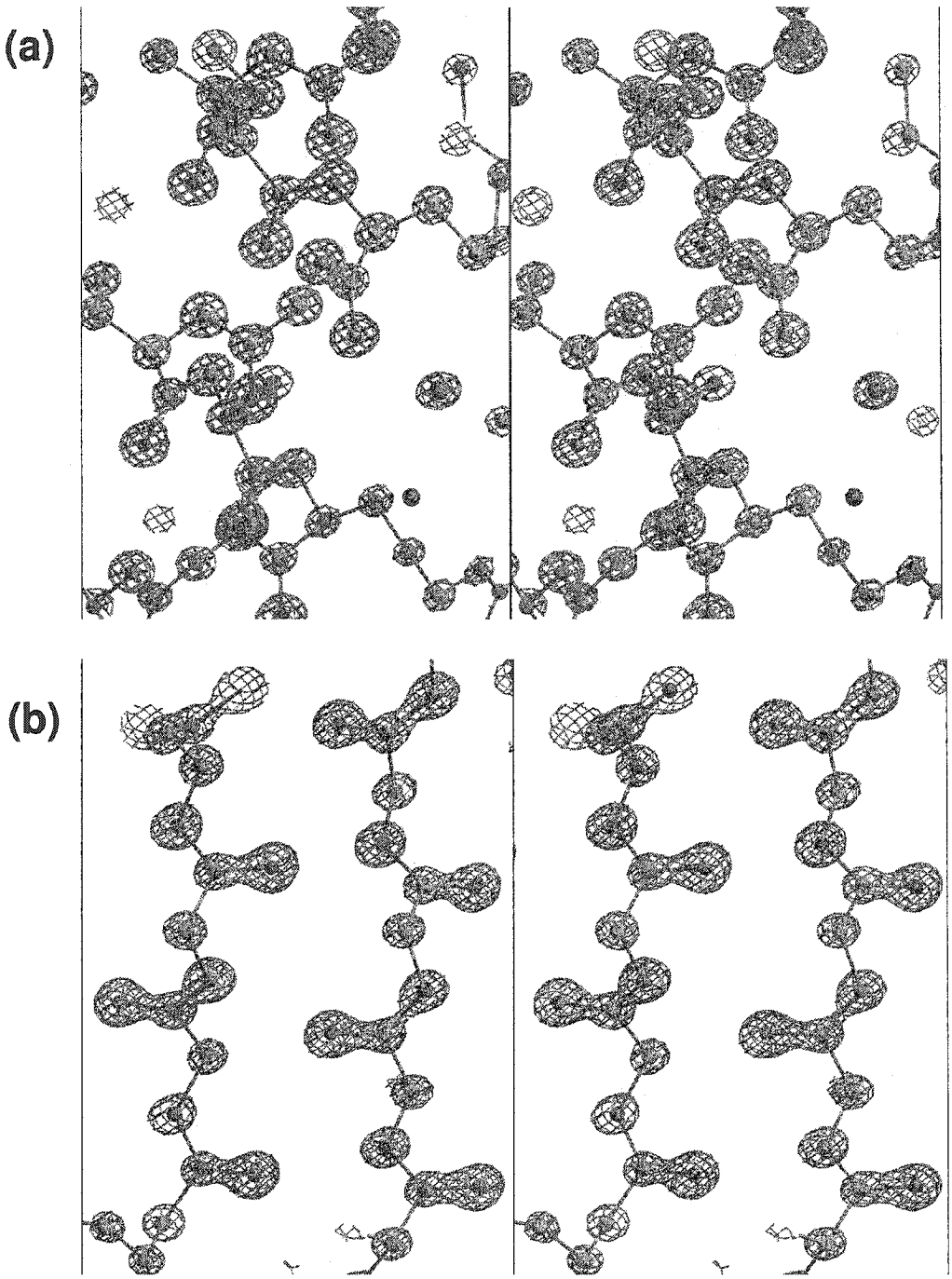

Figure 5.2 Stereographic representations of the electron density maps from the crystal structure of cholesterol oxidase showing (a) an α-helical region and (b) a region of β-sheet structure. The electron density maps were computed using the coefficients 2mFo-Fc and are contoured at 4.0 σ.

As mentioned above each of the 340 residues included in the study were visually classified as either "share", "middle" or "gap" depending on the appearance of the electron density at the carbonyl centers. The "middle" region was included in order to more clearly separate the differences of the two extreme cases. An example of each of the classified carbonyl groups is shown in Figure 5.3. The average distribution of the classified carbonyl densities for the 340 residues included in the study (~70% of the total residues) is shown in Figure 5.4a. An unequal distribution of the two extremes: "gap" and "share" is observed. Only 14 % of the carbonyl residues in the structure were observed to be of the "gap" type while 36 % were observed as the "share" type.

A similar unequal distribution of types of carbonyl groups was observed for residues involved in turns, random coils or 3_{10}-helices (Figure 5.4b). No significant differences were observed for the carbonyl electron density between these three types of secondary structure, so these groups were pooled together and labeled as "coil". This combined "coil" group represents 51% of the residues that were included in the study. The distribution of carbonyl types for the "coil" group is essentially identical to the average distribution observed for all 340 residues.

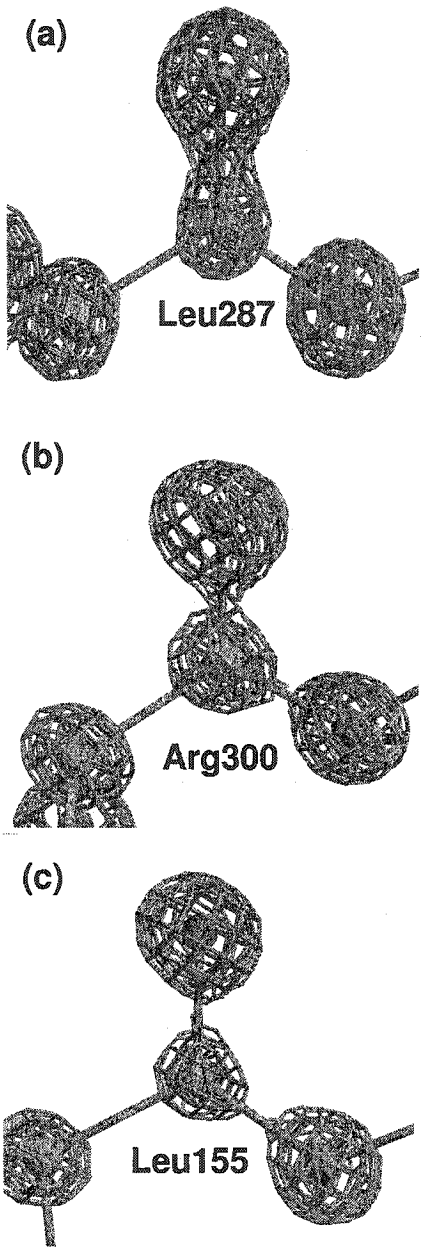

Figure 5.3 The peptide backbone electron density for (a) "share" (b) "middle" and (c) "gap" type carbonyl groups. Both the "share" (residue Leu 287) and the "gap" (residue L155) type carbonyl groups represent typical examples with a carbonyl bond length representative of their respective average. The electron density maps were computed using the coefficients 2mFo-Fc and contoured at 4.0 σ (shown in magenta) and at 5.0 σ (shown in blue).

Despite the compactness and stability of cholesterol oxidase, only 45 % of residues adopt α-helical (25 %) or β-sheet structures (20 %). However, clear differences for the electronic distribution of carbonyl groups between these two types of secondary structure motifs are apparent (Figures 5.4c and 5.4d). Over 50 % of residues that are present in β-sheet structure, exhibit a "share" type of electron density for their backbone carbonyl groups (Figure 5.4c), a 17% increase relative to the average distribution of "share" type carbonyl densities within the structure. In addition, a much higher percentage (53%) of "share" type carbonyl densities are observed in β-sheet structures compared to α-helical structures (compare Figures 5.4c and 5.4d). Correspondingly, there are fewer occurrences of "gap" type carbonyl densities for β-sheet residues. Within β-sheet structures, only 4% of carbonyl groups exhibited "gap" type densities compared to the percentage of "gap" occurrences of 14% for the overall structure.

While a predominance of "share" type carbonyl groups are observed for β-sheets, α-helices exhibit a significantly higher than average occurrence of "gap" type densities (Figure 5.4d). A difference of 18 % was observed between carbonyl groups exhibiting a "gap" type density distribution in α-helices and the overall distribution (compare Figure 5.4a and 5.4d). A more pronounced difference of 28% was observed upon comparison of the gap distribution between α-helical and β-sheet structures (compare Figures 5.4c and 5.4d). The percentage of α-helical residues adopting the "middle" type density distribution is essentially identical as those observed for all the residues and the "coil" group of residues. Thus, the greater occurrence of "gap" type carbonyl densities observed

in α-helices compared to the average distribution can be directly correlated to an 18 % decrease in the "share" type densities.

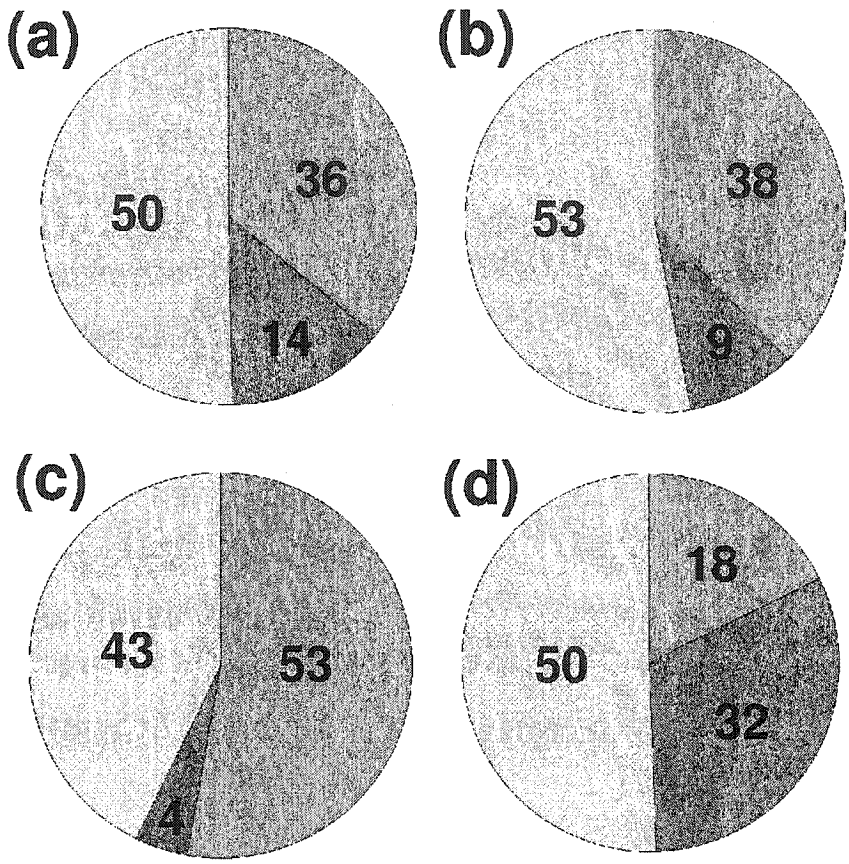

Figure 5.4 Electron density distribution for carbonyl groups in cholesterol oxidase. (a) Overall distribution of carbonyl types present in the enzyme (except those modeled in alternate conformations and those exhibiting thermal parameters greater than 8.0Å^2) (b) Combined pool of the carbonyl groups found in the loop and turn regions of the structure. (c) Carbonyl groups present in β-sheet structure. (d) Carbonyl groups present in α-helical structures. Blue, red and yellow represent carbonyl groups exhibiting "share", "gap" and "middle" type electron densities respectively.

One might expect that the observed polarization of the α-helix carbonyl groups, are associated with longer carbonyl, C=O, bond distances. A comparison of the average carbonyl bond lengths for the two extreme cases: the "gap" case within α-helices and the "share" case within β-sheets, reveal significantly longer distances within helical structures. Within cholesterol oxidase, there are 28 examples of the carbonyl groups within helices that exhibit gap type electron density and 37 examples of carbonyl groups within sheet structures that exhibit share type of density. An analysis of the average C=O bond distance within these populations is 1.245(8) Å for "gap" types within α-helices and 1.230(8) Å for the "share" types within β-sheet structures.

Despite these differences in carbonyl bond distances, there are examples of α-helix carbonyls that are of the "gap" type which have shorter C=O bond distances as well as "share" type β-sheet carbonyl groups with long C=O bond distances. For example, Ser291, present in an α-helix, has a short carbonyl bond distance of 1.231(8) Å and yet its electron density is clearly polarized and thus is classified as a "gap" case (Figure 5.5a). Likewise, Ile16, present in a β-sheet, has a long carbonyl bond distance of 1.248(8) Å and its carbonyl electron density is observed as a "share" case (Figure 5.5b). Although both of these residues have "atypical" carbonyl bond lengths, their electron density distribution is comparable to the "typical" examples presented in Figure 5.3 where the carbonyl bond lengths are close to the calculated average for their respective types of secondary structure.

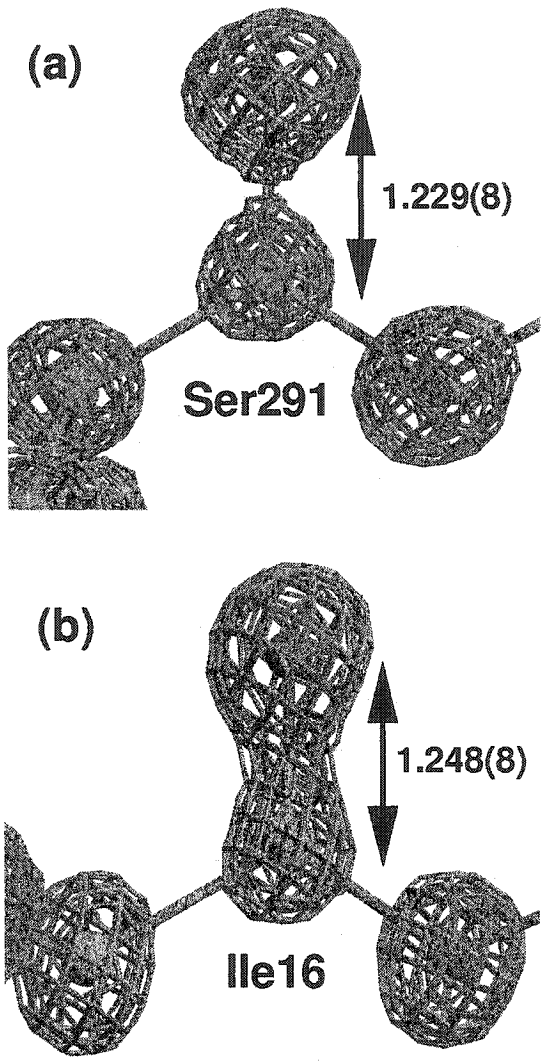

Figure 5.5 The peptide backbone electron density for (a) the α-helical residue, S291 and (b) β-sheet residue, I16. Both residues have atypical carbonyl bond distances despite exhibiting the characteristic carbonyl electron density type. The electron density maps were computed using the coefficients 2mFo-Fc and contoured at 4.0 σ (shown in magenta) and 5.0 σ (shown in blue).

A further study of the geometry between the two extreme types of carbonyl groups has revealed some significant differences as well as some interesting similarities. Quite unexpectedly there were no significant differences in the average amide C-N bond

distances between the gap and share type carbonyl groups, despite the observed differences in C=O bond lengths. However differences were observed in the ranges of C--N bond distances between the two types. When comparing the C-N bond distances for the 37 examples of the sheet "share" type a slightly larger sample range was observed (0.07 Å), than for the 28 examples of the helix "gap" type (0.05Å).

An analysis of peptide planarity was also carried out in order to determine if the classical resonance model could explain the density distribution. Although a larger deviation from planarity was observed for the O-C-N-CA dihedral angle in "share" type carbonyls within sheet structures compared to "gap" carbonyls in helical structures, there was no convincing correlation between the C-N bond distance and the dihedral angle for either type of carbonyl group.

When comparing the bond angles surrounding the carbonyl groups, we found that the average CA-C=O bond angles were essentially identical for different carbonyl types. However, for each of the other two bond angles: CA-C-N and O=C-N, differences of 2 degrees between the "gap" α-helix and "share" β-sheet carbonyl types were observed. The β-sheet "share" type carbonyl groups exhibit a larger average O=C-N bond angle (123.4(6)°) when compared to that found for α-helix "gap' type carbonyl groups (121.6(7)°). The averaged CA-C-N bond angle for the β-sheet "share" type carbonyl is 115.9(6)° and 117.9(6)° for the α-helix "gap" type. Interestingly, the 2 degree difference in the average CA-C-N bond angles between the two types is correlated to the difference in the average O=C-N bond angle suggesting a variation of the position of the nitrogen atom within the plane of the peptide bond.

Considering a resonance model for an amide, one would suppose that the oxygen atom in a polarized carbonyl group would exhibit a larger partial negative charge compared to a less polarized group. In order to ascertain if the geometric and electronic differences observed are a result of differences in their partial charges, a comparison of the peak heights for the amide atoms in the electron density maps was carried out.

The scattering phenomena in a diffraction experiment results from the electron density within the crystal and is characterized by the atomic scattering factors ($f=f_o e^{-B(\sin^2\theta)/\lambda^2}$ where f is the scattering factor for an atom at $\sin\theta/\lambda=0$, f_o is the scattering factor at some non zero value of $\sin\theta/\lambda$ and B is related to the mean-square amplitude of atomic vibration and parameter) . These scattering factors are a direct function of the atomic charge for a particular atom type and are used to calculate the electron density maps, which are based solely on the modeled structure. In addition to the atomic charge, the scattering factor is damped by an exponential function of the atomic vibration, which is not dependent on the atom type. Therefore, any observed differences in the atomic scattering factors for atoms with identical thermal parameters will be due solely to differences in their atomic charge. By comparing the integrated electron density values surrounding the atoms, any differences in atomic charge density should be apparent between atoms with similar isotropic thermal parameters.

Unfortunately, during the crystallographic refinement of the structure, the atomic thermal parameters are adjusted to improve the fit of the map computed using the experimental data, to a map calculated solely on the model and pre-assigned atomic charges. Thus, the difference in the actual atomic charge of the atom, from the pre-

assigned atomic charge, can be "soaked" up by the atomic thermal displacement parameters. In practice, one will observe a higher value for the thermal displacement parameters, to compensate for less electron density than expected at a particular atomic position.

In order to obtain a more realistic view of the actual atomic charge density, the atomic peak height was plotted against the isotropic thermal displacement parameter. This graph was examined for differences in the distributions of the amide atom between the two extreme cases: the "gap" case of α-helix and the "share" cases of β-sheet carbonyl groups (Figure 5.6). Some clustering was observed for the different "types" of carbonyl carbon atoms, however, no clear clustering was observed for either the oxygen or the nitrogen atoms. The carbonyl carbon atoms within α-helical regions of the structure tend to cluster in a region of the graph with higher thermal displacement parameters suggesting that less electron density is observed around these atoms in α-helical regions than in β-sheet regions of secondary structure.

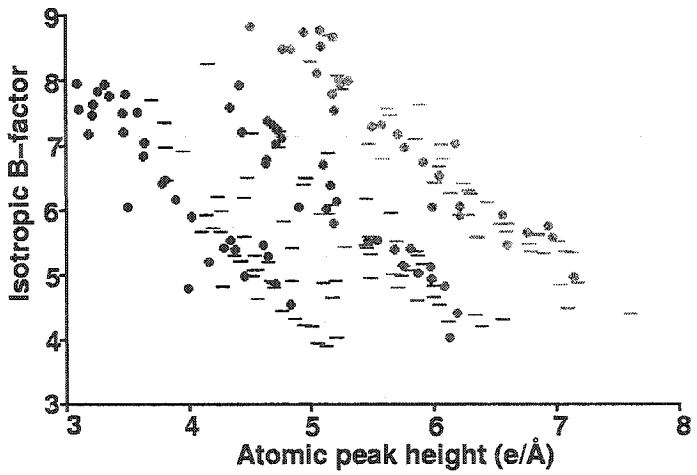

Figure 5.6 Atomic peak height distributions for the amide atoms present in α-helices (•) and β-sheet structure (-). Carbon atoms are represented in black, nitrogen atoms in blue and oxygen atoms in red.

Rather than using peak heights, one may also integrate the electron density within an assigned spatial region. Integrating and summing the electron density within a sphere surrounding the atom, will be more sensitive than using a single grid point (at the atomic peak) to compare atomic charge differences. Using an integration approach will minimize errors associated with differences between a tall sharp density peak seen for a more rigid atom and the flatter density peak of a more mobile atom. When these integrated peak values were plotted against the thermal parameters both the carbon and the oxygen atoms within the carbonyl group exhibit a clustering dependent on the secondary structure (Figure 5.7a). In contrast, no clustering was observed for the amide nitrogen atom (Figure 5.7b). The clustering observed in Figure 5.7a indicates a greater electron density near the atomic centers when the carbonyl group is in a β-sheet versus an α-helix. Interestingly no

significant differences in the electron density was found between the amide nitrogen atoms from different secondary structure elements.

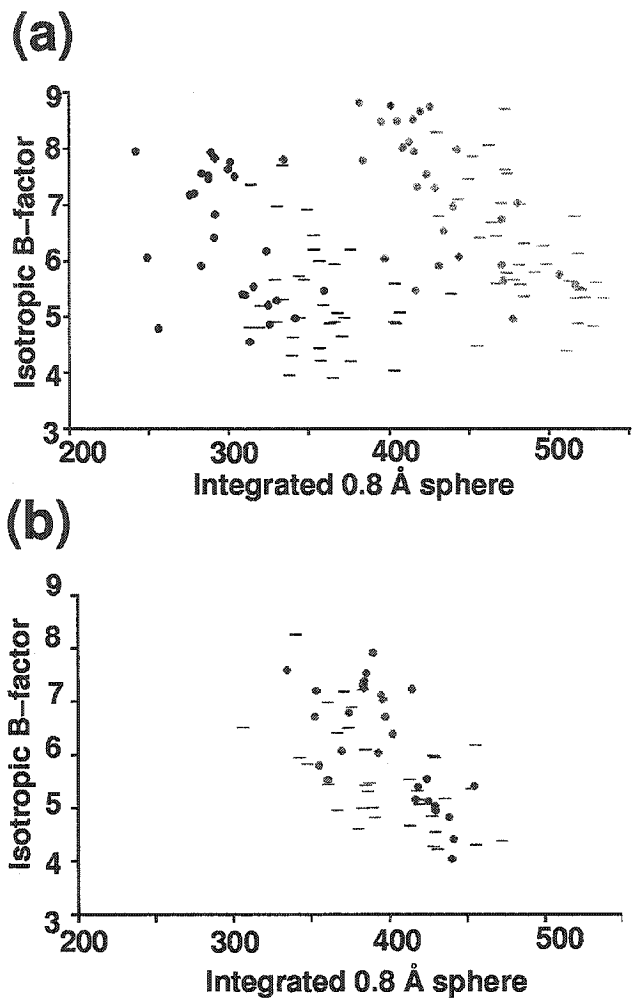

Figure 5.7 The electron density distributions for the amide (a) carbonyl atoms and (b) nitrogen atoms present in α-helices (•) and β-sheet structure (-). Carbon atoms are represented in black, nitrogen atoms in blue and oxygen atoms in red.

5.5 DISCUSSION

The degree of detail that can be observed by crystallographic studies of macromolecules is limited by the attainable resolution of the diffraction pattern. The

ability of electron density maps to represent the "actual" density of a molecule depends on the data resolution, data quality, and accuracy of the refined structural model. Atomic resolution data (≤ 1Å) provides a high-quality representation of the electron density surrounding each atom of the protein and these maps easily differentiate between carbon, nitrogen and oxygen atoms for the residues with low thermal displacement parameters. One-electron differences between atom types can be correlated to the observed differences in the magnitude of the electron density around the atom. Only in a few examples have macromolecules diffracted to extremely high (sub Ångstrom) resolution. Most of these high-resolution structures have been limited to proteins of molecular weight below 30KDa. We present a sub-Ångstrom resolution study of a larger protein thus enabling a better statistical evaluation of structural, electronic, and chemical features. Although such evaluations have been possible in the past using spectroscopic methods, this study provides a unique opportunity to directly visualize differences in the electronic environment of the peptide group as a function of secondary structure elements.

The calculated electron density is represented by contouring a map at various cutoff levels, where 1 sigma is the average root mean square deviation of the noise of the map. When the electron density map for cholesterol oxidase was contoured at 4 sigma (2.2 e/Å^3), interesting differences in the electron density of the backbone carbonyl groups were observed (Figure 5.2). Originally, we noticed that many of the carbonyl groups of residues in β-sheets did not exhibit resolved electron density around the individual carbonyl atoms even when contoured at 5 sigma (2.8 e/Å^3). For most other atoms within

the structure a 5 sigma contour level results in well resolved spherical electron density. This apparent delocalization of the electronic charge between the carbonyl atoms within a β-sheet could be the result of larger charge density relative to carbonyl atoms in α-helices and differences in the shapes of their "atomic" orbitals. These electronic differences are not strictly correlated with C=O bond length since examples of both short and long carbonyl bond distances are observed for both density types; "share" and "gap" (Figures 5.3 and 5.5).

As one might expect, from spectroscopic studies, the carbonyl groups of residues within α-helices have a more polarized electron density than those in β-sheets (Figure 5.2). Indeed, analysis of our structure reveals less electron density between the carbon and oxygen atoms for the α-helix carbonyl groups, when compared to those in β-sheets. The predominance of a gap in the electron density between α-helix carbonyl groups contoured at 2.2 e/Å^3 suggests possible differences in orbital hybridization between α-helices and β-sheets.

The similar distribution of carbonyl types of the pooled "coil" structure to the overall distribution within the protein, agrees well with the calculated ^{13}CO NMR tensor distribution found for the protein, Binase, where no significant differences were observed relative to the overall average (Pang 2000). The largest differences in the tensors were found between the averaged α-helix and the β-sheet values, where the averaged isotropic chemical shift differences were σ_{iso} 178.1(1.4) for α-helix and 174.9(1.4) for β-sheet structures. These results agree well with the electronic differences observed for the

carbonyl groups of cholesterol oxidase, where the α-helix carbonyl charge density is more polarized and less charge density is observed on the carbonyl carbon atom.

This polarization of the α-helix "gap" type carbonyl, does not appear to be the result of differences in the amide bond order or planarity since no significant differences in the C-N bond lengths or the C-O-N-C_a dihedral angle was observed between the carbonyl groups from different secondary structure regions. In addition, the charge density at the amide nitrogen center and within an 0.8 Å radius sphere does not indicate any dependence on the adopted secondary structure. Thus it appears that environmental factors affecting the electron density of the carbonyl group are not associated with electronic differences of the amide nitrogen atoms. Rather, hydrogen bonding and other Coulombic interactions with the carbonyl group, are likely to be responsible for polarizing its electron density.

Carbonyl-carbonyl interactions have been implicated as a significant attractive force in holding main-chain amide groups together in proteins, resulting in the predominance of particular secondary structure motifs (Maccallum, Poet et al. 1995a; Maccallum, Poet et al. 1995b). The electrostatic interaction between oppositely charged oxygen and carbon atoms of carbonyl groups are proposed to be partially responsible for distorting the amide hydrogen bond geometry from planarity. The uncorrelated relationships between the C=O and C-N bond distances and the amide twist angle support such an alternative stabilizing interaction as responsible for the differences in the carbonyl electron density as opposed to the more classical resonance model. If the increased charge density observed for both of the β-sheet carbonyl atoms (Figure 5.7a) was due to donation from the lone pair

nitrogen then a decrease in charge density for the nitrogen atoms from β-sheet residues (Figure 5.7b) should also have been observed. Clearly, these studies indicate that the observed electronic features cannot be explained by differences in amide resonance structures.

In summary our study suggests that, in a protein structure, the ionic nature of a planar amide (Figure 5.1) proposed by Wiberg (Wiberg 1999) appears to be a superior model to the resonance model historically used to describe a peptide group. Although α-helix carbonyl bonds are slightly longer than those found in β-structure, there is no correlation between the carbonyl bond length and amide C-N bond distance. In addition, the charge density of the carbon atom for the polarized α-helix carbonyl is typically lower than that observed for the β-sheet carbonyl. This suggests that, for an α-helix peptide, there is less charge transfer from the nitrogen to the carbon atom despite the tendency of the peptide bond to be more planar than β-sheet peptides.

These observations may help address our understanding of how atomic positions are related to their surrounding electronic environment, and if the strength of a bonding interaction is less dependent on distance than on the orbital shape and charge density. Further work to correlate these findings to both spectroscopic measurements and quantum mechanical calculations will help to test the accuracy and predictability of these methods to represent charge polarization within protein structure.

5.6 ACKNOWLEDGMENTS

We thank Louis Lim, Nicole Sampson, Bill Scott and Glenn Millhauser for useful discussions. We also thank Nicole Sampson for providing purified cholesterol oxidase for this study. This work is supported by the grants from the National Institutes of Health Grant GM63262 and the Canadian Institutes of Health Research Grant MT-13341.

5.7 REFERENCES

Doran, J. D. and P. R. Carey (1996). Alpha-helix dipoles and catalysis: absorption and Raman spectroscopic studies of acyl cysteine proteases. *Biochemistry* **35**(38): 12495-502.

Fraaije, M. W. and A. Mattevi (2000). Flavoenzymes: diverse catalysts with recurrent features. *Trends Biochem. Sci.* **25**: 126-132.

Ghisla, S. and V. Massey (1989). Mechanism of flavoprotein-catalysed reactions. *Eur. J. Biochem.* **181**: 1-17.

Haris, P. I. and D. Chapman (1995). The conformational analysis of peptides using Fourier transform IR spectroscopy. *Biopolymers* **37**(4): 251-63.

Hutchinson, E. G. and J. M. Thornton (1996). PROMOTIF--a program to identify and analyze structural motifs in proteins. *Protein Sci* **5**(2): 212-20.

Kleywegt, G. J. and T. A. Jones (1996). Xdlmapman and Xdldataman - Programs for Reformatting, Analysis and Manipulation of Biomacromolecular Electron-Density Maps and Reflection Data Sets. *Acta Crystallographica Section D-Biological Crystallography* **52**: 826-828.

Maccallum, P. H., R. Poet, et al. (1995a). Coulombic Attractions between Partially Charged Main-Chain Atoms Stabilise the Right-Handed Twist Found in Most Beta-Strands. *J.Mol.Biol.* **248**(2): 374-384.

Maccallum, P. H., R. Poet, et al. (1995b). Coulombic Interactions between Partially Charged Main-Chain Atoms Not Hydrogen-Bonded to Each Other Influence the Conformations of Alpha-Helices and Antiparallel Beta-Sheet - a New Method for Analysing the Forces between Hydrogen Bonding Groups in Proteins Includes All the Coulombic Interactions. *J.Mol.Biol.* **248**(2): 361-373.

McRee, D. E. (1999). XtalView/Xfit--A versatile program for manipulating atomic coordinates and electron density. *J Struct Biol* **125**(2-3): 156-65.

Milner-White, E. J. (1997). The partial charge of the nitrogen atom in peptide bonds."*Protein Science* **6**: 2477-2482.

Pang, Y., Zuiderweg, R.P. (2000). Determination of Protein Backbone 13CO Chemical Shift Anisotropy Tensors in Solution. *J. Am. Chem. Soc.* **122**(19): 4841-4842.

Sheldrick, G. M. and T. R. Schneider (1997). SHELXL: High-resolution refinement. *Methods in Enzymology*. C. W. J. Carter and R. M. Sweet. Boston, Academic Press. **277:** 319-343.

Shinji, Y. (1996). Effects of C(O)-N Bond Rotation on the 13C, 15N, and 17O NMR Chemical Shifts, and Infrared Carbonyl Absorption in a Series of Twisted Amides. *J. Org. Chem.* **61**(3): 941-946.

Vrielink, A., J. Li, et al. (1994). The crystal structure of cholesterol oxdiase. Mechanistic implications for FAD dependent alcohol oxidation. *Flavins and Flavoproteins*. B. Curti, S. Ronchi and G. Zanetti. Berlin, Water de Gruyter & Co.: 175-184.

Wiberg, K. B. (1999). The interaction of carbonyl groups with substituents. Acc. Chem. Res. **32**(11): 922-929.

Wiberg, K. B. and H. Castejon (1995). Carbanions .2. Intramolecular Interactions in Carbanions Stabilized by Carbonyl, Cyano, Isocyano, and Nitro Groups." *J. Org. Chem.* **60**(20): 6327-6334.

Wiberg, K. B. B., C.M. (1992). Resonance interactions in acyclic systems. 3. Formamide internal rotation revisted. Charge and energy redistribution along the C-N bond rotational pathway. *J. Am. Chem. Soc.***114**(3): 831-840.

Yue, Q. K., I. J. Kass, et al. (1999). Crystals Structure Determination of Cholesterol Oxidase from *Streptomyces* and Structural Characterization of Key Active Site Mutants. *Biochemistry* **38**: 4277-4286.

Zuiderweg, Y. P. a. E. R. P. (2000). Determination of Protein Backbone 13CO Chemical Shift Anisotropy Tensors in Solution. *J.Am.Chem.Soc.* **122**(19): 4841-4842.

CHAPTER 6. CONCLUSIONS

6.1 GENERAL DISCUSSION

Cholesterol oxidase from *Streptomyces sp.* (SCOA) is a model enzyme with which to study the catalytic effects of protein structure. The redox cofactor, FAD, in SCOA interacts with the surrounding protein environment through hydrogen bonds, π-stacking and helix dipoles. Closer examination of these interactions has lead to new insights into the roles these interactions play in catalysis. In addition to the classical hydrogen bonds, involving two electronegative atoms sharing a hydrogen atom, it is clear that there are other more subtle interactions with the flavin involving hydrogen bond donations to the isoalloxazine system. Together these protein interactions affect the conformation of the redox cofactor, twisting and adjusting the atomic positions to a shape more favorable for additional electronic charge. It has been well established that the reduced FAD is more stable with a bent isoalloxazine group, however the protein interactions likely also affect the reactivity of FAD by permutating its orbital geometries.

The work presented in this thesis provides more precise experimental geometries and electronic distributions of the isoalloxazine group in a protein. These experimental studies will be invaluable for comparisons to theoretical models as a test of their predictive capability. In addition the studies have indicated that the protein bound isoalloxazine geometry is significantly different than those calculated for isolated groups. This result confirms the necessity of geometry optimization for a protein bound isoalloxazine group in QM-MM studies, if one wants to obtain more representative results.

The observation of differences in the electron density of main chain carbonyl groups indicates that, in addition to the spherical model used to depict the atomic positions, other parameters are needed to describe orbital geometries. Charge density studies, which include polarization terms, will be further pursued in the Vrielink laboratory in order to characterize these electronic features of protein structure. While we were limited in our studies to elucidate the electronic differences in the isoalloxazine system among the five different atomic resolution structures, it is likely that charge density studies will clarify the significant differences observed in the isoalloxazine geometries.

The characterization of the different carbonyl types is just one example a protein structural feature that can be studied with the sub-atomic resolution electron density maps. With the five independently refined structures, the more subtle electronic features of these maps can be examined with added confidence that these observations are significant and not an artifact of the noise in the maps. For example, one could study the effect of polarization in aromatic groups. Perhaps improving our understanding of why these groups are involved in both repulsive and attractive π - π interactions. Further insights into the structural features that are responsible for the electronic stabilization in particular secondary structural motifs such as α-helices and turns may be discovered with further analyses of these structures.

6.2 Future crystallographic studies of the FAD cofactor

Now that we are aware of the sensitivity of the FAD cofactor to X-ray irradiation, further tests can be carried out in order to isolate the different redox species of the

isolloxazine system. Perhaps the absence of glycerol as a cryo-protectant would significantly slow down the artificial reduction of the crystals. Efforts are currently underway to obtain a microspectrometer that can be used in conjunction with data collection to obtain absorption spectra of single crystals during the course of the diffraction experiment. This would allow us to quantatively measure the reduction of the SCOA crystals during the course of the experiment. Clearly, comparisons of a fully oxidized crystal and the fully reduced crystal would be invaluable for experimentally determining where the two additional electrons in the reduced state are distributed in the isoalloxazine system. These observations could then be compared to theoretical calculations and correlated with kinetic data.

Our studies also strongly suggest that side chains of residues move in the frozen crystals during the course of the experiment as a function of the reduction rate. This phenomenon can be examined in more detail using a method of combined data collections as described by Berglund et al. (Berglund et al., 2002). Diffraction data is collected on many crystals randomly orientated in a cryo-loop. With this data, one can effectively obtain relatively complete data sets corresponding to different X-ray irradiation exposure times, by pooling together data collected with similar exposure times. For example, using multiple SCOA crystals at pH 5.0, one could pool together data collected in the first hour from these crystals and effectively have a complete data set for an oxidized enzyme. The results presented in this thesis have shown that the reduction rates of SCOA are dependent on the mother liquor matrix, likely the glycerol concentration. This observation can be utilized by finding the optimal condition where reduction of the crystal is gradual over the course of the experiment. Then by collecting

multiple data sets, pooling the data together by exposure times and refining each pooled data set independently, a dynamic picture should result that reveals how the protein and isoalloxazine change as a function of reduction.

6.3 Future studies of a flavoenzyme mecahnism

Another goal of this thesis was to determine the catalytic roles of the residues surrounding the isoalloxazine system in SCOA. Multiple roles have been observed for the asparagine residue, N485. By positioning its side chain towards the pyrimidine ring of the isoalloxazine system N485 stabilizes the additional charge on the reduced cofactor and, through a network of interactions, this movement gates the opening of a narrow hydrophobic tunnel leading to the isoalloxazine system. It is highly probable that this is the route that molecular oxygen takes to access the active site and reoxidize the cofactor.

Many hydride transfer reactions catalyzed by flavoenzymes are proposed to be activated by a preceding proton abstraction of the substrate by an active site base. The active site histidine residue, H447 had, prior to these studies, been characterized as the active site base for the oxidation reaction. The work presented in this thesis has shown that H447 is not the active site base, but rather plays a crucial role in orienting the substrate relative to the isoalloxazine system. The histidine residue is conserved among the glucose-methanol-choline (GMC) family of enzymes (Cavener, 1992; Kiess et al., 1998). Further assessment and revaluation of the role of the histidine in those enzymes could be useful in evaluating the necessity of an active site base for flavin assisted hydride transfer reactions. It is unclear through examination of the structure of glucose oxidase (GOX), a structurally homologous enzyme to SCOA, what the role of its

analogous histidine is in the oxidation reaction. Mutagensis and kinetic studies, of GOX where the histidine is mutated to an asparagine, could perhaps provide some insights into its role in oxidation. If the analogous histidine is in fact an active site base in GOX then this would present an example where conservation of a residue does not necessary indicate conservation of its function.

All of the crystallographic structures presented in this thesis were carried out in the absence of the substrate. A complex structure of the *Brevibacterium sterolicum* cholesterol oxidase (BCO1) is known (Li et al., 1993), however we propose that the bound steroid substrate is not in the position necessary for oxidation, but rather positioned as an artifact of the reduced state of the FAD cofactor in that structure. Clearly more conclusive evidence would result from a substrate complex with the fully oxidized cofactor. Methods for trapping the Michaelis complex (cholesterol & oxidized FAD) include using mutants like N484L where the oxidative activity is dampened. The use of mutants can be problematic due to a mis-positioning of the substrate. Despite this limitation, particular mutants can be selected where the isomerization activity is unaffected by the mutation as these structural studies have suggested that the isomerization activity is expected to be optimal when the substrate is close to, or in, its proposed binding position for oxidation. Another method for slowing enzyme turnover, and trapping the complex, could include crystallization or transfer of the crystals to very basic pH solutions where the oxidative activity is severely dampened. This method could be applied to both wild type and mutant enzymes.

Complex crystals are either obtained by co-crystallization of the substrate and protein or by soaking experiments where the protein crystals are in a solution containing

the substrate. Both methods are being actively carried out to obtain the elusive Michaelis complex of SCOA. The tight crystal packing in SCOA could be the cause of our inability to obtain a steroid complex via the latter method. Co-crystallization experiments have lead to potential complex structures, however to date these crystals, do not diffract to sufficient resolution to determine if cholesterol is bound in the active site. As shown here the wild type SCOA crystals diffract to sub-atomic resolution. Further soaking experiments with smaller substrates, such as cyclohexanol and 3-cyclohexene-1-ol, could determine how the hydroxyl ring of cholesterol binds for oxidation. In addition, with sub-atomic resolution crystals, one could trap the enzyme with these substrates during different points in the reaction pathway thus providing a unique view of the pathway followed during substrate oxidation and isomerization.

Chapters 3, 4 and 5 of this thesis demonstrate the value of pursuing atomic resolution structures. The additional detail provided by sub-atomic resolution maps, as compared to 1.5 Å, resulted in a ten-fold increase in the observation of discretely disordered residues. Resolving these alternate residue conformations is invaluable for understanding the dynamics of a protein and provides important insights into the catalytic mechanism of an enzyme.

6.4 References

Berglund, G. I., Carlsson, G. H., Smith, A. T., Szoke, H., Henriksen, A. & Hajdu, J. (2002). The catalytic pathway of horseradish peroxidase at high resolution. *Nature* **417**(6887), 463-468.

Cavener, D. (1992). GMC oxidoreuctases. A newly defined family of homologous proteins with diverse catalytic activities. *J. Mol. Biol.* **223**, 811-814.

Kiess, M., Hecht, H.-J. & Kalisz, H. M. (1998). Glucose oxidase from *Penicillium amagasakiense*: Primary structure and comparison with other glucose-methanol-choline (GMC) oxidoreductases. *Eur. J. Biochem.* **252**, 90-99.

Li, J., Vrielink, A., Brick, P. & Blow, D. M. (1993). Crystal structure of cholesterol oxidase complexed with a steroid substrate: Implications for flavin adenine dinucleotide dependent alcohol oxidases. *Biochemistry* **32**, 11507-11515.

ACS PUBLICATIONS DIVISION GUIDELINES

FOR THESES AND DISSERTATIONS

ATTN: STUDENTS, STUDENT ADVISORS, AND TEACHERS

Permission is now automatically granted to include your paper(s) or portions of your paper(s) in your thesis; please pay special attention to the implications paragraph below. The Joint Board/Council Committees on Copyrights and Publications recently approved the following:

> Copyright permission for published and submitted material from theses and dissertations
> ACS extends blanket permission to students to include in their theses and dissertations their own articles, or portions thereof, that have been published in ACS journals or submitted to ACS journals for publication, provided that the ACS copyright credit line is noted on the appropriate page(s).
>
> Publishing implications of electronic publication of theses and dissertation material
> Students and their mentors should be aware that posting of theses and dissertation material on the Web prior to submission of material from that thesis/dissertation to an ACS journal may affect publication in that journal. Whether Web posting is considered prior publication may be evaluated on a case-by-case basis by the journal's editor. If an ACS journal editor considers Web posting to be "prior publication", the paper will not be accepted for publication in that journal.

If your paper has **not** yet been published by ACS, we have no objection to your including part or all of it in your thesis in print and microfilm formats; please note, however, that electronic distribution or Web posting of the unpublished paper as part of your thesis in electronic formats might jeopardize publication of your paper by ACS. Please print the following credit line on the first page of your article: "Reproduced (or 'Reproduced in part') with permission from [JOURNAL NAME], in press (or 'submitted for publication'). Unpublished work copyright [CURRENT YEAR] American Chemical Society." Include appropriate information.

If your paper has already been published by ACS and you want to include part or all of it in your thesis or dissertation, please print the ACS copyright credit line on the first page of your article: "Reproduced (or 'Reproduced in part') with permission from [FULL REFERENCE CITATION.] Copyright [YEAR] American Chemical Society." Include appropriate information.

Note: If you plan to submit your thesis to UMI or to another dissertation distributor, you should not include the unpublished ACS paper in your thesis if the thesis will be disseminated electronically, until ACS has published your paper. After publication of the paper by ACS, you may release the entire thesis for electronic dissemination; ACS's copyright credit line should be printed on the first page of the ACS paper.

Permission is not granted to post any published or unpublished ACS articles on any Web site.

Questions? Call ACS Publications Division Copyright Office staff at 3, or e-mail us at

PERMISSIONS DEPARTMENT

WILEY
Publishers Since 1807

October 8, 2002

Ms.Paula Lario

Dear Ms. Lario:

RE: Your October 2, 2002 request for permission to republish Figure 4 from Proteins: Structure, Function and Genetics [43:420-432(2001)]. This material will appear in your forthcoming PhD thesis, to be published by McGill University.

1. Permission is granted for this use, except that if the material appears in our work with credit to another source, you must also obtain permission from the original source cited in our work.

2. Permitted use is limited to your edition described above, and does not include the right to grant others permission to photocopy or otherwise reproduce this material except for versions made for use by visually or physically handicapped persons. Up to five copies of the published thesis may be photocopied by a microfilm company.

3. Appropriate credit to our publication must appear on every copy of your thesis, either on the first page of the quoted text, in a separate acknowledgment page, or figure legend. The following components must be included: Title, author(s) and /or editor(s), journal title (if applicable), Copyright © (year and owner). Reprinted by permission of John Wiley & Sons, Inc.

4. This license is non-transferable. This license is for non-exclusive **English language print** rights and microfilm storage rights by McGill University only, throughout the world. *For translation rights, please reapply for a license when you have plans to translate your work into a specific language.*

Sincerely,

Judith Spreitzer
Manager, Copyright & Permissions

UNIVERSITY OF CALIFORNIA, SANTA CRUZ

BERKELEY • DAVIS • IRVINE • LOS ANGELES • RIVERSIDE • SAN DIEGO • SAN FRANCISCO SANTA BARBARA • SANTA CRUZ

Alice Vrielink
Department of Molecular Cellular and Developmental Biology and
Department of Chemistry and Biochemistry

January 28, 2003

Paula Lario
D.H. Copp Building, Dept of Biochemistry

Attention: Paula Lario

As per your request, I herby grant you permission to include our unpublished manuscript titled "Effect of pH on the atomic resolution structures of cholesterol oxidase: FAD reduction by synchrotron radiation" in your thesis.

Sincerely yours,

Alice Vrielink, PhD
Associate Professor

STONY BROOK
STATE UNIVERSITY OF NEW YORK

DEPARTMENT OF CHEMISTRY
Nicole S. Sampson
Professor *Secretary:*

January 28, 2003

Paula Lario
D.H. Copp Building, Dept of Biochemistry

Attention: Paula Lario

As per your request, I herby grant you permission to include our unpublished manuscript titled "Effect of pH on the atomic resolution structures of cholesterol oxidase: FAD reduction by synchrotron radiation" in your thesis.

Yours sincerely,

Nicole S. Sampson

PERMISSIONS DEPARTMENT

WILEY
Publishers Since 1807

October 8, 2002

Ms.Paula Lario
Biology Department/UCSC

Dear Ms. Lario:

RE: Your October 2, 2002 request for permission to republish Figure 4 from Proteins: Structure, Function and Genetics [43:420-432(2001)]. This material will appear in your forthcoming PhD thesis, to be published by McGill University.

1. Permission is granted for this use, except that if the material appears in our work with credit to another source, you must also obtain permission from the original source cited in our work.

2. Permitted use is limited to your edition described above, and does not include the right to grant others permission to photocopy or otherwise reproduce this material except for versions made for use by visually or physically handicapped persons. Up to five copies of the published thesis may be photocopied by a microfilm company.

3. Appropriate credit to our publication must appear on every copy of your thesis, either on the first page of the quoted text, in a separate acknowledgment page, or figure legend. The following components must be included: Title, author(s) and /or editor(s), journal title (if applicable), Copyright © (year and owner). Reprinted by permission of John Wiley & Sons, Inc.

4. This license is non-transferable. This license is for non-exclusive **English language print** rights and microfilm storage rights by McGill University only, throughout the world. *For translation rights, please reapply for a license when you have plans to translate your work into a specific language.*

Sincerely,

Judith Spreitzer
Manager, Copyright & Permissions

Thesis 8-02.doc

ELSEVIER
SCIENCE

08 November 2002

Our ref: HW/vm/nov02.047

Paula I Lario

Dear Ms Lario

JOURNAL OF MOLECULAR BIOLOGY, Subject to Acceptance, Lario et al: "Sub-atomic resolution crystal structure of cholesterol oxidase: What atomic resolution ..."

As per your letter dated 05 November 2002, we hereby grant you permission to reprint the aforementioned material at no charge **in your thesis** subject to the following conditions:

1. If any part of the material to be used (for example, figures) has appeared in our publication with credit or acknowledgement to another source, permission must also be sought from that source. If such permission is not obtained then that material may not be included in your publication/copies.

2. Suitable acknowledgment to the source must be made, either as a footnote or in a reference list at the end of your publication, as follows:

   "Reprinted from Publication title, Vol number, Author(s), Title of article, Pages No., Copyright (Year), with permission from Elsevier Science".

3. Reproduction of this material is confined to the purpose for which permission is hereby given.

4. This permission is granted for non-exclusive world **English** rights only. For other languages please reapply separately for each one required. Permission excludes use in an electronic form. Should you have a specific electronic project in mind please reapply for permission.

5. This includes permission for UMI to supply single copies, on demand, of the complete thesis. Should your thesis be published commercially, please reapply for permission.

Yours sincerely

Helen Wilson
Rights Manager

Your future requests will be handled more quickly if you complete the online form at
www.elsevier.com/homepage/guestbook/?form=permis

ACS PUBLICATIONS DIVISION GUIDELINES

FOR THESES AND DISSERTATIONS

ATTN: STUDENTS, STUDENT ADVISORS, AND TEACHERS

Permission is now automatically granted to include your paper(s) or portions of your paper(s) in your thesis; please pay special attention to the implications paragraph below. The Joint Board/Council Committees on Copyrights and Publications recently approved the following:

> Copyright permission for published and submitted material from theses and dissertations
> ACS extends blanket permission to students to include in their theses and dissertations their own articles, or portions thereof, that have been published in ACS journals or submitted to ACS journals for publication, provided that the ACS copyright credit line is noted on the appropriate page(s).
>
> Publishing implications of electronic publication of theses and dissertation material
> Students and their mentors should be aware that posting of theses and dissertation material on the Web prior to submission of material from that thesis/dissertation to an ACS journal may affect publication in that journal. Whether Web posting is considered prior publication may be evaluated on a case-by-case basis by the journal's editor. If an ACS journal editor considers Web posting to be "prior publication", the paper will not be accepted for publication in that journal.

If your paper has not yet been published by ACS, we have no objection to your including part or all of it in your thesis in print and microfilm formats; please note, however, that electronic distribution or Web posting of the unpublished paper as part of your thesis in electronic formats might jeopardize publication of your paper by ACS. Please print the following credit line on the first page of your article: "Reproduced (or 'Reproduced in part') with permission from [JOURNAL NAME], in press (or 'submitted for publication'). Unpublished work copyright [CURRENT YEAR] American Chemical Society." Include appropriate information.

If your paper has already been published by ACS and you want to include part or all of it in your thesis or dissertation, please print the ACS copyright credit line on the first page of your article: "Reproduced (or 'Reproduced in part') with permission from [FULL REFERENCE CITATION.] Copyright [YEAR] American Chemical Society." Include appropriate information.

Note: If you plan to submit your thesis to UMI or to another dissertation distributor, you should not include the unpublished ACS paper in your thesis if the thesis will be disseminated electronically, until ACS has published your paper. After publication of the paper by ACS, you may release the entire thesis for electronic dissemination; ACS's copyright credit line should be printed on the first page of the ACS paper.

Permission is not granted to post any published or unpublished ACS articles on any Web site.

Questions? Call ACS Publications Division Copyright Office staff at or e-mail us at copyright@acs.org.

August 1998